

NASA Contractor Report 3476

Experimental and Analytical Studies of Advanced Air Cushion Landing Systems

E. G. S. Lee, A. B. Boghani, K. M. Captain,
H. J. Rutishauser, H. L. Farley, R. B. Fish,
and R. L. Jeffcoat

CONTRACT NAS1-15051
NOVEMBER 1981

NASA

NASA
CR
3476
c.1



LOAN COPY: RETURN TO
AFWL TECHNICAL LIBRARY
KIRTLAND AFB, N.M.



NASA Contractor Report 3476

Experimental and Analytical Studies of Advanced Air Cushion Landing Systems

E. G. S. Lee, A. B. Boghani, K. M. Captain,
H. J. Rutishauser, H. L. Farley, R. B. Fish,
and R. L. Jeffcoat
Foster-Miller Associates, Inc.
Waltham, Massachusetts

Prepared for
Langley Research Center
under Contract NAS1-15051



National Aeronautics
and Space Administration

**Scientific and Technical
Information Branch**

1981

CONTENTS

	<u>Page</u>
SUMMARY	1
PART I - NOVEL ACLS CONCEPTS	3
INTRODUCTION	3
CANDIDATE ACLS CONCEPTS	5
Introduction	5
Description of Concepts	7
INITIAL SCREENING	13
TEST METHODOLOGY AND APPARATUS	15
Method of Evaluation	15
Test Apparatus	15
EVALUATION OF THE ADVANCED CONCEPTS	19
The Baseline Cushion	19
The Damped Trunk	24
The Filled Trunk	30
The Compartmented Trunk	30
The Segmented Trunk	34
Roll Feedback Control	34
CONCEPT COMPARISON	41
COMPUTER SIMULATION	47

CONTENTS (Continued)

	<u>Page</u>
FULL-SCALE DESIGN OF AN ADVANCED ACLS CONCEPT . . .	55
Design Features	55
Design Details	57
Fabrication, Installation and Preliminary Tests .	62
SCALE MODEL TESTS OF THE NASA ACLS TEST VEHICLE . .	67
Design Features and Details	67
Test Apparatus	69
Static Tests	70
Stability Analysis	75
Dynamic Tests	77
Computer Simulation	77
DYNAMIC TESTING OF SCALED ACLS MODELS	81
Principles of Dynamic Scaling	81
Scaling Techniques	82
Application to Scaled NASA Test Vehicle	86
Scale Model Tests for Model Validation	89
CONCLUSIONS AND RECOMMENDATIONS	91
PART II - WATERBORNE ACLS STUDIES	93
INTRODUCTION	93
Background	93
Summary	93

CONTENTS (Continued)

	<u>Page</u>
TESTING	95
Test Objectives	95
Test Equipment	95
Test Results	97
ANALYSIS	109
Approach	109
Model Development	109
System Frequency	113
Simulation Results	117
Model Limitations	124
CONCLUSIONS AND RECOMMENDATIONS	127
APPENDIX A - DESCRIPTION OF NOVEL ACLS CONCEPTS	129
APPENDIX B - COMPARISON BETWEEN SIMULATION AND EXPERIMENT.	141
APPENDIX C - STABILITY ANALYSIS OF NASA TEST VEHICLE	163
APPENDIX D - FLUID SYSTEM ELEMENT REPRESENTATION	167
APPENDIX E - FLUID MECHANICAL ANALYSIS	169
REFERENCES	175

FIGURES

<u>Figure No.</u>		<u>Page</u>
1	Novel ACLS concepts	9
2	The test rig	16
3	The test cushion	17
4	Fan flow test rig	20
5	Pressure-flow characteristics of the tip-turbine fan	21
6	Roll stiffness - baseline cushion	22
7	Heave dynamics - baseline cushion	23
8	Trunk material damping test rig	25
9	Flexural damping constant of various trunk materials	27
10	Roll stiffness - damped trunk	28
11	Heave drop test - damped trunk	29
12	Foam filler installation	31
13	Roll stiffness - filled trunk	32
14	Heave drop - filled trunk	33
15	Roll stiffness - compartmented trunk	35
16	Heave drop test - compartmented trunk	36
17	Heave drop test - segmented trunk	37
18	Conceptual representation of roll feedback control.	39
19	Roll stiffness characteristics	40
20	Trunk height comparison	42

FIGURES (Continued)

<u>Figure No.</u>		<u>Page</u>
21	Heave stiffness comparison	43
22	Damping ratio and roll stiffness comparison	44
23	Comparison between simulation and experiment - baseline system	48
24	Comparison between simulation and experiment - damped trunk	49
25	Comparison between simulation and experiment - filled trunk	50
26	Comparison between simulation and experiment - compartmented trunk	51
27	Comparison between simulation and experiment - segmented trunk	52
28	NASA test vehicle trunk design - top view .	56
29	Characteristics of NASA test vehicle hub-turbine fan	58
30	NASA test vehicle trunk design - cross sectional shape	59
31	NASA test vehicle trunk design - trunk attachment detail	60
32	NASA test vehicle trunk design - location of trunk attachment holes	61
33	The checkerboard pattern of the NASA test vehicle orifices	63
34	The segmented trunk for the NASA ACLS test vehicle (lobe covers removed)	64
35	NASA test vehicle operating with the segmented trunk	65
36	Design configuration for one-third scale test vehicle	68

FIGURES (Continued)

<u>Figure No.</u>		<u>Page</u>
37	Trunk profile versus load	71
38	Hard surface clearance versus load for one-third scale test vehicle	72
39	Pressure versus load for one-third scale test vehicle	73
40	Side trunk characteristic polynomial	74
41	Static roll test results	76
42	Drop test results for one-third scale test vehicle; 2.4 cm (6 in.)	78
43	Comparison between simulation and experiment (heave position and trunk pressure)	79
44	Comparison between simulation and experiment (cushion pressure and heave acceleration)	80
45	Comparison between simulation and experiment trunk pressure - full-scale NASA test vehicle	90
46	Waterborne ACLS test rig	96
47	Cushion pressure frequency: ACLS test rig	100
48	Cushion pressure: ACLS test rig; 1-m gap; $X_0 = 2.5$ cm (1 in.)	101
49	Cushion pressure: ACLS test rig; 1-m gap; $X_0 = 5$ cm (2 in.)	102
50	Cushion pressure: ACLS test rig; 10-cm gap; $X_0 = 2.5$ cm (1 in.)	103
51	Cushion pressure: ACLS test rig; 10-cm gap; $X_0 = 5$ cm (2 in.)	104
52	Cushion pressure: ACLS test rig; 10-cm gap with baffle; $X_0 = 2.5$ cm (1 in.)	105

FIGURES (Continued)

<u>Figure No.</u>		<u>Page</u>
53	Cushion pressure: ACLS test rig; 10-cm gap with baffle; $X_0 = 2$ cm (5 in.)	106
54	Cushion pressure step response: ACLS test rig; 1-m gap	107
55	Cushion pressure step response: ACLS test rig; 10-cm gap	108
56	Waterborne ACLS test rig model	109
57	ACLS test rig simulation: 1-m gap; $X_0 = 2.5$ cm (1 in.); $Q_i = 0.42$ m ³ /min (15 ft ³ /min)	120
58	ACLS test rig simulation: 1-m gap; $X_0 = 5$ cm (2 in.); $Q_i = 0.42$ m ³ /min (15 ft ³ /min)	121
59	ACLS test rig simulation: 10-cm gap; $X_0 = 2.5$ cm (1 in.); $Q_i = 0.42$ m ³ /min (15 ft ³ /min)	122
60	ACLS test rig simulation: 10-cm gap; $X_0 = 5$ cm (2 in.); $Q_i = 0.42$ m ³ /min (15 ft ³ /min)	123
61	Cushion pressure-trunk discharge phase portrait; ACLS test rig simulation; 10-cm gap	125
62	Damped trunk	130
63	Coated trunk	131
64	Filled trunk	132
65	Compartmented trunk	133
66	Segmented trunk	134
67	Plenum relief valve	135
68	Contoured gap trunk	136
69	Circular trunk	137
70	Finger skirt trunk	138

FIGURES (Continued)

<u>Figure No.</u>		<u>Page</u>
71	Roll feedback control	139
72	Comparison between simulation and experiment heave position - baseline system	142
73	Comparison between simulation and experiment heave acceleration - baseline system	143
74	Comparison between simulation and experiment cushion pressure - baseline system	144
75	Comparison between simulation and experiment trunk pressure - baseline system	145
76	Comparison between simulation and experiment heave position - damped trunk	146
77	Comparison between simulation and experiment heave acceleration - damped trunk	147
78	Comparison between simulation and experiment cushion pressure - damped trunk	148
79	Comparison between simulation and experiment trunk pressure - damped trunk	149
80	Comparison between simulation and experiment heave position - filled trunk	150
81	Comparison between simulation and experiment heave acceleration - filled trunk	151
82	Comparison between simulation and experiment cushion pressure - filled trunk	152
83	Comparison between simulation and experiment trunk pressure - filled trunk	153
84	Comparison between simulation and experiment heave position - compartmented trunk	154
85	Comparison between simulation and experiment heave acceleration - compartmented trunk	155

FIGURES (Continued)

<u>Figure No.</u>		<u>Page</u>
86	Comparison between simulation and experiment cushion pressure - compartmented trunk	156
87	Comparison between simulation and experiment trunk pressure - compartmented trunk	157
88	Comparison between simulation and experiment heave position - segmented trunk	158
89	Comparison between simulation and experiment heave acceleration - segmented trunk	159
90	Comparison between simulation and experiment cushion pressure - segmented trunk	160
91	Comparison between simulation and experiment trunk pressure - segmented trunk	161
92	Test rig fluid element circuit	167
93	Streamline construction for evaluating the Bernoulli equation	170

TABLES

<u>Table No.</u>		<u>Page</u>
1	Novel ACLS Concepts	6
2	Simulation Model Verification Summary	53
3	ACLS Trunk Cost Data	66
4	Comparison of Static Test Data Between One-Third and Full-Scale Models	69
5	Scale Factors for the One-Third Scaled NASA Test Vehicle	88
6	Test Rig Data	115
7	System Frequency	118
8	Model Parameters	118

SUMMARY

In Part I of this report, several new concepts are developed for Air Cushion Landing Systems (ACLS) which have the potential for improving performance characteristics (roll stiffness, heave damping, and trunk flutter), and reducing fabrication cost and complexity. After an initial screening, the following five leading concepts are evaluated in detail:

1. Damped trunk
2. Filled trunk
3. Compartmented trunk
4. Segmented trunk
5. Roll feedback control.

The evaluation is based on tests performed on scale models. Test results show that trunks fabricated with materials with high inherent damping can alleviate the problems of heave stability and trunk flutter. A modest increase in roll stiffness can be achieved with new trunk configurations, but it will be necessary to implement a roll feedback system in order to substantially increase the roll stiffness.

The ACLS dynamic simulation developed earlier has been updated so that it can be used to predict the performance of full-scale ACLS incorporating these refinements. The simulation was validated through scale-model tests.

A full-scale ACLS based on the segmented trunk concept is described. It has been fabricated and installed on the NASA ACLS test vehicle, where it is currently being used to support advanced system development.

A geometrically-scaled model (one-third full scale) of the NASA test vehicle has been fabricated and tested. This model, evaluated by means of a series of static and dynamic tests, is used to investigate scaling relationships between reduced and full-scale models. The analytical model developed earlier is applied to simulate both the one-third scale and the full-scale response.

Principles of scale model testing are briefly discussed, along with procedures used to scale the NASA test vehicle.

Part II of this report describes the experiments, analysis, and computer simulations resulting from a preliminary investigation

into the behavior of a waterborne ACLS. The work described consisted of the following three tasks:

1. Construction of a two-dimensional, reduced-scale, rigid-impermeable-trunk test rig.
2. Formulation of analytical models for the test rig and the trunk discharge process.
3. Computer simulation and model verification against test data.

Test results show that an air discharge path from the cushion to the atmosphere is alternately opened and sealed by the water, and that this discontinuous trunk discharge process is characterized by periodic limit-cycle behavior. Initial simulations indicate that the basic trunk discharge process can be predicted with relatively simple analytical models. This low-frequency discharge process has important practical implications with regard to the over-water performance of the amphibious aircraft equipped with ACLS.

PART I - NOVEL ACLS CONCEPTS

INTRODUCTION

An important milestone in the development of ACLS technology has been reached. Technical and operational feasibility of the concept has now been established through the development and testing of three full-scale designs for the Jindivik, XC-8A and LA-4 aircraft. Before further aircraft-specific designs are prepared, it is appropriate to take a fresh look at the basic landing system with a view to overcoming some known shortcomings and developing concepts and designs that provide improved dynamic performance at lower cost. This report, which summarizes the work performed thus far under Contract No. NAS1-15051, Advanced ACLS Configuration Studies, takes an initial step in this direction.

Initially, 10 new concepts for ACLS were generated. These concepts had the potential for improving performance and/or reducing fabrication cost and complexity. Although there are other practical considerations such as ease of retraction, steering, and maintenance, it was decided to concentrate initially on improving system performance. The system refinements were based on increased fluid damping, differential trunk pressures, increased trunk material damping, alternate trunk geometry, and feedback control. After an initial screening process, the following five concepts were evaluated in detail:

1. Damped trunk
2. Filled trunk
3. Segmented trunk
4. Compartmented trunk
5. Roll feedback control.

The evaluation was based on tests performed on scale models. Heave drop, roll stiffness, and other tests were carried out to assess the basic dynamic behavior of the various systems. The results showed that a substantial increase in damping and stability can be achieved with the new trunk designs, but that a major increase in roll stiffness will require some form of roll feedback control. The segmented trunk configuration appeared to be the easiest to fabricate and assemble at low cost.

The ACLS dynamic simulation developed earlier has been updated so that the performance simulation of a full-scale ACLS incorporating these concepts can be carried out. The computer program and user's manual are available from Computer Software Management and Information Center (COSMIC), 112 Barrow Hall, University of Georgia, Athens, GA 30602, and are identified as COSMIC LAR-12303.

A full-scale segmented trunk design for the NASA test vehicle is carried out. This trunk, assembled from four segments, is made from Kevlar®* coated with polyurethane. The key features of the design are described along with other design details and the fabrication procedure.

Names of several manufacturers and their products have been referred to in the report. This does not constitute official endorsement of such products or manufacturers, either expressed or implied, by the National Aeronautics and Space Administration.

The authors wish to acknowledge the assistance of Professor D.N. Wormley of the Massachusetts Institute of Technology in the performance of the contract.

*Kevlar® is a trademark of the E. I. du Pont de Nemours & Company, Inc.

CANDIDATE ACLS CONCEPTS

Introduction

One of the major objectives in investigating new concepts for an ACLS is to overcome some of the deficiencies that have been observed in earlier designs. These deficiencies include:

1. Low roll stiffness
2. Low damping and hence poor stability
3. Trunk flutter.

Another objective is to generate new ACLS concepts that can be implemented at reduced cost.

Through an initial concept generation phase, 10 basic ACLS concepts were identified, which have the potential of overcoming the shortcomings mentioned above. These concepts, described later, are listed in Table 1, along with an initial indication of the areas where performance improvements are likely. There are four categories in which the proposed concepts can be classified. These are:

1. Increased fluid damping (with or without differential trunk pressure)
2. Increased trunk material damping
3. Alternate trunk geometry
4. Feedback control.

It must be recognized that these four categories can themselves be combined, so that an improved ACLS design for a specific aircraft will consist of a synthesis of these concepts to give an overall design best suited to the application in question. For the work described herein, however, each concept has been evaluated independently to determine its basic merits independent of other factors.

A brief description of the various concepts is given below. Additional details are presented in Appendix A. At this stage, the concepts are generic in nature, and could be implemented in a variety of ways. Subsequently, after the initial evaluation is carried out, five of the leading concepts are reduced to practice and tested to further evaluate the improvement in performance.

TABLE 1. - NOVEL ACLS CONCEPTS

No.	Concept	Category	Potential Improvement			
			Increased roll stiffness	Increased damping	Reduced flutter	Reduced cost
1	Damped trunk	Increased trunk material damping		X	X	
2	Coated trunk			X	X	
3	Filled trunk		X	X		
4	Compartmented trunk	Increased fluid damping and differential trunk pressures	X	X		
5	Segmented trunk		X	X		X
6	Plenum relief valve	Increased fluid damping		X		
7	Contoured gap trunk	Alternate trunk geometry			X	
8	Circular trunk				X	X
9	Finger skirt trunk		X		X	
10	Roll feedback control	Feedback control	X	X		

Description of Concepts

A description of the various concepts is given below. Sketches of the concepts are shown in Figure 1. Additional details are presented in Appendix A.

The damped trunk. - In this concept (Figure 1(a)) the trunk is made out of a "lossy" material that provides additional damping during tension and flexure. Such a system will help improve the damping and stability of the ACLS. However, in order to get sufficiently high damping, a composite or sandwich-type trunk material may be needed.

The coated trunk. - This concept (Figure 1(b)) is similar to the damped trunk, except that trunk damping is provided by covering a conventional trunk with a coating of lossy material, instead of making up the trunk from a high-loss substrate directly. With this approach, the coating thickness can be increased in the high-flexure regions, to obtain additional damping. The coating could be applied internally to prevent wear. This concept is dynamically similar to the damped trunk, and should be easier to fabricate. However, it may not be compatible with certain trunk materials and designs.

The filled trunk. - In this concept (Figure 1(c)) the trunk is filled with a high-loss foam or other type of material that will introduce additional damping when the trunk cross-section changes under dynamic load. It will be relatively easy to implement, and should be compatible with a wide variety of trunk designs.

The compartmented trunk. - In this concept (Figure 1(d)) the trunk is divided into several compartments by flexible, porous partitions. During dynamic operation, the losses caused by flow through the partitions introduce additional damping. In addition, different pressure levels in the various trunk compartments help increase angular stiffness.

The segmented trunk. - In this concept (Figure 1(e)) the trunk is made up of four or more separate, independently-fed segments, fastened together to form a unit. It is dynamically equivalent to a compartmented trunk with nonporous partitions. The system will be easier to fabricate since it is made up of smaller, less complex segments, having fewer curves. In fact, one attractive configuration of this trunk consists of four straight segments fastened together in the form of a picture frame. Such a trunk shape has been chosen for the NASA free body test vehicle and is described in more detail subsequently.

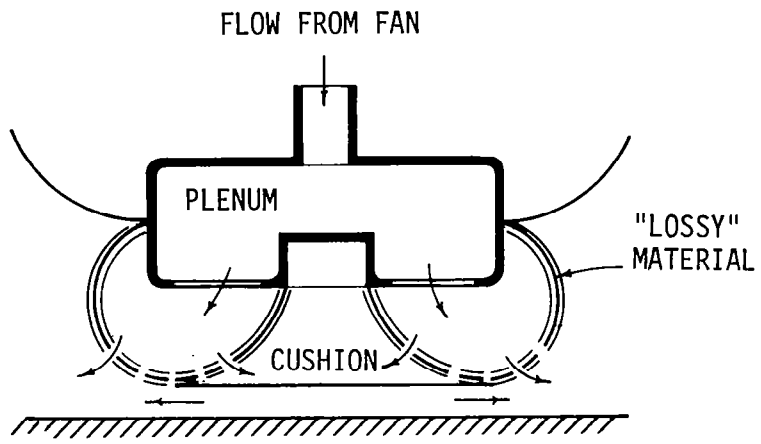
Pressure relief valve. - In this concept (Figure 1(f)) a pressure relief valve vents the plenum flow whenever the pressure level exceeds a preset value. This approach increases damping and improves stability by introducing an additional source of energy dissipation. The principal advantage of this concept is that it is very easy to implement and is compatible with almost all ACLS designs.

The contoured gap trunk. - In this concept (Figure 1(g)) the exit gap is contoured by means of elements such as strips attached or molded to the trunk bottom. This approach ensures that the gap area never reduces to zero, even under the most severe dynamic loading. Since flow blockage is eliminated, fan stall and other severe transients are alleviated, and system stability is improved. The change in the dynamic pressure force loading in the exit gap has been found to reduce flutter.

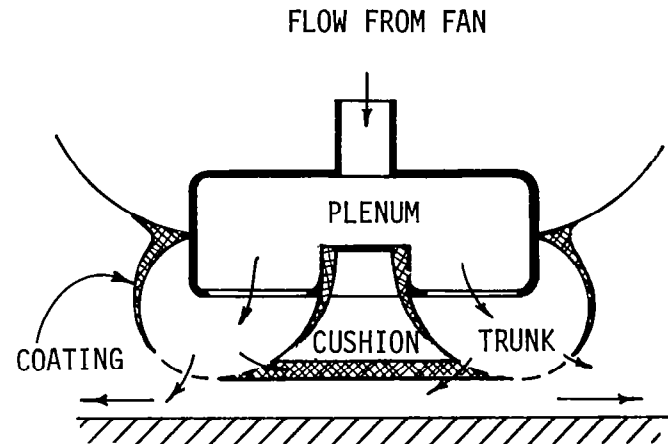
The circular trunk. - In this concept (Figure 1(h)) the plan-form configuration of the trunk is a circle instead of the conventional oval. With such a shape, the trunk will have higher heave stiffness because hoop stresses will prevent the sides from moving outwards. Although roll and pitch stiffness will be lower, this configuration lends itself to multiple cushions so that the heave forces of multiple cushions acting over the separating moment arm will provide a high angular stiffness for the full ACLS.

The finger skirt trunk. - This concept (Figure 1(i)) is a variation of a system currently used in air cushion transporters. It consists of a trunk surrounded by an air-lubricated finger skirt that absorbs part of the dynamic load and helps increase angular stiffness. It will, however, result in a relatively complex system that may be difficult to fabricate at low cost.

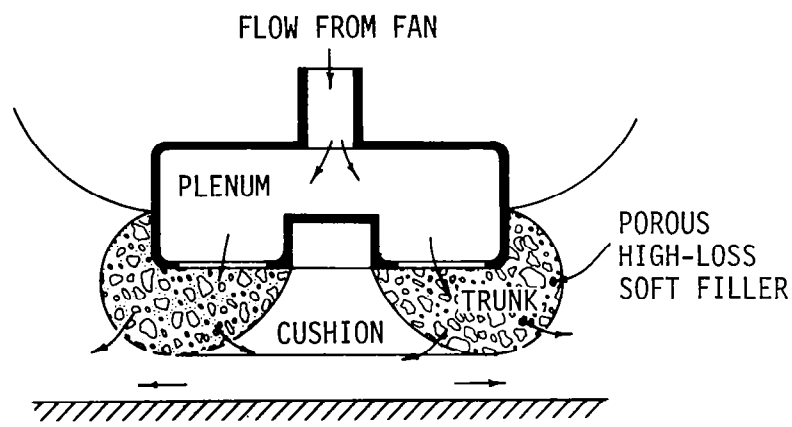
Roll feedback control. - In this concept (Figure 1(j)) the roll angle signal, suitably processed, is used to modulate the inlet airflow to various sections of the trunk. Such a system will only be effective in combination with segmented or compartmented trunks where different pressure levels can be established in different trunk sections. In this way, the roll stiffness of the ACLS will increase substantially.



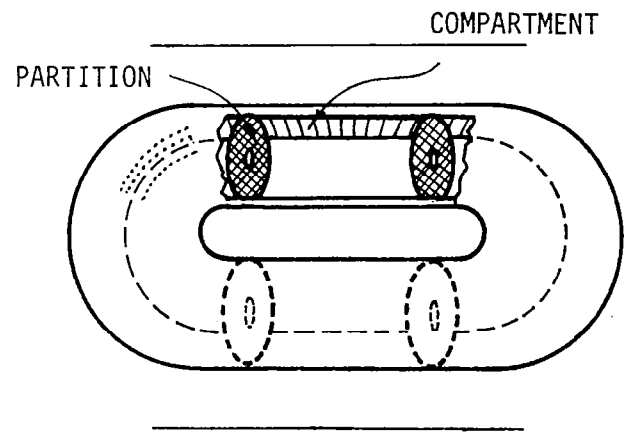
(a) Damped Trunk.



(b) Coated Trunk.

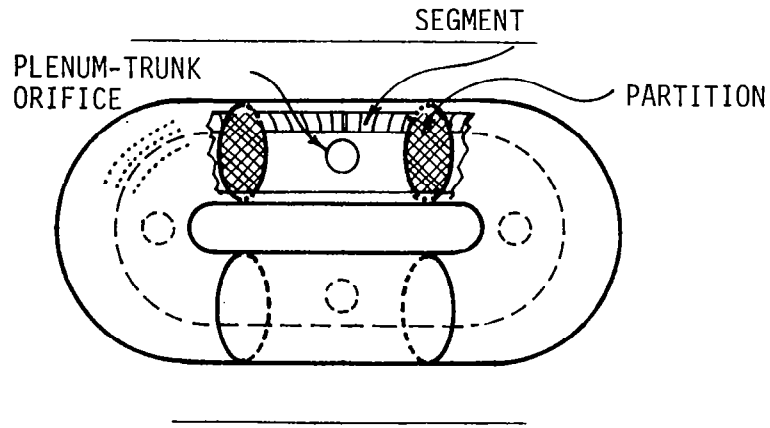


(c) Filled Trunk.

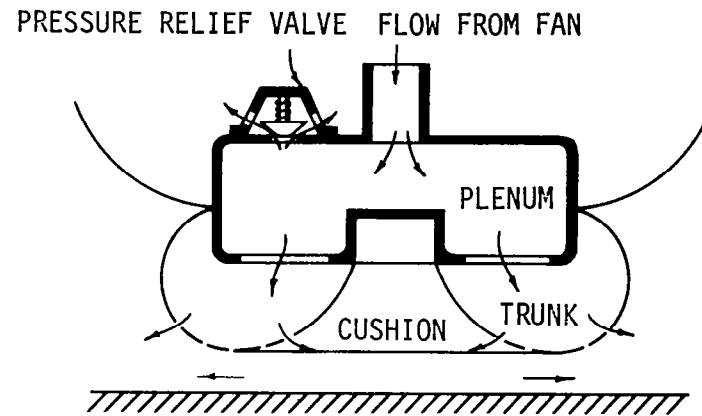


(d) Compartmented Trunk.

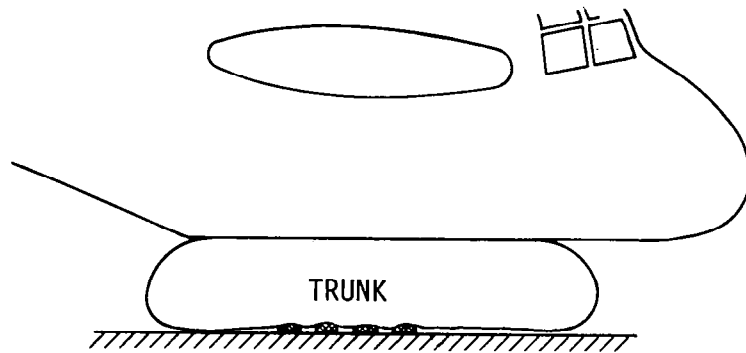
Figure 1. - Novel ACLS concepts.



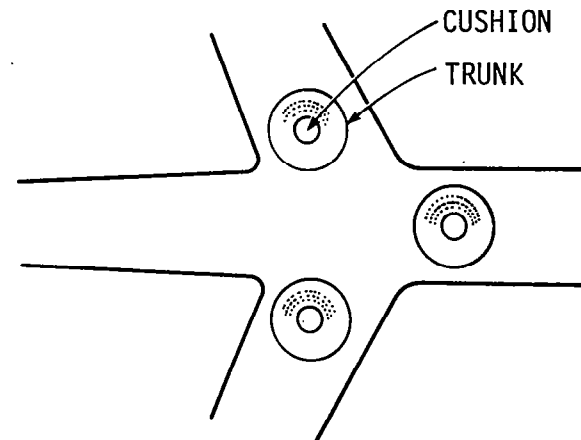
(e) Segmented Trunk.



(f) Plenum Relief Valve.

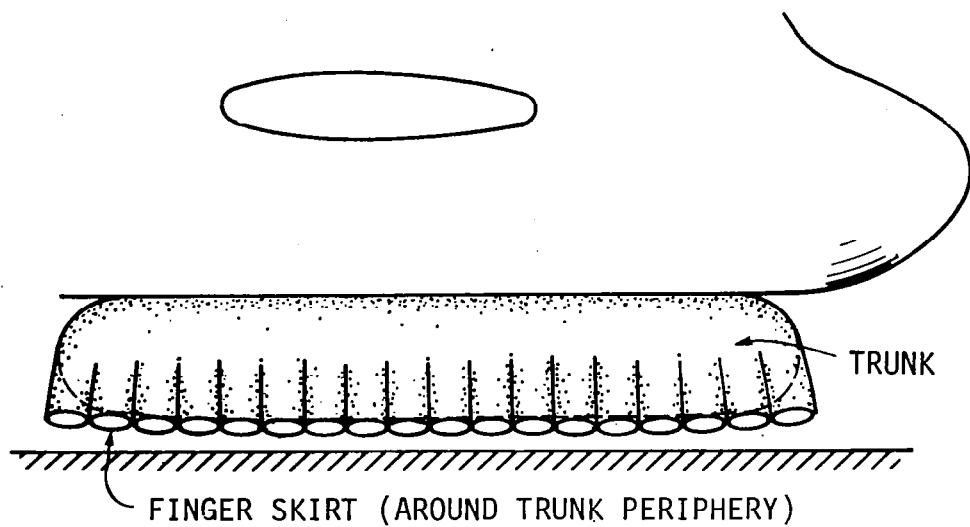


(g) Contoured Gap Trunk.

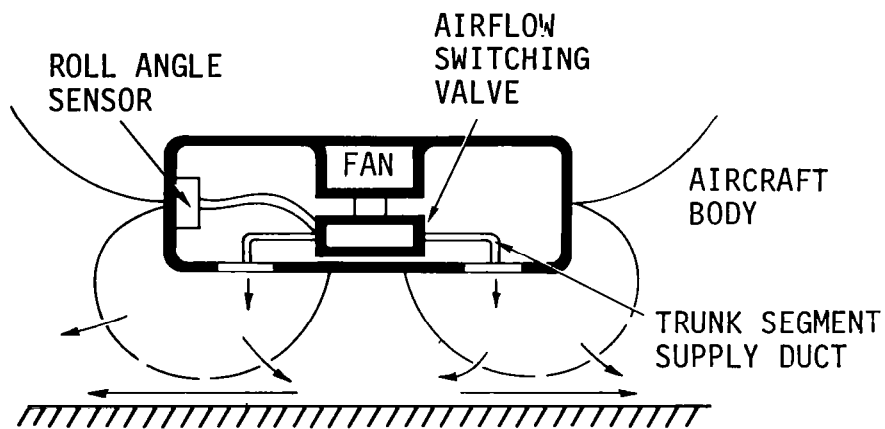


(h) Circular Trunk.

Figure 1. - Continued.



(i) FINGER SKIRT TRUNK



(j) ROLL FEEDBACK CONTROL

Figure 1. - Concluded.

INITIAL SCREENING

All the 10 concepts described earlier were subjected to an initial screening. The criteria used to judge each concept were as follows:

Ease of fabrication. - Past experience has shown that a sophisticated design has often led to difficulties in construction and maintenance. For this reason, each concept was viewed critically to see how it could be implemented easily and at low cost.

Performance improvement. - Providing adequate roll stiffness and damping, and eliminating flutter are three key requirements for an improved ACLS. All concepts were evaluated to assess their potential for improvements in these areas.

Based on these criteria, the following concepts were selected for further evaluation:

1. Damped trunk
2. Filled trunk
3. Compartmented trunk
4. Segmented trunk
5. Roll feedback control.

TEST METHODOLOGY AND APPARATUS

Method of Evaluation

After the initial screening, the chosen concepts were evaluated in further detail. This was carried out by preparing a design for each concept, fabricating scale models, and evaluating the performance through heave drop tests (at zero forward speed) and roll stiffness tests. The flutter behavior of the trunk was also assessed. Although scale-model costs were not considered realistic enough for comparison, a qualitative comparison of the ease of fabrication of the new trunk concepts was carried out. Also, the single concept chosen for full-scale design was compared in cost with historical cost data for conventional trunks.

In addition, the computer simulation developed earlier (ref. 1) was modified to simulate all of the concepts evaluated. Test data obtained with the scale models were used to validate the basic computer model. The object of this effort was to have available a computer program that could accurately predict the behavior of advanced ACLS configurations being designed.

Test Apparatus

The apparatus used to test the ACLS designs was developed earlier and is described in a previous report (ref. 1). The test rig is shown in Figure 2. It allows the ACLS to be constrained in heave, pitch, or roll, and tested independently in any of these modes. It is fully instrumented, and provides a dynamic readout of variables such as heave displacement and acceleration, roll and pitch angles and acceleration, cushion and trunk pressures, and fan flow.

The frame for the test cushion was also developed earlier (ref. 1). A sketch of the overall frame configuration is shown in Figure 3(a) to 3(c). It consists of an aluminum structure which forms the plenum and provides the attachment points for the trunk. The fan is mounted directly on the plenum at one end. It is an air-driven tip turbine centrifugal fan made by the Technology Development Corporation, Dayton, OH.

A variety of configurations was tested during the evaluation phase of the program. They were all formed from one basic trunk that was modified as the testing progressed. The basic trunk was fabricated by Hovercraft Fabrics, Ltd. It was made up from a Kevlar substrate coated with polyurethane. Unlike conventional trunks with punched orifices, porosity for this trunk was achieved by retaining the inherent porosity of the Kevlar fabric through a reduction of the polyurethane coating in the orifice region. Details of trunk configuration are shown in Figure 3(d).

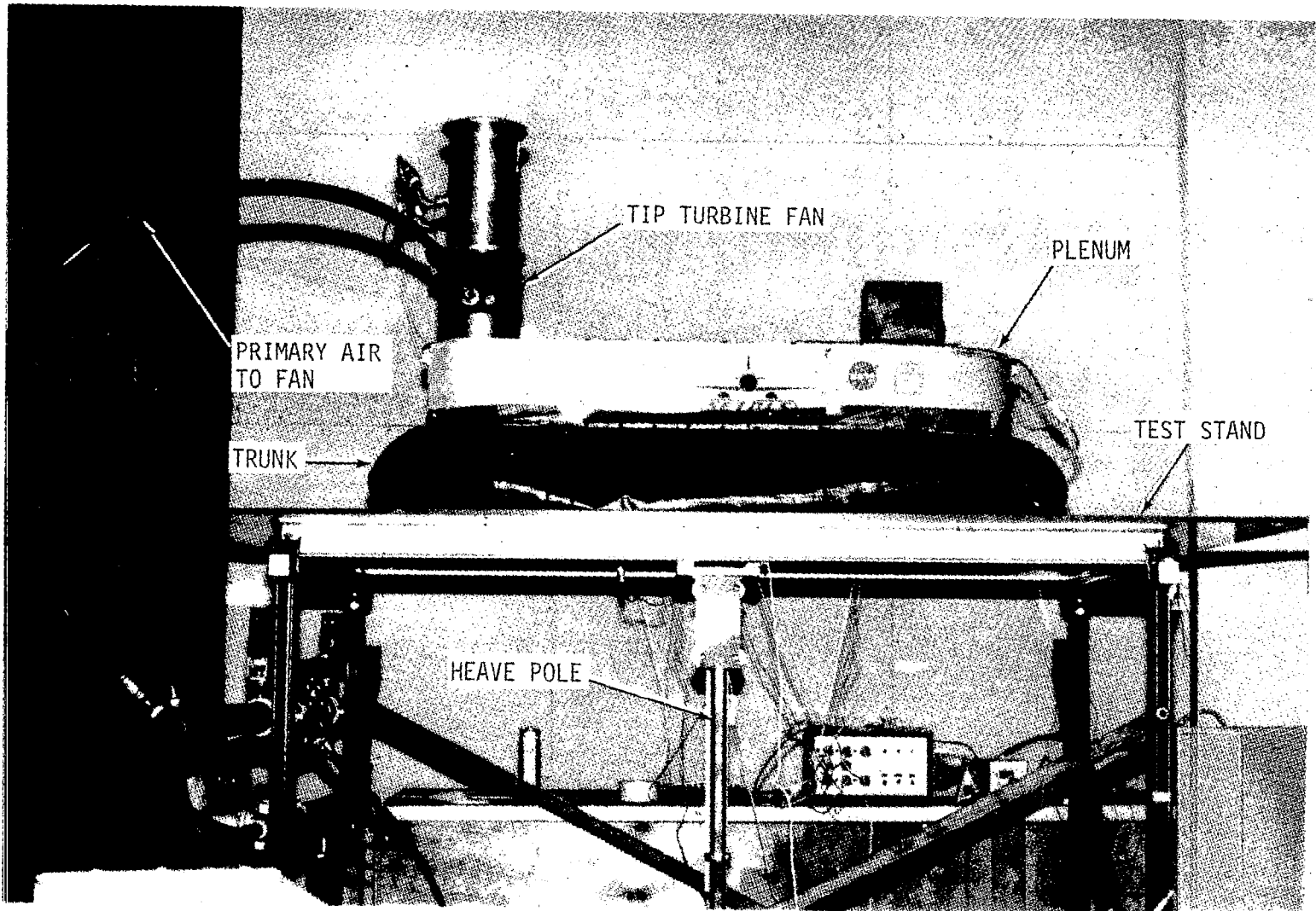
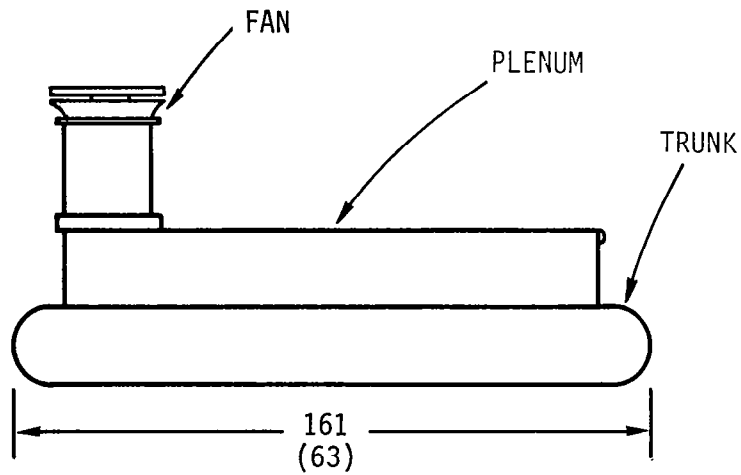
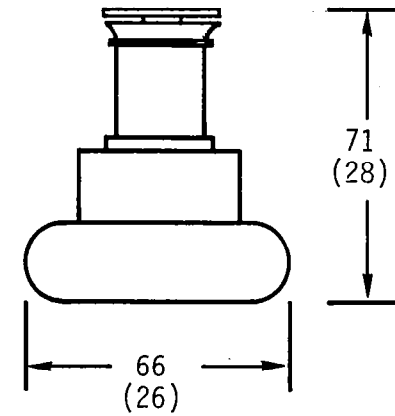


Figure 2. - The test rig.

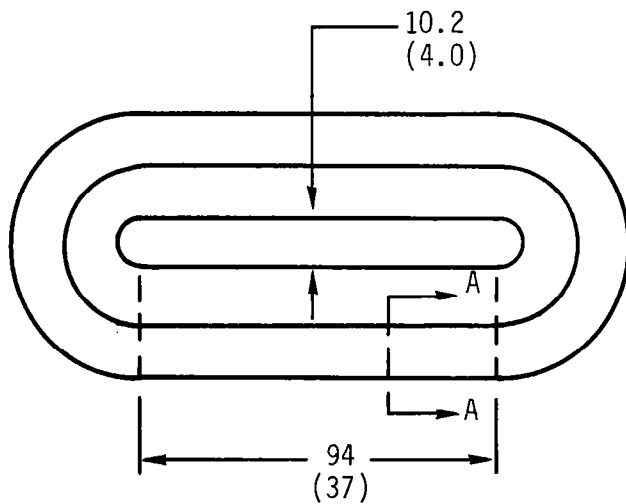


(a) Side View.

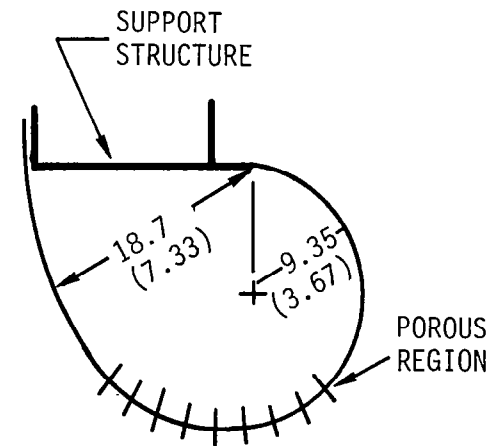


(b) End View.

NOTE: DIMENSIONS IN
CENTIMETERS
(INCHES)



(c) Bottom View.



(d) Trunk Cross-Section (A-A).

Figure 3. - The test cushion.



EVALUATION OF THE ADVANCED CONCEPTS

The Baseline Cushion

An ACLS designed and built several years ago by the Boeing Company, Seattle, WA, was chosen as the baseline cushion (ref. 2). It was supplied with a trunk made of Dacron®* fabric covered with polyurethane. This system was evaluated to provide baseline data against which the new concepts could be compared.

Fan characteristics. - The baseline cushion, and all other concepts, were evaluated using the same tip turbine fan. The characteristics of this fan depend on the primary air supply pressure. The initial tests showed a discrepancy between the data supplied by the manufacturer and flow-pressure readings obtained during the tests. Therefore, a fan test rig was built to check the accuracy of the data. This rig is shown in Figure 4. The fan flow was measured for various outlet valve openings using an orifice flowmeter. The corresponding fan pressure was measured using water manometers connected to the pressure taps.

The measured fan data are shown in Figure 5 along with the manufacturer's data. The difference between the two is probably due to the worn condition of the fan blades. It should be noted that this centrifugal tip turbine fan does not exhibit the stall characteristic of the axial fan originally supplied with the baseline cushion and evaluated in ref. 1.

All the computer simulations described later were carried out using the measured characteristics rather than the manufacturer's specifications.

Static tests. - The roll stiffness of the cushion was evaluated by measuring the roll angle for various values of roll moment. The test results are shown in Figure 6. The curves for increasing and decreasing roll angle are different due to hysteresis caused by friction due to rubbing of the trunk lobes on the ground plane.

Drop tests. - A representative heave drop test record is shown in Figure 7. Heave position and heave acceleration following a 15 cm (6 in.) drop are shown. As can be seen, this baseline case represents a relatively undamped system that is fairly typical of many ACLS designs.

*Dacron® is a trademark of the E. I. du Pont de Nemours & Company, Inc.

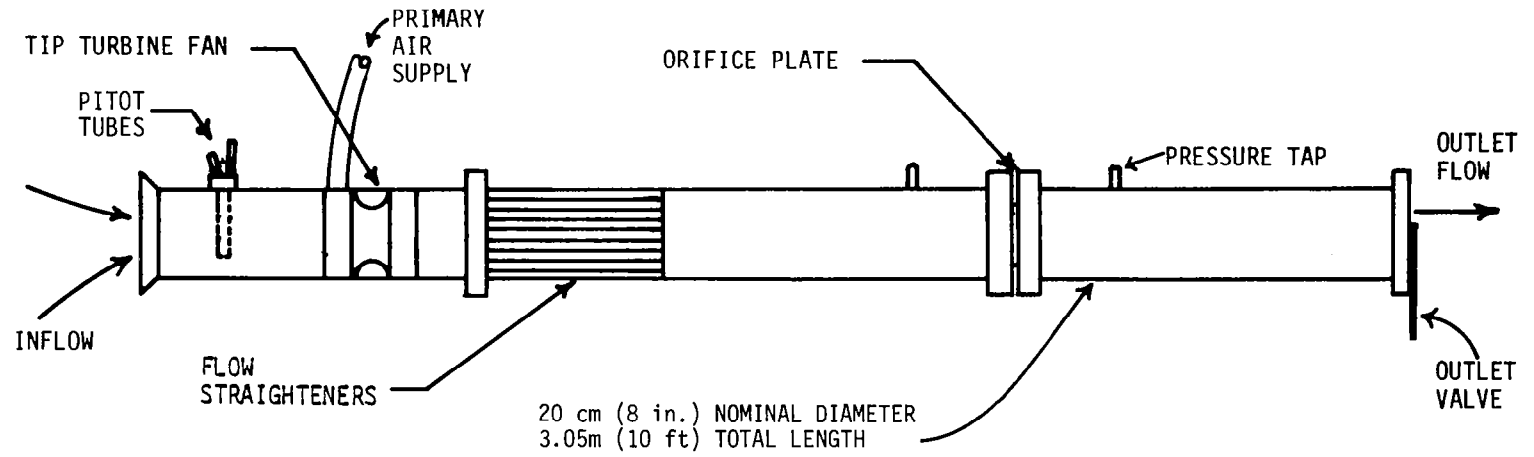


Figure 4. - Fan flow test rig.

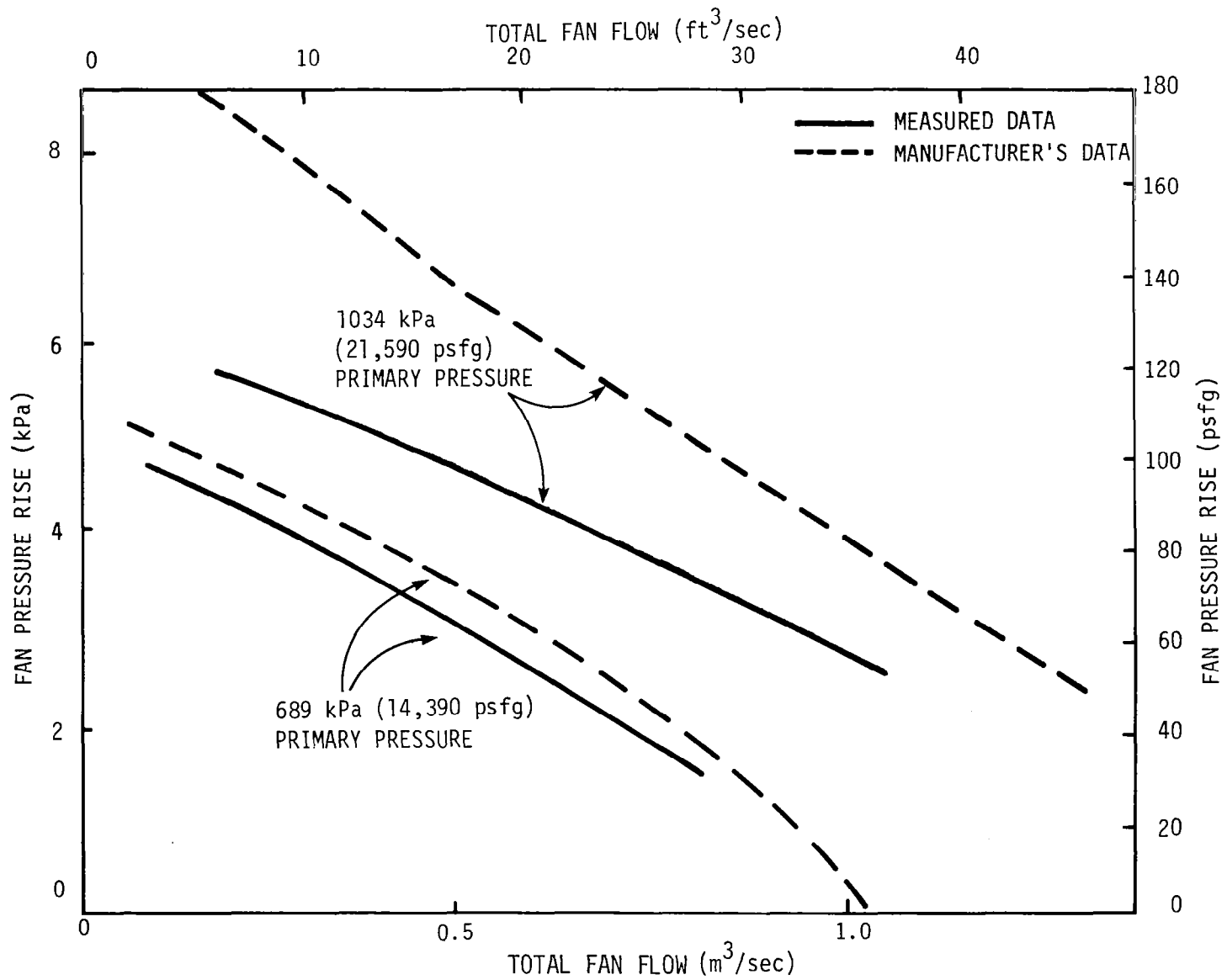


Figure 5. - Pressure-flow characteristics of the tip-turbine fan.

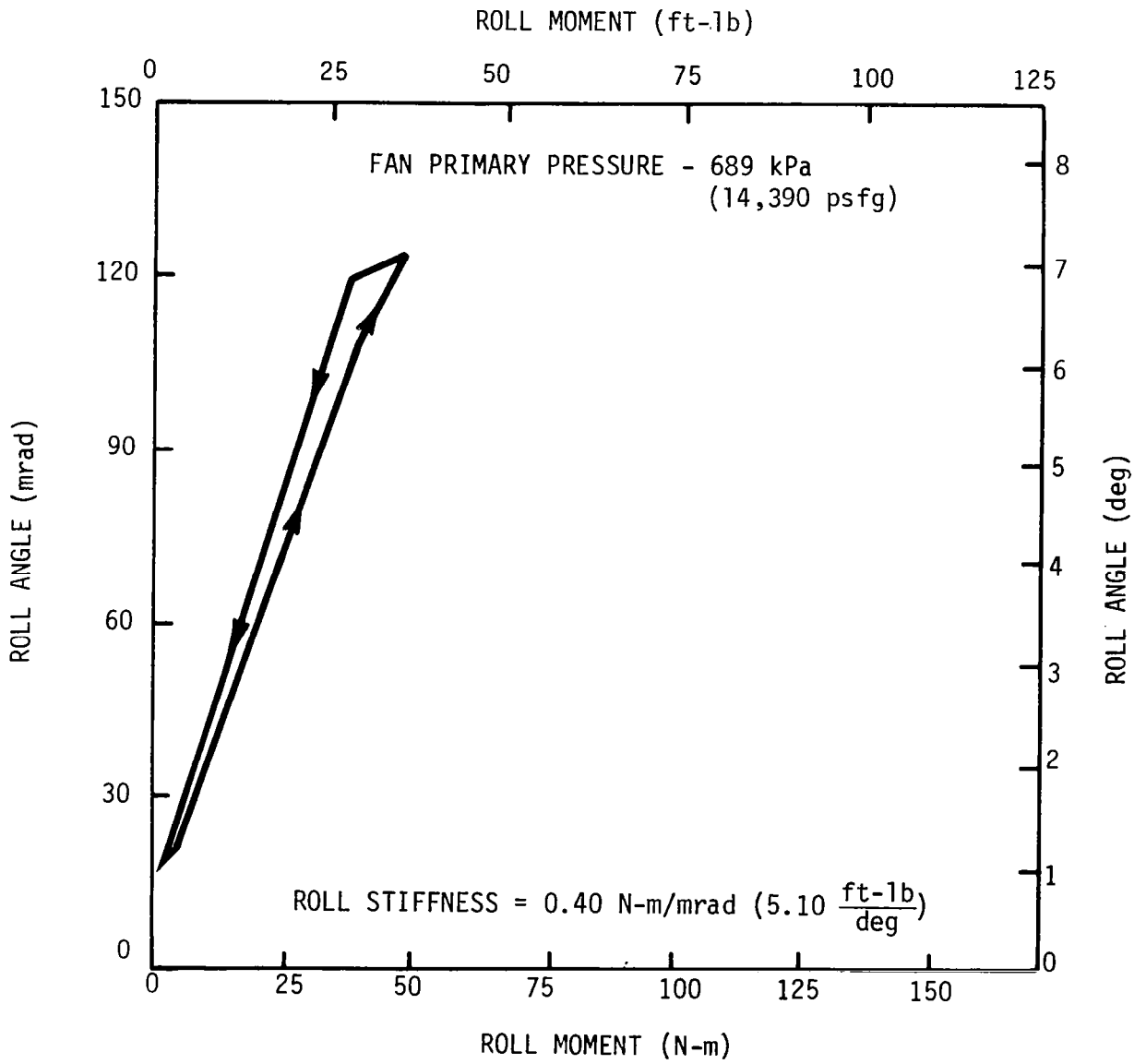


Figure 6. - Roll stiffness - baseline cushion.

PRIMARY FAN PRESSURE = 689 kPa

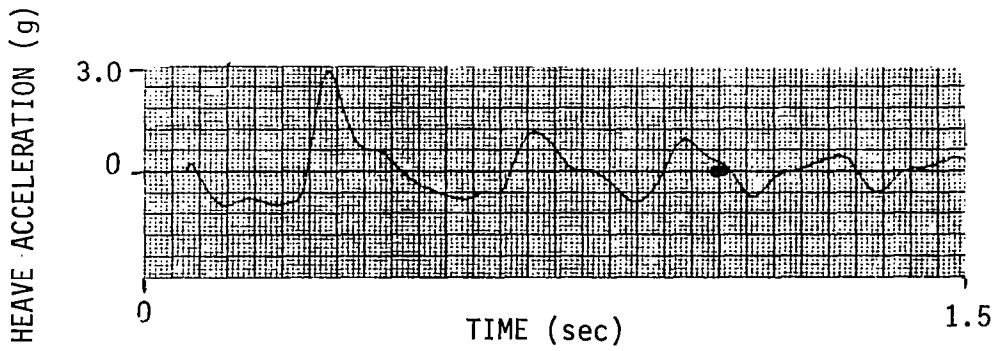
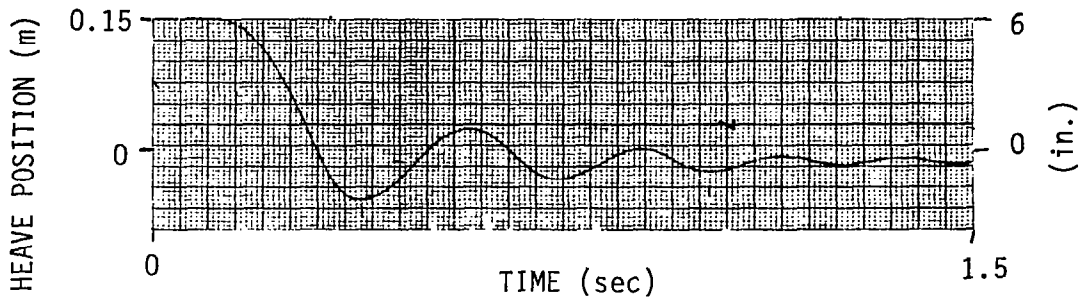


Figure 7. - Heave dynamics - baseline cushion.

Flutter observations. - The baseline trunk exhibits considerable flutter. The amount of flutter is found to be a function of load. The primary flutter frequency is 42 Hz. The flutter amplitude increases as the load is increased to 845N (190 lb) (nominal weight of model) then reduces to almost zero at a 1192N (268-lb) load. When the load is further increased from 1192N (268 lb), flutter reappears at a higher frequency (~130 Hz).

The Damped Trunk

One of the ways in which the damping of an ACLS could be improved is by increasing the damping of the trunk material. As information on the damping characteristics of candidate trunk materials does not exist in the industry, it was necessary to perform tests to assess the damping loss of trunk materials subjected to strains similar to those experienced during ACLS operation.

Material damping tests. - Most of the strain, and hence damping loss, in the ACLS trunk occurs due to flexure. For this reason, a pendulum test was conceived and implemented to measure trunk material damping in flexure. The test rig is shown in Figure 8.

The test specimen consists of a strip of trunk material 2.54 cm (1 in.) wide and 10 to 13 cm (4 to 5 in.) long. It is suspended from a support like a pendulum and a weight is attached to the lower end. The angular deflection of the pendulum is measured by means of a protractor placed behind the unit. The entire assembly is placed inside a vacuum chamber to eliminate air drag. A release electromagnet is included in the system to allow the pendulum to be released automatically from a preset initial angle after the vacuum has been established.

The test consisted of measuring the decay rate of the oscillations, and from this rate, determining the flexural damping constant of the material. The test was carried out as follows. The pendulum was released from an initial angle of 0.34 rad (20 deg) and the decay time t_d needed for this angle to reduce by one-half was noted. The pendulum length was chosen to give an oscillation frequency comparable to the heave frequency of typical ACLS. Initial tests showed that in the range of 1 to 2 Hz, frequency had no effect on the decay time.

The equation of motion for the pendulum, assuming a linear damping model, is as follows:

$$Wl^2 \ddot{\theta} - B_k \dot{\theta} = Wl \sin\theta$$

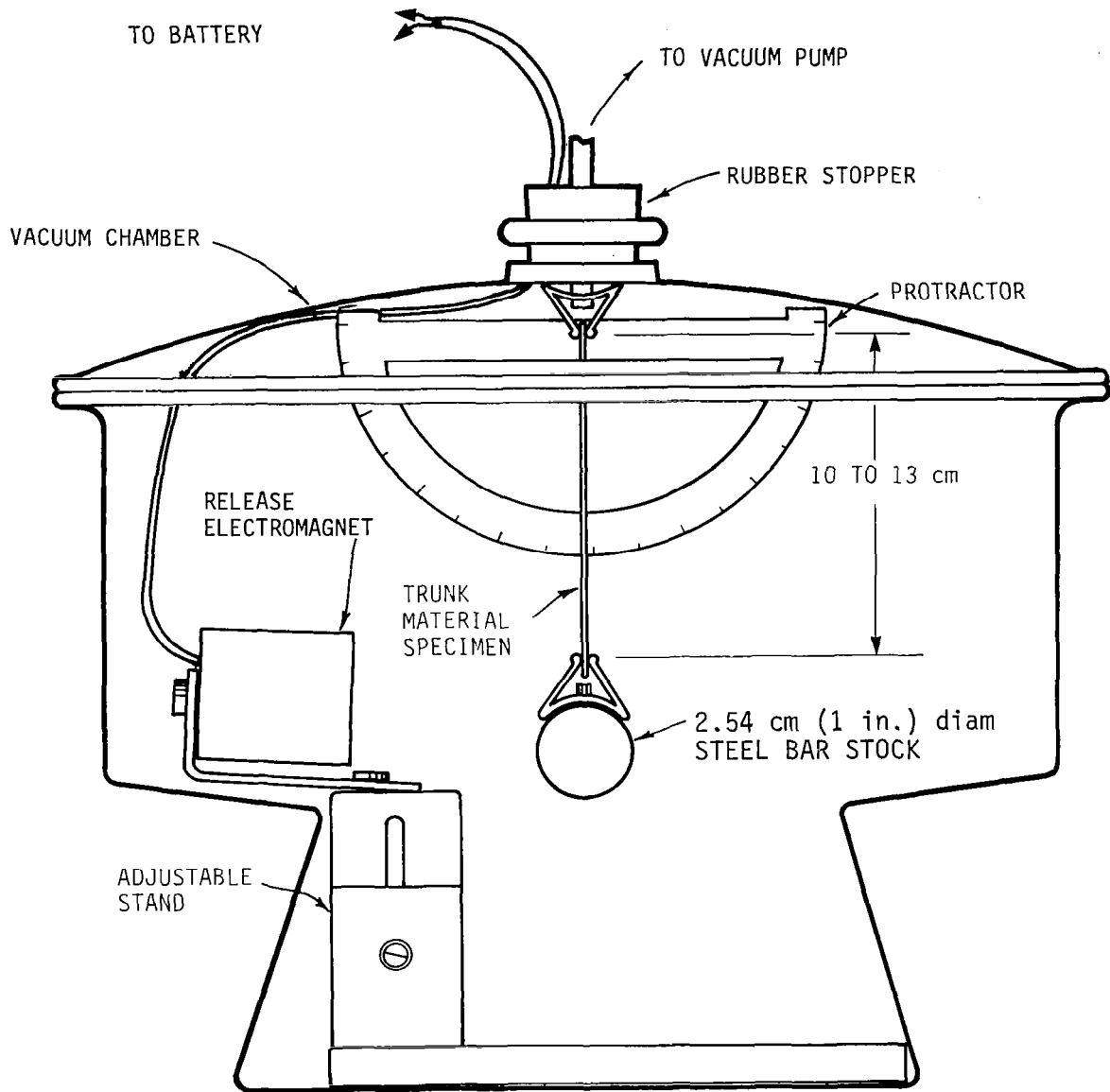


Figure 8. - Trunk material damping test rig.

where

- W = Weight of pendulum bob
- l = Pendulum length
- B_k = Flexural damping constant of trunk material
- θ = Angular displacement

This equation was integrated between the limits $t = 0$, $\theta = 0.34$ rad and $t = t_d$, $\theta_2 = 0.17$ rad to find the value of the trunk material damping constant B_k . The resulting values of B_k for various materials are shown in Figure 9.

From these results, the following conclusions can be reached:

1. For the same material, B_k increases as the thickness is increased. For the materials and thicknesses tested, the increase is fairly linear.
2. The trunk damping constant B_k is independent of frequency over the range of interest to ACLS.
3. Kevlar coated with polyurethane exhibited significantly more flexural damping than Dacron coated with polyurethane.

Based on the above results, it was decided to fabricate a trunk made of a Kevlar-polyurethane composite of the same size as the baseline Dacron-polyurethane trunk. This trunk was made of a triaxial basket weave of Kevlar coated with 1.5 mm (60 mil) of polyurethane. The triaxial weave was chosen since it is more stable than a biaxial weave. A fabric with a biaxial weave tends to stretch and distort when loaded on an angle from the direction of the warp and weft. This can cause high stresses in the area of the fabric/urethane interface. Cyclic loading will eventually cause failure due to delamination of the fabric and urethane. The triaxial weave, by contrast, stretches and distorts far less when loaded in any direction. All subsequent work, including the implementation of the other concepts, was carried out by modifying this basic trunk.

Static Tests. - The results of the roll stiffness tests are shown in Figure 10. Comparing these results with those of the baseline trunk (Figure 6) shows that the average roll stiffness has increased using the Kevlar trunk.

Drop tests. - Typical drop test records are shown in Figure 11. Comparing this figure with Figure 7 shows how the changed trunk material has increased the overall system damping.

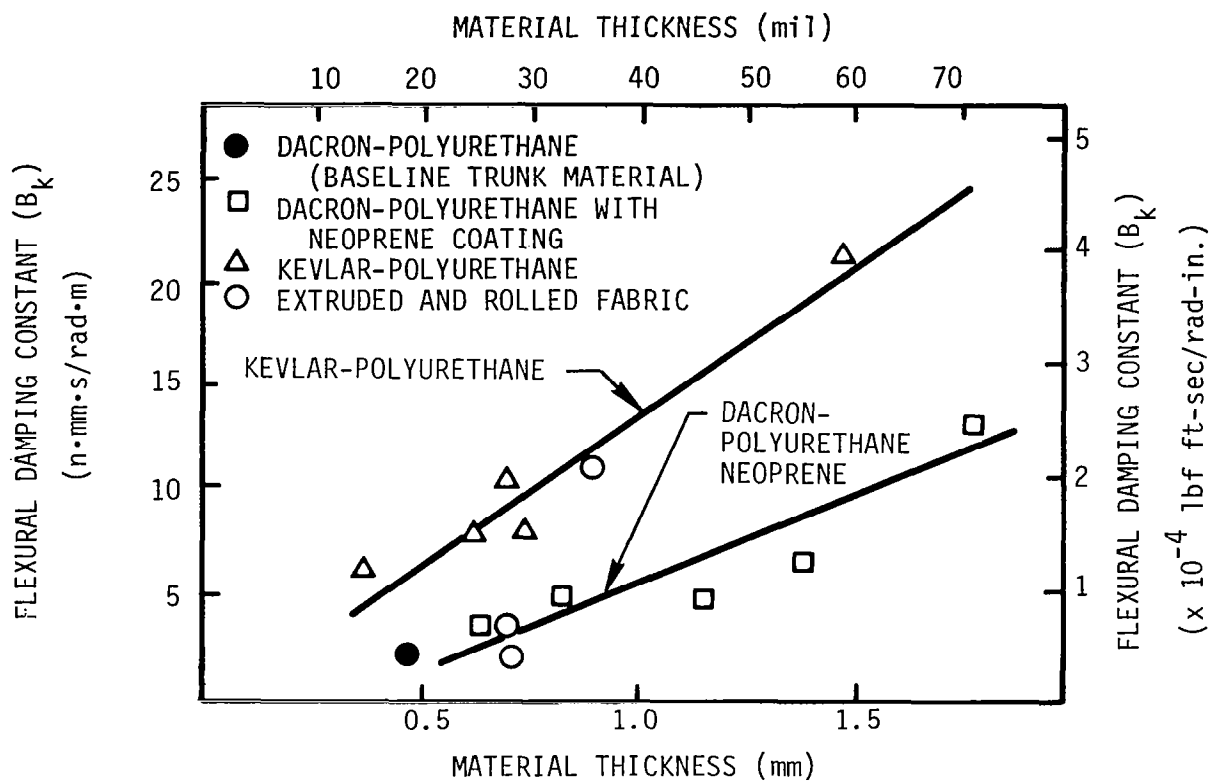


Figure 9. - Flexural damping constant of various trunk materials.

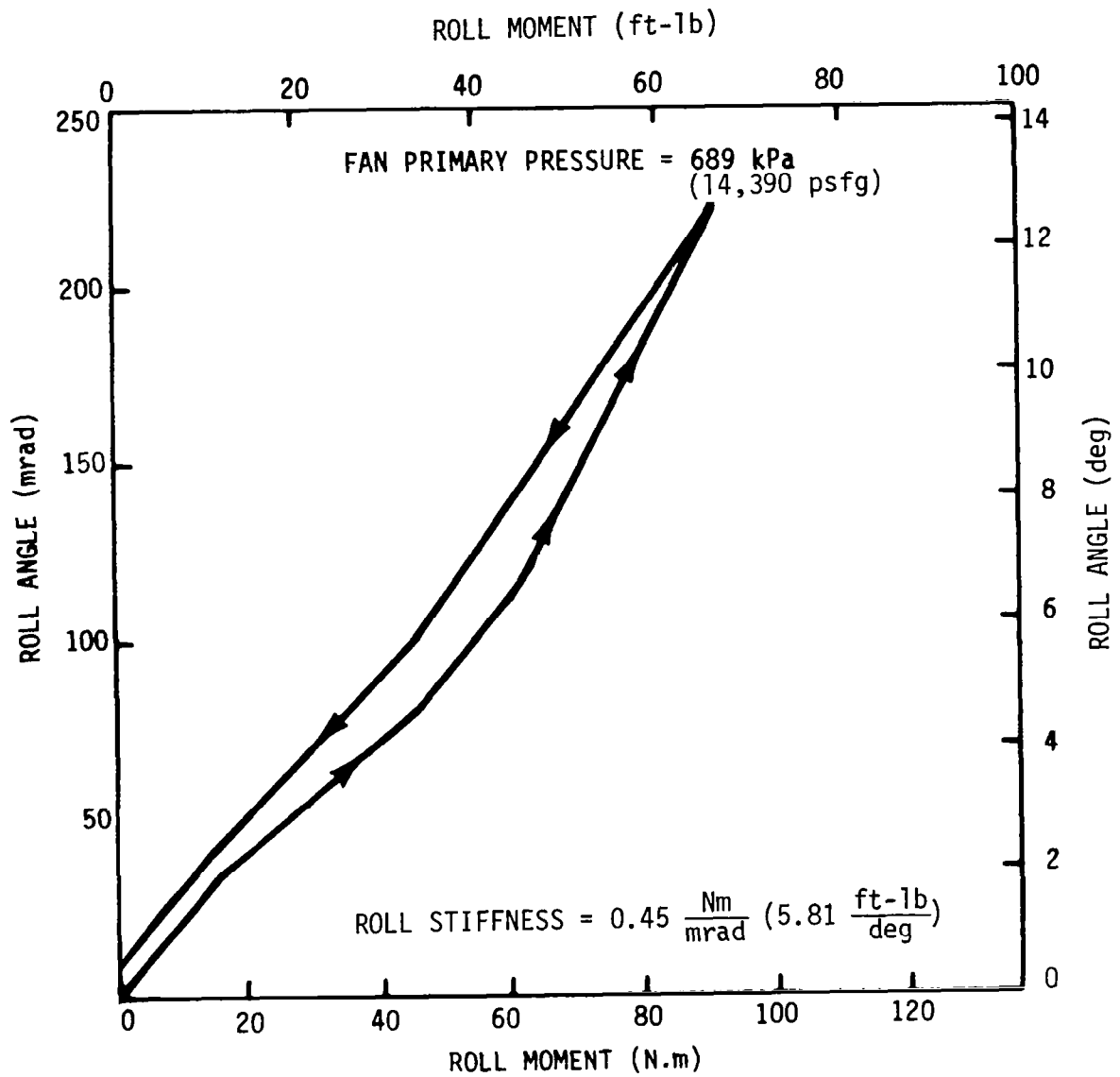


Figure 10. - Roll stiffness - damped trunk.

PRIMARY PRESSURE = 689 kPa

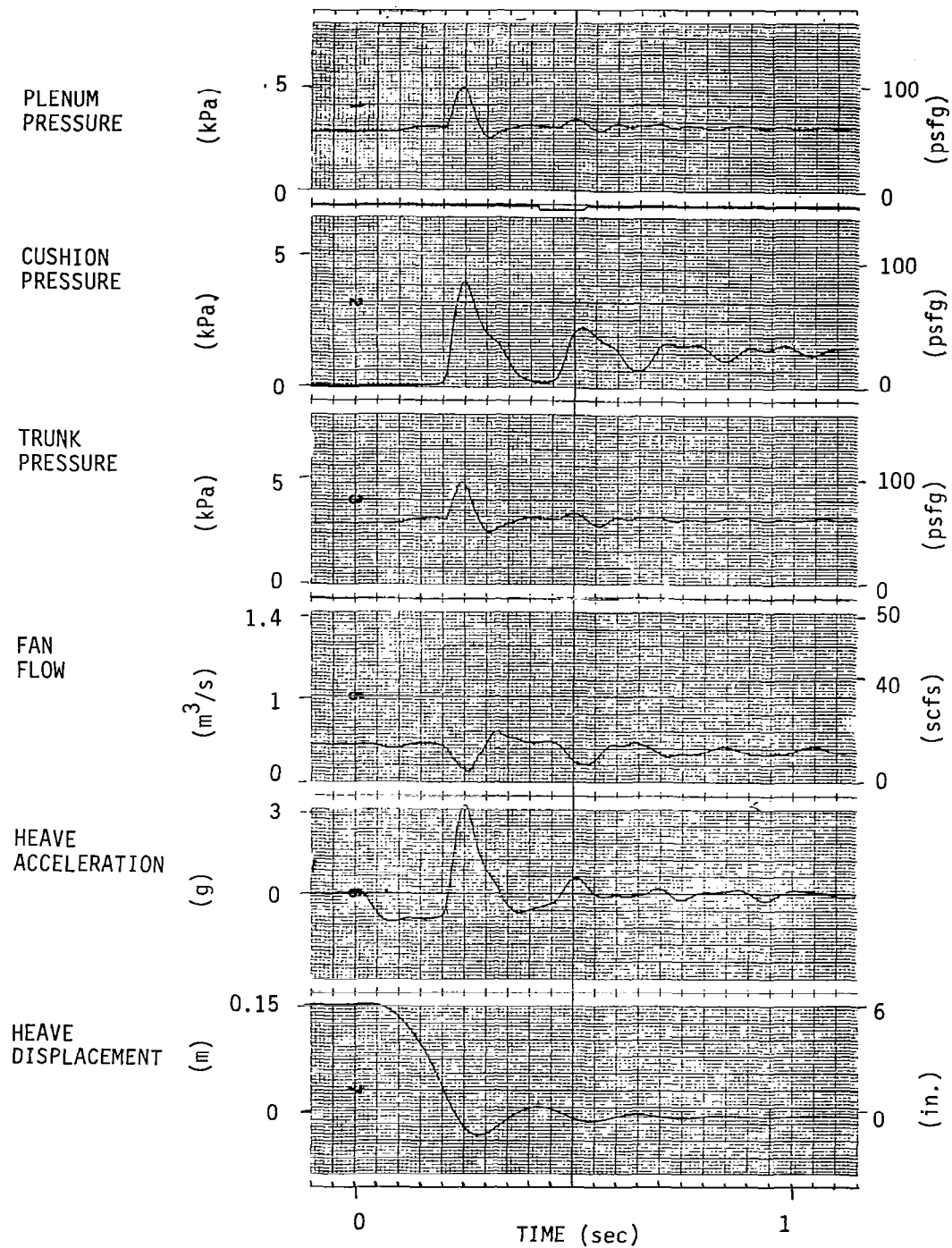


Figure 11. - Heave drop test - damped trunk.

Flutter observations. - Probably because of the higher material damping, no flutter was observed during any of the tests. This behavior differs significantly from the flutter behavior of the baseline Dacron-polyurethane trunk.

The Filled Trunk

The filled trunk concept represents a technique for increasing system damping by introducing a foam filler into the trunk. The configuration tested in this study consisted of the basic Kevlar-polyurethane trunk with high damping foam installed at several locations as shown in Figures 1(d) and 12. There are several advantages to this configuration, including:

1. The damping is provided directly by the foam filler between the hard surface and the bottom of the trunk.
2. The amount of damping can be easily changed by varying the amount and location of the foam.
3. The damping is independent of the trunk material characteristics.
4. By providing orifices in the foam partitions, the filled trunk concept can be easily modified to implement the compartmented trunk concept discussed later.

The foam chosen for this study was an open-cell polyurethane foam (T-38 Temper-Foam) manufactured by the Edmont-Wilson Company, Cashocon, OH.

Static tests. - Roll stiffness test data are shown in Figure 13.

Drop tests. - Typical heave drop test records are shown in Figure 14.

Flutter observations. - No flutter was observed during any of the tests.

The Compartmented Trunk

In the compartmented trunk concept, the trunk is divided into compartments by porous partitions. The trunk chambers thus formed can have different pressures under dynamic loading, and this pressure differential causes flow across the partitions and increases system damping. The configuration evaluated in this study was a modified version of the basic Kevlar-polyurethane trunk. Four foam partitions were attached to the inside of the trunk. Partition porosity was established by a single central orifice 38.1 mm (1.5 in.) in diameter in each partition. Air-flow from the tip turbine fan, via the plenum, was fed directly to the side compartments. The end compartments were fed from the side compartments through the partition orifices.

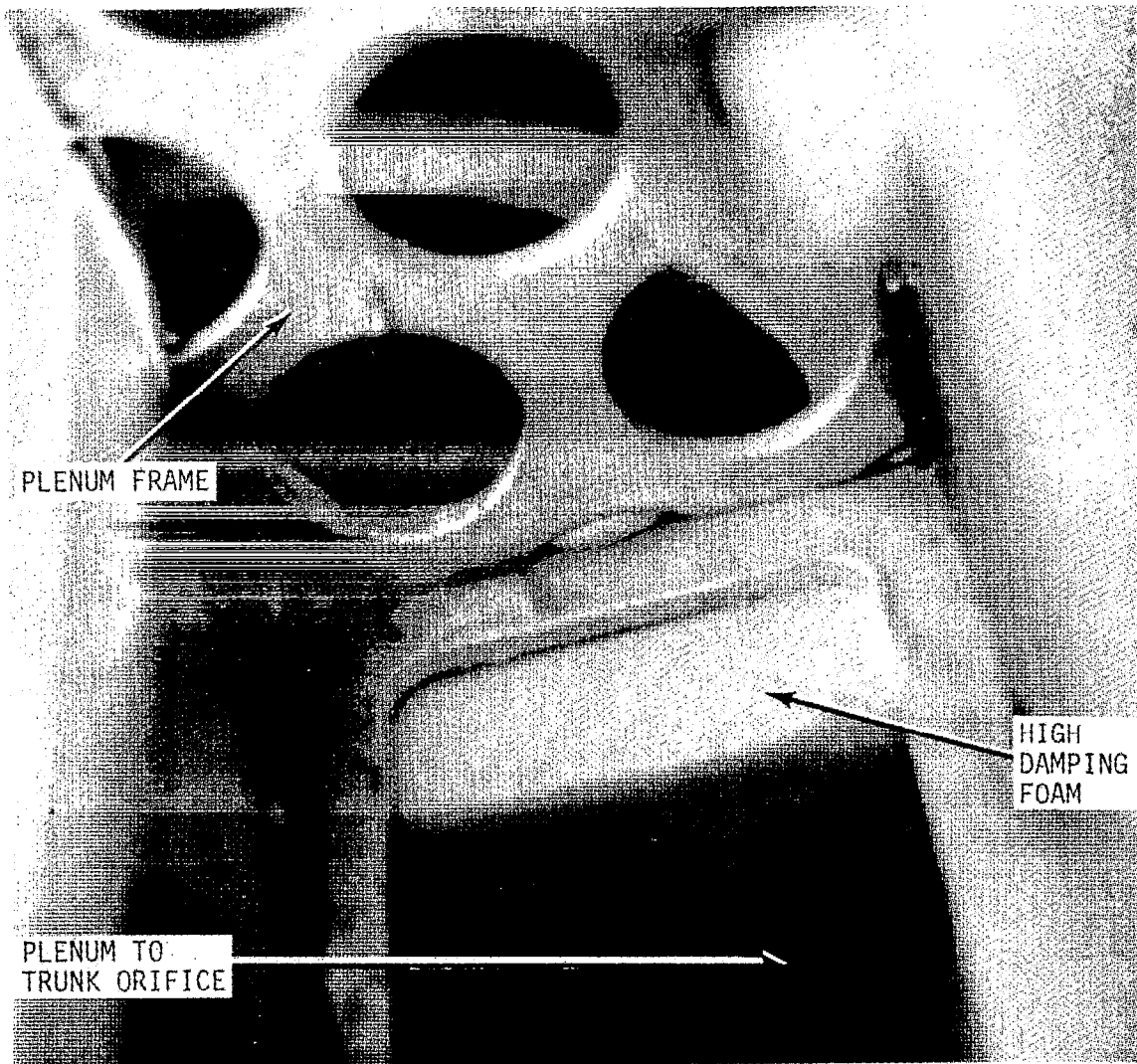


Figure 12. - Foam filler installation.

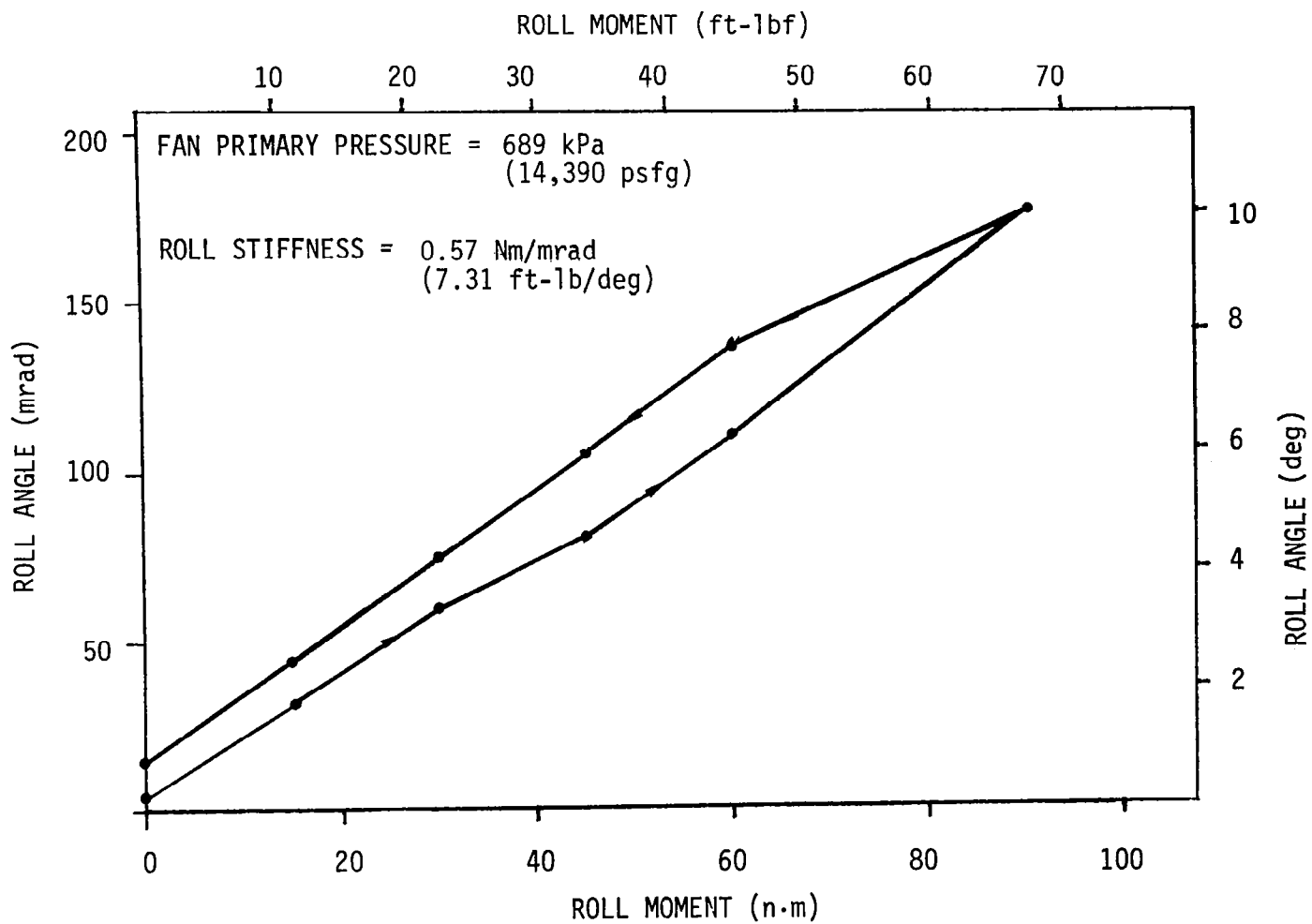


Figure 13. - Roll stiffness - filled trunk.

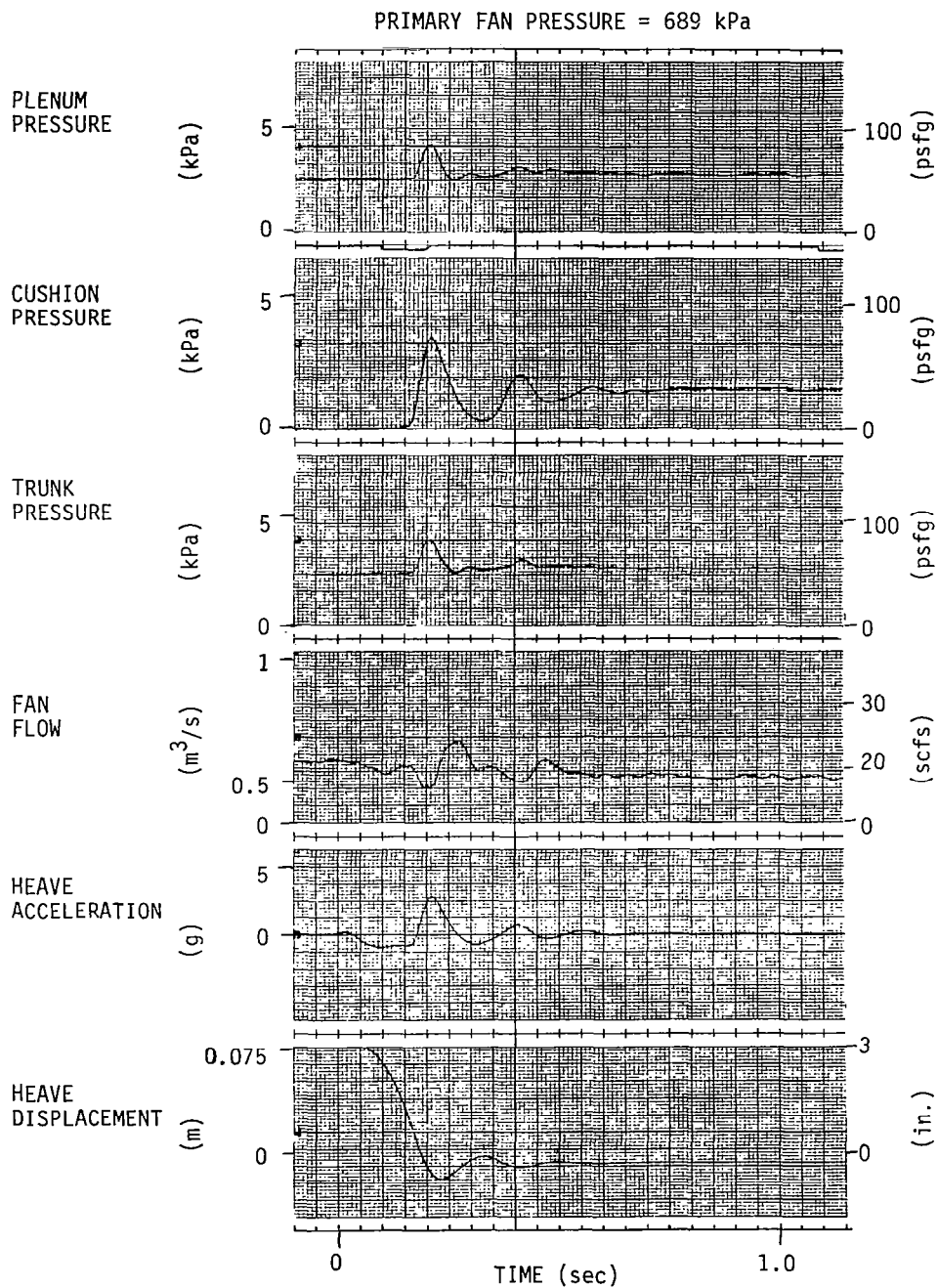


Figure 14. - Heave drop - filled trunk.

Static tests. - Roll stiffness test data are shown in Figure 15.

Drop tests. - Typical heave drop test records are shown in Figure 16.

Flutter observations. - No flutter was observed during any of the tests.

The Segmented Trunk

The segmented trunk concept incorporates independent trunk lobes individually fed by the air source. Since the trunk is fabricated in separate lobes, it is expected to be less expensive to fabricate than conventional trunks. Also, the side lobes can be operated at a higher pressure to increase roll stiffness. Finally, by providing flow controllers to the ducts leading to the lobes, a feedback control scheme can be realized which can modulate the individual trunk flows to provide optimum heave, pitch, and roll stiffness and damping.

In this study, the basic Kevlar-polyurethane trunk was modified by placing four impervious but flexible foam partitions in the trunk to form the four independent trunk lobes. The lobes were fed individually by orifices placed between the plenum and trunk segments. These orifices had twice the area of the trunk outflow orifices. All lobes were fed from the common tip turbine fan.

Static tests. - Initial operating experience showed that the static behavior paralleled that of the compartmented trunk tested earlier.

Drop tests. - Typical heave drop test records are shown in Figure 17.

Flutter observations. - No flutter was observed during any of the tests.

Roll Feedback Control

The concepts described earlier were primarily aimed at increasing system damping, either by increased trunk material damping or by additional fluid damping. The concept described below, however, is aimed at increasing the roll stiffness of the system by means of feedback.

Conceptually, this system consists of a roll sensor that redirects the flow to one side of the trunk to counteract any

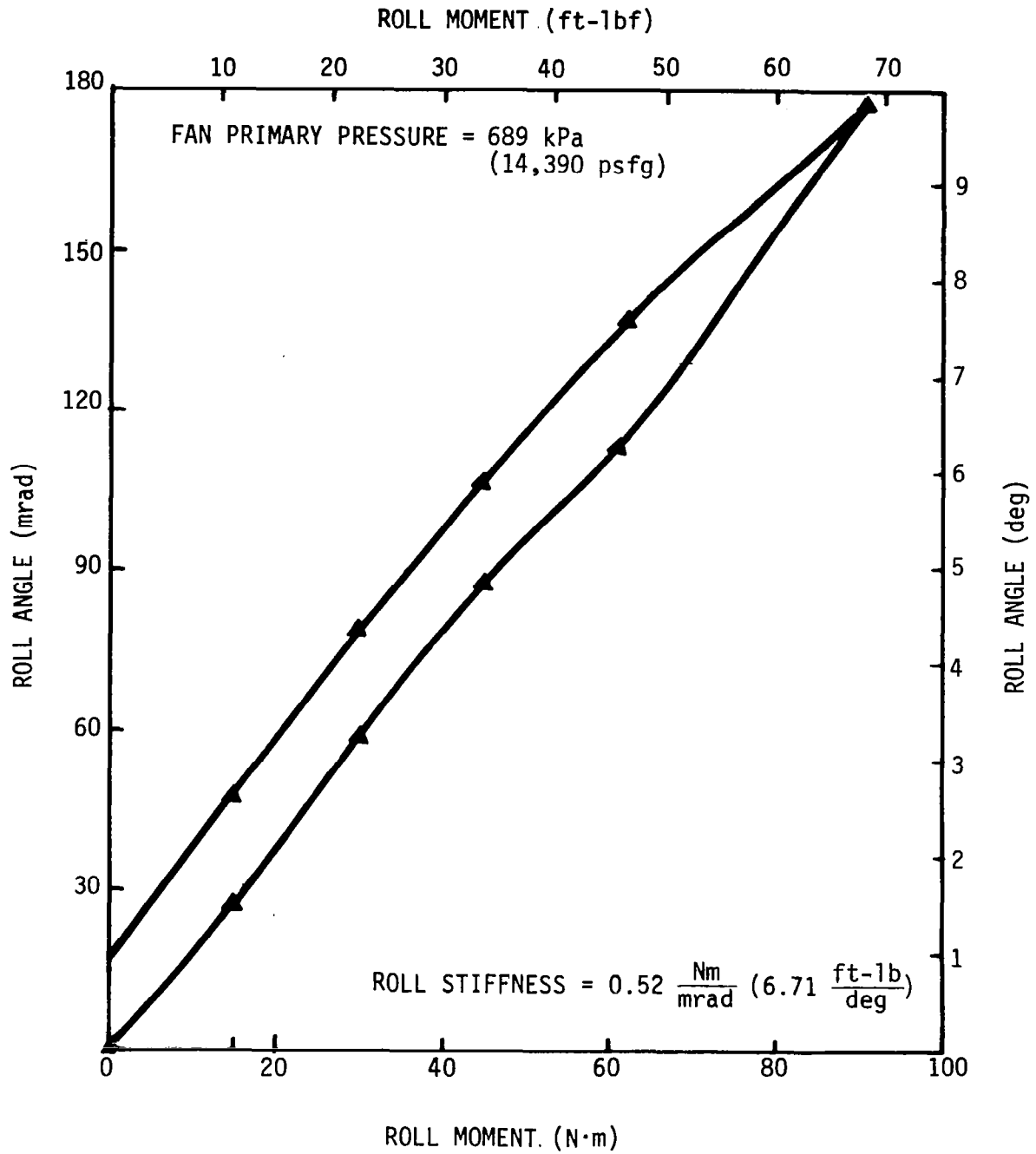


Figure 15. - Roll stiffness - compartmented trunk.

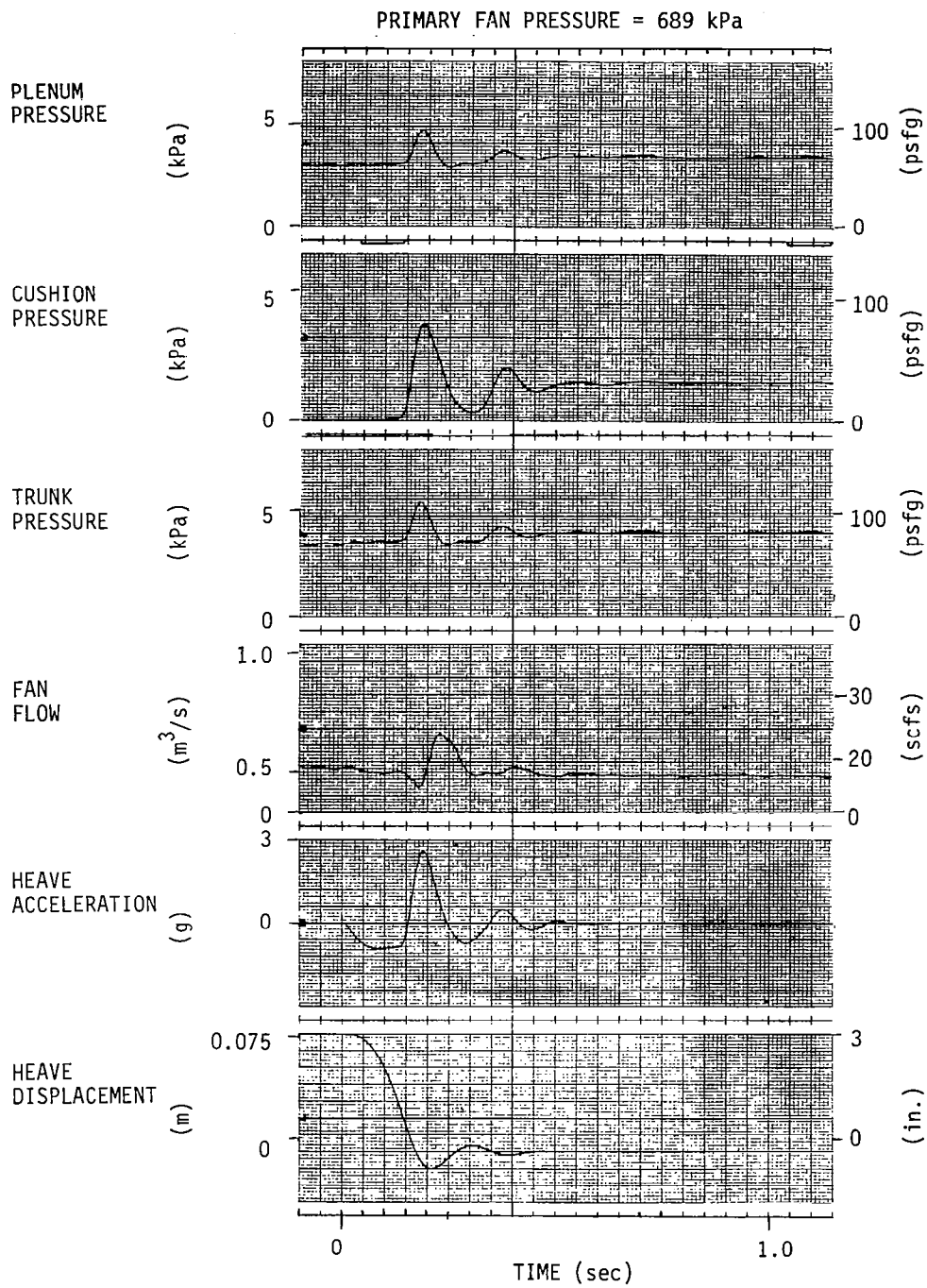


Figure 16. - Heave drop test - compartmented trunk.

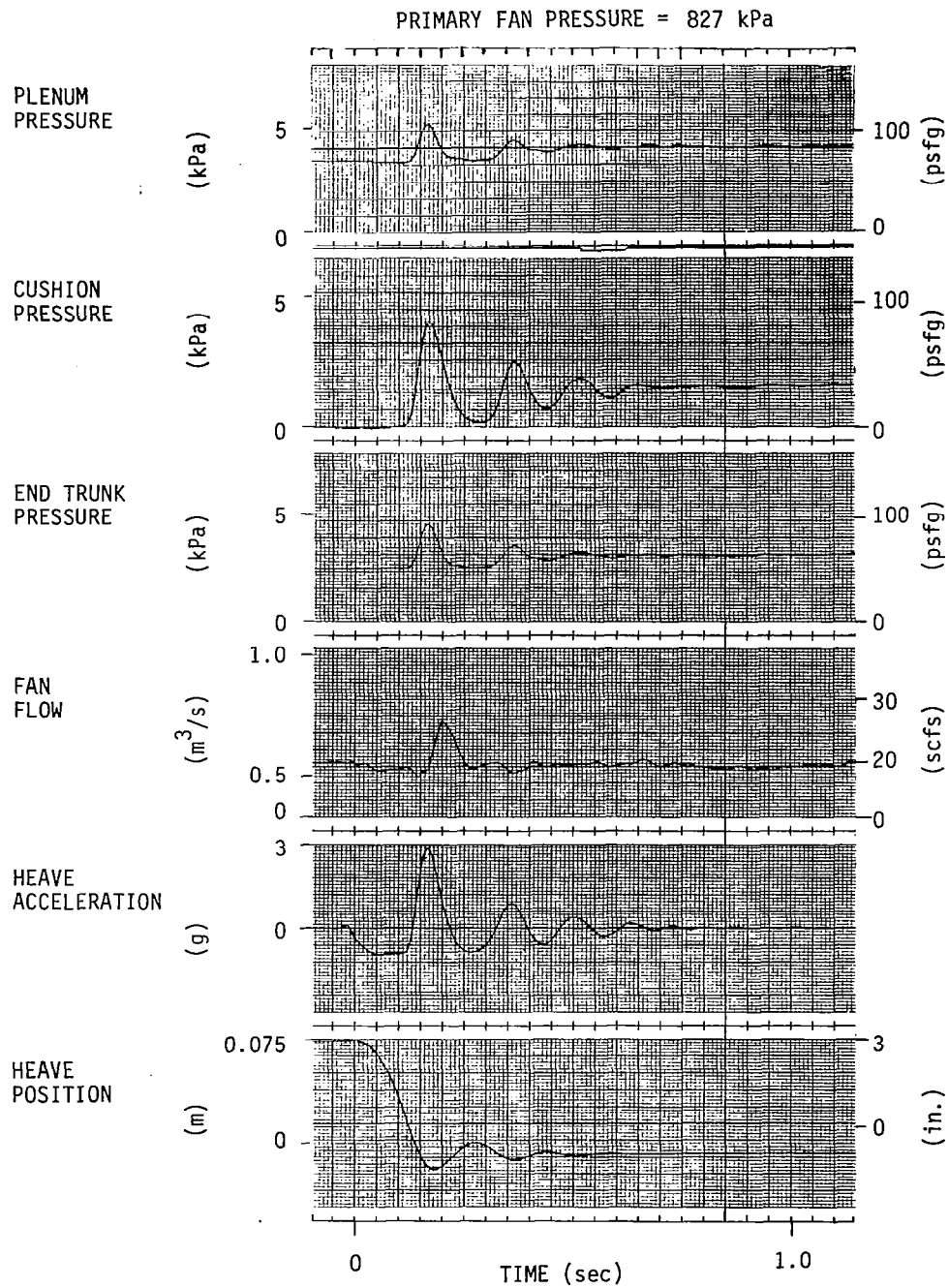


Figure 17. - Heave drop test - segmented trunk.

roll moment. A typical arrangement of the system used with a compartmented trunk is shown in Figure 18. When the system is level, without any roll angle, the roll sensor causes the switching valve to remain in a neutral position, and thereby supply each side trunk segment with the same amount of airflow. However, when the system tilts in roll, the roll sensor causes the switching valve to direct more air to the side that is lower to the ground, thus counteracting the tilt and increasing the roll stiffness. In practice, several refinements would be incorporated into the system, such as a roll threshold setpoint to be exceeded before flow switching can occur and a dynamic compensation system to modulate the switching valve in an optimal manner.

In this study the effectiveness of the concept was evaluated by closing the loop manually — that is, the roll angle sensor output signal was observed during the static roll tests and the switching valve activated by hand to redirect the flow. Curve A (Figure 19) shows the roll stiffness characteristic of the compartmented trunk without roll feedback. Curve B shows the increase in roll stiffness obtained by manual redirection of the flow with a "bang-bang" control strategy.

As mentioned earlier, an optimal scheme for the roll control system will include a threshold setpoint to suppress continual oscillations about the null position, and a compensation system to reduce the high transient loading that is associated with bang-bang control. The roll stiffness characteristic after the inclusion of such refinements is shown qualitatively in Curve C. With such a scheme, the cushion behaves just like the basic compartmented trunk cushion (that is, without roll feedback) for small roll disturbances. As the roll disturbances become more severe, however, the system behavior switches gradually to that obtained with bang-bang roll control. Although the actual roll stiffness of such a scheme will depend on the threshold and compensation system details, the initial test data shown in Figure 19 indicate that a doubling of the roll stiffness appears reasonable.

Drop tests. - Since the roll control system does not affect the heave dynamics of the ACLS, its heave performance will be the same as that obtained with the compartmented trunk described earlier.

Flutter observations. - No flutter was observed during any of the tests.

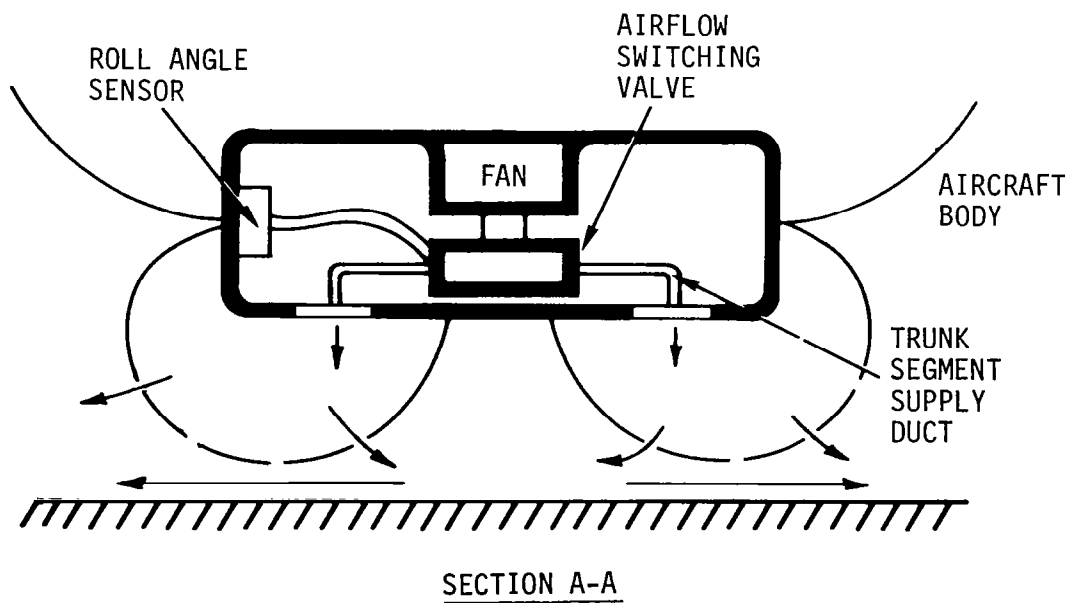
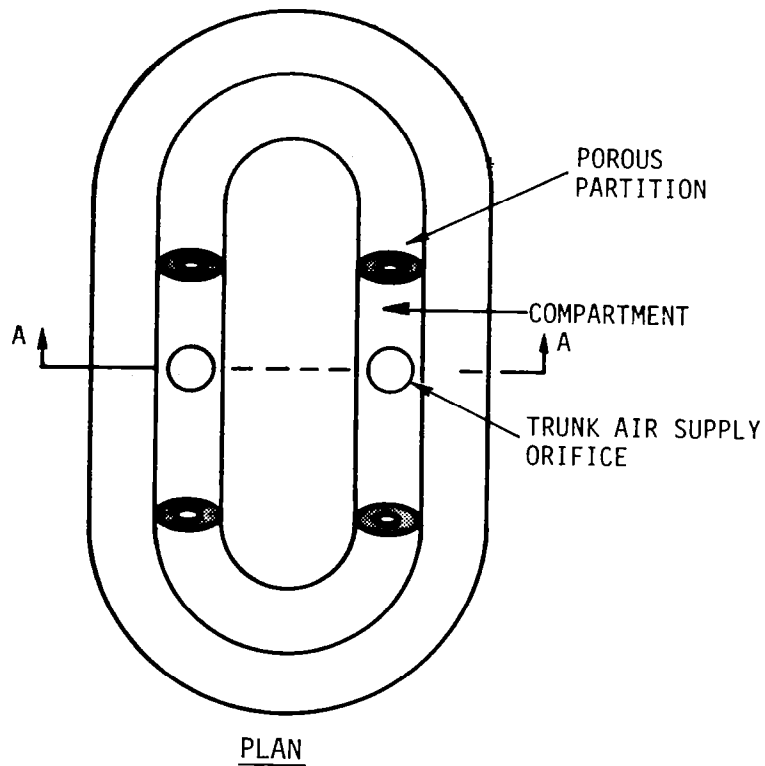


Figure 18. - Conceptual representation of roll feedback control.

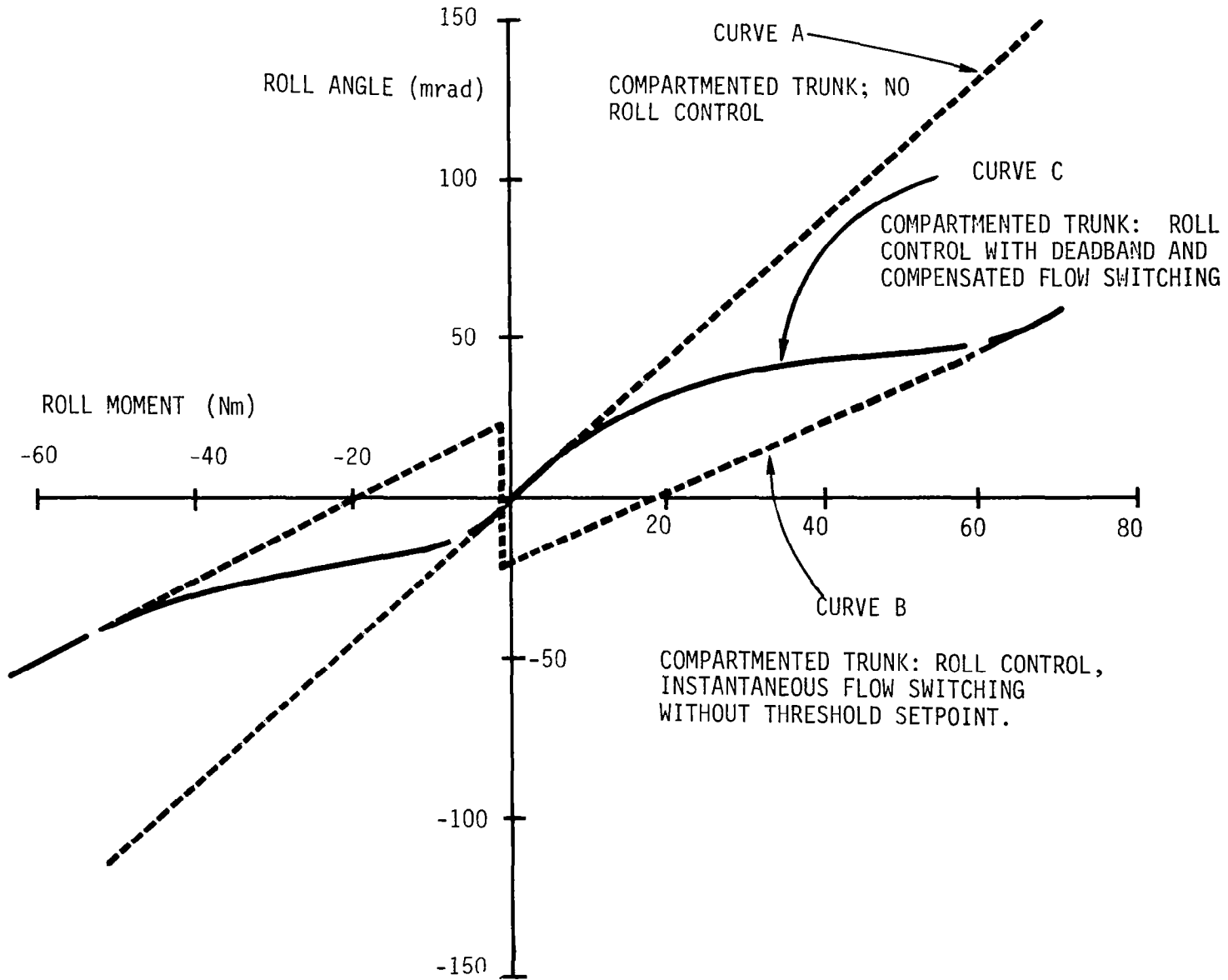


Figure 19. - Roll stiffness characteristics.

CONCEPT COMPARISON

The concepts evaluated earlier were compared on the basis of trunk characteristics, static heave and roll stiffness, heave damping, and flutter. A qualitative assessment of fabrication complexity was also made.

Trunk shape. - Figure 20 shows the trunk height as a function of the pressure for the two types of trunk tested. The X-axis of the curve is the ratio of the cushion pressure P_c to the trunk pressure P_t . The Y-axis is the ratio of the trunk height H_y at a given cushion pressure to the trunk height H_{yi} at zero cushion pressure.

As the cushion pressure increases, the trunk lobes bow outwards, thus reducing the trunk height. For a given pressure ratio, the Kevlar trunk shows a smaller height reduction than the Dacron trunk. This is to be expected, since the Kevlar trunk is made of thicker and stiffer material than the Dacron trunk.

Heave stiffness. - The hard surface clearance as a function of the heave load is shown in Figure 21. The inverse slope of the curve represents the heave stiffness of the system. The results confirm that the Kevlar trunk is stiffer than the Dacron trunk. Since the two trunks are geometrically similar, this increase in stiffness is due to the increased bending stiffness of the Kevlar material used to make the trunk.

Roll stiffness. - The roll stiffness of the various ACLS concepts is compared in Figure 22(a). The results show that the new trunk configurations exhibit a modest increase in roll stiffness over the baseline system. This is probably due to the increased material stiffness of the Kelvar trunk used to implement the concepts. A more substantial increase in roll stiffness is achieved with the roll feedback control scheme. With this approach, the redistribution of air supplied to the trunk causes a significant change in footprint pressure distribution and results in an increase in the roll stiffness by a factor of four.

Damping ratio. - The heave damping ratio for all the cases is shown in Figure 22(b). In general, the new systems have about twice as much damping as the baseline case, this increase occurring due to the increased material damping of the trunk, along with additional fluid damping from other sources.

Flutter. - The flutter observations confirm that the Kevlar trunk does not exhibit any flutter behavior. This behavior is

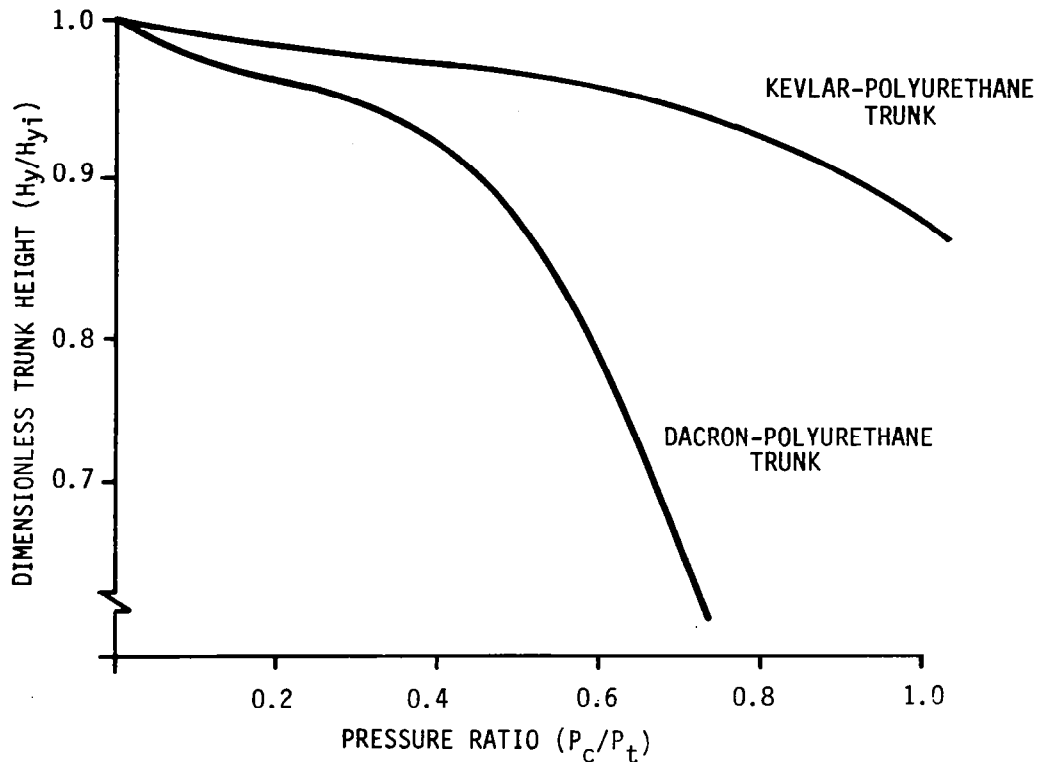


Figure 20. - Trunk height comparison.

in contrast to the baseline trunk, which was observed to flutter significantly when loaded. The flutter-free operation of the Kevlar trunk is probably due to the superior damping properties of the trunk material.

Fabrication ease. - Ease of fabrication is an important characteristic for an ACLS trunk. Previous experience has shown that sophisticated trunk designs have been difficult (and expensive) to fabricate and maintain.

The new trunk configurations appear to be easier to fabricate than existing designs. They are made by laying up the Kevlar fabric on molds and then spraying the assembly with polyurethane to the desired thickness. The required porosity of the trunk is obtained by taping up appropriate regions of the trunk prior to spraying, to avoid sealing the natural porosity of the fabric. This method of providing trunk porosity is superior to the earlier technique of punched orifices because the tendency for stress cracking around the punched holes is eliminated.

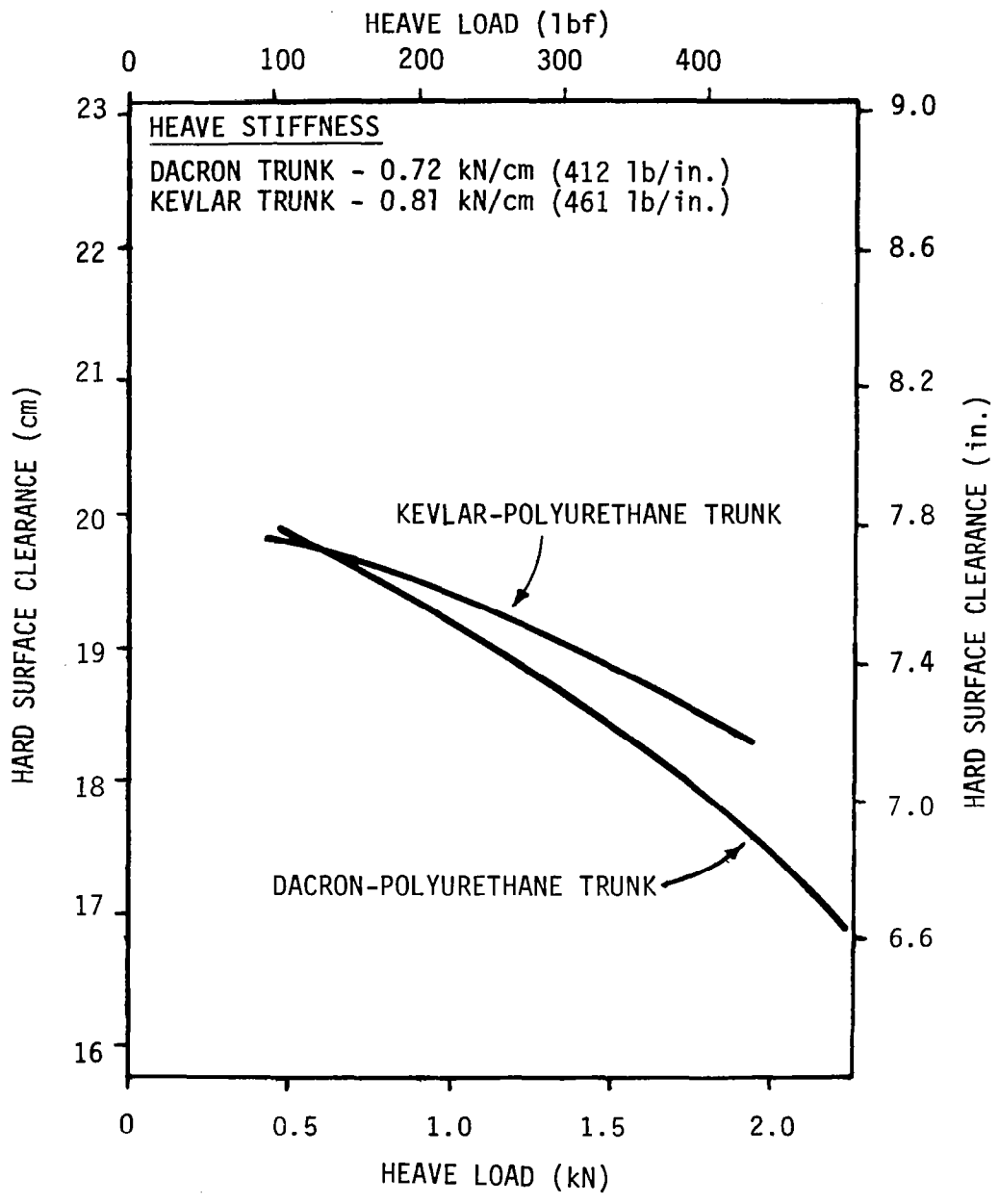


Figure 21. - Heave stiffness comparison.

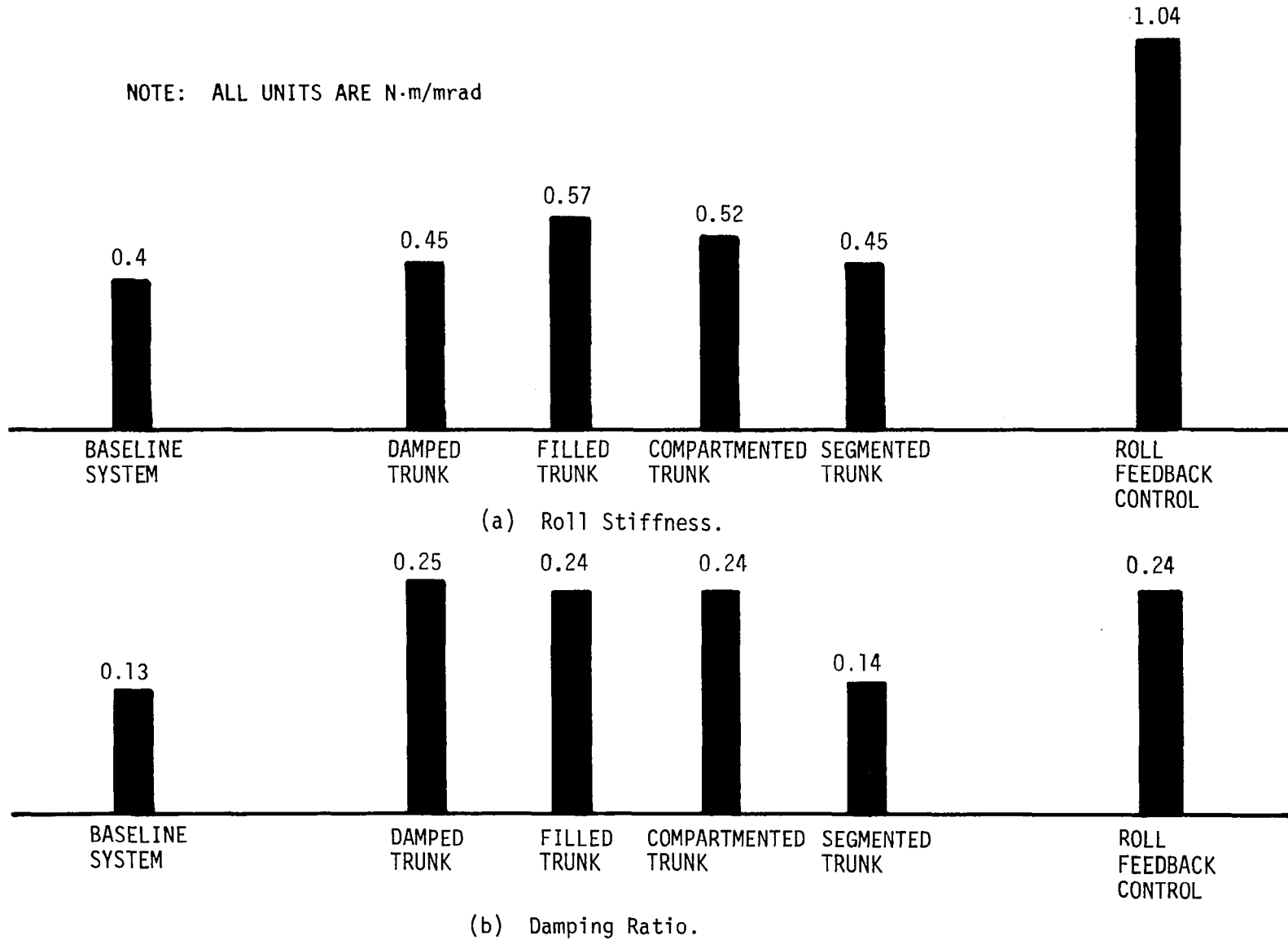


Figure 22. - Damping ratio and roll stiffness comparison.

Of the trunk configurations studied, the segmented trunk concept was found to be the easiest to fabricate. This trunk is made up of four straight segments and assembled like a picture frame. With this approach, each segment can be fabricated relatively easily, since there is no compound curvature in the segment shape. In addition, during development and testing, the overall size and aspect ratio of the cushion can be conveniently altered by replacing the side or end segments of the trunk. This ability to replace segments independently also improves the maintenance aspects of the system. For these reasons, it was decided that the segmented trunk configuration should be chosen for the NASA ACLS test vehicle. The design and fabrication of this trunk and its installation on the test vehicle are described in the section entitled "Full-Scale Design of an Advanced ACLS Concept."

COMPUTER SIMULATION

The existing computer program, developed through an earlier contract (ref. 1), was updated to allow simulation of the leading concepts described in the previous section. This task was carried out to keep the basic simulation program current with the latest developments so that it remains available for the analytical evaluation of optimal designs. The validity of this program was checked by comparing the simulation results with heave drop test data. The comparison for heave displacement and cushion pressure for the baseline system and four of the new concepts is shown in Figures 23 to 27. A full set of results, including the comparisons for other variables of interest, is included in Appendix B.

Although the complete time history of vibration provides very useful data on ACLS operation, the real value of the model as a design tool lies in its ability to determine the peak levels of the critical system parameters during touchdown and slideout. For instance, the maximum trunk pressure and dynamic trunk deflection form direct inputs to the layout and structural design of the trunk. Similarly, the impact value of heave acceleration and damping ratio provide a very good initial indication of the smoothness and stability of the landing. It is therefore appropriate to evaluate the model based on its ability to predict the peak parameters of interest. A comparison of the key peak (and steady-state) parameters has been carried out using the data shown in Appendix B. The results of this comparison are summarized in Table 2.

The figures shown in the tables are average values for all the concepts evaluated. The static model values represent the differences between theory and experiment for the steady-state condition. The dynamic model values (except damping ratio and frequency) represent the corresponding peak levels that occur during heave impact. As the table shows, the simulation can predict the static characteristics of the ACLS within a 10 percent margin of error. For the dynamic model, however, this margin ranges from 10 to 40 percent. Although the computer model could be further refined should a particular application warrant it, it will serve as a valuable design and evaluation tool for use in developing improved ACLS designs, even as it stands.

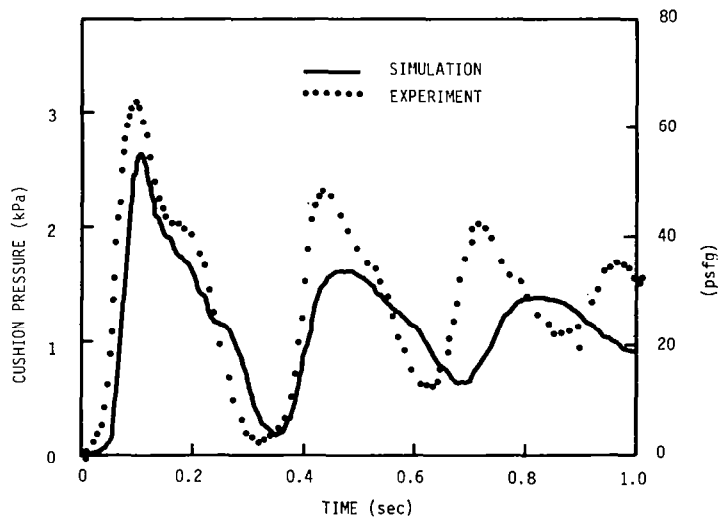
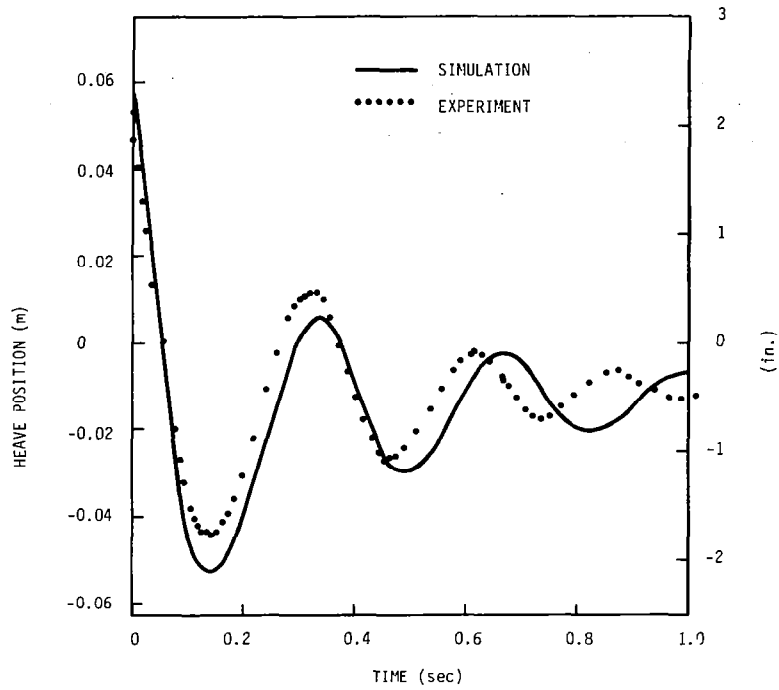


Figure 23. - Comparison between simulation and experiment - baseline system.

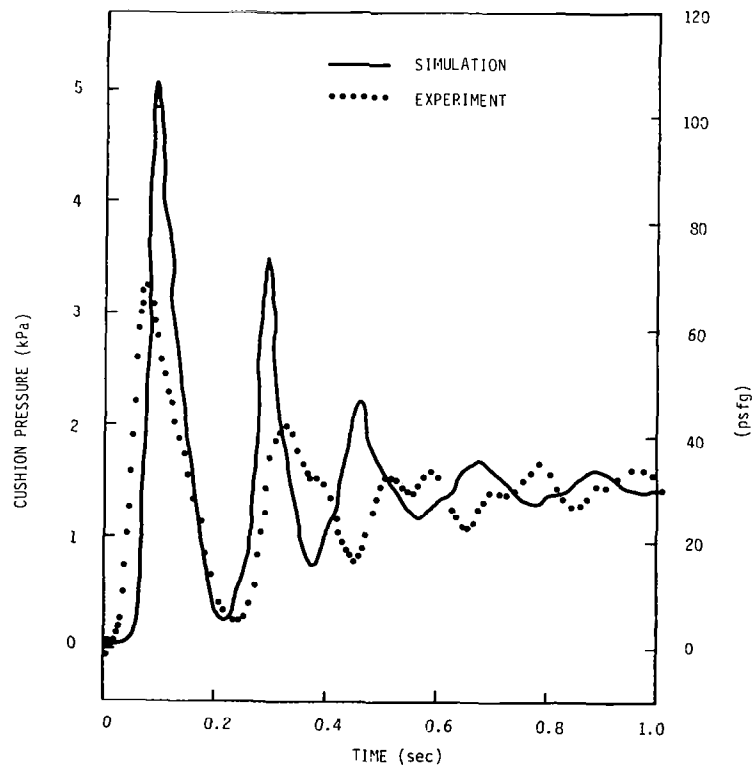
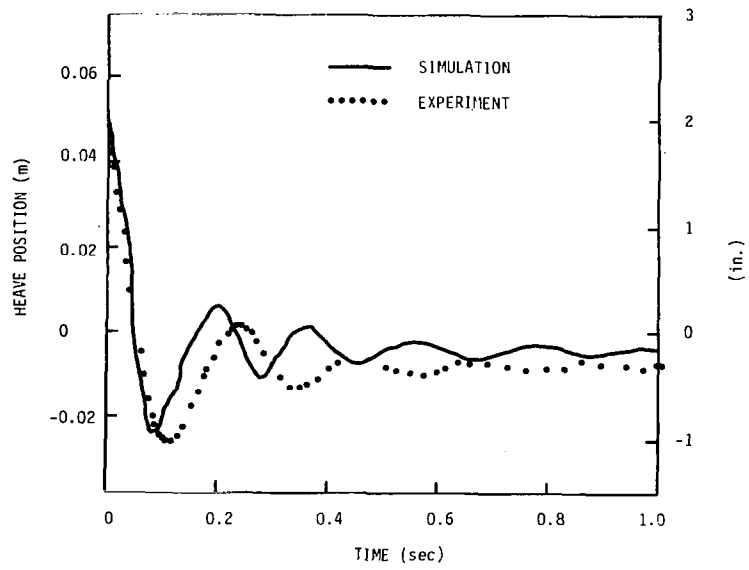


Figure 24. - Comparison between simulation and experiment - damped trunk.

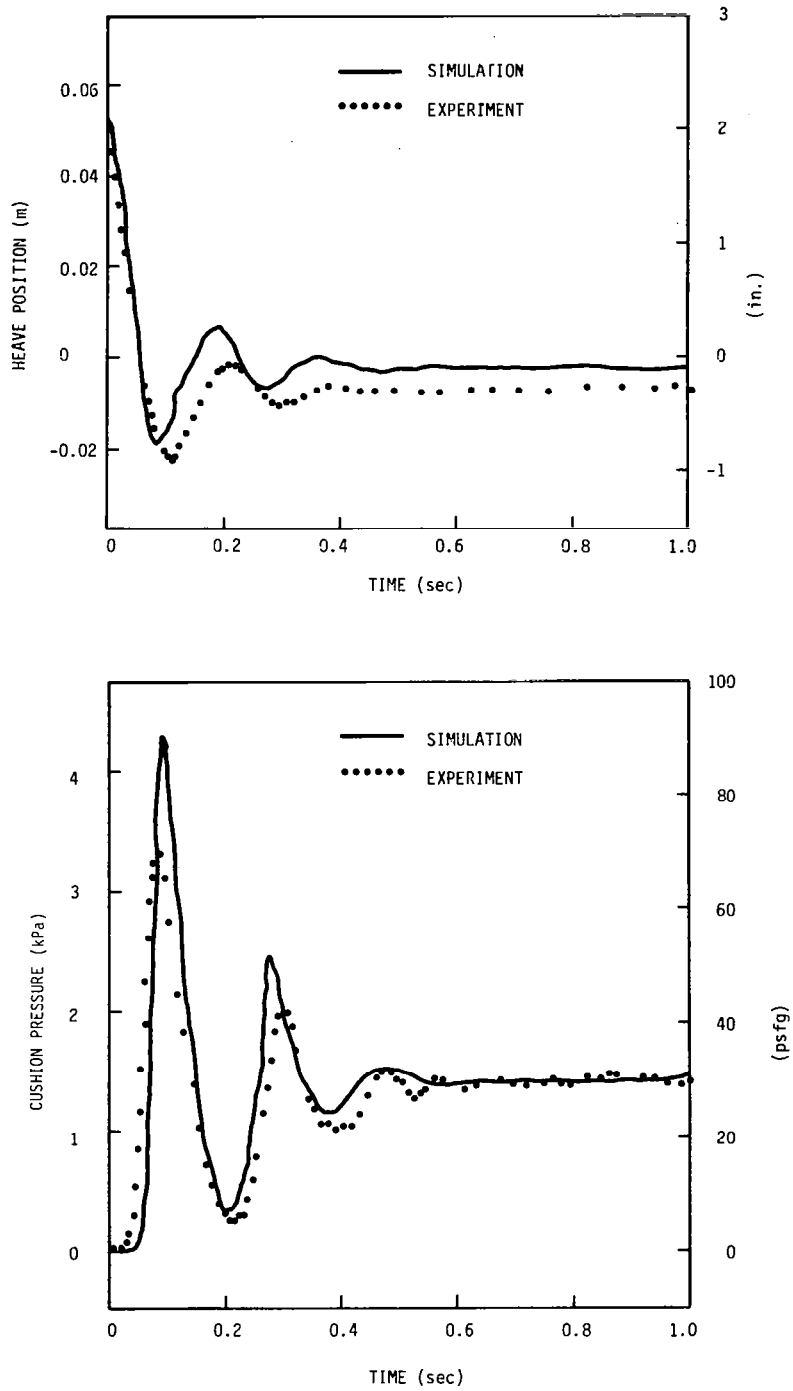


Figure 25. - Comparison between simulation and experiment - filled trunk.

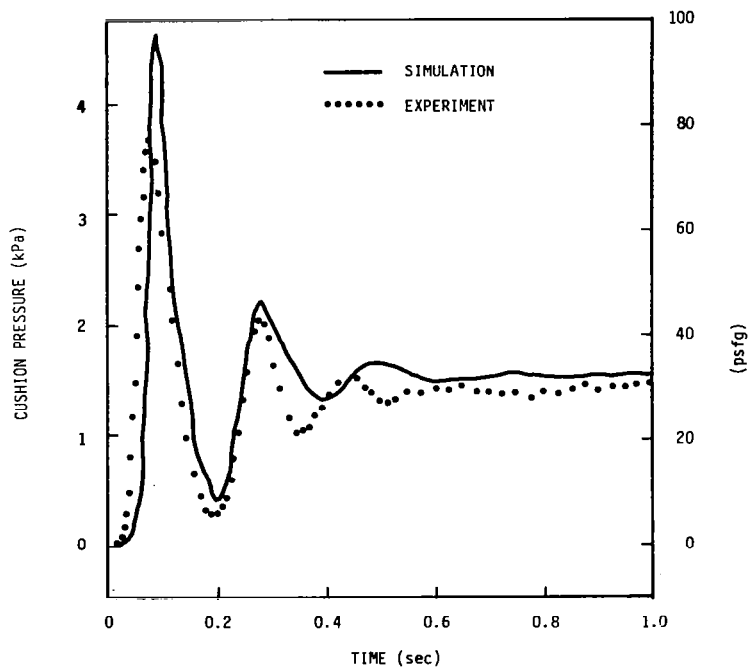
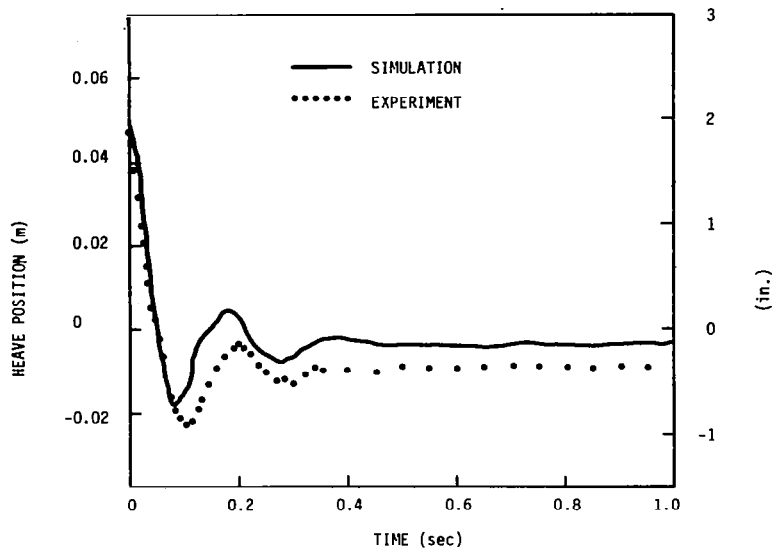


Figure 26. - Comparison between simulation and experiment - compartmented trunk.

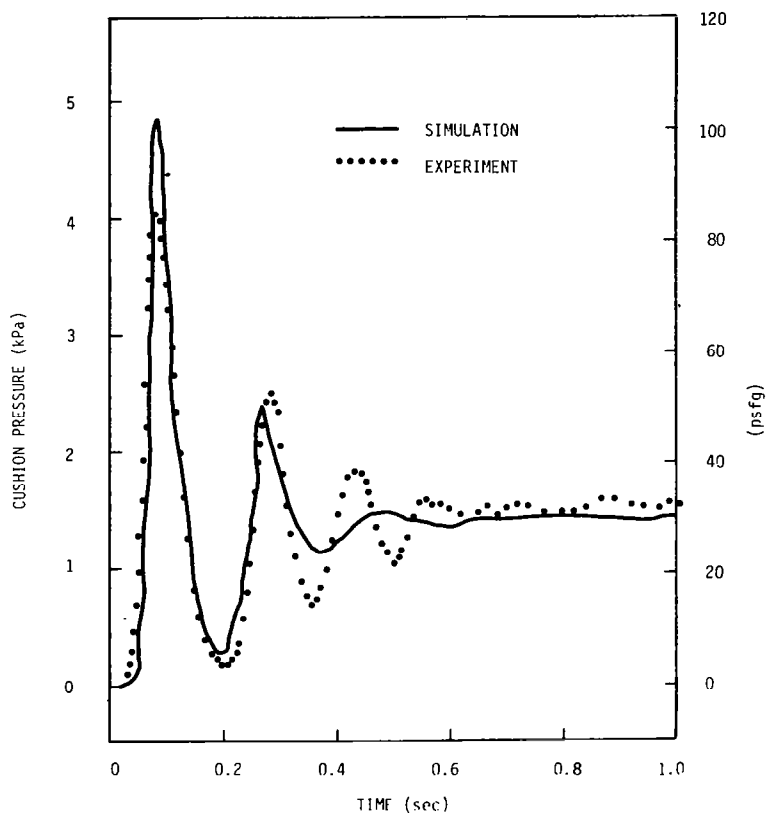
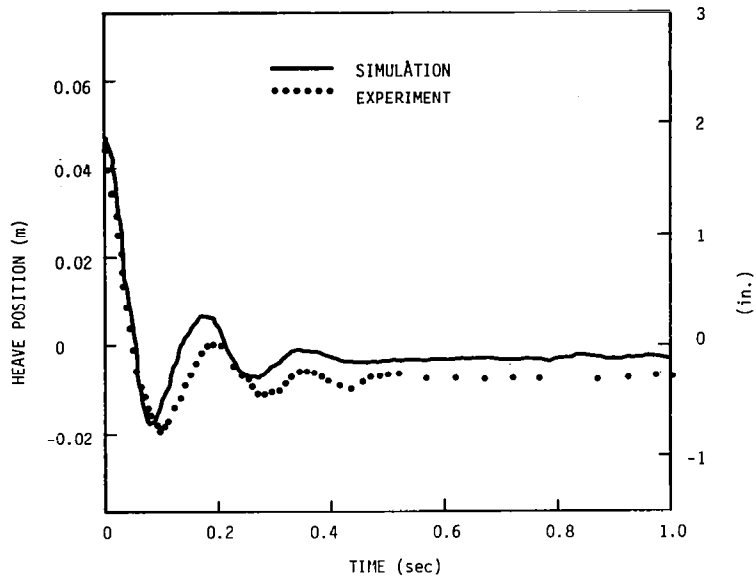


Figure 27. - Comparison between simulation and experiment - segmented trunk.

TABLE 2. - SIMULATION MODEL VERIFICATION SUMMARY

Parameter	Rms Prediction Error Margin	
	Static model	Dynamic model
Clearance	2%	3%
Clearance reduction	n/a	25%
Trunk pressure	9%	7%
Cushion pressure	6%	23%
Heave acceleration	n/a	42%
Damping ratio	n/a	18%
Heave frequency	n/a	9%



FULL-SCALE DESIGN OF AN ADVANCED ACLS CONCEPT

In order to investigate the segmented trunk concept further and to provide NASA with a test ACLS which could be used to investigate various braking and steering concepts, FMA designed and fabricated a trunk for the ACLS test vehicle at NASA. The details of the trunk are described in the following subsections.

Design Features

The design developed for the test vehicle trunk incorporates several new features:

1. The trunk consists of four independent lobes as shown in Figure 28.

2. The end segments are straight (unlike the curved ends employed in present designs).

3. The trunk lobes are fed from a plenum through several ducts incorporating independently controlled valves.

4. The basic trunk material is Kevlar coated with polyurethane.

5. The trunk orifices are not punched in the fabric, but are obtained by selective coating in such a way that the space between the fabric weave in the orifice region is not completely blocked.

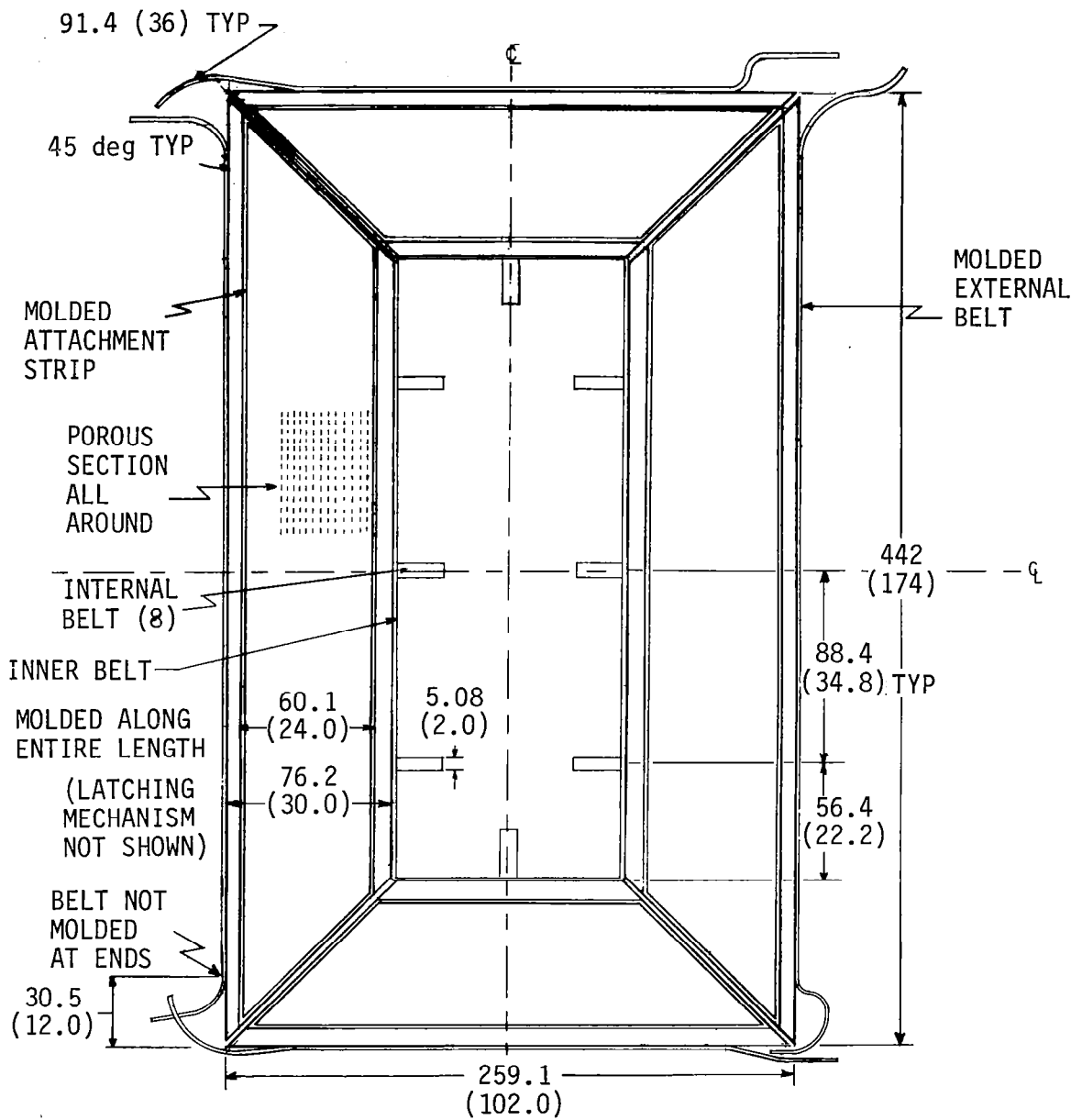
The advantages of these design features are:

1. The independent lobe design makes the trunk relatively inexpensive and easy to fabricate. The lobes can be made out of similar molds and the width or the length of the trunk can be changed simply by replacing the end or side lobes as required.

2. The use of independent lobes also simplifies the task of replacing any damaged or worn out trunk sections.

3. Because the lobes are fed independently, the pressures in the side lobes can be increased if necessary to increase roll stiffness.

4. The configuration lends itself to active control. For a future active control scheme, the valves controlling the flow to the lobes can be modulated actively to optimize heave, pitch, and roll damping.



NOTE: DIMENSIONS IN CENTIMETERS (INCH)

Figure 28. - NASA test vehicle trunk design - top view.

5. The bottom of the trunk is stronger than that of conventional designs because of the absence of punched orifice holes which reduce trunk strength.

Design Details

The trunk dimensions and pressures are chosen so that the ACLS can operate with the available fan. The fan presently available at NASA is a Model 875 centrifugal air-driven, hub-turbine fan made by the Technology Development Corporation, Dayton, OH, the characteristics of which are shown in Figure 29.

The trunk pressure is selected to be 9.57 kPa (200 psfg) and the cross-sectional dimensions are selected as shown in Figure 30. These numbers are for design and are not necessarily those achieved. With this choice, the trunk can support the entire test vehicle weight, 2500 kg (5500 lb), even if the cushion air is vented out due to a break in the lobe joint or while negotiating a large ditch. In normal operation, however, the cushion pressure will not be zero. An initial analysis for operation over a smooth surface indicates that the cushion pressure will be maintained at about 2.4 kPa (50 psfg).

The design trunk-ground contact width, assuming that the trunk takes the entire load, is 0.23m (0.764 ft) and the total air flow corresponding to a trunk pressure of 9.57 kPa (200 psfg) is 3.68 kg/s (8.11 lbm/sec, 107 ft³/sec). Assuming that the trunk has orifices over double the contact area (see Figure 30), the required porosity works out to be 0.00757*. This is lower than the porosity of 0.023 for the XC-8A ACLS and 0.028 for the prototype trunk used in the tests described earlier. If a more powerful fan is available, the porosity can be increased while keeping the same trunk pressure. For this reason, the trunk has been fabricated with provisions for incorporating higher porosity in the future. When used with the present hub-turbine fan, some portions of the porous area are covered up so that the porosity is set at 0.00757.

The attachment details for the trunk are shown in Figure 31. The trunk is attached to the inside of the aluminum frame member. With this configuration, the trunk pressure actually strengthens the seal. Several metal strips are also molded in the trunk to provide structural strength at the attachment holes, the location of which is shown in Figure 32.

*Porosity is defined as the orifice area divided by the total trunk area in the orifice zone.

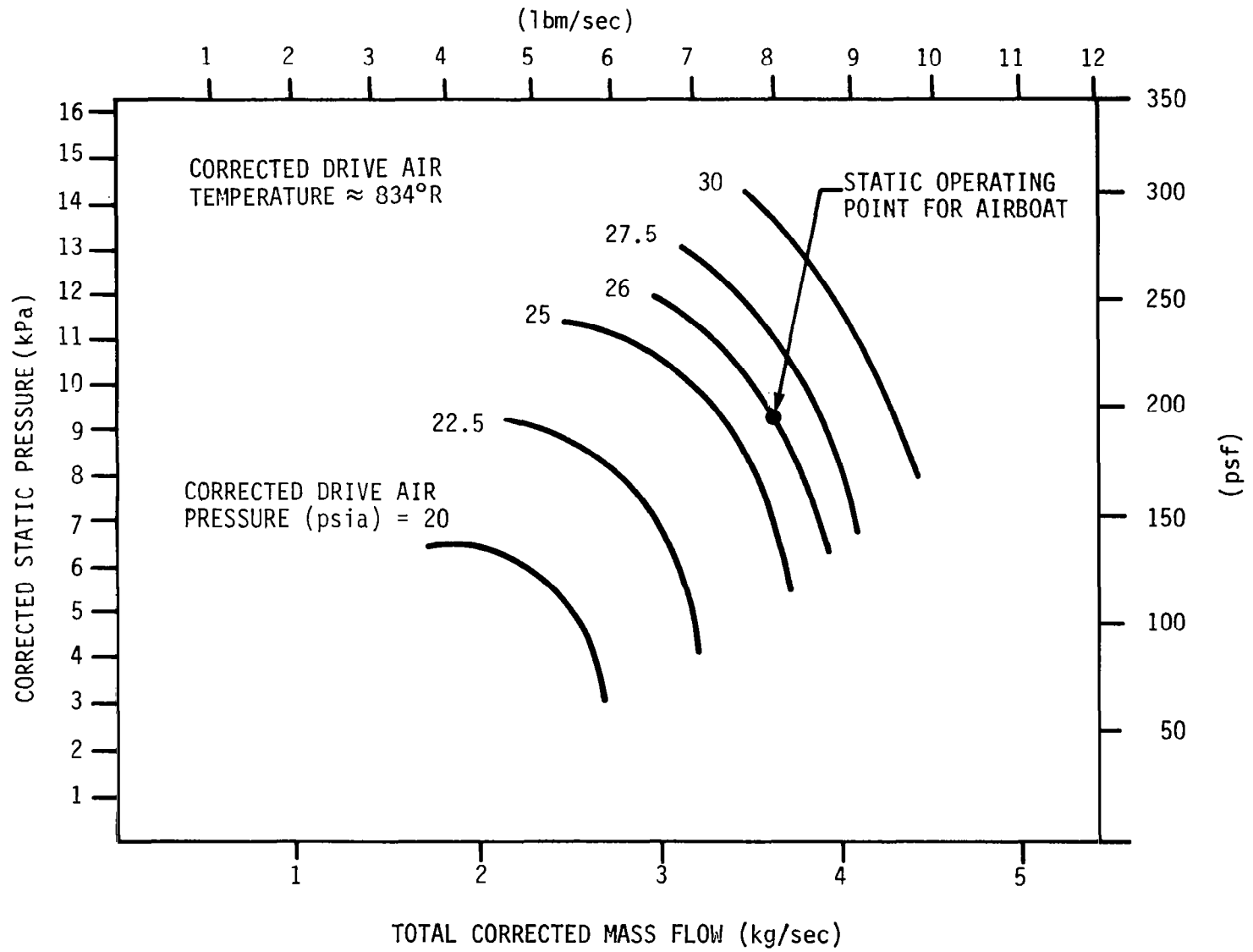
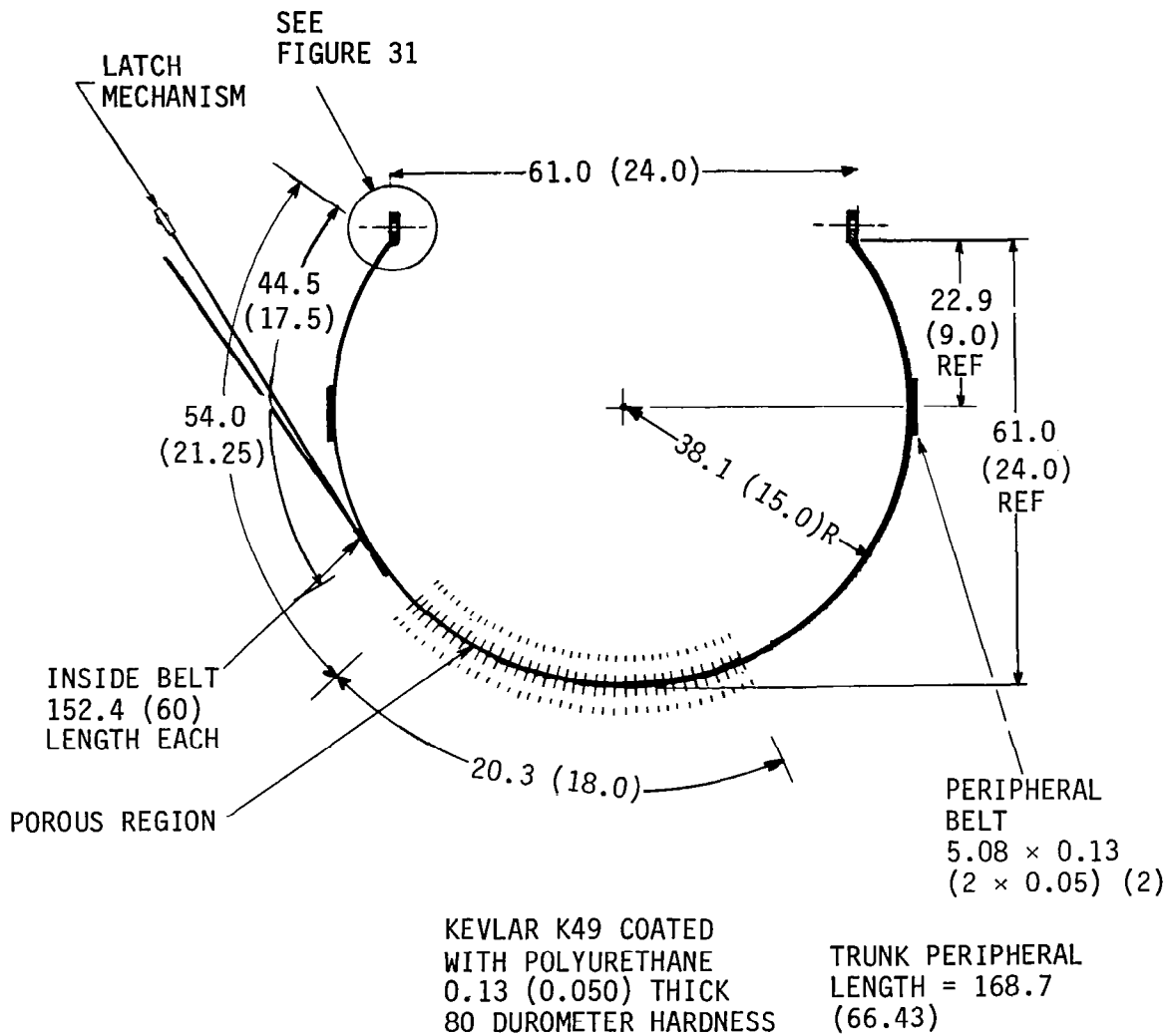
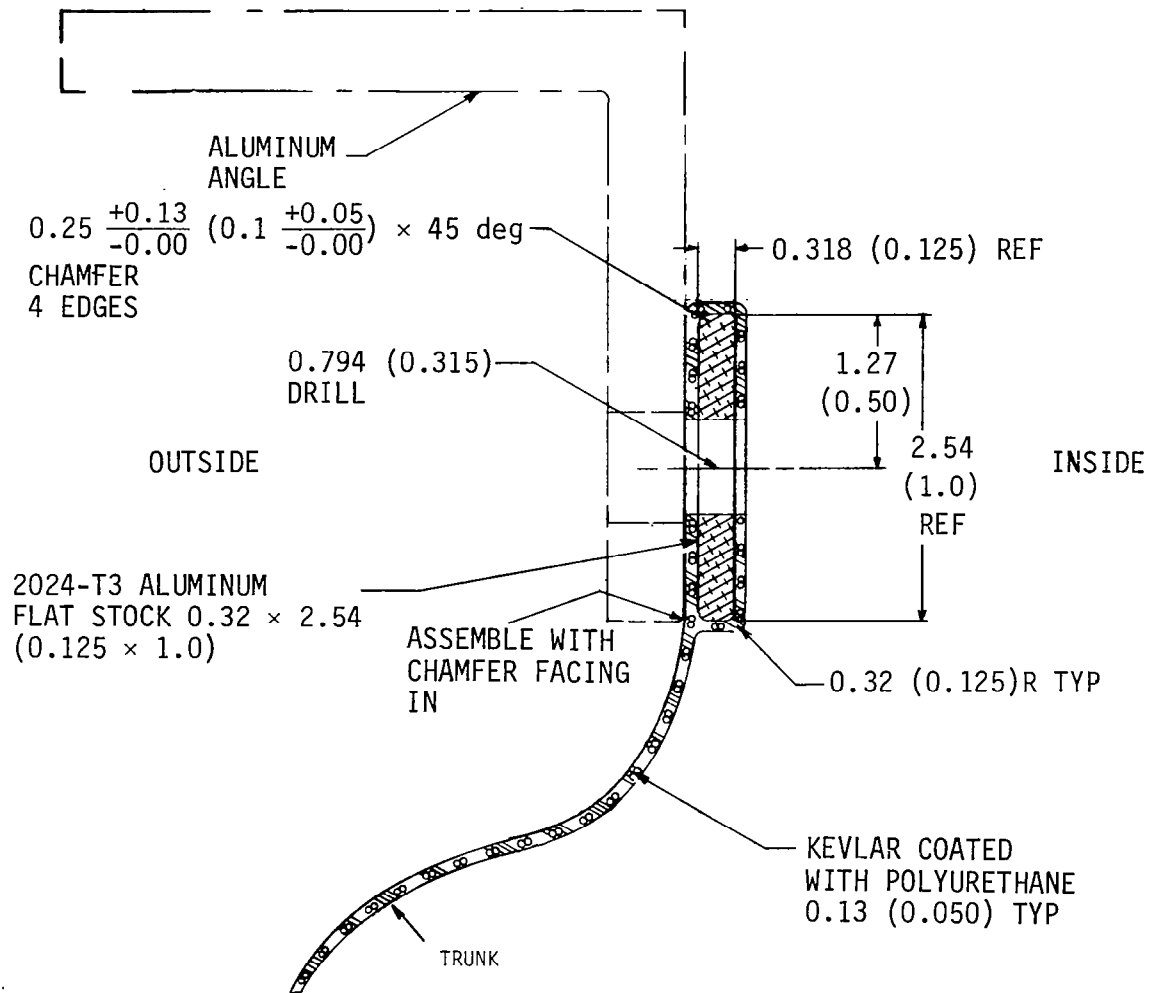


Figure 29. - Characteristics of NASA test vehicle hub-turbine fan.



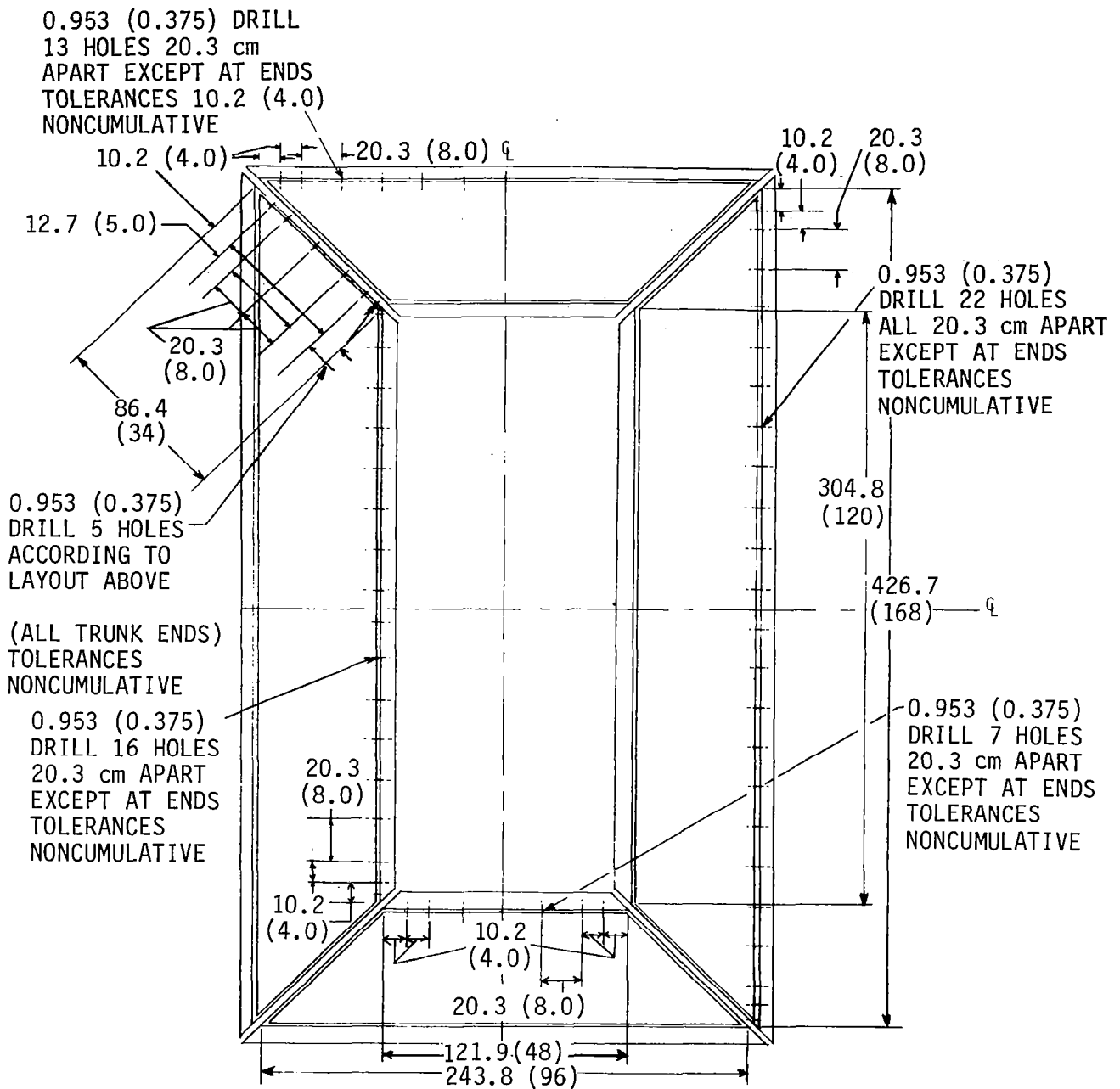
NOTE: ALL DIMENSIONS IN CENTIMETERS (INCH)

Figure 30. - NASA test vehicle trunk design - cross-section shape.



NOTE: DIMENSIONS IN CENTIMETERS (INCH)

Figure 31. - NASA test vehicle trunk design - trunk attachment detail.



NOTE: DIMENSIONS IN CM (IN.)

Figure 32. - NASA test vehicle trunk design - location of trunk attachment holes.

In order to keep the trunk lobes from moving outward due to the cushion pressure, restraining belts are provided as shown in Figure 30. These belts are integrally attached to the trunk during the fabrication process.

Fabrication, Installation and Preliminary Tests

The trunk was fabricated by Hovercraft Fabrics, Ltd. of Toronto, Canada. The fabrication involved making a male mold in the shape of the trunk. This mold was sanded smooth and a coat of wax applied. Several coats of polyurethane were sprayed and the Kevlar fabric was laid on before the polyurethane had a chance to dry. Finally, more polyurethane was sprayed to complete construction.

The porous region (orifice zone) was formed by laying tape on the bottom in a checkerboard pattern and spraying lightly with polyurethane. The resulting orifices are shown in Figure 33. The aluminum strips in the attachment zone and the restraining belts were secured in place and then made integral with the trunk by spraying with polyurethane.

After the fabrication of the lobes, they were shipped to NASA where they were put together (see Figure 34). The complete assembly was then fastened to the test vehicle (Figure 35).

Preliminary tests performed on the test vehicle showed that the trunk provided very good roll and pitch stiffness. Initially, the lobe joints leaked and required stronger restraint than that provided by the belts. The problem was solved by bolting the lobes together at the ends. This modification resulted in higher cushion pressures and subsequent instability of the system. Pressure relief valves installed at each lobe restored system stability while still maintaining good lubrication in the cushion air gap. The test vehicle has passed its initial checkout tests and is currently serving as a test bed for the investigation of advanced steering and braking concepts.

Cost data on ACLS trunks are difficult to compare because the trunks are fabricated as one-of-a-kind developmental items rather than routine production units. Nevertheless, with this consideration in mind, an initial guide to trunk cost and fabrication complexity can be obtained from historic cost data for some of the larger ACLS trunks. These data are shown in Table 3.

It is clear that an elastic trunk — that is, one that retracts by its own elasticity — is an order of magnitude more expensive than an inelastic trunk. The other one-piece trunks, both molded and stitched, are at least two to three times more

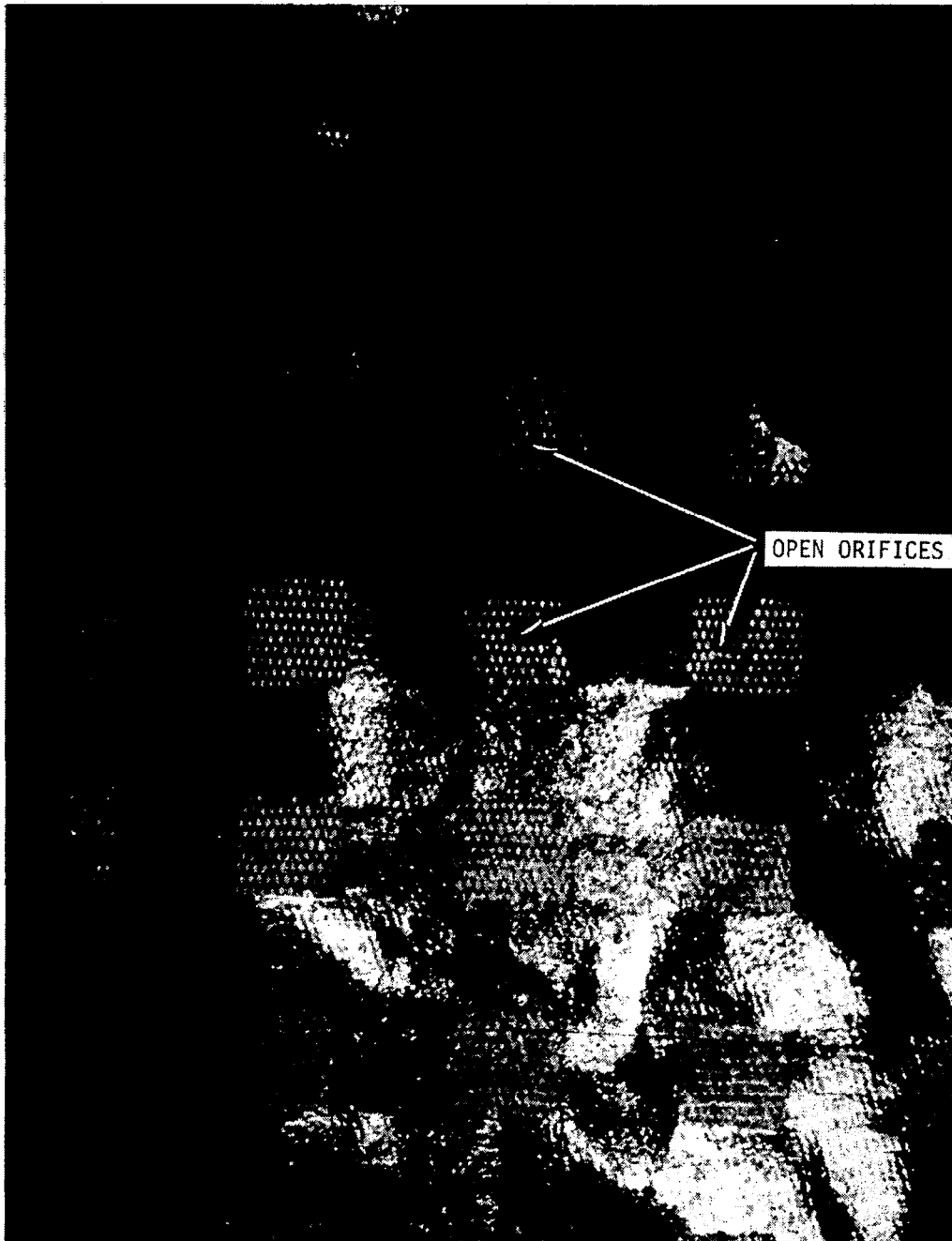


Figure 33. - The checkerboard pattern of the NASA test vehicle trunk orifices.

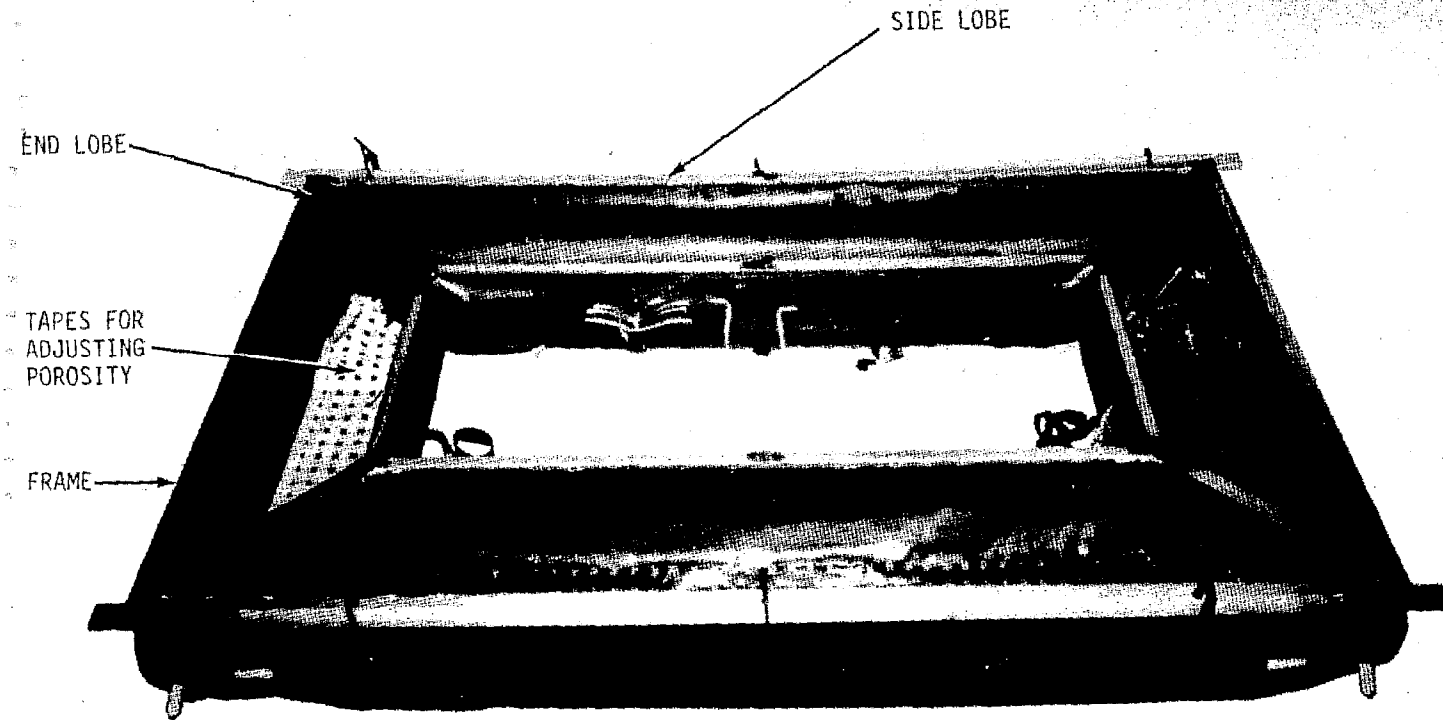


Figure 34. - The segmented trunk for the NASA ACLS test vehicle (lobe covers removed).

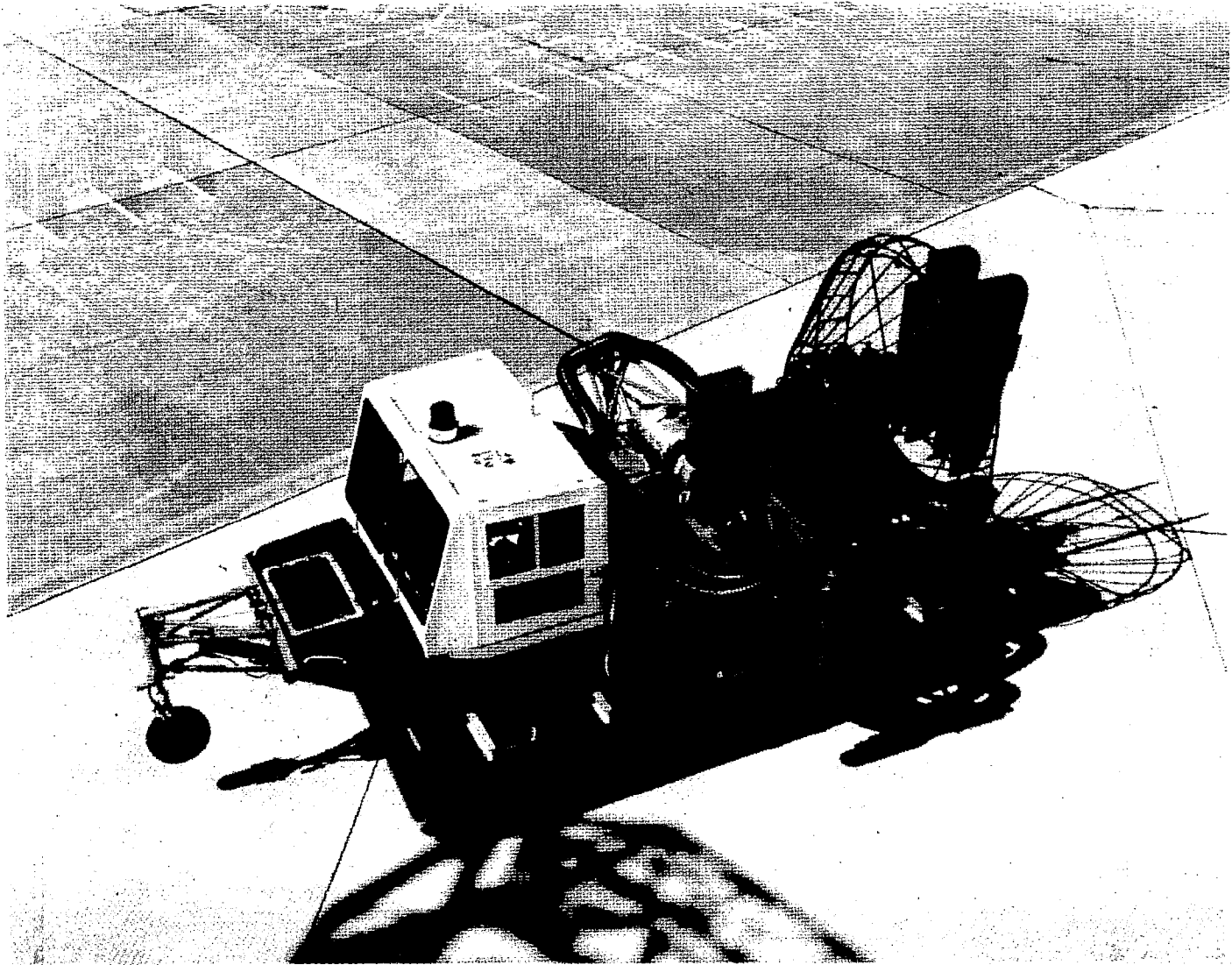


Figure 35. - NASA test vehicle operating with the segmented trunk.

TABLE 3. - ACLS TRUNK COST DATA

Test Aircraft/ vehicle	Shape and size	Cost	Year	Type
1. Buffalo (XC-8A) (ref. 2)	Oval, 9.9 × 4.2m (32.4 × 13.9 ft)	\$300,000	1973	One piece elastic rubber trunk, stitched and bonded to shape
2. A4-D (1/3 scale) (ref. 2)	Oval, 161 × 66 cm (63 × 26 in.)	\$ 22,000	1974	One piece inelastic Dacron-polyurethane trunk, molded to shape
3. Jindivik (ref. 2)	Oval, 320 × 135 cm (126 × 53.3 in.)	\$ 15,000	1975	One piece inelastic nylon-neoprene trunk, stitched and bonded to shape
4. NASA test vehicle	Rectangular, 426.7 × 243.8 cm (168 × 96 in.)	\$ 9,000	1978	Four segment Kevlar- polyurethane trunk, molded to shape

expensive than the segmented trunk developed through this study, especially after cost inflation is taken into account. This is because the segmented trunk is made up of four independent lobes, which individually have no compound curvature, thus making them easier to fabricate.

SCALE MODEL TESTS OF THE NASA ACLS TEST VEHICLE

Because of the central role played by scale model testing in the development of new vehicle systems, it was decided to conduct a series of analytical and experimental investigations using an accurate geometrical scale model of the full-scale NASA ACLS test vehicle described in the previous section. The existence of well instrumented test articles at two scales provides an unusual opportunity to determine scaling relationships and to establish guidelines for interpreting the results of scale model testing.

Design Features and Details

A one-third scale model was designed to reproduce as closely as possible, the geometry of the full-scale NASA test vehicle. The linear dimensions of the new trunk system were designed to be one-third the values of those of the full-scale vehicle. Like the full-scale trunk system, the new trunk system has four straight independent segments. Air flows from a fan into a plenum and then through several ducts which direct the flow into the trunks. Like the full-scale trunk, the trunk orifices of the one-third scale trunk system are not punched into the fabric, but by selectively coating the base material such that the space between the fabric weave in the orifice region is not completely covered. The overall configuration of this design is shown in Figure 36.

The operating trunk and cushion pressures were chosen such that they would be at the properly scaled values of the full-scale vehicle. The trunk ends were fastened together and polyurethane foam inserted between the trunk segments to reduce the leakage from the cushion, and to increase the cushion pressure to enhance the air lubrication between the trunk and ground. "Y" fittings similar to those used on the full-scale vehicle, were obtained and implemented on the model. The duct system was then adjusted in order to obtain high trunk pressures with little variation in pressure among the trunk segments. The optimum duct configuration was found to be the same as that in the original design of the system. The fan used in this design was the tip turbine fan used in the previous tests. The desired trunk and cushion pressures were obtained by adjusting the primary air pressure of the fan and altering the porosity of the trunk lobes by blocking off part of the flow area at the porous section of the trunk. Table 4 is a comparison of data between the full-scale and one-third scale models. There is generally good correlation between the models.

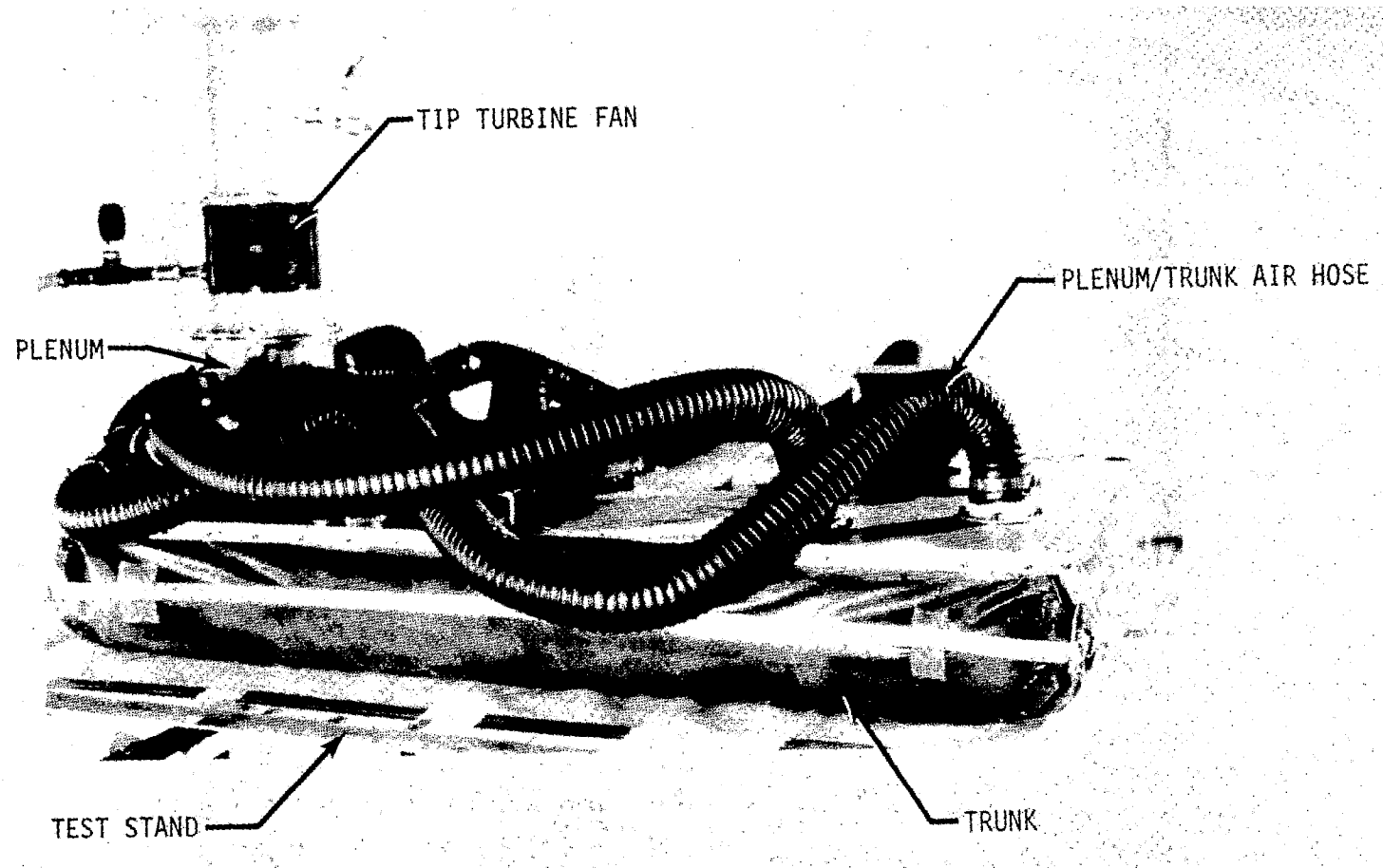


Figure 36. - Design configuration for one-third scale test vehicle.

TABLE 4. - COMPARISON OF STATIC TEST DATA BETWEEN ONE-THIRD AND FULL-SCALE MODELS

Parameter	Full-scale	One-third scale (theoretical)	One-third scale (actual)
Weight kg (lbm)	2291.0 (5050.00)	85.00 (187.00)	107.00 (235.00)
Plenum pressure kPa (psf)	13.5 (282.00)	4.50 (94.00)	3.35 (70.00)
Trunk pressure (average) kPa (psf)	8.0 (170.00)	2.70 (57.00)	2.88 (58.00)
Cushion pressure kPa (psf)	3.0 (62.00)	1.00 (20.70)	0.81 (17.00)
Fan flow kg/sec (lbm/sec)	4.4 (9.750)	0.29 (0.63)	0.49 (1.07)

The trunk material is composed of a polyester fabric with a triaxial weave (B66P), coated with polyurethane. In the design of scale models, it is desirable to use identical materials for similar components in both the model and prototype. There was, however, no Kevlar fabric available that could come close to giving properly scaled dynamic performance of the prototype, and it was thus necessary to use a different material. The polyester fabric was chosen because its weave is similar to that of the Kevlar K49 fabric. Although no dynamic testing of this material had been performed, we felt that it would have fewer reliability problems than encountered previously with other designs, and that the dynamic performance of the system would be more accurately represented by a trunk of this material than one fabricated from poorly scaled Kevlar.

Since the full-scale and one-third scale trunk systems are similar, they both share certain advantages in their basic designs. These are listed in the section "Full-Scale Design of an Advanced ACLS Concept."

Test Apparatus

The test apparatus used for the one-third scale model is the same one used in the evaluation of the five concepts previously discussed. The only change that was implemented on the test rig for these tests was the geometry of the yoke assembly used for the roll tests. This was done so that the one-third scale model could

easily be implemented on the NASA test rig at Langley Research Center. This change did not, however, adversely affect the tests conducted in this study.

Static Tests

To obtain a better understanding of the new ACLS trunk system, and to generate more accurate data for computer simulation, several static tests were conducted on the one-third scale trunk system. These included the determination of the heave and roll stiffness characteristics, and steady state values of other system parameters.

Since the ACLS concepts considered previously (ref. 1) incorporate straight sides and semicircular ends, the Hybrid Trunk model was clearly preferred for the computer simulation. However, the trunk configuration under investigation has four straight sections with straps to prevent outward movement (and attendant high leakage) of the trunk as the cushion load increases. Figure 37 shows that both the side and end trunk sections bow outwards slightly with increased load. This outward movement of the side and end trunk sections is not as significant as found in previous designs, probably due to the presence of the nylon straps. These data on trunk shape were converted to "trunk polynomials" for use in the computer analysis.

Figure 38 shows a plot of the hard surface clearance versus load. The stiffness of the system, which is the inverse slope of the curve, increases as the load increases. The shape of the curve is similar to that found for the previous ACLS concepts. The stiffness of the system is 986.1 N/cm (546 lbf/in.), which is slightly higher than the Kevlar trunk 950.9 N/cm (543 lbf/in.) with the semicircular ends.

Figure 39 shows the variation in the trunk and cushion pressures as a function of the load. As expected, the trunk pressure increases with increasing load, then levels off at higher loads because of the fan characteristics. The cushion pressure increases linearly with load, but at a lower rate than experienced with the other designs. This is due to the leakage through the gap between the trunk segments. This leakage phenomenon of the test vehicle design has been considered and work has been done to implement it into the computer simulation discussed earlier.

Figure 40 shows a plot of the results of a third-order regression analysis of the side trunk characteristics which was generated from the static heave stiffness data. The results are compared to two previous ACLS designs. It can be seen that the trunk behavior falls between a pure membrane model and the system using the Kevlar K49 fabric.

Roll tests were conducted to complete the static evaluation of the one-third scale model. Sheets of Teflon®* were mounted on top of the plexiglas test platform to minimize friction between

*Teflon® is a trademark of the E.I. du Pont de Nemours & Company, Inc.

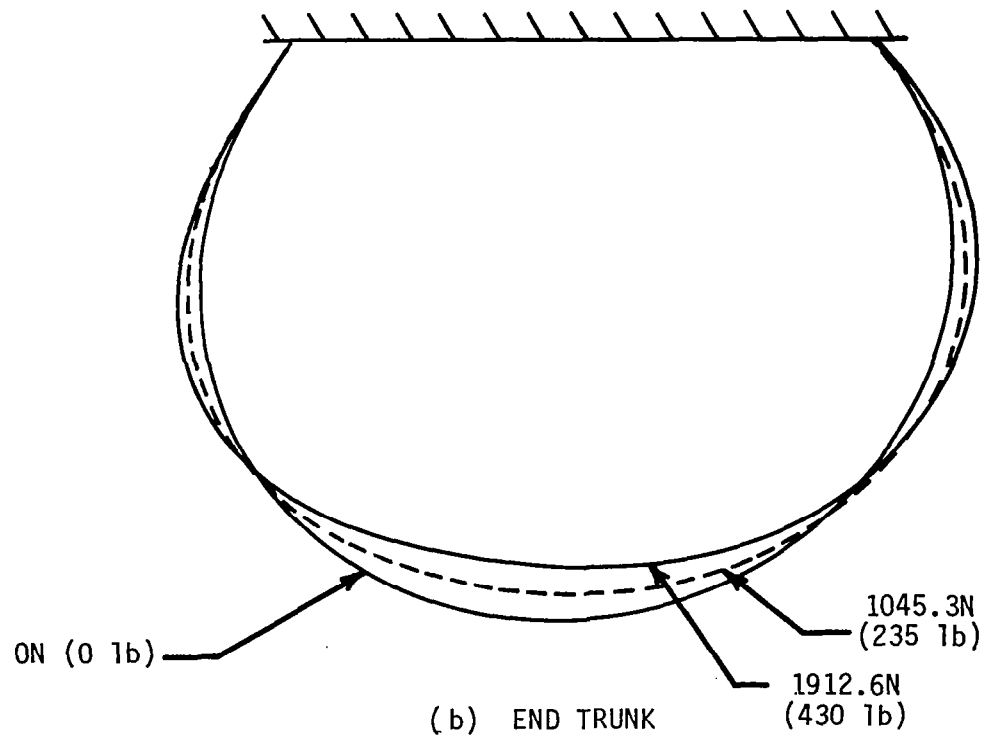
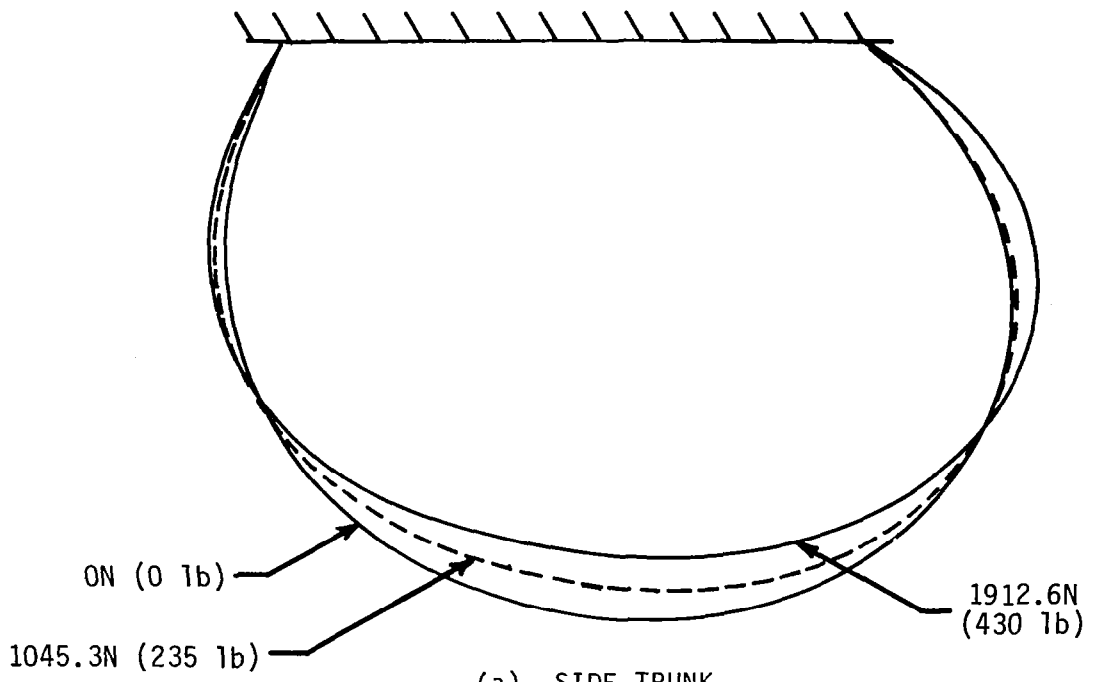


Figure 37. - Trunk profile versus load.

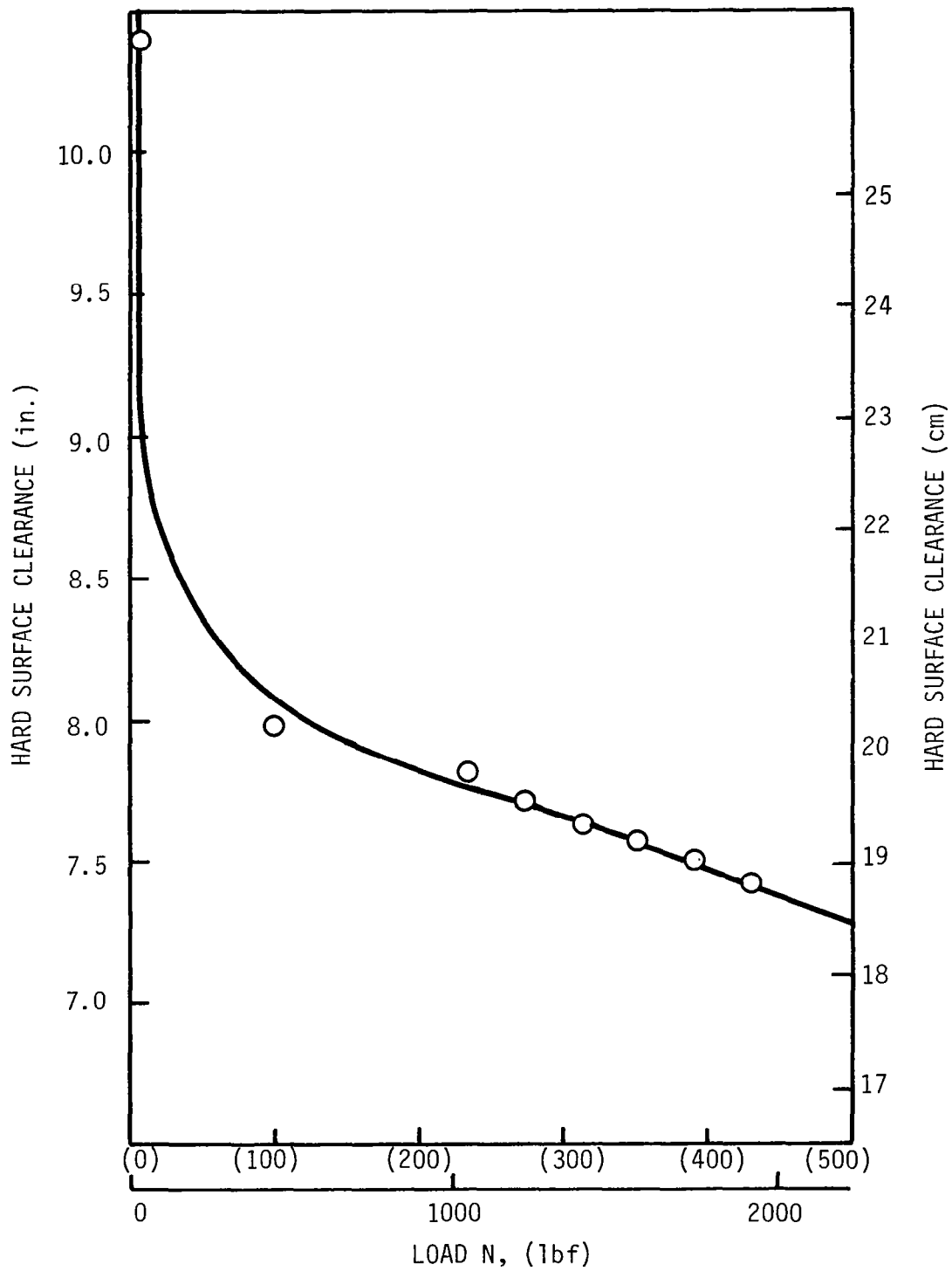


Figure 38. - Hard surface clearance versus load for one-third scale test vehicle.

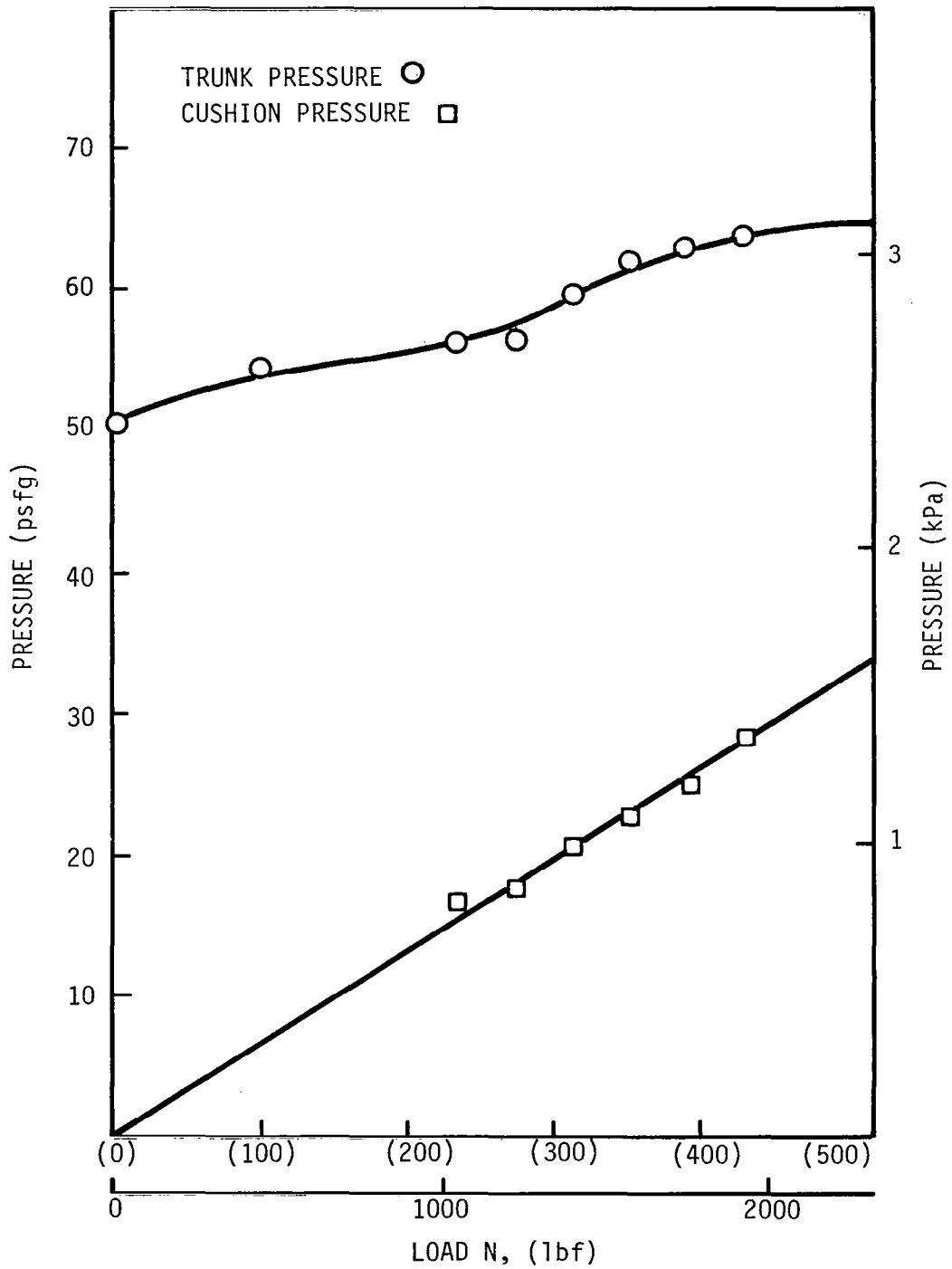
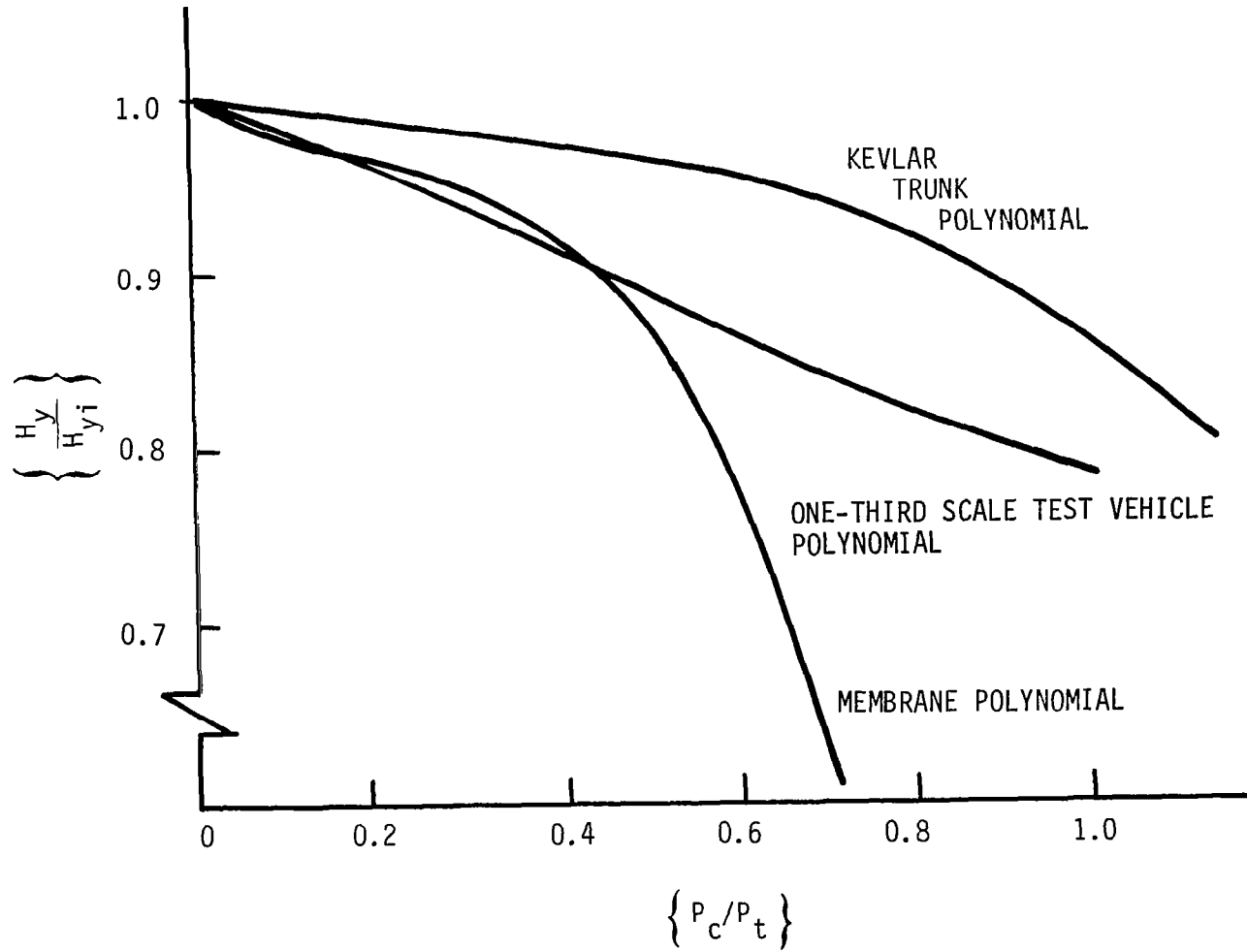


Figure 39. - Pressure versus load for one-third scale test vehicle.



$$\left\{ \frac{H_y}{H_{yi}} \right\} = A_{ho} + A_{hi} \left\{ \frac{P_c}{P_t} \right\} + A_{h2} \left\{ \frac{P_c}{P_t} \right\}^2 + A_{h3} \left\{ \frac{P_c}{P_t} \right\}^3$$

Figure 40. - Side trunk characteristic polynomial.

the trunk and the "ground." The test results are shown in Figure 41 and compared to two other ACLS configurations. The roll stiffness of 3.14 Nm/mRad is much higher than originally expected from this system. This was apparently due to the lack of a lubrication at the corners of the trunk. Although the Teflon sheets were used during the tests, the trunk adhered to the ground as the roll movement increased. This effect is also evident from the hysteresis in the test results.

Stability Analysis

The one-third scale model is quite stable during operation (even when subjected to large perturbations of the trunk system), whereas the full-scale model became unstable soon after the trunk ends were bolted together. To understand the reason for this difference, a stability analysis of the one-third scale model was conducted, using the methods developed in ref. 3. Analysis details are contained in Appendix C. The results of the analysis can be used to determine whether or not the system should be stable or unstable. If the ratio of the lead time constant to the lag time constant, τ_1/τ_2 , is greater than unity, stable operation is indicated. If τ_1/τ_2 is less than unity, unstable operation is indicated. Using test data, the analysis indicates that the ratio of the lead time constant to the lag time constant, τ_1/τ_2 , is 3.55. In comparison, $\tau_1/\tau_2 = 0.451$ for the full-scale system. The results are consistent with the observed results of both model and prototype.

Two factors have been identified as the probable causes for the difference in stability between the one-third scale and full-scale systems: the characteristics of the fan used in the scaled model; and the scaling effects on absolute pressures. A constraint is imposed on the one-third scale model by the use of the tip turbine fan, which does not have the proper scaled pressure/flow characteristics of the hub turbine fan used in the full-scale test vehicle. Comparison of the theoretical and actually attained scaled values in Table 4 indicates that to obtain properly scaled pressures, fan flow is 70 percent higher than would have been expected. The increased air mass flow rate of the one-third scale contributes significantly to the observed stable performance. However, further calculations show that even with the proper geometric and flow scaling, $\tau_1/\tau_2 = 1.32$, and stable operation is still obtained. The remaining factor contributing to the stability of the scaled system is that both the one-third and full-scale models are operated at atmospheric pressure; and while gauge pressures scale, absolute pressures do not. Hypobaric testing, which is not feasible with the present apparatus, would be required to duplicate the damping properties of the full-scale system. Principles of dynamically scaled models are addressed in a later section.

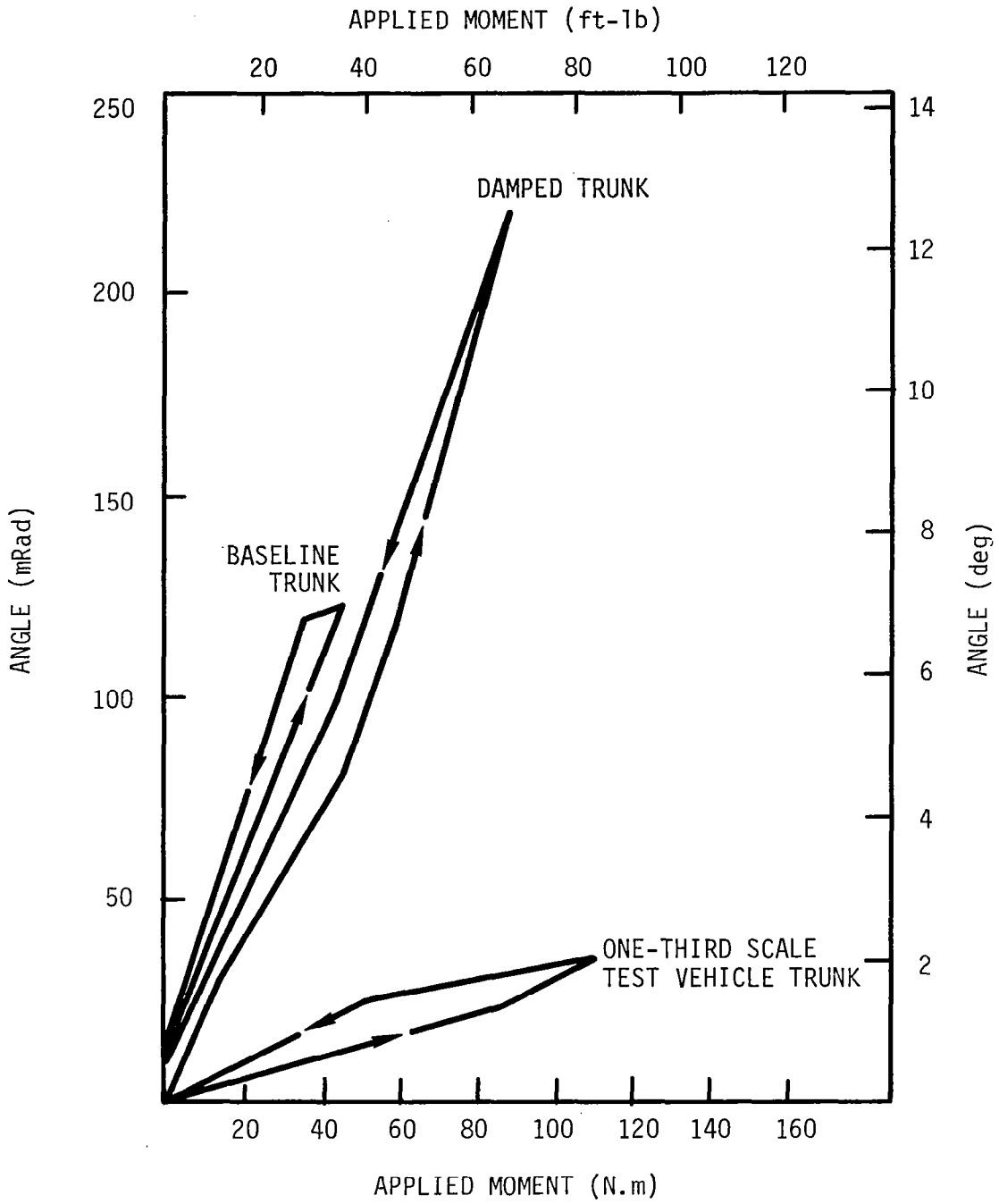


Figure 41. - Static roll test results.

Dynamic Tests

Heave drop tests of 2.54, 7.62, and 15.24 cm (1, 3, and 6-in.) amplitude were conducted to monitor the transient response of the scaled model. In order to preserve the similarity of relevant parameters (such as trunk and cushion pressure) between the one-third and full-scale systems, a fan supply pressure of 100 psig was used. Since these operating parameters are nearly equivalent to those found in other ACLS concepts, this segmented trunk concept can be compared directly to the other configurations studied thus far. The result of a typical drop test is shown in Figure 42. The heave position plot shows that the system is highly damped ($\zeta = 0.36$). This is due to the high damping properties of the base material used to fabricate the trunk. There could also be an additional energy dissipation mechanism in this system: a form of fluid damping caused by the cushion pressure venting to the atmosphere through the trunk lobe interfaces as the trunk is compressed on impact. Although the trunk ends are fastened together with bolts, and foam has been inserted between the lobe interfaces to prevent leakage, there is still a significant amount of flow through this area at impact when the cushion gap is closed. This unintentional cushion vent tends to stabilize the system.

Computer Simulation

Computer simulations of 15.24 cm (6-in.) drop tests of the one-third scale NASA test vehicle were conducted using the program discussed earlier. The parameters of interest (such as trunk pressure, cushion pressure, heave position, and heave acceleration) are plotted in Figures 43 and 44 along with the corresponding experimental results. The computer results were processed through a 10 Hz first-order filter in order to approximate the second-order filters in the signal processor and in the experimental instrumentation. The results are in good agreement.

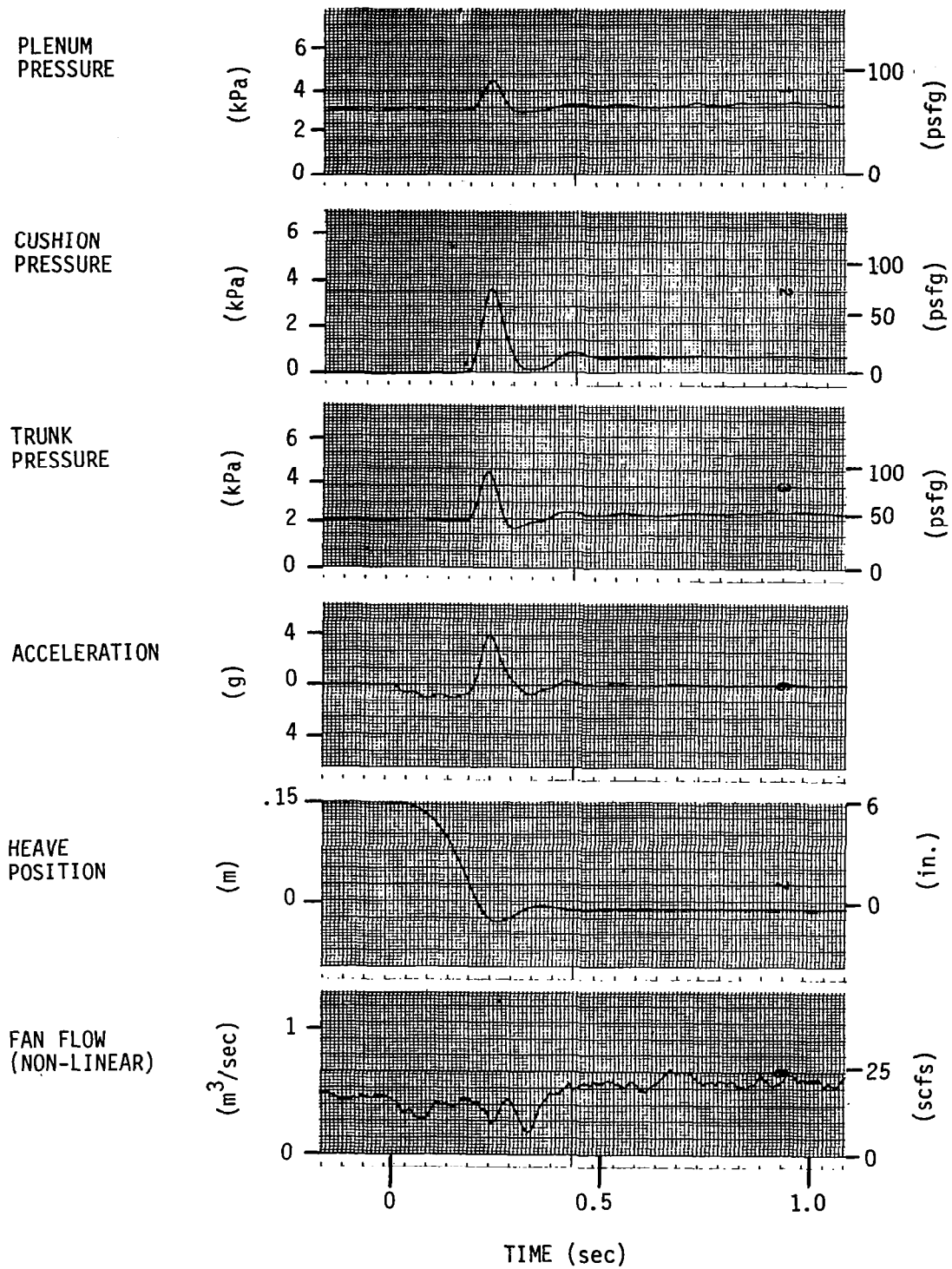


Figure 42. - Drop test results for one-third scale test vehicle; 2.4 cm (6 in.).

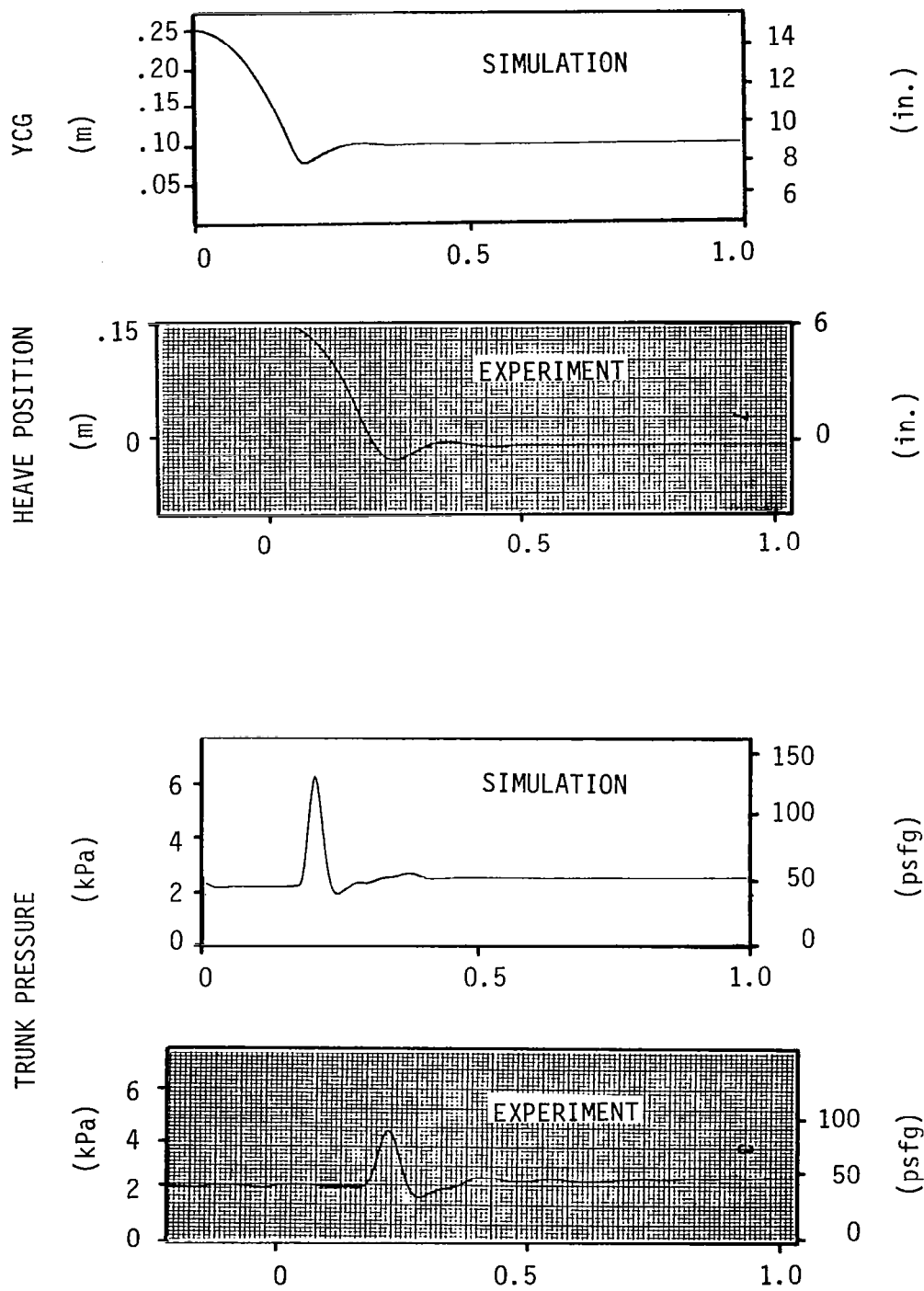


Figure 43. - Comparison between simulation and experiment (heave position and trunk pressure).

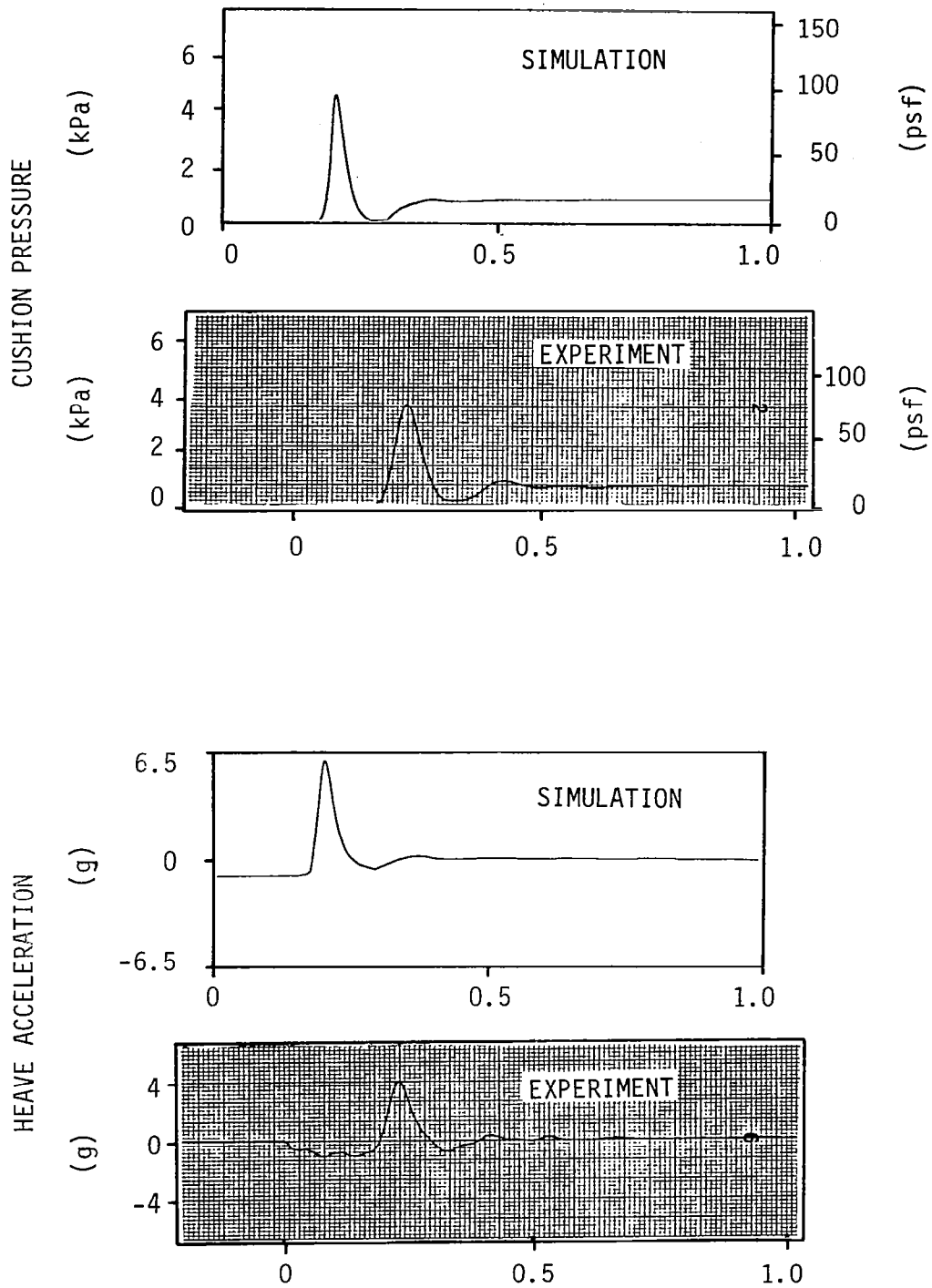


Figure 44. - Comparison between simulation and experiment (cushion pressure and heave acceleration).

DYNAMIC TESTING OF SCALED ACLS MODELS

A major portion of the study described in this report has been based on the use of reduced-scale physical models to validate mathematical models of ACLS dynamic behavior. This section presents a brief discussion of the principles of scale model testing as applied to ACLS. We review the type of scaling used in our laboratory experiments, and indicate the modifications necessary to obtain dynamic similitude. The use of scale model results to validate analytical models is emphasized.

Principles of Dynamic Scaling

Reduced-scale physical models are useful when experimental results are necessary, but full-scale hardware testing is not warranted. Techniques for scaling have been refined primarily in the maritime and aircraft industries, where the complex nature of fluid flow makes reliable analytical treatment very difficult. The benefits of a validated scale model include:

1. Lower cost than full-scale tests
2. More rapid testing
3. Greater fidelity than analytical models
4. A better understanding of overall system behavior (including unexpected features).

This subsection describes basic scaling techniques, with emphasis on their relationship to the ACLS application.

The goal in scale modeling is to predict the behavior of a prototype by subjecting a scale model to conditions similar to those encountered by the prototype. For simple systems, this process can be almost trivial; but for most systems of interest (including the NASA test vehicle), this can be a difficult task. What must be done in order to scale complicated systems is to divide the larger system into a number of subsystems. Each corresponding subsystem of the model and prototype is then analyzed for pertinent physical parameters such as the size, weight, or stiffness, etc. Similar or homologous behavior is achieved if quantities such as those above the model can be found by multiplying the quantity of the corresponding element of the prototype by a constant or scale factor. The only constraint for a homologous system is that the scale factor for given quantities between the prototype and model must be the same for all like quantities for the remaining subsystems.

For example, if x represents the length of a component on the prototype and x' represents the corresponding component on the model, then x^* is the scale factor to transform the model length to the prototype length ($x = x^*x'$). Here x^* must represent the common scale factor for every length in the system, whether it be the length of a component or the displacement of the component when subjected to a load. Fulfilling this criterion alone, however, is not sufficient to yield a true dynamically scaled model. Other quantities (such as stress, acceleration, strain, power, etc.) must also be scaled in order to achieve a valid scaled model. Since all such quantities can be expressed as a function of five or fewer variables - primary quantities (length, time, force, temperature, and electric current) - only these five quantities need to be accounted for in system scaling. Quantities such as stress or acceleration scale factors, called secondary scale factors, can easily be computed once the primary scale factors are derived.

Scaling Techniques

There are various methods used to develop properly scaled models. Three of these are commonly known as (ref. 4):

1. The law method
2. The equation method
3. The parameter method (dimensional analysis).

If a model and prototype are homologous, the physical laws that govern the behavior of each system must be identical. The law approach is applied by using these law(s) and processing them until the primary scale factors which relate model quantities to prototype quantities can be extracted. The equation approach involves a transformation or normalization of the differential equations that describe both the model and prototype. Primary scale factors are found directly when the equation transformation is performed. The parameter method involves identifying the parameters defined in the governing laws, and subjecting them to dimensional analysis in order to obtain the scaling relations.

All of these methods require knowledge of the physical laws governing the system, either explicitly or by inference. If the structure of the system is well understood, the law approach is somewhat more direct than the others. For this reason, it will be used in the following discussion of ACLS scaling.

The first step in system scaling is to properly identify the physical laws that govern the system. A series of steps is then conducted to transform these laws into expressions for the primary scale factors. The steps in deriving primary scale factors include:

1. Identification of physical laws governing behavior of system
2. Conversion of physical laws to representative quantities
3. Derivation of "Pi" numbers
4. Extraction of primary scale factors from Pi numbers

To demonstrate these concepts, we will derive primary scale factors for an actual subsystem of the NASA test vehicle. One particular subsystem of interest is the trunk material used on various ACLS designs. Performance parameters that are of interest in evaluating trunk systems are the stiffness and damping characteristics of the trunk material. Let us assume that a typical section of the trunk can be modeled as a vibrating beam. The physical laws which govern the behavior of the beam are:

1. Hooke's law, which describes the elasticity of the material:

$$\sigma = E\epsilon$$

where

$$\begin{aligned} \sigma &= \text{is stress} \\ E &= \text{is Young's modulus} \\ \epsilon &= \text{is the strain} \end{aligned}$$

2. Newton's law, which describes the inertial force on the material:

$$dF = d(ma)$$

where

$$\begin{aligned} F &= \text{the force} \\ m &= \text{mass} \\ a &= \text{acceleration} \end{aligned}$$

3. Energy dissipation or internal damping of the material, described by:

$$dU = (dV)c^3$$

where

dU = energy dissipation per cycle of the volume dV

c = a material constant.

The next step is to convert each of the laws above into representative quantities. A representative quantity stands for like quantities. For example, V is a representative quantity for volume, whether it be cushion, trunk or plenum volume of the NASA test vehicle. Another example is the acceleration term, $a = d^2 x/dt^2$. Converting this into representative form gives $a \hat{=} x/t^2$, where x is the representative length term and t is the representative time term. The symbol $\hat{=}$ means "equivalent to". Thus, the representative quantities for the laws above are:

$$\sigma \hat{=} E \varepsilon$$

$$F \hat{=} ma$$

$$U \hat{=} Vc^3$$

In scale modeling, a Pi number (denoted by π), is a dimensionless relation made up of representative quantities whose value must be equal for the model and prototype. In this case:

$$\pi_1 = \sigma/E\varepsilon$$

$$\pi_2 = F/ma$$

$$\pi_3 = U/Vc^3$$

The Pi numbers in the forms above do not help in identifying the scale factors necessary for a scale model. When the variables are rewritten in terms of primary quantities and material properties the resulting Pi numbers are:

$$\pi_1 = F/E\ell^2\varepsilon$$

$$\pi_2 = Ft^2/\rho\ell^4$$

$$\pi_3 = F\sqrt{c}/\ell^2.$$

Therefore, the quantities concerning elasticity, inertia, and damping will be similar if the relations above are equal for both model and prototype. Assume for the moment that the trunk material is identical for both model and prototype. Then, $E = E'$, $c = c'$, and $p = p'$. The Pi numbers then reduce to:

$$\pi_1 = F/\ell^2 \epsilon$$

$$\pi_2 = Ft^2/\ell^4$$

$$\pi_3 = F/\ell^2$$

In addition, if the trunk for the model and prototype are geometrically similar, $\epsilon = \epsilon'$, then the relations reduce to:

$$\pi_1 = F/\ell^2$$

$$\pi_2 = Ft^2/\ell^4$$

$$\pi_3 = F/\ell^2$$

Combining these Pi numbers, the result is:

$$\pi_4 = t/\ell \text{ or } t \hat{=} \ell$$

This implies that $t^* = \ell^*$. If t_d and t_d' , are representative decay times for the prototype and the model respectively, $t_d = \ell^* t_d'$, which means that for one-third scale model ($\ell^* = 3$) the decay time of the model will be one-third of that of the prototype. This assumes, of course, that the trunk material is identical for both model and prototype, and that the trunk is geometrically scaled.

The method just described seems straightforward; but for complicated systems which are governed by numerous physical laws, conflicting Pi numbers can result. For example, two Pi numbers used to describe a system could result in relations such as $t = \ell$ and $t = \ell^2$. As more physical laws are used to describe a system, more Pi numbers must be satisfied; this leads in turn to more constraints on primary quantities. Therefore, the physical

laws describing a system must be kept to a minimum and judiciously chosen. There may also arise a Pi number which is mathematically correct, but is in fact impractical or physically impossible to apply.

Scaling is very much an art, and there are no set rules to follow to avoid complications such as those just described. Relaxation techniques exist, however, which can be used to circumvent potential scaling problems. Relaxation techniques are not formulas or straightforward procedures of resolving these problems. They are simply generalized iterative methods which have evolved as useful aids in scale modeling. This section will not address the variety of relaxation techniques available, but will deal with those applied to the scaled NASA test vehicle.

Application to Scaled NASA Test Vehicle

A one-third geometric scale model of the NASA ACLS test vehicle was implemented on the FMA test stand. The choice of scale was dictated by the need to make direct comparisons with previous tests on other configurations.

A basic criterion for scaling the dynamic behavior of fluid-mechanical systems is that the ratio of the inertial forces and the viscous forces, and the ratio of the inertial forces and the gravitational forces be identical for both model and prototype. These two ratios can be reduced to the well-known Pi numbers referred to as the Reynolds number and the Froude number, respectively. The expressions for these Pi numbers are:

$$Re = \ell v / \nu$$

$$Fr = v / \sqrt{g \ell}$$

where

ℓ = representative length

v = representative velocity

g = gravitational acceleration

ν = kinematic viscosity.

For these Pi numbers to be the same for the model and prototype (assuming they are tested in the same fluid), then $l/l' = v'/v \times$ and $v'/v = \sqrt{l'/l}$. It is obvious that these two requirements can be satisfied only at full-scale, and that in order to achieve dynamic similarity, the model and prototype must be tested in different fluids. In particular, for the one-third scale ACLS model, the kinematic viscosity of the fluid in which the model is tested should be approximately one-fifth of that of ambient air.

This could be accomplished by using very cold air or other gas as the working fluid, but the cold would alter the properties of the flexible trunk. Since the inertial and gravitational laws predominate in this application, the one-third scale model was designed such that the Froude number is identical for both model and prototype. This kind of compromise is common in scale modeling. Since the two Pi numbers, Re and Fr, result in conflicting constraints on the model and prototype, the dominant law (law of gravitation) was retained while the weaker (laws of viscous friction) was discarded. From this result and the length primary scale factor ($l^* = 3$), the other system parameters can be derived as shown in Table 5.

The derivation of Pi numbers governing trunk behavior was used as an illustration of scaling using the law approach. Since it has been found that the trunk material has a significant effect on the performance of an ACLS (see the section on "Evaluation of Advanced Concepts"), the derivation will be reviewed here in light of the present scale model design. The Pi numbers that resulted from the analysis were:

$$\pi_1 = F/E\ell^2\epsilon$$

$$\pi_2 = Ft^2/\rho\ell^4$$

$$\pi_3 = F\sqrt{c}/\ell^2$$

Ideally, the next step would be to eliminate material properties common to both model and prototype. In practice, however, it is virtually impossible to produce a trunk material which is both geometrically and dynamically scaled. Judging from the tests that FMA conducted on various trunk materials (see Figure 9), a dynamically scaled trunk should consist of a material much more flexible than that used on the baseline trunk fabricated by the Boeing Company. Since even the light, flexible material used for the baseline trunk system has proven to be unreliable, it was decided to use a polyester/urethane fabric similar to, but lighter than, the one used on the large-scale design. Dynamic properties

TABLE 5. - SCALE FACTORS FOR THE ONE-THIRD
SCALED NASA TEST VEHICLE

Parameter	Scaled Factor
<u>Design Parameter</u>	
Linear Dimensions	3
Weight	(3) ³
Moment of Inertia	(3) ⁵
Cushion and Trunk Pressure	3
Total Air Flow	(3) ^{5/2}
Cushion Area	(3) ²
Trunk Porosity	1
Heave Stiffness	(3) ²
Heave Damping Constant	(3) ^{5/2}
Heave Natural Frequency	(3) ^{1/2}
Fan Characteristic Slope ($\frac{\Delta P}{\Delta Q}$)	(3) ^{3/2}
Plenum Volume	(3) ³
Trunk Volume	(3) ³
Cushion Volume	(3) ³
Plenum Trunk Resistance	(3) ^{3/2}
Trunk Damping Factor (B_K)	(3) ^{9/2}
<u>Test Parameters</u>	
Forward Velocity	(3) ^{1/2}
Sink Rate	(3) ^{1/2*}
Friction Coefficient	1
Roughness of Surface**	3
<u>Measured Parameters</u>	
Time	(3) ^{1/2}
Displacement	3
Velocity	(3) ^{1/2}
Acceleration	1
Angle	1
Angular Velocity	(3) ^{1/2}
Angular Acceleration	1/3
*Approximate	
**Roughness of the surface is represented by A, where the double sided spectral density of the ground irregularity is given by $S_y(\omega) = \frac{Av}{\omega^2}$, where v is the velocity of the vehicle and ω is frequency in rad/sec.	

of the material, however, do not scale accurately with respect to the trunk material used on the large-scale design. This illustrates a problem often encountered in designing scale models: materials with the required physical properties may be unobtainable or impractical.

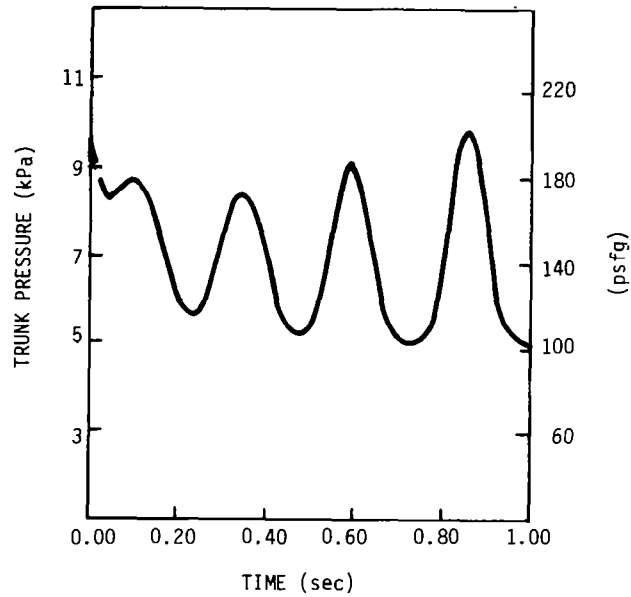
A third important factor that affects the dynamic performance of ACLS is the supply fan operating characteristics. It is important that the pressure-flow curve of the fan used in the small model be scaled properly with respect to the one used on the prototype. The one-third scale test procedure required adjusting the primary air supply pressure until the trunk and cushion pressures were at the scaled values. Once this was done, it was found that the air mass flow rate was much higher than necessary for a dynamically scaled model. Since the air flow rate has a significant effect on the stability of an ACLS, performance of the model and prototype should be expected to differ (see section on "Model Tests of the NASA ACLS Test Vehicle").

Scale Model Tests for Model Validation

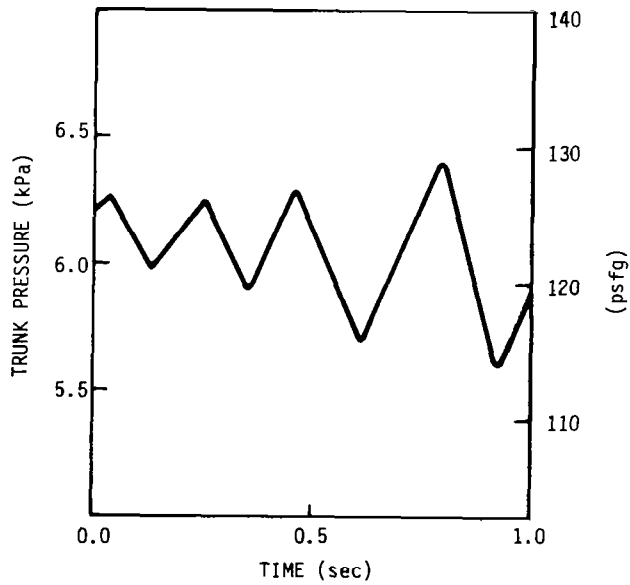
Although the one-third scale and full scale models were designed to be geometrically and not dynamically similar, tests on the scale model can be used to great advantage in conjunction with computer simulations to understand the performance of the prototype.

Remember that a mathematical model consists of a structure and a set of parameters. The structure of the reduced-scale physical model should be the same as the full-scale article, and the same mathematical model should therefore serve to simulate both (with suitable changes in parameter values). If a computer program predicts the behavior of a one-third scale model on the basis of parameter values measured or calculated a priori, then we have strong reason to believe that the fit will also be good with regard to the prototype. It is not necessary for the scale model to "mimic" the full-scale vehicle's behavior in order to validate the analytical model; but a validated model can be confidently applied at full-scale. Notice, however, that one's degree of confidence in the mathematical model declines sharply as it becomes necessary to adjust the a priori parameter values to fit the observed response.

The FMA 5 computer program has been validated for both static and dynamic behavior using scale model data. The good correlation achieved between full-scale static tests and the computer simulation (see Figure 45) also suggests that the program can be effectively extrapolated to trunks of other dimensions.



(a) SIMULATION RESULTS



(b) EXPERIMENTAL RESULTS

Figure 45. - Comparison between simulation and experiment trunk pressure - full-scale NASA test vehicle.

CONCLUSIONS AND RECOMMENDATIONS

The objective of this project has been to generate and evaluate novel ACLS concepts which can alleviate the shortcomings of present designs. These shortcomings include low damping, low roll stiffness, trunk flutter, and complexity of fabrication. The analytical findings of this study have been confirmed by experimental work on reduced scale models. The conclusions reached from this study are summarized below.

1. Damping and Stability. System damping and stability can be increased significantly by incorporating a trunk configuration with higher inherent damping such as the damped trunk or other trunk concepts evaluated in "Evaluation of the Advanced Concepts". Such trunk configurations also show a tendency to suppress flutter.

2. Roll Stiffness. Although some increase in roll stiffness can be achieved with new trunk configurations, a major increase in roll stiffness may require multiple cushions or roll feedback control.

3. Fabrication Cost and Complexity. For any new trunk type, fabrication cost and complexity can be significantly reduced by making the trunk out of four straight segments, and putting them together with a suitable restraint system as demonstrated by the segmented trunk concept developed for the NASA ACLS test vehicle.

4. Scale Model Tests. It is very difficult to achieve full dynamic similarity between reduced and full-scale models. Nevertheless, the dynamic response of each respective system was accurately simulated using the computer program. Therefore, this validated computer program can be used confidently in the development of full-scale systems.

5. System Design. No single ACLS concept evaluated to date can be considered ideal for all applications. In fact, the optimum design for a particular application will emerge from a synthesis of concepts that include high-damping trunk materials, segmented or other novel trunk configurations, pressure relief valves, and feedback control. In this regard, the computer program can simulate a variety of novel ACLS options, and will thus be a very useful tool in the initial evaluation of optimal designs.

With the completion of this work, the technology base available for the design of an optimum ACLS for a given application has grown significantly. Further work must be done to extend our

knowledge and upgrade the design tools available for advanced ACLS development. This work includes the following two items:

1. Computer-Aided Reduced and Full-Scale Tests. It has been shown that the present computer program can accurately predict the behavior of reduced and full-scale systems for certain configurations. Dynamic tests, however, have been confined to pure heave at zero forward speed only. The validity of the analytical model has not been fully tested for multiple degrees of freedom. This program should be further refined and tested in conjunction with the one-third scale model for other degrees of freedom.

2. Development of a Video Output Computer Simulation. The present analytical model and computer simulation has grown to a point where it is very difficult and time consuming to interpret the large volume of printed output data. In order to retain the capability of using the analytical model rapidly and efficiently, it is now necessary to expand the output capabilities of the simulation to display the results of ACLS landing dynamics in real-time on a video display. This can be achieved either through a hybrid digital-to-analog simulation or by means of a post-processing display of recorded output. In either case, such a capability will ensure that the large number of alternative configurations and parameter options for ACLS can be evaluated rapidly and efficiently to arrive at an optimum design.

PART II - WATERBORNE ACLS STUDIES

INTRODUCTION

Background

Past investigations of ACLS have concentrated on analyses of ACLS operation over hard surfaces. Because one of the most promising applications of ACLS is in amphibious operations, it is essential to extend this work to over-water dynamic behavior.

The following sections summarize the first stage of waterborne ACLS research, in which the basic analysis of a two-dimensional, reduced-scale, rigid-impermeable-trunk test rig has been developed and subjected to preliminary investigation. On the basis of these findings, recommendations are made for further analytical and experimental work.

Summary

At the outset of the waterborne ACLS studies described here, little was known concerning the behavior of an air cushion trunk submerged in water, particularly with respect to the details of the trunk discharge mechanism. Before serious analytical efforts could be undertaken, it was necessary that some observational understanding be gained of the process by which a trunk gap is formed in water, permitting the discharge of air from the cushion to the atmosphere.

The first phase of the study program, therefore, was the construction of a two-dimensional, reduced-scale, rigid-impermeable trunk test rig. Experiments conducted with the test rig provided both a qualitative understanding of the discharge process for model development and quantitative data for model verification.

The presence of a periodic, discontinuous trunk discharge process is perhaps the most significant experimental observation. In view of the complexities of the discharge process, initial analytical efforts concentrated on developing lumped parameter models which would permit a rapid means of investigating different trunk gap formation mechanisms. Following the verification of such a model, an analysis based on fundamental principles was initiated. In this report, simulation results are based on a lumped parameter model, with most of the essential parameter values being determined from the fundamental principles analysis.

A rigid-impermeable trunk was used in this investigation to simplify the problem for initial studies. Introduction of a flexible or permeable trunk complicates the dynamics of the discharge process and could possibly have obscured the gap formation mechanisms observable with a rigid-impermeable trunk. It is anticipated that a discontinuous trunk discharge process will also be observed with a nonrigid-permeable trunk, but it is difficult to predict its actual behavior on the basis of the results of this study.

TESTING

Test Objectives

The objective of laboratory testing was to obtain both a qualitative and quantitative understanding of air cushion behavior over water. Prior to conducting experiments with the test rig, little was known concerning the details of the trunk discharge mechanism. Experience with trunk flutter in overland ACLS experiments (ref. 5), and reports of a pulsating discharge from the leading trunk section of operational hovercraft indicated the necessity of conducting preliminary tests before serious analytical modeling efforts should be attempted.

In addition to providing a qualitative understanding of the discharge behavior, testing provided quantitative data for model parameter evaluation and model verification. Tests were originally planned to determine a discharge coefficient for an orifice model of the trunk gap flow experimentally, in a manner similar to that used in overland ACLS studies (ref. 1). Static measurements of the pressure distribution in the trunk gap, however, were not feasible due to the gap formation dynamics.

All the tests performed were static tests in the sense that the inlet airflow and the depth of the trunk in the water were held constant. As described below, however, these steady operating conditions resulted in a steady oscillation of the system states.

Test Equipment

The trunk for the over-water test rig was adapted from a two-dimensional, one-third scale overland test rig constructed earlier by FMA for NASA (ref. 1). It is fabricated from sheet metal and is rigid and impermeable. The trunk is suspended from the top of a Plexiglas tank, as shown in Figure 46.

Two basic test configurations were employed: one with the gap length extending along the entire 94-cm (37-in.) trunk; and one with the gap length constrained by a partition to a 10-cm (4-in.) section of the trunk as shown in Figure 46. For simplicity, these two configurations will hereafter be referred to as the 1-m gap and 10-cm gap, respectively. Various baffles and weirs were fabricated to aid in studies of tank size and water surface wave effects. One such baffle, placed behind the 10-cm gap on the cushion side, is also illustrated in Figure 46.

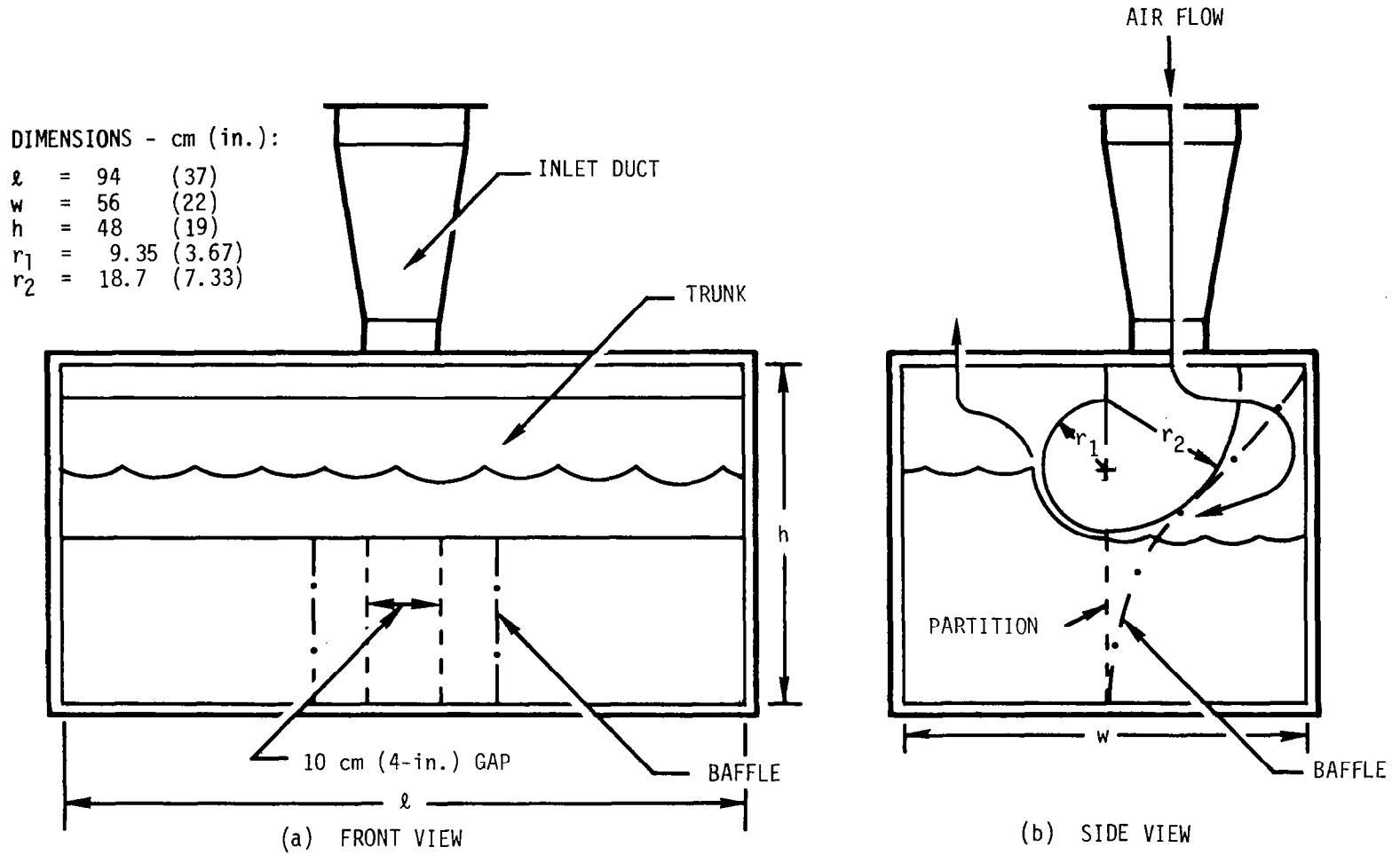


Figure 46. - Waterborne ACLS test rig.

The dimensions of the test rig limit mean cushion pressures to about 1.5 kPa (6 in. H₂O) -- that is, to the level to which the water can rise above trunk bottom on the atmospheric side. A compressed air supply with a short-term capacity of about 0.57 m³/min (20 ft³/min) was used for the inlet air source. The actual maximum useful flow for experimental purposes is about 0.43 m³/min (15 ft³/min), and is limited by the turbulence generated in the tank rather than the supply capacity.

Instrumentation of the test rig consisted of a static flowmeter (0.085 to 0.85 m³/min; 3 to 30 ft³/min) measuring air inlet flow, and a dynamic pressure transducer (± 17 kPa; ± 68 in. H₂O) measuring cushion pressure. Water levels in the tank at the beginning of all tests were measured with a scale relative to the bottom of the trunk. Air flow was controlled with a pressure regulator.

Signal processing was required only for the pressure transducer. A first-order filter was included in the signal processor to attenuate high frequency noise. The noise level relative to the full-scale output of the transducer was small but bothersome at the low pressure levels being measured. The roll-off frequency of the filter was set near 500 Hz (-3 dB bandwidth), well above any frequencies of interest.

Test Results

Test results are presented on both a qualitative and quantitative basis.

Qualitative results. - The most significant characteristic of air cushion behavior over water is the discontinuous trunk discharge. As the cushion is pressurized, the cushion-side water surface lowers to trunk bottom level. Cushion air is then discharged to the atmosphere in discrete packets or bubbles at regular intervals. Initial observations seemed to indicate that waves on the cushion-side water surface could play a significant role in this process (that is, in the formation and resealing of the discharge path). Since the surface waves frequently appeared to be standing waves, tank-size effects were considered. Experiments with baffles and weirs introduced to alter the tank configuration at and below the water surface (on both the cushion and atmospheric sides), however, did not substantially alter the discontinuous discharge process. Also, under no circumstances was it possible to produce a continuous discharge. Inlet flow variations were, therefore, considered as a contributing factor, but any significant inlet flow dynamics were probably not detectable with the flowmeter, and consequently the stiffness of the existing air supply was not determined.

With the 1-m gap, the discharge took the form of air bubbles emerging one by one at apparently random points along the trunk; there was no tendency toward simultaneous discharge along the entire trunk length. At high-flow levels, longitudinal sloshing of the water on the cushion side would promote discharges alternately near each trunk end. To investigate the basic mechanisms at work in the gap formation process, the variation of discharge frequency with test conditions was measured. With the 10-cm gap, the discharge always occurred across the entire gap length, and a distinct trunk discharge frequency could be readily measured. For this test configuration it was noted that the cushion pressure and trunk discharge frequencies were identical.

A number of experiments were conducted to determine the significant conditions associated with the discharge process. Qualitative results established from these experiments include:

1. Discharge and cushion pressure frequencies are insensitive to inlet flow, mean cushion pressure, and surface wave action.
2. Significant cushion pressure dynamics are present, with the discharge occurring near the pressure peaks.
3. There is some coordination between the discharge and the motion of the surface near the trunk.
4. Discontinuous discharge persists up to the maximum flow obtainable from the air supply.

Although the experiments did not identify the essential mechanisms behind the discontinuous discharge process, it was evident that a complex model for the water surface behavior would probably not be required, except possibly in near proximity to the trunk. In general, the presence of small surface waves obscured the gross motion of the cushion-side water surface. The apparent coordination of the cushion-side water surface near the trunk with the discharge was inferred from observations of the trunk from below: with the 1-m gap, each discharge was preceded by a general reduction of the wetted trunk surface area on the cushion side along most of the trunk length.

Quantitative results. - Cushion pressure recordings were made at various inlet flows, Q_i , and at two initial water levels, X_0 , above the trunk bottom with the following test rig configurations: the 1-m gap; the 10-cm gap; and the 10-cm gap with the baffle shown in Figure 46. Mean cushion pressures, \bar{P}_C , of 0.75 to 0.87 kPa (3 to 3.5 in. H₂O) and 1.25 to 1.37 kPa

(5 to 5.5 in. H₂O) result from initially filling the unpressurized test tank to 2.5 cm (1 in.) and 5 cm (2 in.) respectively, above the trunk bottom. Cushion pressure frequency as a function of inlet airflow for these test cushions is summarized in Figure 47. Frequency is relatively insensitive to all the test conditions except gap length.

The dynamic pressure recordings for several of the data points in Figure 47 are presented in Figures 48 through 53. The following characteristics of the pressure oscillations are noted: they are approximately sinusoidal, especially at the lower flow levels; and they are roughly of constant amplitude in many cases. There is some inconclusive evidence of regular "beats" in the amplitude envelopes. The presence of sustained oscillations that are of fixed amplitude and almost sinusoidal is a characteristic of a special class of nonlinear systems called "quasi-harmonic oscillators" (ref. 6). The presence of the beats in some of the amplitude envelopes may be due to standing wave effects in the tank. It is significant that the fundamental oscillation frequency does not appear to be altered by the presence of the beats; thus surface waves apparently do not affect the discharge frequency.

Step response tests were conducted to determine the natural frequency of the water dynamics, that is, the frequency of free water flow between the cushion side and the atmospheric side. The data from these tests were used to identify analytical model parameter values. Step inputs were generated by pressurizing the cushion to a constant value and rapidly releasing the pressure through a large exhaust port. Cushion pressure step response records are shown in Figures 54 and 55 for the 1-m gap and 10-cm gap respectively. In Figure 54, two frequency components are observed: a relatively undamped 30 Hz component; and a moderately damped ($\zeta \approx 0.4$) 1 Hz component. The higher frequency component is attributed to the air cushion dynamics and the lower frequency component to the water dynamics. Note that the same frequency is observed for both initial water levels; the difference in water mass between the two cases is small compared to the total water mass. In Figure 55 only the 30 Hz component is observed; the low frequency water component may be too highly damped to be readily measured.

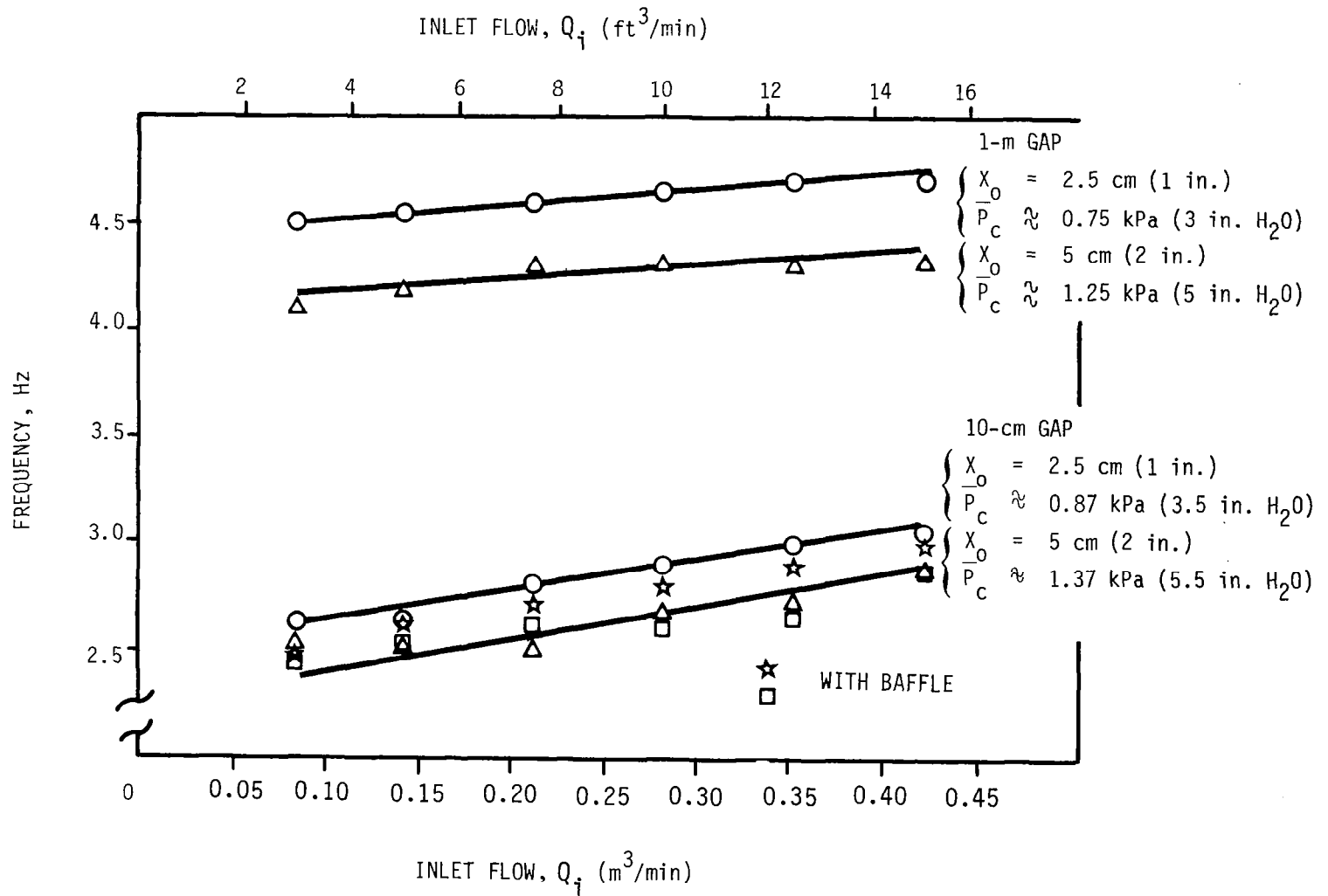
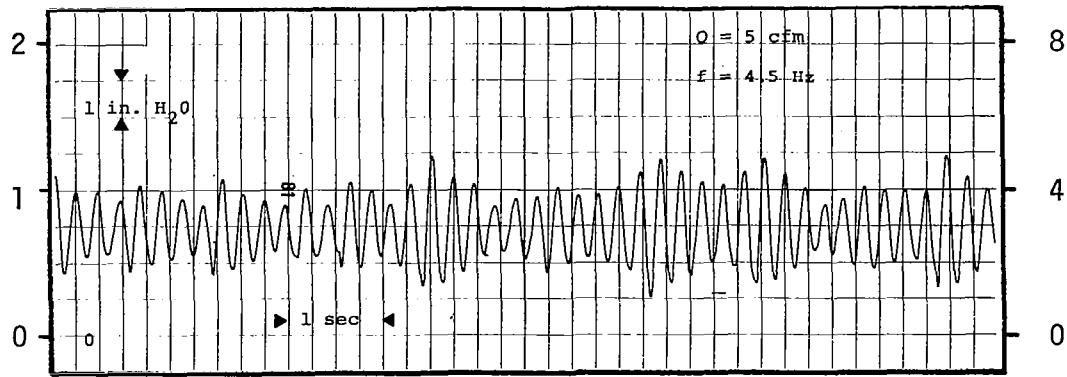
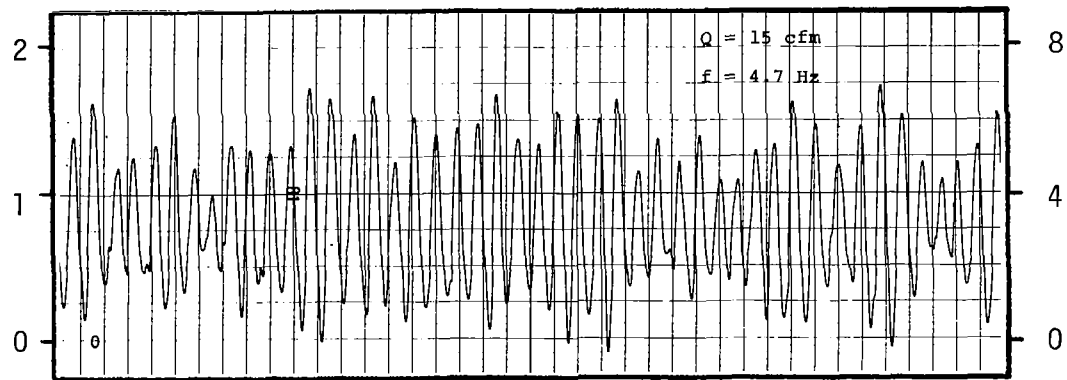


Figure 47. - Cushion pressure frequency: ACLS test rig.



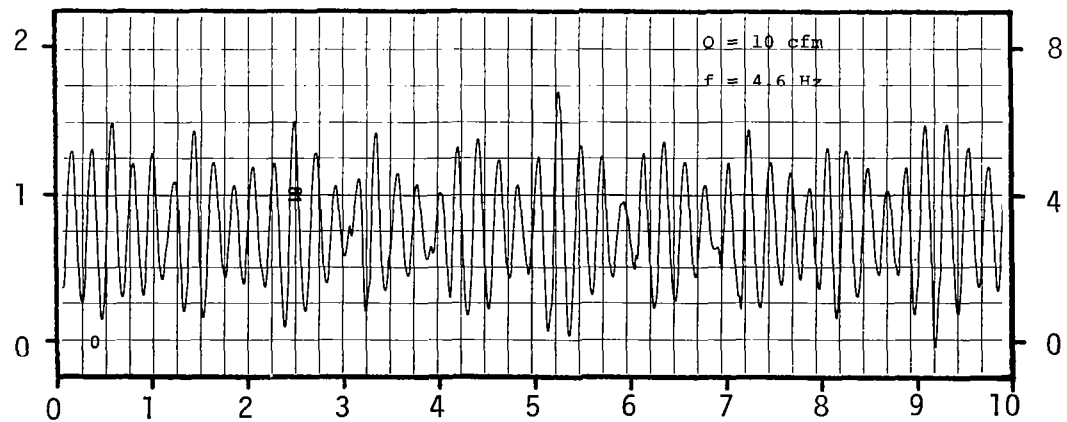
(a) INLET FLOW, $Q_i = 0.14 \text{ m}^3/\text{min}$ ($5 \text{ ft}^3/\text{min}$)

CUSHION PRESSURE, P_c (kPa)



(b) INLET FLOW, $Q_i = 0.28 \text{ m}^3/\text{min}$ ($10 \text{ ft}^3/\text{min}$)

CUSHION PRESSURE, P_c (in. H_2O)



(c) INLET FLOW, $Q_i = 0.42 \text{ m}^3/\text{min}$ ($15 \text{ ft}^3/\text{min}$)

Figure 48. - Cushion pressure: ACLS test rig;
1-m gap; $x_o \approx 2.5 \text{ cm}$ (1 in.)

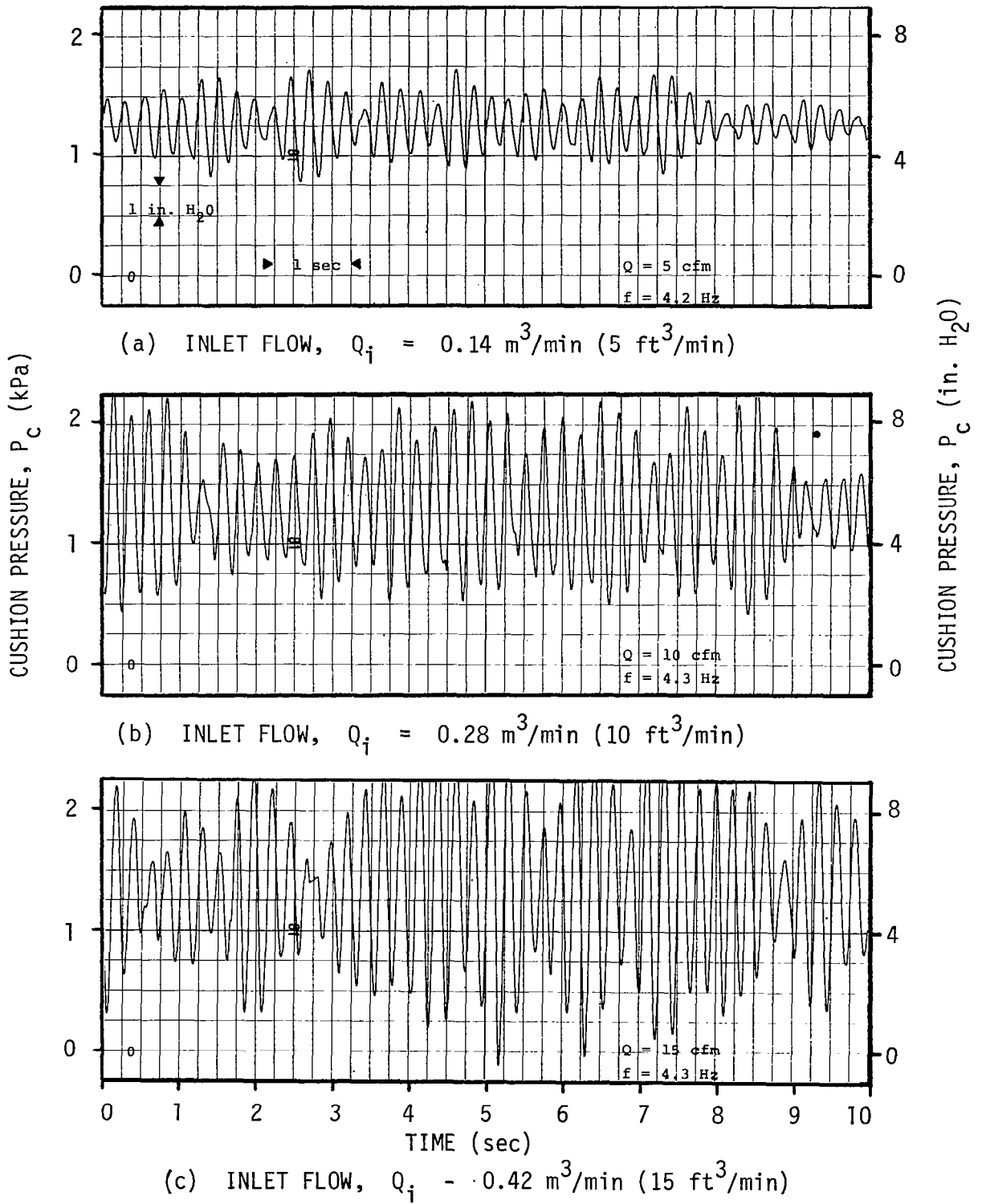
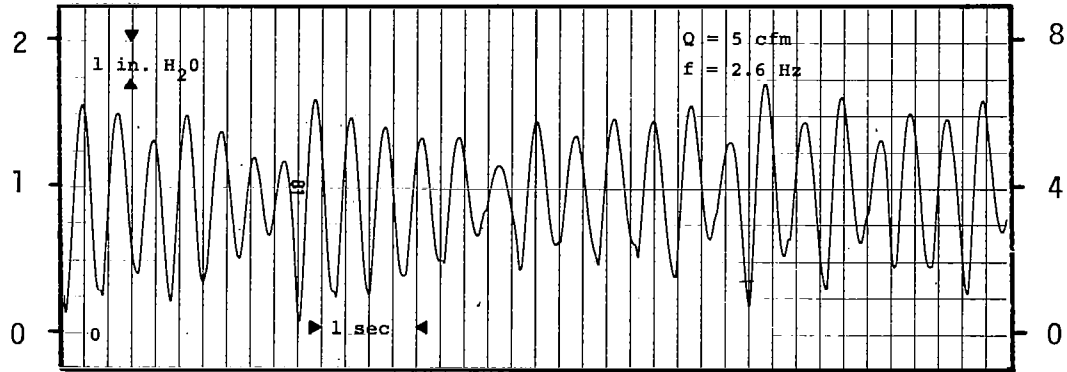
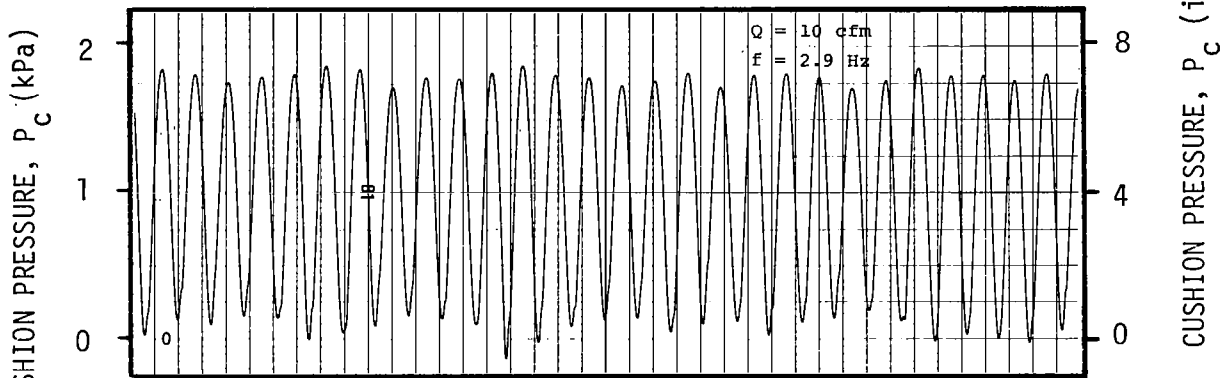


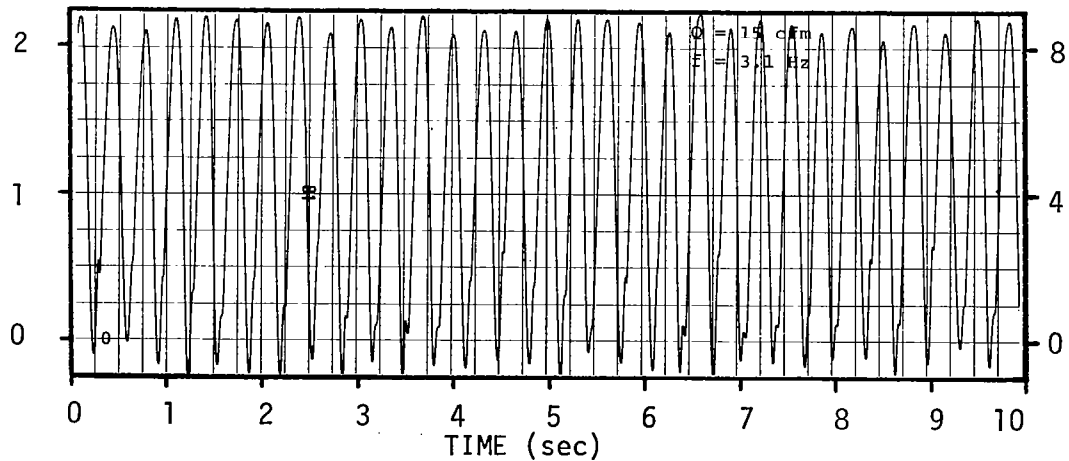
Figure 49. - Cushion pressure: ACLS test rig; 1-m gap; $X_0 = 5 \text{ cm}$ (2 in.).



(a) INLET FLOW, $Q_i = 0.14 \text{ m}^3/\text{min}$ ($5 \text{ ft}^3/\text{min}$)



(b) INLET FLOW, $Q_i = 0.28 \text{ m}^3/\text{min}$ ($10 \text{ ft}^3/\text{min}$)



(c) INLET FLOW, $Q_i = 0.42 \text{ m}^3/\text{min}$ ($15 \text{ ft}^3/\text{min}$)

Figure 50. - Cushion pressure: ACLS test rig;
10-cm gap; $X_o = 2.5 \text{ cm}$ (1 in.)

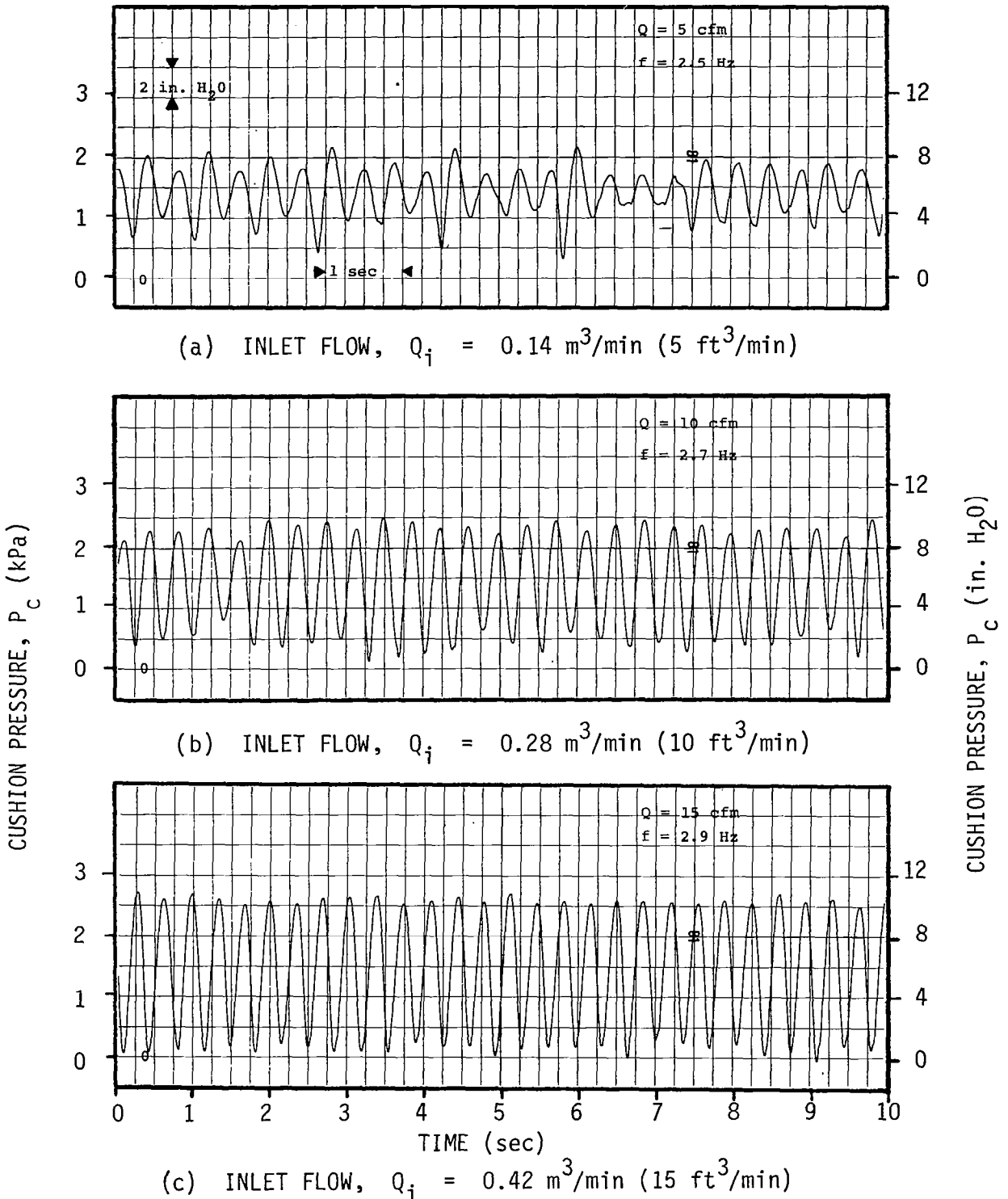
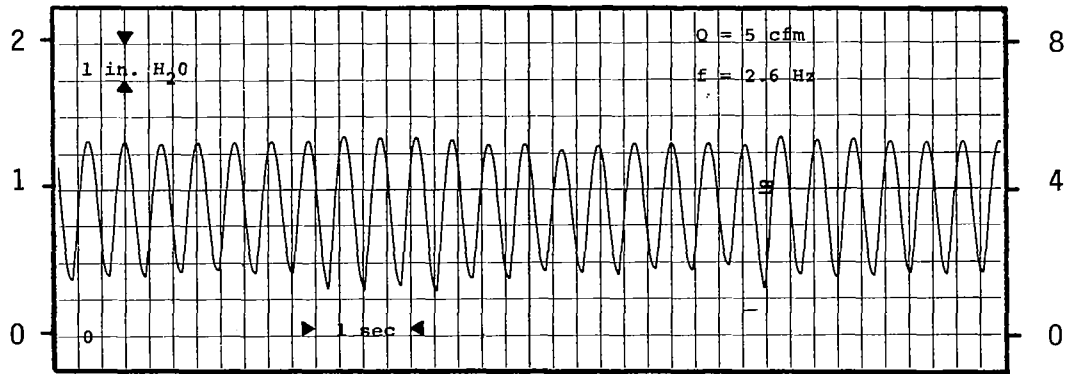
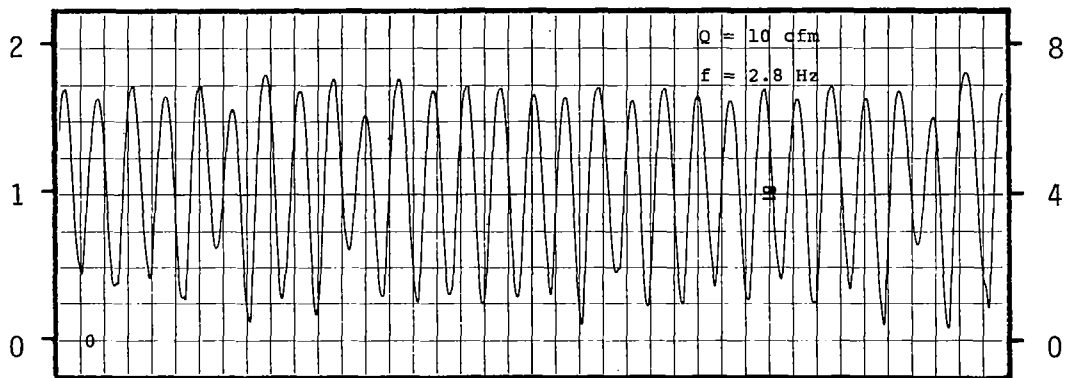


Figure 51. - Cushion pressure: ACLS test rig; 10-cm gap; $X_0 = 5 \text{ cm}$ (2 in.).



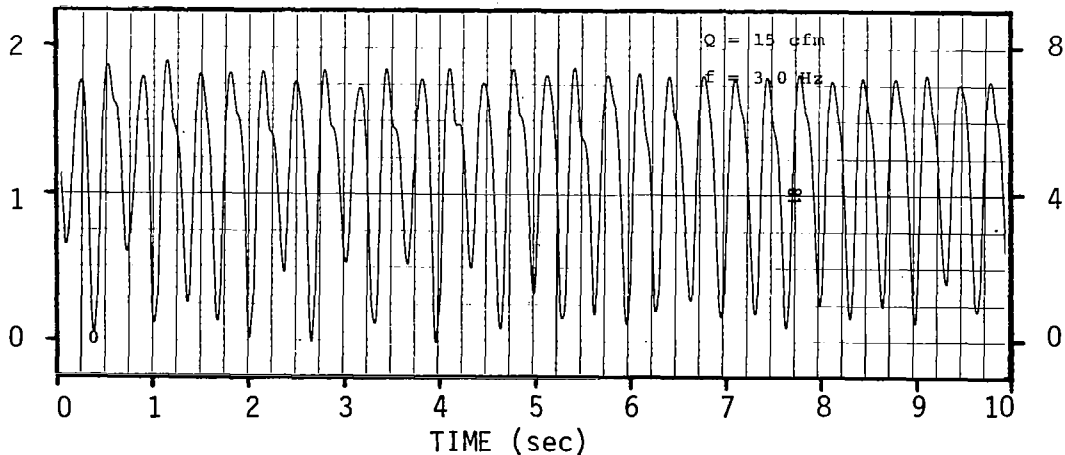
(a) INLET FLOW, $Q_i = 0.14 \text{ m}^3/\text{min}$ ($5 \text{ ft}^3/\text{min}$)



(b) INLET FLOW, $Q_i = 0.28 \text{ m}^3/\text{min}$ ($10 \text{ ft}^3/\text{min}$)

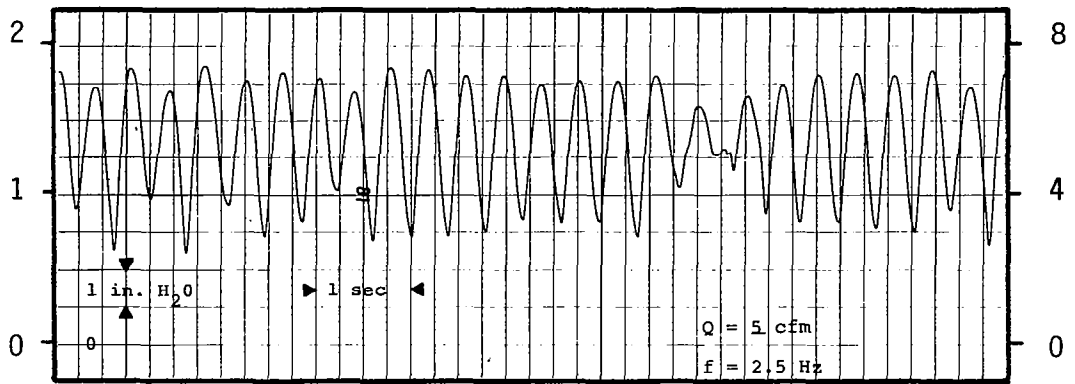
CUSHION PRESSURE, P_c (kPa)

CUSHION PRESSURE, P_c (in. H_2O)



(c) INLET FLOW, $Q_i = 0.42 \text{ m}^3/\text{min}$ ($15 \text{ ft}^3/\text{min}$)

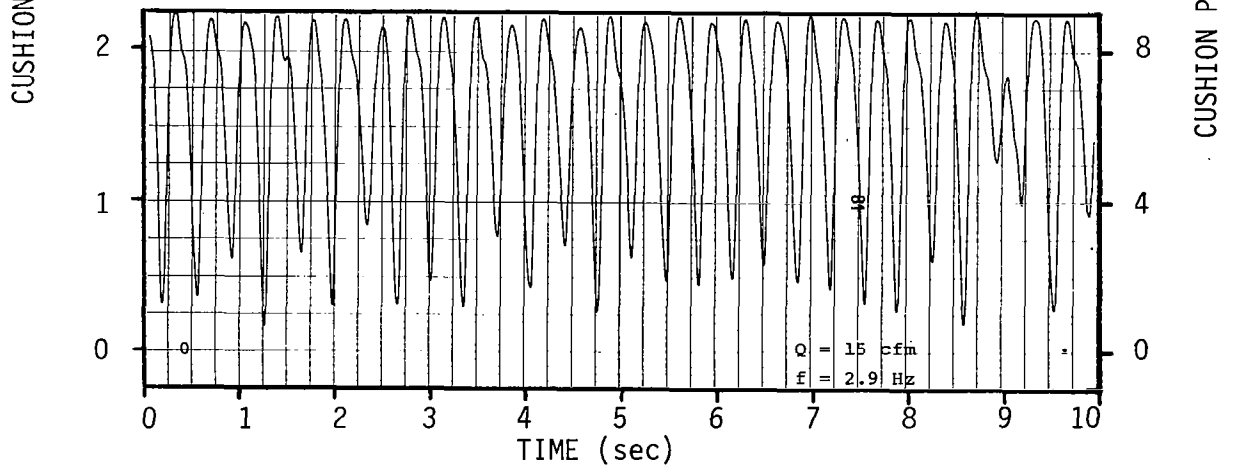
Figure 52. - Cushion pressure: ACLS test rig;
10-cm gap with baffle; $X_o = 2.5 \text{ cm}$ (1 in.).



(a) INLET FLOW, $Q_i = 0.14 \text{ m}^3/\text{min}$ ($5 \text{ ft}^3/\text{min}$)

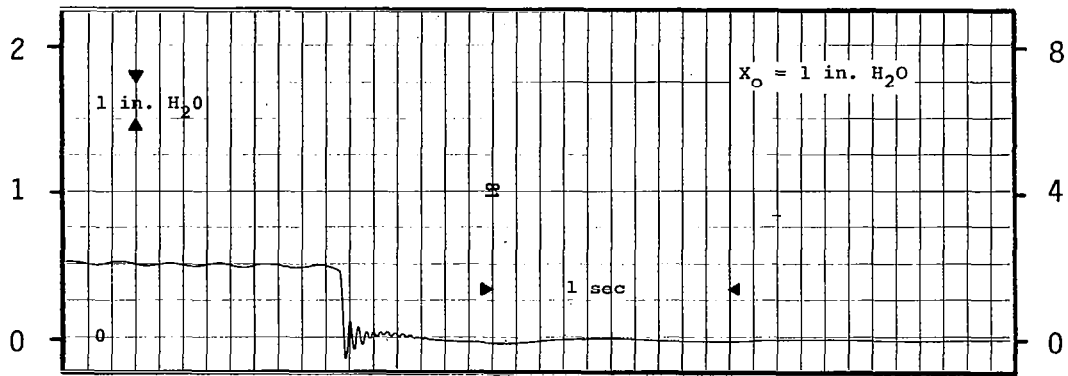


(b) INLET FLOW, $Q_i = 0.28 \text{ m}^3/\text{min}$ ($10 \text{ ft}^3/\text{min}$)



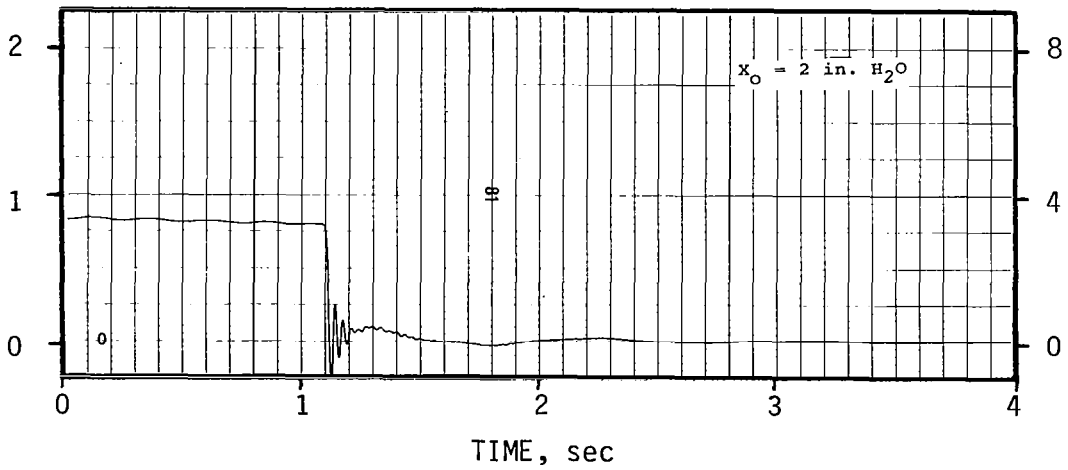
(c) INLET FLOW, $Q_i = 0.42 \text{ m}^3/\text{min}$ ($15 \text{ ft}^3/\text{min}$)

Figure 53. - Cushion pressure: ACLS test rig;
10-cm gap with baffle; $X_0 = 2 \text{ cm}$ (5 in.)



(a) $X_0 = 2.5 \text{ cm (1 in.)}$

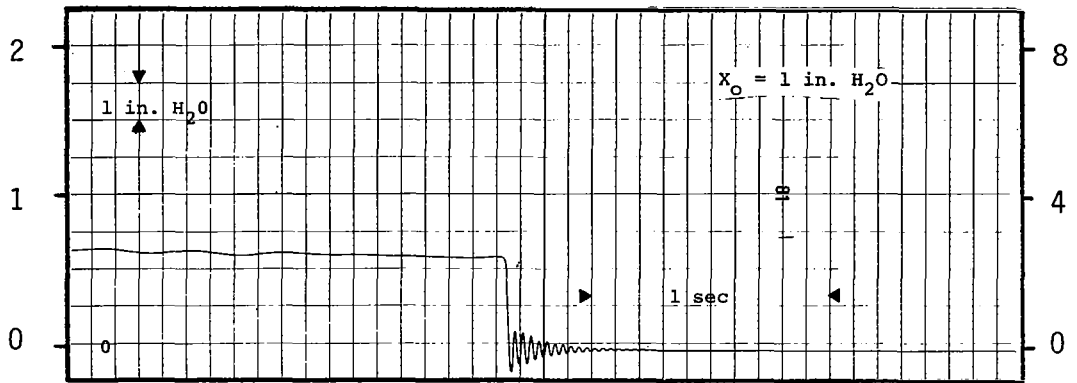
CUSHION PRESSURE, P_C (kPa)



(b) $X_0 = 5 \text{ cm (2 in.)}$

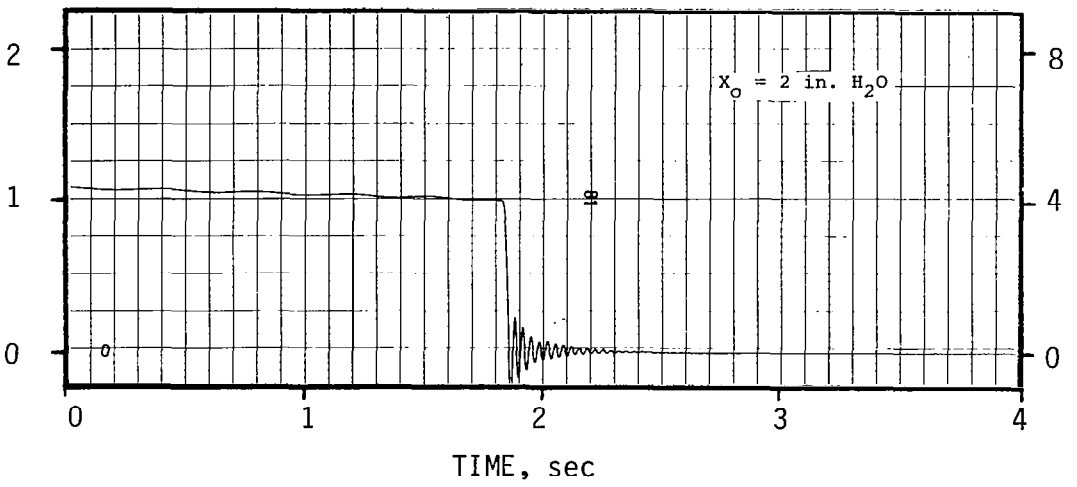
CUSHION PRESSURE, P_C (in. H_2O)

Figure 54. - Cushion pressure step response:
 ACLS test rig; 1-m gap.



(a) $X_0 = 2.5 \text{ cm (1 in.)}$

CUSHION PRESSURE, P_c (kPa)



CUSHION PRESSURE, P_c (in. H₂O)

(b) $X_0 = 5 \text{ cm (2 in.)}$

Figure 55. - Cushion pressure step response:
 ACLS test rig; 10-cm gap.

ANALYSIS

Approach

Given the complexity of the trunk discharge process as observed on the test rig, an initial analysis of the water dynamics based on fundamental fluid mechanical principles was not practical. The approach taken was to develop a simple lumped parameter model using empirical data to estimate parameter values. Two forms of dynamic system elements were found to be useful: mechanical system elements for developing a simulation model; and fluid system elements for investigating and identifying the essential mechanisms at work. After a basic understanding of the water dynamics was obtained, a more direct and rigorous derivation was formulated using the Bernoulli equation. The results of this derivation, however, remain to be incorporated in the simulation model. The analysis of the airflow dynamics is similar to that used in previous ACLS studies (ref. 1) and is based on fundamental fluid mechanical principles. The trunk gap flow is modeled by an orifice.

Model Development

The test rig model used for analysis is shown in Figure 56. The entire water system is represented by lumped parameter elements consisting of a mass, spring, and dashpot (M-K-B system).

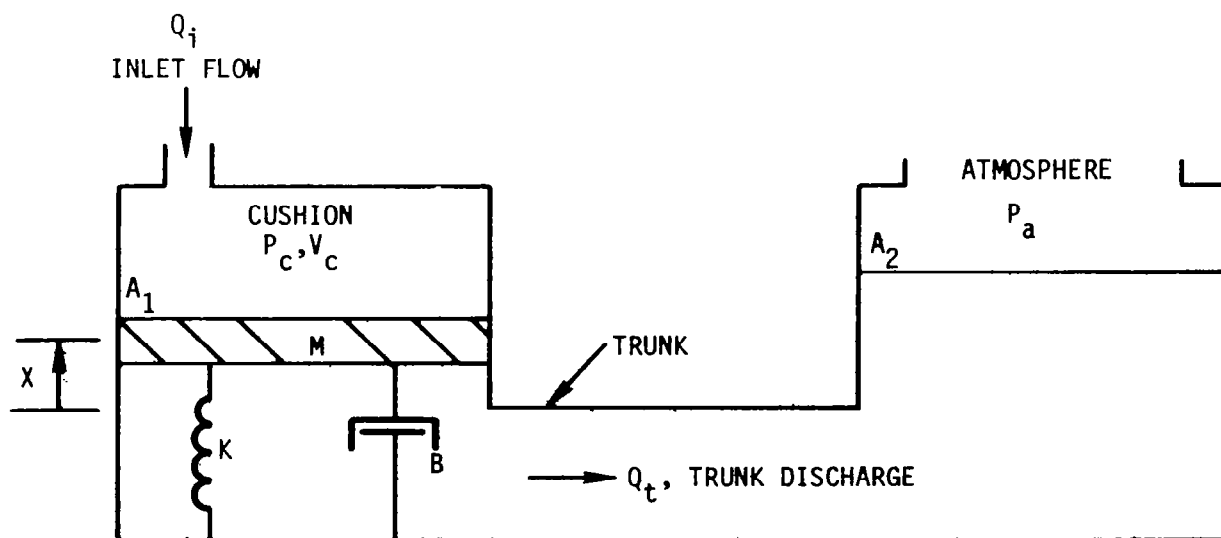


Figure 56. - Waterborne ACLS test rig model.

Mass position, X , relative to the trunk bottom represents the cushion-side water surface level. The essential assumption of the model is that the trunk gap is an orifice formed between the cushion-side water level and the trunk bottom -- that is, the gross motion of the water surface defines the gap formation process and the gross position of the water surface defines the orifice opening.

Water dynamics. - The dynamics of the water system are described by the second-order equation of motion for the mass,

$$M\ddot{X} + B\dot{X} + K(X - X_0) = -P_C A_1 \quad (1)$$

where

- M = the total effective water mass
- B = the damping of water flow from the cushion side to the atmospheric side
- K = the water compliance
- X = the water surface position
- X_0 = the initial water surface position (unpressurized cushion: $P_C = 0$)
- P_C = the cushion pressure (gauge)
- P_a = the atmospheric pressure (absolute)
- A_1 = the cushion side water surface area
- A_2 = the atmospheric side water surface area

The water compliance can be calculated directly from the model geometry:

$$K = \frac{\rho g A_1}{\left(1 + \frac{A_1}{A_2}\right)} \quad (2)$$

In the actual test rig, A_1 and A_2 vary slightly with X . For calculations, A_1 and A_2 are measured at $X = 0$ -- that is, near the operating point.

Given that the natural frequency, $f_n(\text{water})$, of the water system is known, the effective water mass can be calculated from

$$M = \frac{K}{(2\pi f_n(\text{water}))^2} \quad (3)$$

The damping coefficient for a specified damping factor, ζ , is given by

$$B = 2\zeta\sqrt{KM} \quad (4)$$

Air dynamics. - Conservation of mass flow requires that

$$\frac{d}{dt} (\rho_a V_c) = \rho_a (Q_i - Q_g) \quad (5)$$

where

V_c = the total cushion-side air volume

ρ_a = the air density

Q_i = the inlet flow

Q_t = the discharge through the trunk gap

From the polytropic (adiabatic) pressure-density relation,

$$\frac{P_c + P_a}{\rho_a^\gamma} = \text{constant} \quad (6)$$

where

$$\gamma \approx 1.4.$$

From equations (5) and (6),

$$\dot{P}_c = \frac{\gamma(P_c + P_a)}{V_c} (Q_i - Q_t - \dot{V}_c) \quad (7)$$

For small changes in the cushion-side water surface position, the water surface remains essentially constant, so that near the operating point

$$\dot{V}_c = -A_1 \dot{X} \quad (8)$$

and

$$V_c = V_{c0} - A_1 X \quad (9)$$

where V_{c0} is the total cushion-side air volume at $X = 0$.

Trunk gap flow. - The flow through the trunk gap is based on an orifice model,

$$Q_t = C_d A \sqrt{\frac{2 \Delta P}{\rho}}$$

where

C_d = the discharge coefficient

A = the orifice area

ΔP = the pressure across the orifice

ρ = the water density

For the water and air dynamics models given above,

$$Q_t = \begin{cases} C_d \times l_g \sqrt{\frac{2P_c}{\rho}} & ; X < 0 \text{ and } P_c > 0 \\ 0 & ; \text{otherwise} \end{cases} \quad (10)$$

where l_g is the gap length. Note that l_g is defined by the test rig geometry and is not necessarily the orifice length formed during the discharge process.

System dynamics. - Equations (1) and (7) describe a third-order nonlinear dynamic system. Note that a nonlinearity arises out of the interaction of the air and water dynamics through the cushion volume terms in equation (7), as well as in the expression for the trunk gap flow in equation (10).

System Frequency

Investigation of the natural frequency characteristics of the water and air dynamics provides additional insight into the operation of the test rig. Fluid system elements are used to derive lumped parameter models for the air dynamics and water dynamics. Determination of the combined air-water system natural frequency then follows by simple analysis.

Fluid system element analysis. - The fluid system elements of interest here are those which characterize the mechanisms of fluid energy storage. A description of dynamic linear system representation using these elements is given in ref. 7. The analysis here, therefore, is based on a linearization of the air and water systems.

The fluid capacitance of the cushion air and the water can be readily calculated from the geometry of the test rig. They are given, respectively, by

$$C_a = \frac{V_c}{\gamma(P_c + P_a)}$$

and

$$C_w = \frac{A_1}{\left(1 + \frac{A_1}{A_2}\right) \rho g}$$

where all variables are as previously defined.

The fluid inertance, on the other hand, is not readily related to obvious geometrical quantities. However, if the natural frequencies of each system can be determined, then the fluid inertances of the cushion air and the water can be approximated, respectively, by

$$I_a = \frac{1}{C_a (2\pi f_n(\text{air}))^2}$$

and

$$I_w = \frac{1}{C_w (2\pi f_n(\text{water}))^2}$$

where $f_n(s)$ is the natural frequency of system, "s".

The fluid element representation of the test rig is a series connection of the above inertances and capacitances (Appendix D). The natural frequency of the linearized air-water system is given by

$$f_n(s) = 2\pi \left[\frac{C_a + C_w}{C_a C_w} \frac{1}{I_a + I_w} \right]^{1/2}$$

For the test rig, $C_w \gg C_a$ and $I_w \gg I_a$; hence,

$$f_n(s) \approx \sqrt{\frac{I}{C_a I_w}} = \sqrt{\frac{C_w}{C_a}} f_n(\text{water}) \quad (11)$$

The system natural frequency can be determined from the geometry of the test rig and the measured value of the water system natural frequency. Using the data on Table 6 and $f_n(\text{water}) = 1$ Hz, equation (11) gives $f_n(s) = 4.4$ Hz for the 1-m gap.

TABLE 6. - TEST RIG DATA

X_o	Units cm(in.)	1-m Gap		10-cm Gap	
		2.5(1.0)	5.0(2.0)	2.5(1.0)	5.0(2.0)
A_1	m^2 (ft ²)	0.305(2.83)	a	a	a
A_2	m^2 (ft ²)	0.201(1.86)	0.221(2.06)	b	b
A_3	m^2 (ft ²)	0.242(2.25)	c	0.0262(0.243)	c
V_{CO}	m^3 (ft ³)	0.100(2.83)	a	a	a
l_g	m(in.)	0.94(37.0)	c	0.10(4)	c
l_1	m(in.)	0.10(4.0)	a	a	a
l_2	m(in.)	0.18(7.0)	a	a	a
l_3	m(in.)	0.10(4.0)	a	a	a
θ_1	rad	1.57	a	a	a
θ_2	rad	1.38	1.19	b	b

NOTES:

a = Constant for all gap configurations and water levels, X_o .

b = Constant for same X.

c = Constant for same gap configuration.

Comparison with the test values in Figure 47 suggests strongly that the discharge frequency is evidently determined by natural frequency of the air-water system. Moreover, equation (11) indicates that the essential system elements are the water inertance and the air capacitance; or by analogy to their mechanical equivalents, the water mass and the air compliance. Further verification of this result is provided in the following section. It should be stressed that the relative importance of air and water storage mechanisms depends strongly on the geometry and operational parameters, so that the approximations above must be re-examined for other (e.g., full-scale) cases.

Fluid mechanical analysis. - The results of the fluid system element analysis indicate that accurate predictions of the discharge frequency can be determined provided the natural frequency of the water system is known. Such an empirical method is less than ideal for design purposes. As an alternative to using test data, a more rigorous derivation of the water system dynamics was formulated using the Bernoulli equation. The result is a second-order nonlinear differential equation with a characteristic system frequency (Appendix E) given by

$$f_n(\text{water}) = 2\pi \left[\frac{g(1+a)}{\ell_1 \theta_1 + \ell_2 \theta_2 a + \ell_3 b} \right] \quad (12)$$

where

$$a = A_1/A_2$$

$$b = A_1/A_3$$

$$A_1, A_2 = \text{as previously defined}$$

$$A_3 = \text{the gap area (defined by the gap length, } \ell_g \text{ and the height of the trunk bottom above the tank floor)}$$

$$\ell_1, \ell_2, \ell_3 = \text{streamline lengths}$$

$$\theta_1, \theta_2 = \text{streamline parameters in evaluating the Bernoulli equation (Appendix E)}$$

The calculated system frequency, using equations (11) and (12) and the test rig data in Table 6 are presented in Table 7 along with the measured values (Figures 48 through 53) and the simulated values (next section). The calculated values are in close agreement with both the measured and simulated values. Note that the form of equation (12) is particular to the geometry of the test rig and caution must be exercised if it is to be applied to other ACLS configurations.

Simulation Results

Computer simulation of the test rig was carried out using the lumped parameter M-K-B model described above. Parameter values for this model were established by calculating the compliance, K , from equation (2), the mass, M , from equation (3), the water system frequency, $f_n(\text{water})$, from equation (12), and the damping coefficient, B , from equation (4). The only test data used in evaluating these parameters are the damping factors; $\zeta = 0.4$, the value established for the 1-m gap, is used for both the 1-m gap and 10-cm gap configurations, since in the latter case it could not be determined from the step response tests. Table 8 summarizes the data for the parameter model values. Note that although the compliance, K , is the same for both the 1-m gap and the 10-cm gap configurations, the mass, M , is significantly different. The distance with which a fixed volume of water must move to pass through the gap is much larger for the 10-cm gap than the 1-m gap. Thus the effective mass for the 10-cm gap is larger. The discharge coefficient C_d , for the 10-cm gap was set substantially greater than unity in order to obtain a satisfactory match between the observed and simulated discharge behavior.

TABLE 7. - SYSTEM FREQUENCY

X_o , cm (in.)	1-m Gap		10-cm Gap	
		2.5 (1.0)	5.0 (2.0)	2.5 (1.0)
Measurement, Hz*	4.5 to 4.7	4.2 to 4.3	2.6 to 3.1	2.5 to 2.9
Calculation, Hz	4.2	4.1	2.6	2.6
Simulation, Hz*	4.2 to 3.9	3.8 to 4.1	2.6 to 2.3	2.5 to 2.4

*For inlet flows, Q_i , of 0.14 to 0.42 m³/min (5 to 15 ft³/min).

TABLE 8. - MODEL PARAMETERS

X_o	Units	1-m Gap		10-cm Gap	
	cm(in.)	2.5(1.0)	5.0(2.0)	2.5(1.0)	5.0(2.0)
M	kg(slug)	177(12.1)	188(12.9)	457(31.3)	468(32.0)
K	N/m(lb/ft)	5.04(453)	4.74(426)	5.04(453)	4.74(426)
B	$\frac{N\text{-sec}}{m}$ ($\frac{lb\text{-sec}}{ft}$)	864(59.2)	865(59.3)	1390(95.3)	1363(93.4)
C_d	-	0.5	0.5	4.0	4.0

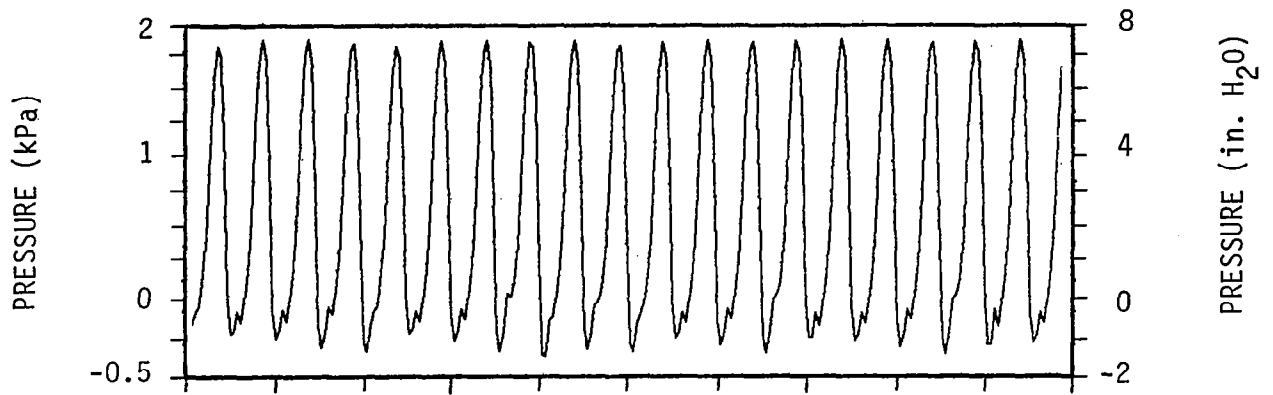
As a result, the product of the orifice area and discharge coefficient is almost the same for the 1-m and 10-cm gap configurations.

Cushion pressure frequencies obtained from the simulations are summarized on Table 7. Simulated values are in close agreement with the calculated and measured values. However, the simulation in most cases predicts the opposite trend in frequency change with inlet flow when compared with the measured data. This may be due to an overly simplistic trunk gap flow model (orifice model).

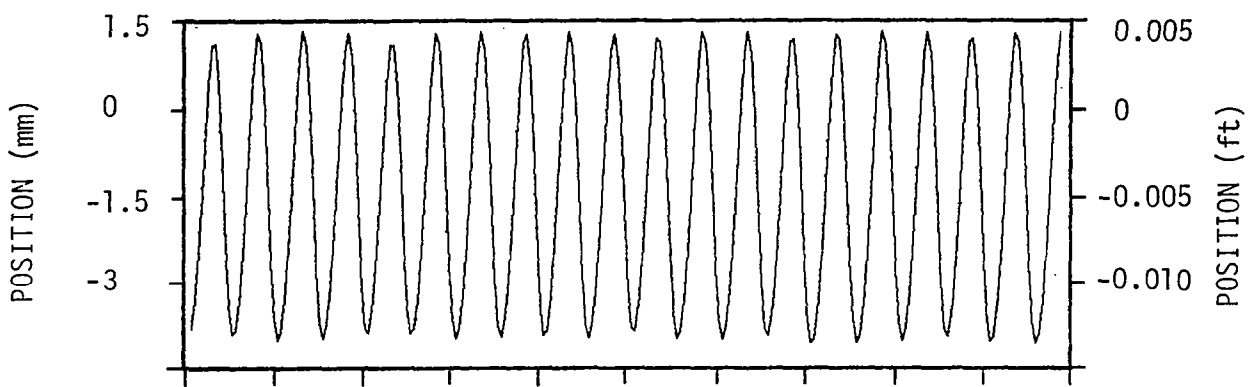
Cushion pressure and cushion-side water surface position and velocity profiles for selected simulation runs are shown in Figures 57 through 60. The pressure profiles are quite similar in shape to the measured profiles except that amplitude envelope modulation is not present (surface wave effects are not modeled). There is also some similarity in the small perturbations in the vicinity of the zero pressure point. In the simulated profiles, these perturbations occur regularly near zero pressure implying some probable connection with the negative pressure cutoff point in the gap flow model. In the measured profiles, however, the perturbations are not always present and frequently occur at low positive pressures. These differences have not been resolved but may also be partly due to unmodeled surface wave effects. The simulated peak-to-peak pressure amplitudes are somewhat greater than the maximum measured peak-to-peak values. There are two probable causes for this difference: in the test rig, the water surface does not act entirely like a piston, as in the model; and in the model, no damping has been included in the air dynamics. Increasing the water damping alone is insufficient to bring the peak-to-peak values into agreement.

Comparison of the phasing of the cushion pressure and water surface position and velocity profiles provides some insight into the dynamics of the test rig. Cushion pressure is strongly coupled to the water surface velocity: the pressure rises when the velocity is positive and falls when the velocity is negative (piston effect). The slope of the pressure profile is somewhat steeper on the falling side due to the trunk discharge. The trunk gap is closed (positive surface position) at peak pressures, and the pressure begins to fall before the gap opens (negative surface position). Inlet flow effects are negligible.

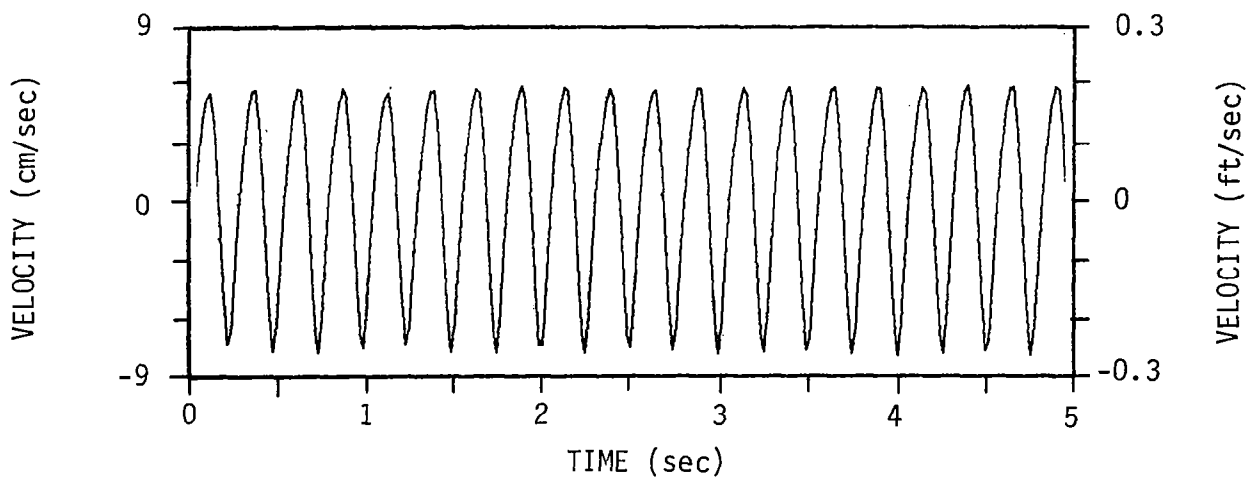
The fact that the simulation reproduces the fundamental characteristics of the test rig, despite probable modeling inaccuracies in the discharge process, would seem to be due to the basic behavior of the system as a quasiharmonic oscillator. The frequency of such an oscillator is determined primarily by the values of the energy storage elements (in this case, the water



(a) CUSHION PRESSURE, P_c



(b) CUSHION-SIDE WATER SURFACE POSITION, X



(c) CUSHION-SIDE WATER SURFACE VELOCITY, \dot{X}

Figure 57. - ACLS test rig simulation: 1-m gap;
 $X_0 = 2.5 \text{ cm (1 in.)}$; $Q_1 = 0.42 \text{ m}^3/\text{min (15 ft}^3/\text{min)}$

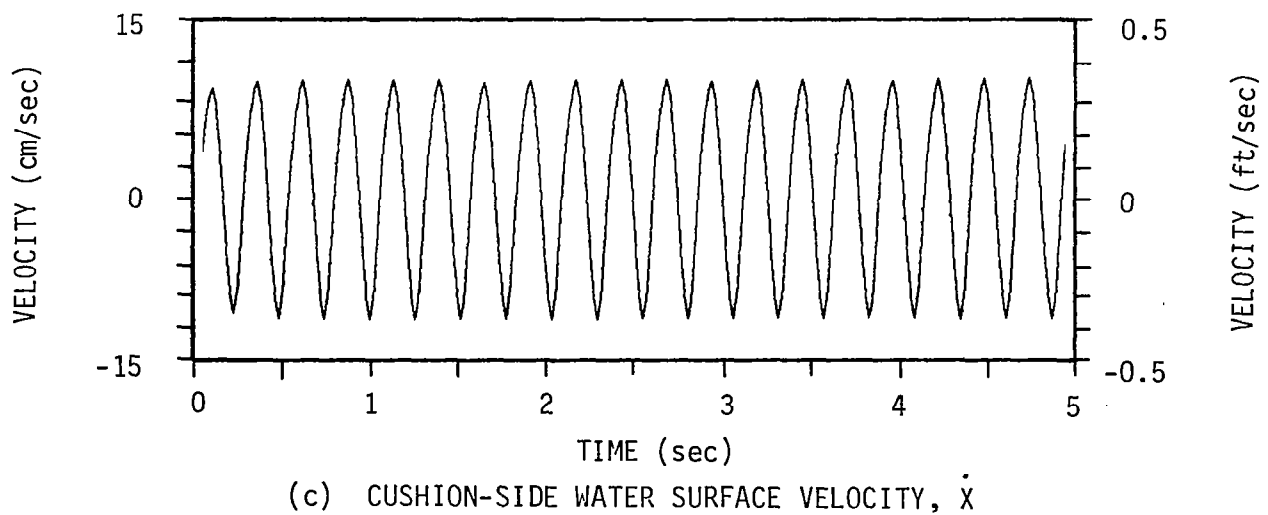
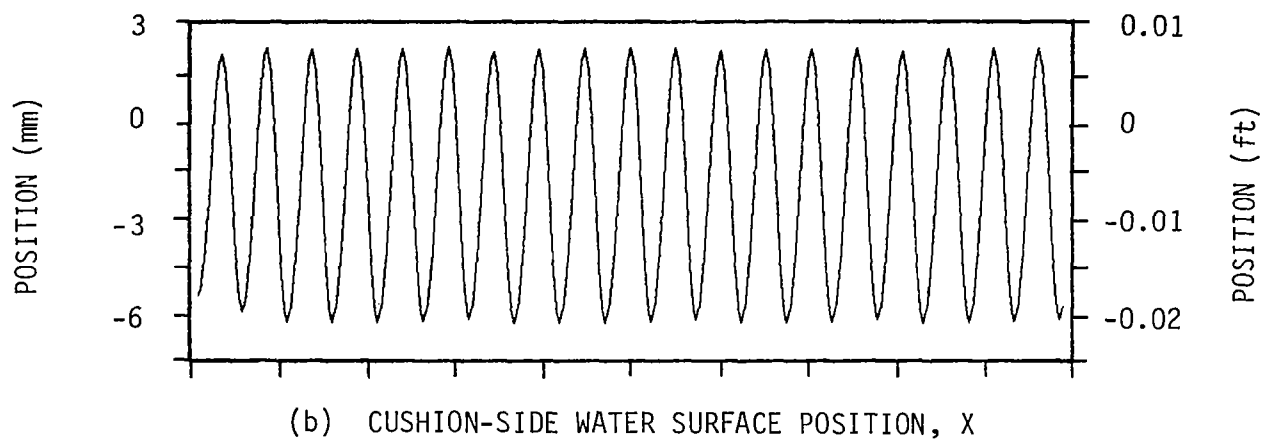
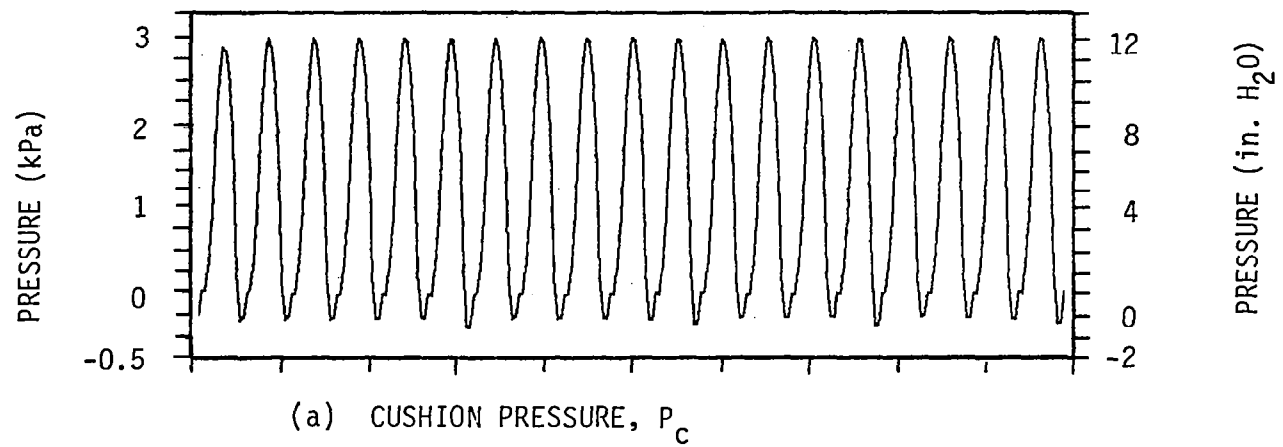
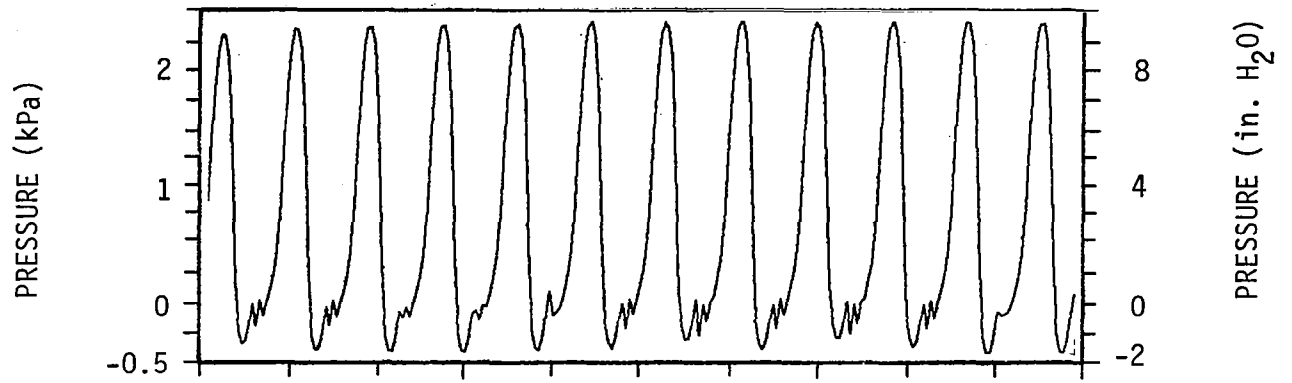
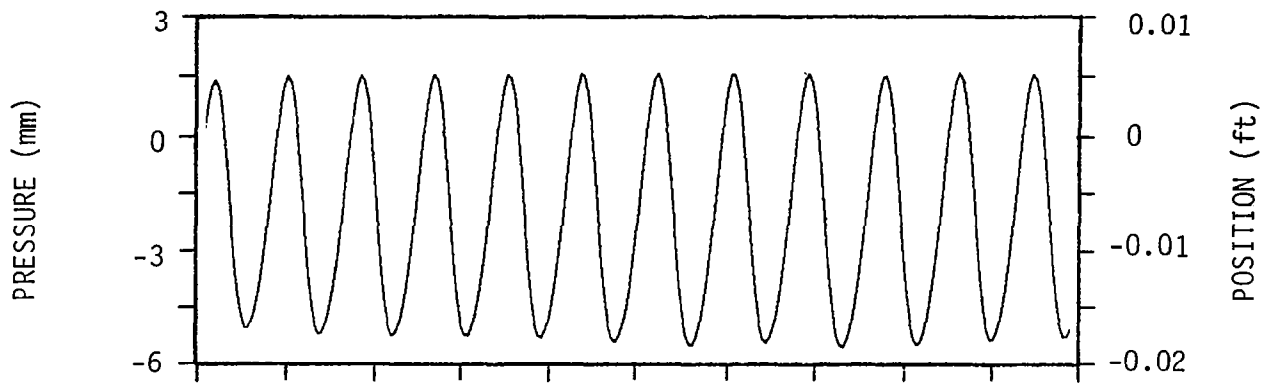


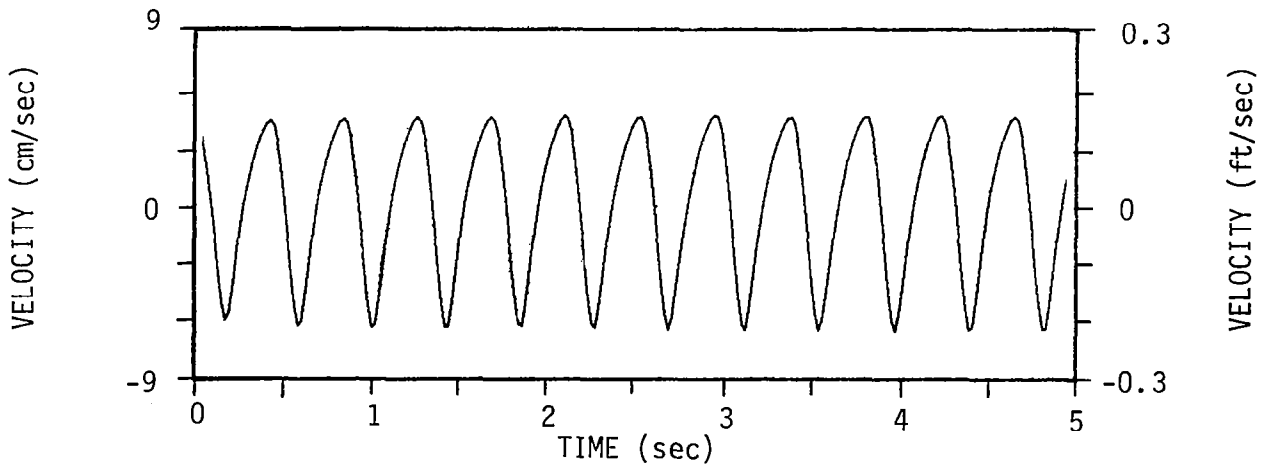
Figure 58. - ACLS test rig simulation: 1-m gap;
 $X_o = 5 \text{ cm (2 in.)}$; $Q_i = 0.42 \text{ m}^3/\text{min (15 ft}^3/\text{min)}$



(a) CUSHION PRESSURE, P_c

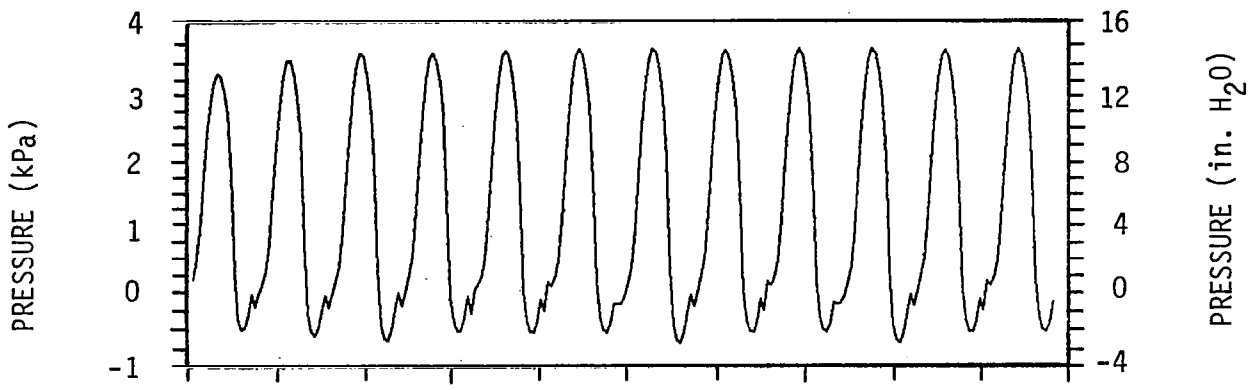


(b) CUSHION-SIDE WATER SURFACE POSITION, X

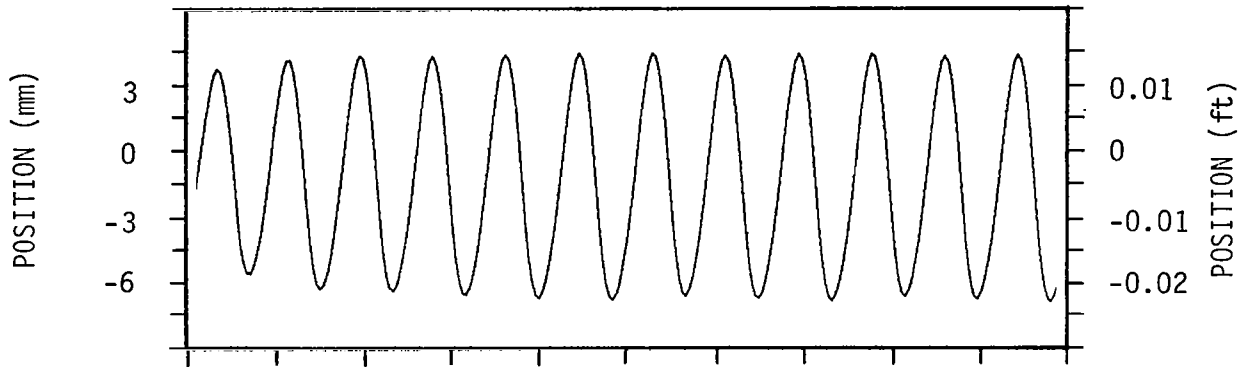


(c) CUSHION-SIDE WATER SURFACE VELOCITY, \dot{X}

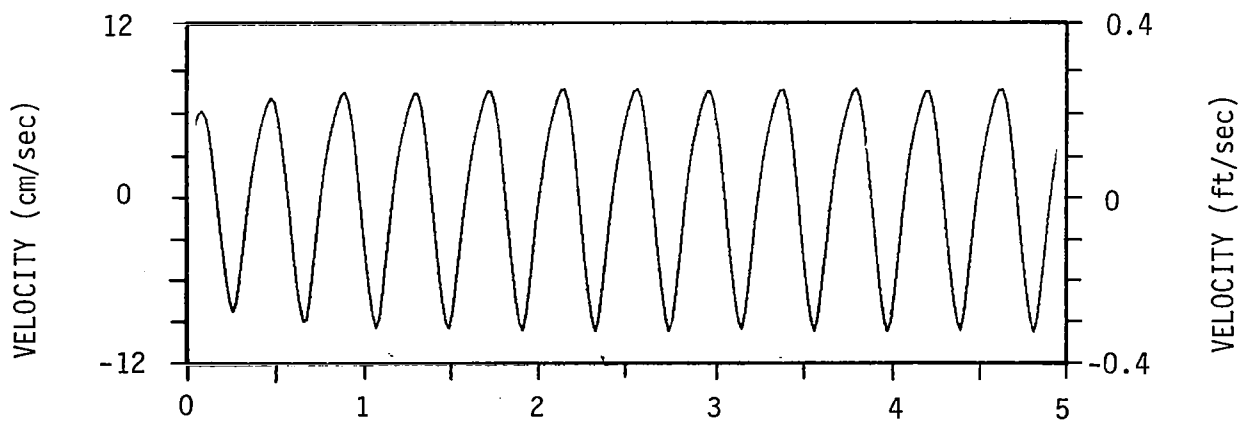
Figure 59. - ACLS test rig simulation: 10-cm gap;
 $X_0 = 2.5 \text{ cm (1 in.)}$; $Q_i = 0.42 \text{ m}^3/\text{min (15 ft}^3/\text{min)}$



(a) CUSHION PRESSURE, P_C



(b) CUSHION-SIDE WATER SURFACE POSITION, X



(c) CUSHION-SIDE WATER SURFACE VELOCITY, \dot{X}

Figure 60. - ACLS test rig simulation: 10-cm gap;
 $X_0 = 5 \text{ cm (2 in.)}$; $Q_i = 0.42 \text{ m}^3/\text{min (15 ft}^3/\text{min)}$

inertance and the air compliance) in the system and not by any elements which dissipate or supply energy (the trunk discharge and the inlet flow) (ref. 6).

Figure 61 illustrates a typical phase-plane portrait for the cushion pressure and the trunk discharge. The overall characteristic is that of a limit cycle. Due to the flow cutoff when the cushion pressure is negative, the limit cycle does not assume the nearly circular pattern expected for a quasiharmonic oscillator.

Model Limitations

Although the predictions of the test rig model and the computer simulation results are in reasonably close agreement with experimental data, several model features require further examination.

The shortcomings of the trunk gap flow model have already been noted, and further work is required to produce a more realistic discharge characteristic. The formation and discharge of bubbles is fundamentally a discontinuous mechanism which is only crudely represented by an orifice model; future work should involve a closer examination of bubble mechanics. A full-scale waterborne ACLS may not be characterized by a quasiharmonic oscillator, and the details of the trunk discharge process may have a greater impact on system behavior than in the test rig.

Although the lumped parameter M-K-B model for the water system has a sound physical basis, it is an indirect model and is partially empirical. Direct use of the differential equations resulting from the analysis using the Bernoulli equation would be a substantial improvement, but some means of incorporating damping into the equations needs to be investigated. Both approaches to modeling the water dynamics treat the water surface as a single element. This may have some impact on the development of an improved trunk gap flow model. Also, the single-element assumption may not extend to a full-scale waterborne ACLS, especially considering the close coupling between the cushion pressure and the water surface dynamics.

Finally, the model is restricted to a rigid, impermeable trunk, fixed in a small two-dimensional test rig. Extension to other geometries - especially to large areas of open water - appears feasible but has not been investigated. A flexible trunk would introduce its own dynamics, as would a finite vehicle mass. The simple model nevertheless represents a good basis for subsequent analysis.

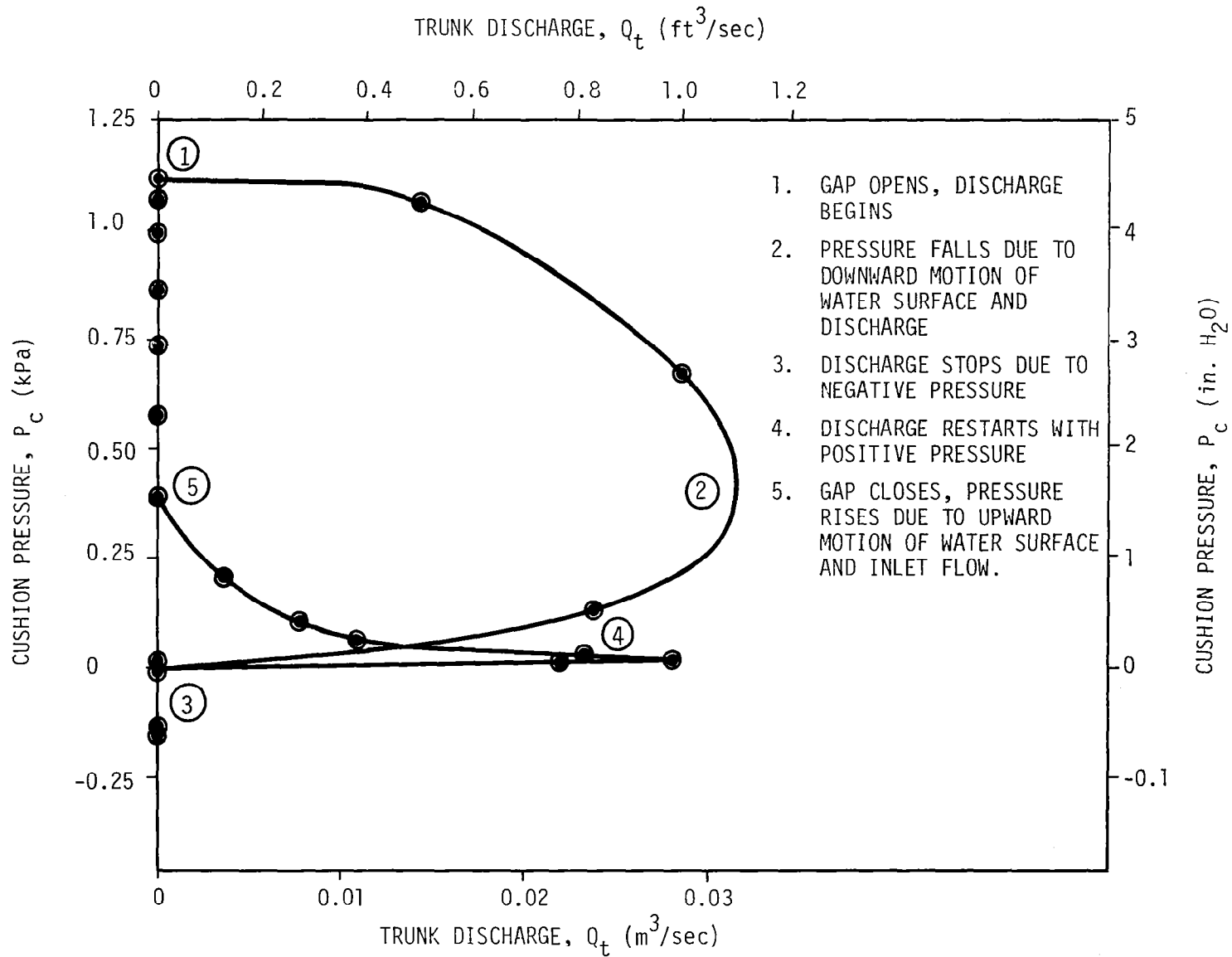


Figure 61. - Cushion pressure-trunk discharge phase portrait; ACLS test rig simulation; 10-cm gap.

CONCLUSIONS AND RECOMMENDATIONS

A two-dimensional, reduced-scale, rigid-impermeable-trunk test rig has been constructed, and an analytical model and computer simulation have been developed to investigate the trunk discharge dynamics of a waterborne air cushion landing system (ACLS). Testing has shown that the discharge from the air cushion to the atmosphere is a discontinuous, periodic process occurring at a frequency dependent primarily on the geometry of the test rig. Through analysis, the relationships between the geometry and lumped parameter model elements have been established, and the essential elements responsible for the frequency of the discharge process identified. Comparison of initial simulation results with test data shows that the model can predict much of the system behavior within a margin of 5 to 25 percent.

Results to date are of a distinctly preliminary character, and additional analytical work still remains to be performed despite the successes of the dynamic model in matching experiments. The model of the test rig is nonlinear and displays the characteristics of a quasiharmonic oscillator - that is, the oscillation frequency is established primarily by the values of energy storage elements in the system, and not by any elements which dissipate or supply energy. Consequently, shortcomings in some of the model elements, notably the trunk gap flow model, are not particularly obvious. Also, the lumped parameter model used for simulation purposes is an indirect analog and is partially empirical. A second model, derived from fundamental principles, has been initiated and used to evaluate some of the model parameters in lieu of test data. Both models treat the cushion-side water surface as a single element or piston, so wave motion is ignored. Finally, the rigid trunk and mounting system do not show dynamic coupling which would be observed in practice.

The presence of moderate to low frequency oscillations in an aircraft landing system is a serious concern, since they may result in undesirable excitation of the aircraft body structural modes. The current state of the model, however, does not purport to be adequate to predict full-scale system performance. Although the results to date are encouraging, further work is required. Recommendations for the next phase of development include:

1. Establishing the existing model concept on the basis of fundamental principles.
2. Modifying the trunk gap flow model for greater realism.

3. Investigation of a multi-element cushion-side water surface model.

4. Computer simulation and verification against test rig data.

5. Conversion of the test rig to accommodate flexible trunks.

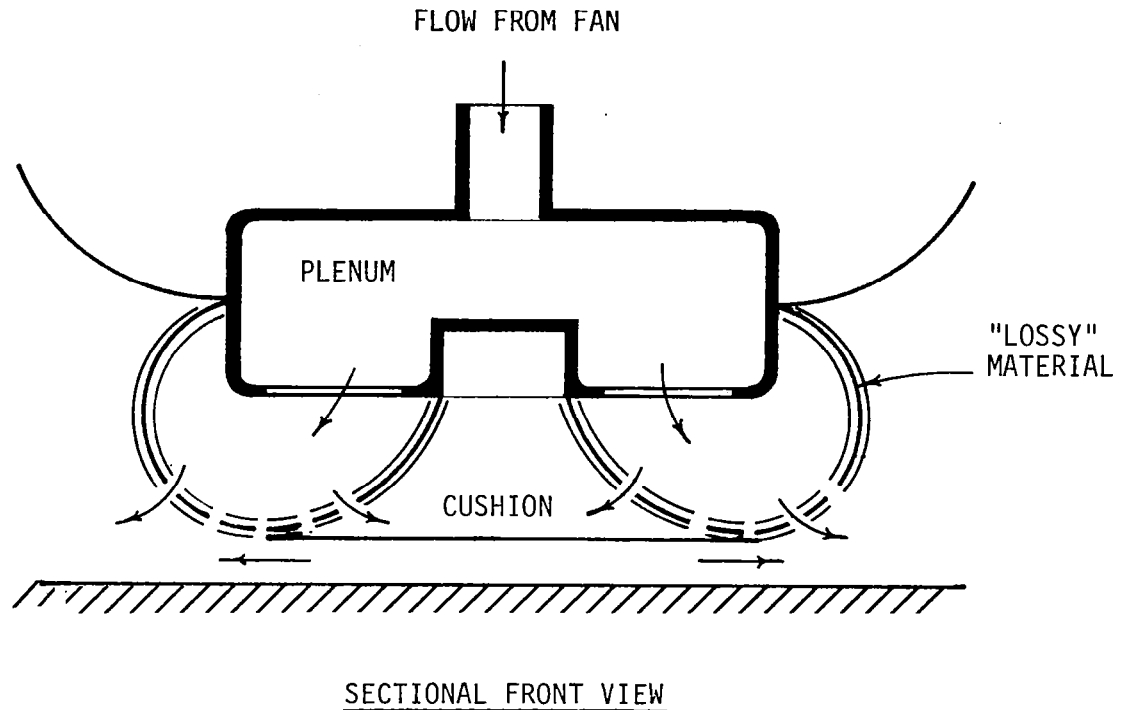
6. Development of a basic heave model for the analysis of the vehicle-trunk-water system.

In addition, a more thorough examination of hovercraft literature should be carried out in order to identify similarities to ACLS waterborne operation.

APPENDIX A

DESCRIPTION OF NOVEL ACLS CONCEPTS

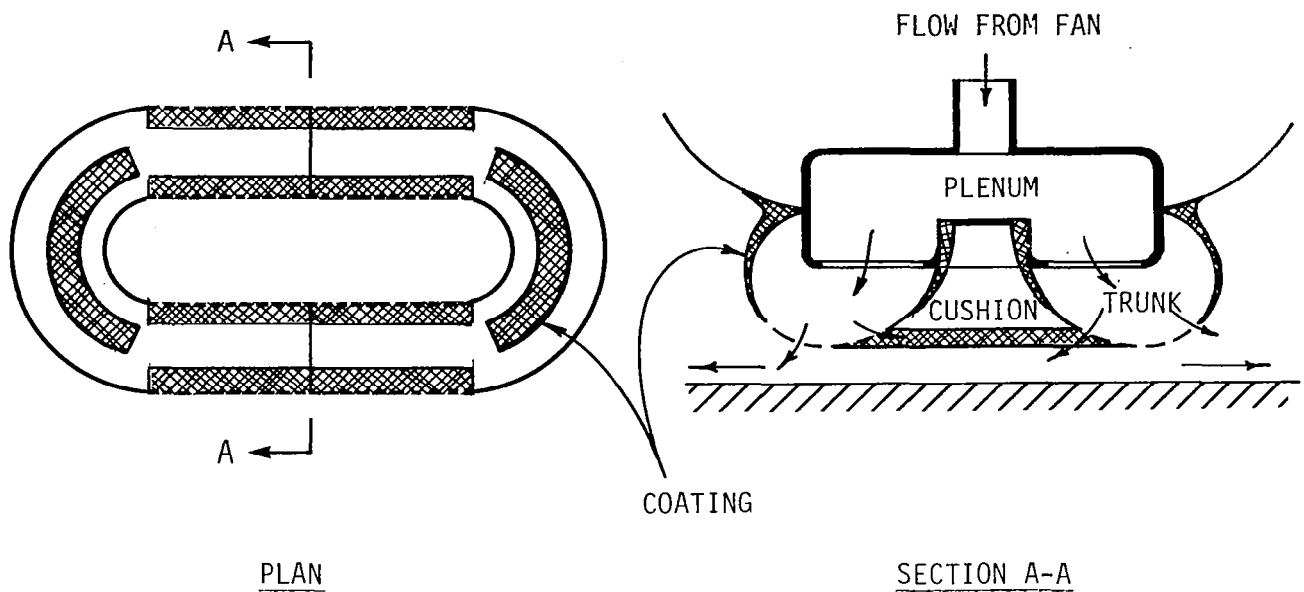
The initial concept generation phase identified 10 novel concepts for improved ACLS. These concepts are described in Figures 62 through 71.



DESCRIPTION: TRUNK MADE OUT OF A LOSSY MATERIAL TO INCREASE OVERALL DAMPING AND IMPROVE SYSTEM STABILITY.

- FEATURES:
- HIGH FLEXURAL DAMPING OF THE TRUNK MATERIAL
 - CAN BE MADE FROM SINGLE MATERIAL OR SANDWICH COMPOSITE.

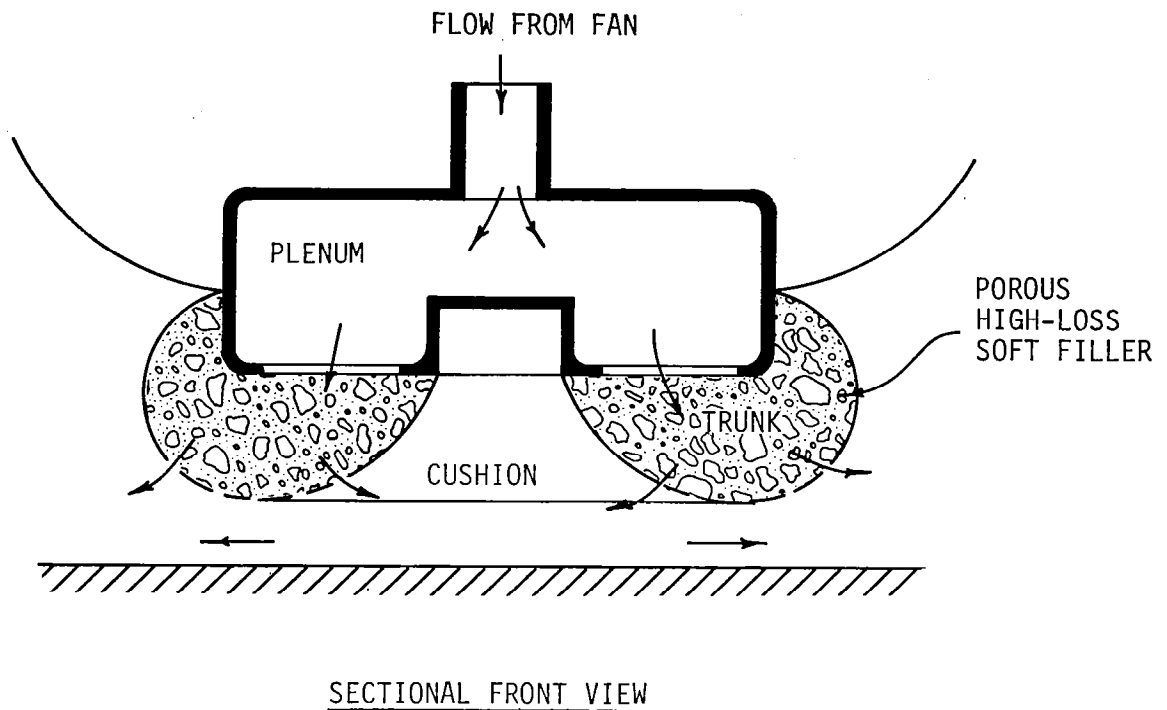
Figure 62. - Damped trunk.



DESCRIPTION: THE TRUNK IS COATED WITH HIGH DAMPING MATERIAL AT SELECTED ZONES OF HIGH FLEXURE. THESE PLACES INCLUDE THE BOTTOM OF THE TRUNK ENDS AND THE TRUNK ATTACHMENT REGION. INCREASING THE DAMPING OF THE TRUNK SHOULD IMPROVE THE DAMPING AND STABILITY OF THE OVERALL SYSTEM.

- FEATURES:
- INCREASES FLEXURAL LOSSES AT PLACES WHERE THE TRUNK UNDERGOES HIGH FLEXURE
 - COATING MAY BE APPLIED ON THE INSIDE TO PREVENT WEAR
 - MAY BE EASIER TO FABRICATE THAN THE DAMPED TRUNK.

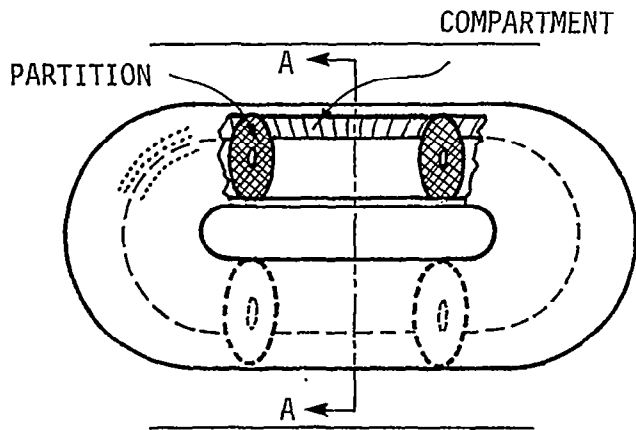
Figure 63. - Coated trunk.



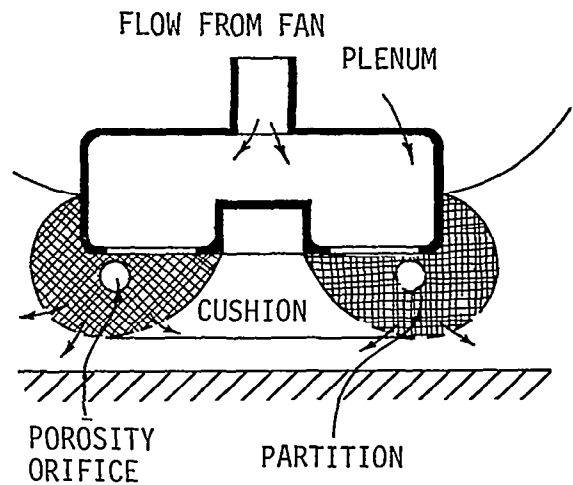
DESCRIPTION: THE TRUNK IS FILLED WITH A POROUS HIGH-LOSS SOFT MATERIAL (SUCH AS FOAM) THAT PROVIDES EXTRA DAMPING WHEN THE TRUNK CROSS-SECTION CHANGES DYNAMICALLY.

- FEATURES:
- SIMPLE TO IMPLEMENT AND COMPATIBLE WITH A WIDE VARIETY OF TRUNK DESIGNS
 - INCREASES TRUNK DAMPING INDEPENDENT OF THE TRUNK MATERIAL CHARACTERISTICS
 - DIFFICULT FOR RETRACTION AND STOWAGE.

Figure 64. - Filled trunk.



PLAN



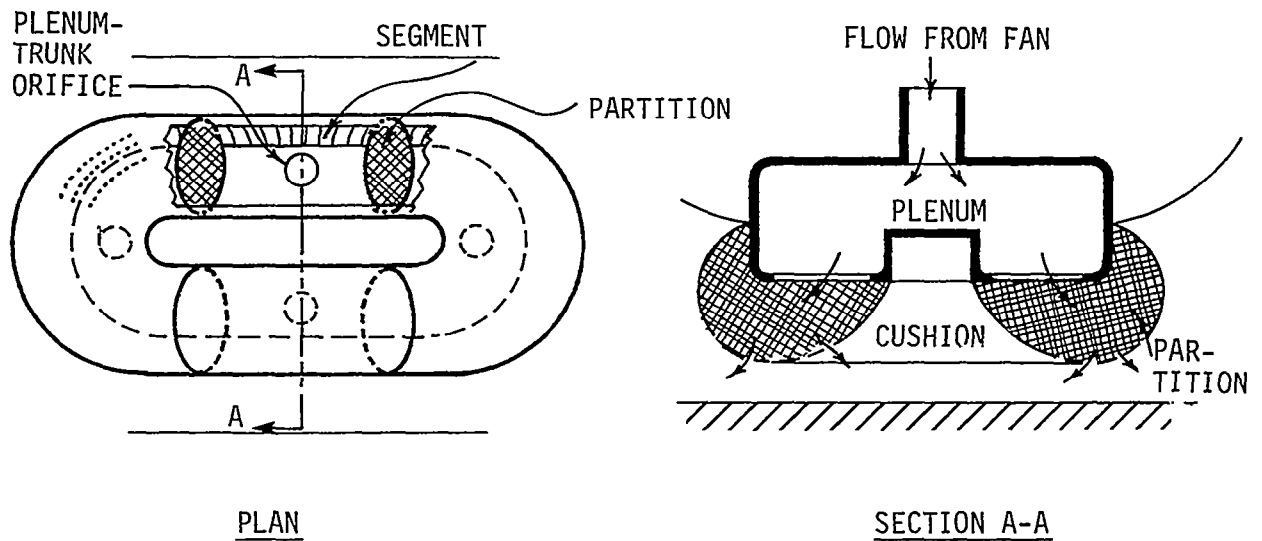
SECTION A-A

DESCRIPTION: THE TRUNK IS DIVIDED INTO SEVERAL COMPARTMENTS BY FLEXIBLE PARTITIONS WITH ORIFICES. THE TRUNK CAN BE FED BY ONE OR MORE ORIFICES.

FEATURES:

- ORIFICES IN THE PARTITIONS INCREASE FLUID DAMPING
- IN DYNAMIC OPERATION, THE PRESSURE DIFFERENCE BETWEEN THE VARIOUS COMPARTMENTS WILL INCREASE ROLL (AND PITCH) STIFFNESS
- THE POTENTIAL FOR FAN STALL IS REDUCED BECAUSE THE ORIFICES HELP ISOLATE THE TRUNK COMPARTMENTS FROM THE AIR SOURCE.

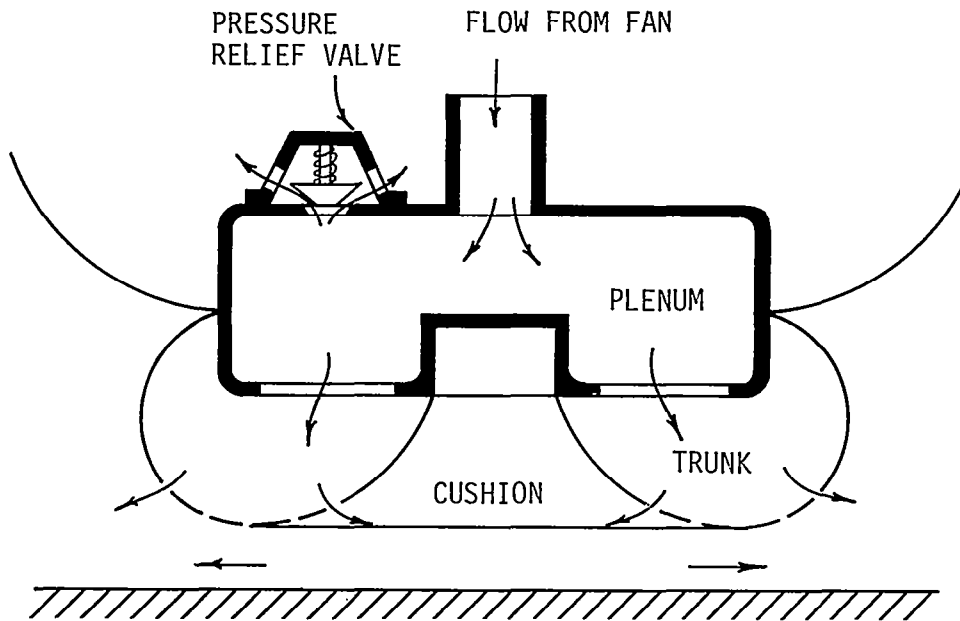
Figure 65. - Compartmented trunk.



DESCRIPTION: THE TRUNK IS MADE UP OF FOUR OR MORE INDEPENDENT SEGMENTS. FASTENERS AT THE SEGMENT INTERFACES MAY BE REQUIRED. THE SEGMENTS CAN BE FED BY ONE OR MORE AIR SOURCES.

- FEATURES:
- SHOULD BE EASY TO FABRICATE
 - ROLL AND PITCH STIFFNESS CAN BE INCREASED DUE TO PRESSURE DIFFERENCE BETWEEN TRUNK SEGMENTS
 - WITH MULTIPLE AIR SOURCES, COUPLING WILL BE REDUCED
 - FLUID DAMPING CAUSED BY FLOW THROUGH THE PLENUM-TRUNK ORIFICES SHOULD INCREASE.

Figure 66. - Segmented trunk.

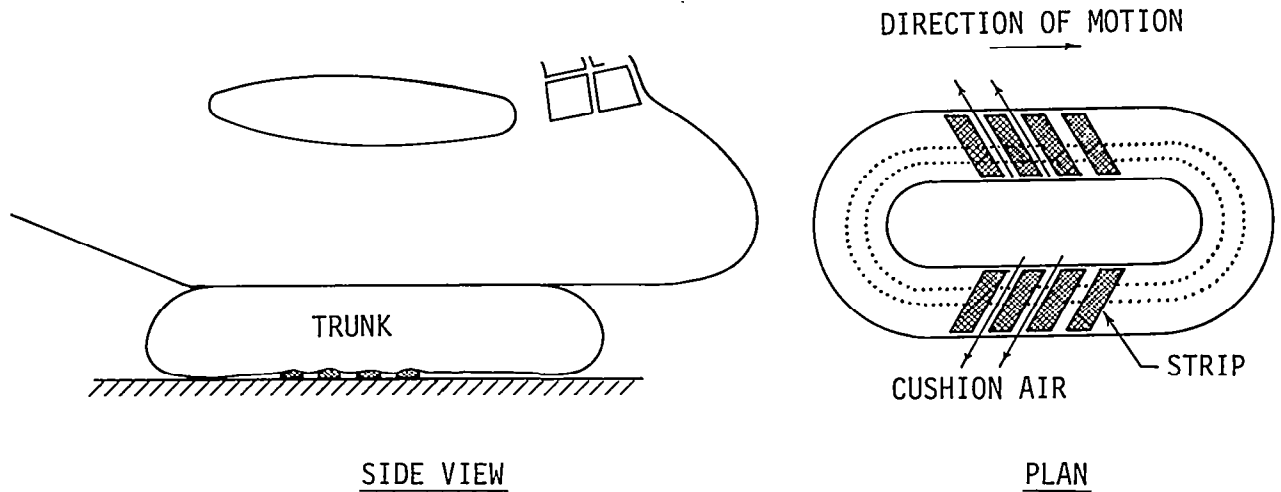


SECTIONAL FRONT VIEW

DESCRIPTION: A PRESSURE RELIEF VALVE TO VENT THE FLOW WHEN A PRESET PLENUM PRESSURE IS EXCEEDED.

- FEATURES:
- PROVIDES BETTER IMPACT ENERGY ABSORPTION AND IMPROVED STABILITY DUE TO ENERGY DISSIPATION IN THE FORM OF PRESSURIZED AIR LOSS
 - EASY TO IMPLEMENT, AND COMPATIBLE WITH MOST ACLS CONFIGURATIONS.

Figure 67. - Plenum relief valve.

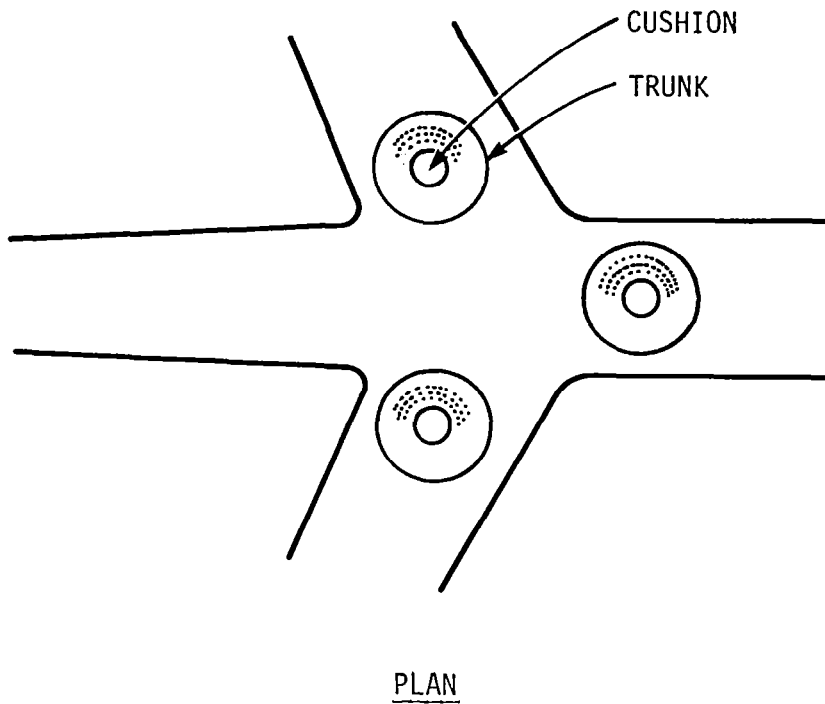


DESCRIPTION: THE EXIT GAP IS CONTOURED BY MEANS OF STRIPS ATTACHED (OR MOLDED) TO THE TRUNK BOTTOM. THE STRIPS CAN BE ORIENTED STRAIGHT ACROSS OR AT AN ANGLE AS SHOWN.

FEATURES:

- TRUNK FLUTTER SHOULD REDUCE
- HEAVE STABILITY WILL IMPROVE SINCE THE GAP AREA NEVER BECOMES ZERO
- IF STRIPS ARE MADE OF LOSSY MATERIAL, SYSTEM DAMPING WILL INCREASE
- THE POTENTIAL FOR FAN STALL WILL BE REDUCED, BECAUSE COMPLETE FLOW BLOCKAGE DURING LANDING IMPACT WILL NOT OCCUR.

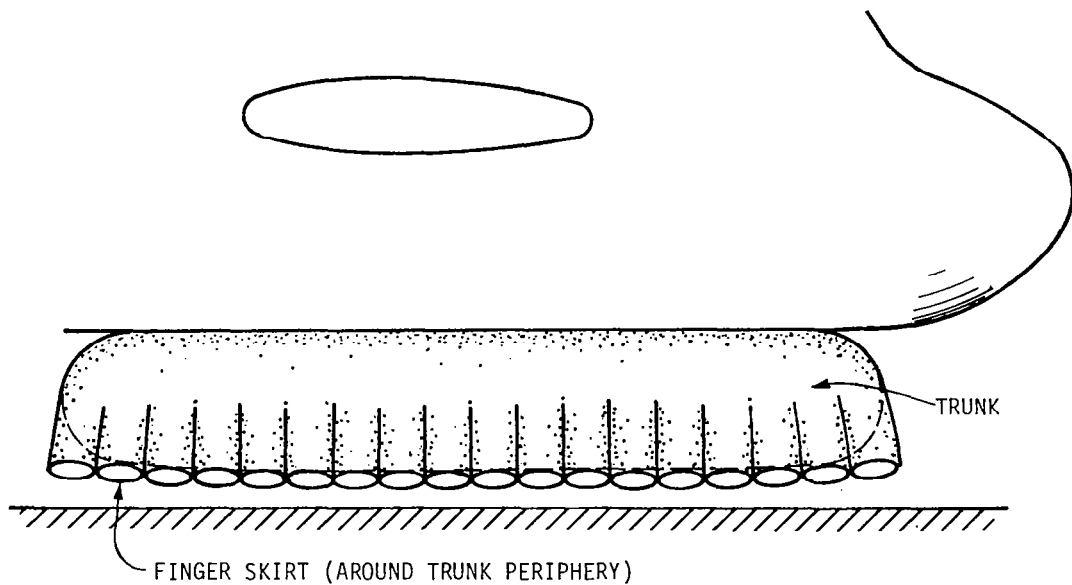
Figure 68. - Contoured gap trunk.



DESCRIPTION: IN PLAN, THE TRUNK IS CIRCULAR INSTEAD OF OVAL.

- FEATURES:
- HIGH HEAVE STIFFNESS, SINCE HOOP STRESSES PREVENT THE TRUNK SIDES FROM MOVING OUTWARDS
 - THIS CONFIGURATION LENDS ITSELF TO MULTIPLE CUSHIONS, SO THAT THE HIGH HEAVE FORCES ACTING OVER THE MOMENT ARM PROVIDE HIGH ANGULAR STIFFNESS.

Figure 69. - Circular trunk.

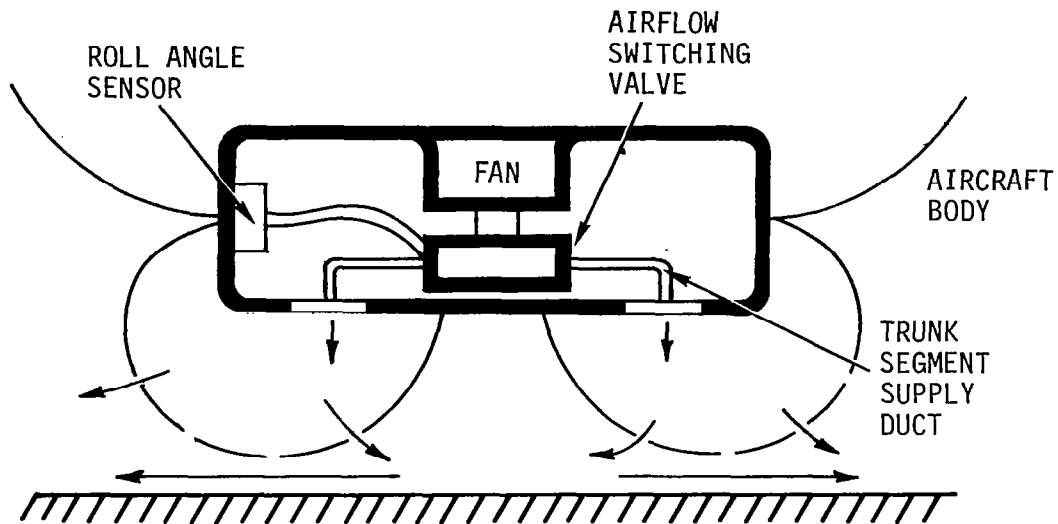


SIDE VIEW

DESCRIPTION: THE FINGER SKIRT IS CURRENTLY USED IN AIR CUSHION TRANSPORTERS. IT CONSISTS OF A SERIES OF FLEXIBLE TUBES WHICH CREATE A LIFT FORCE WHEN NEAR THE GROUND. IN THIS APPLICATION, THE SKIRT CAN BE MADE INTEGRAL WITH THE TRUNK AND LOCATED AROUND THE ENTIRE CUSHION PERIPHERY.

- FEATURES:
- THE ROLL AND PITCH STIFFNESS WILL INCREASE
 - MAY BE EXPENSIVE TO IMPLEMENT AND MAINTAIN.

Figure 70. - Finger skirt trunk.



SECTIONAL FRONT VIEW

DESCRIPTION: ROLL ANGLE SIGNAL, SUITABLY PROCESSED, IS USED TO MODULATE INLET FLOW TO THE SIDE TRUNK SEGMENTS.

- FEATURES:
- ROLL STIFFNESS SHOULD INCREASE SIGNIFICANTLY
 - MUST BE USED IN COMBINATION WITH A SEGMENTED OR COMPARTMENTED TRUNK.

Figure 71. - Roll feedback control.

APPENDIX B

COMPARISON BETWEEN SIMULATION AND EXPERIMENT

The comparison between simulation and experiment for a typical heave drop test for the baseline system and each of the leading ACLS concepts is shown in Figures 72 through 91. The variables compared include heave displacement and acceleration and trunk and cushion pressure.

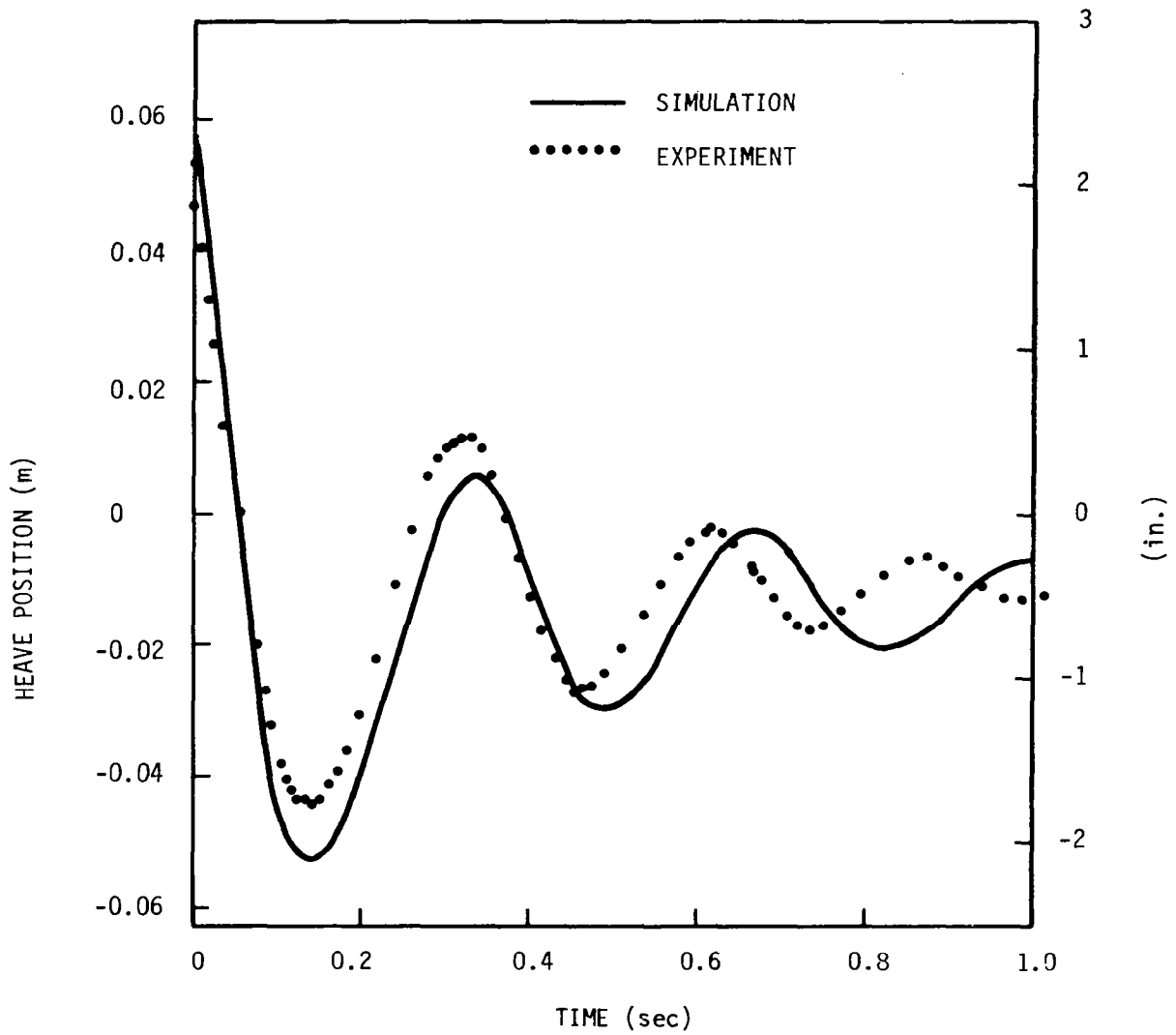


Figure 72. - Comparison between simulation and experiment heave position - baseline system.

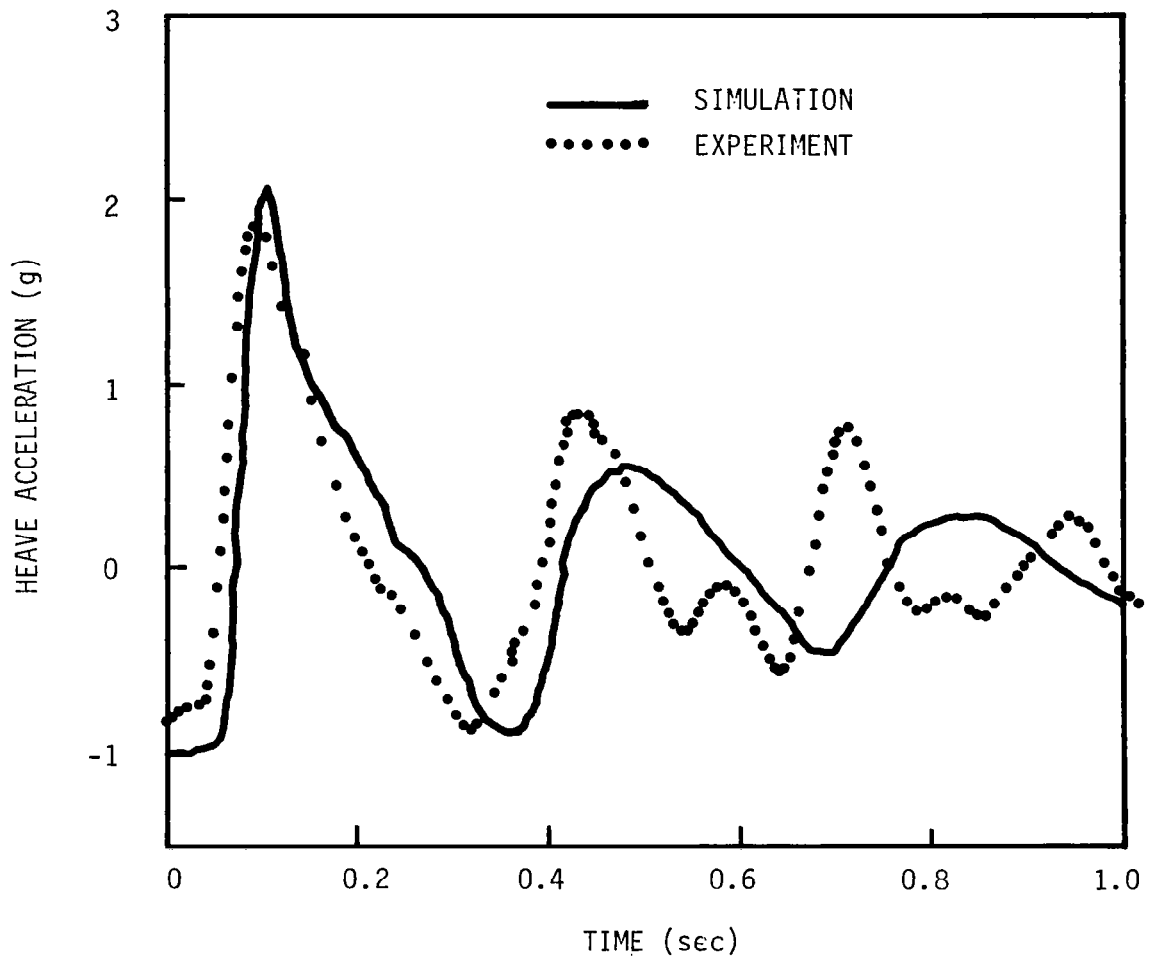


Figure 73. - Comparison between simulation and experiment heave acceleration - baseline system.

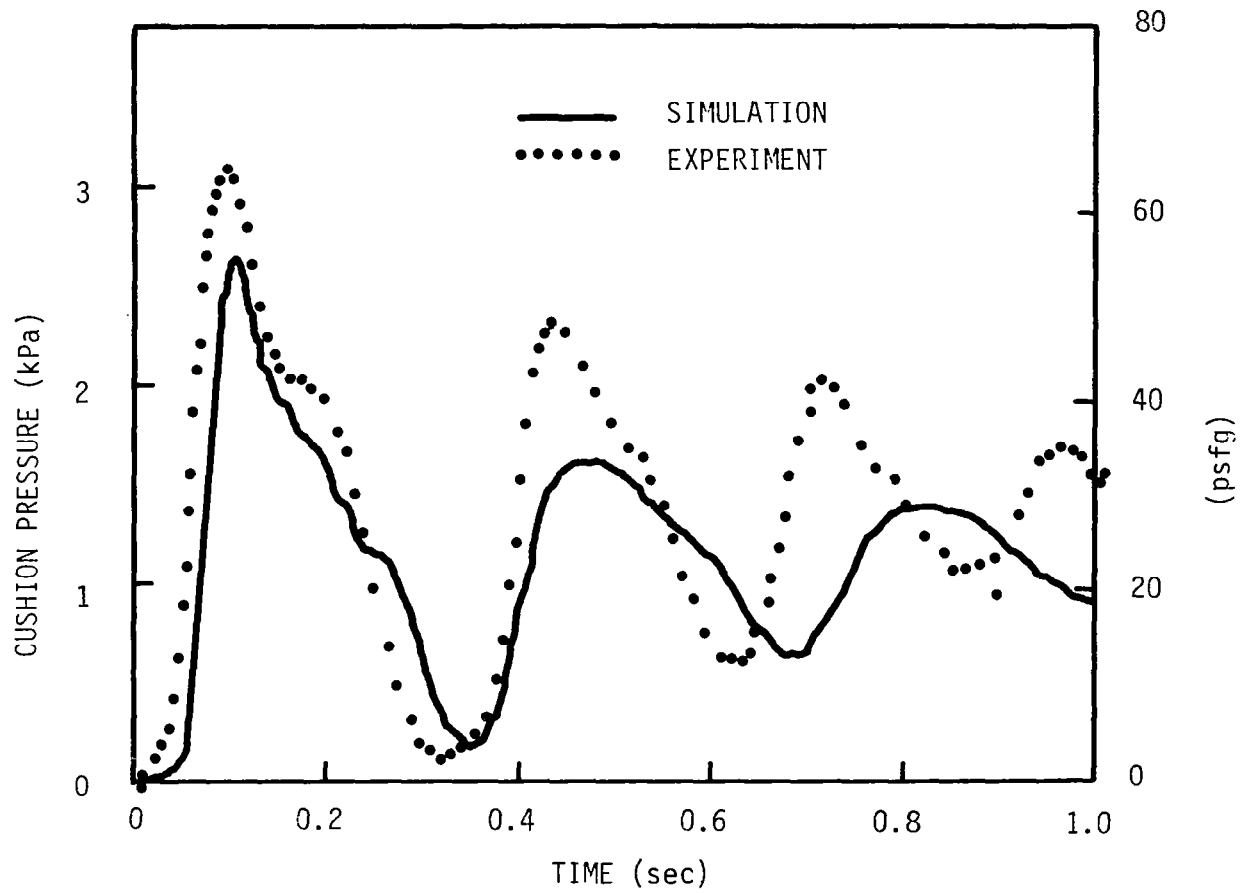


Figure 74. - Comparison between simulation and experiment cushion pressure - baseline system.

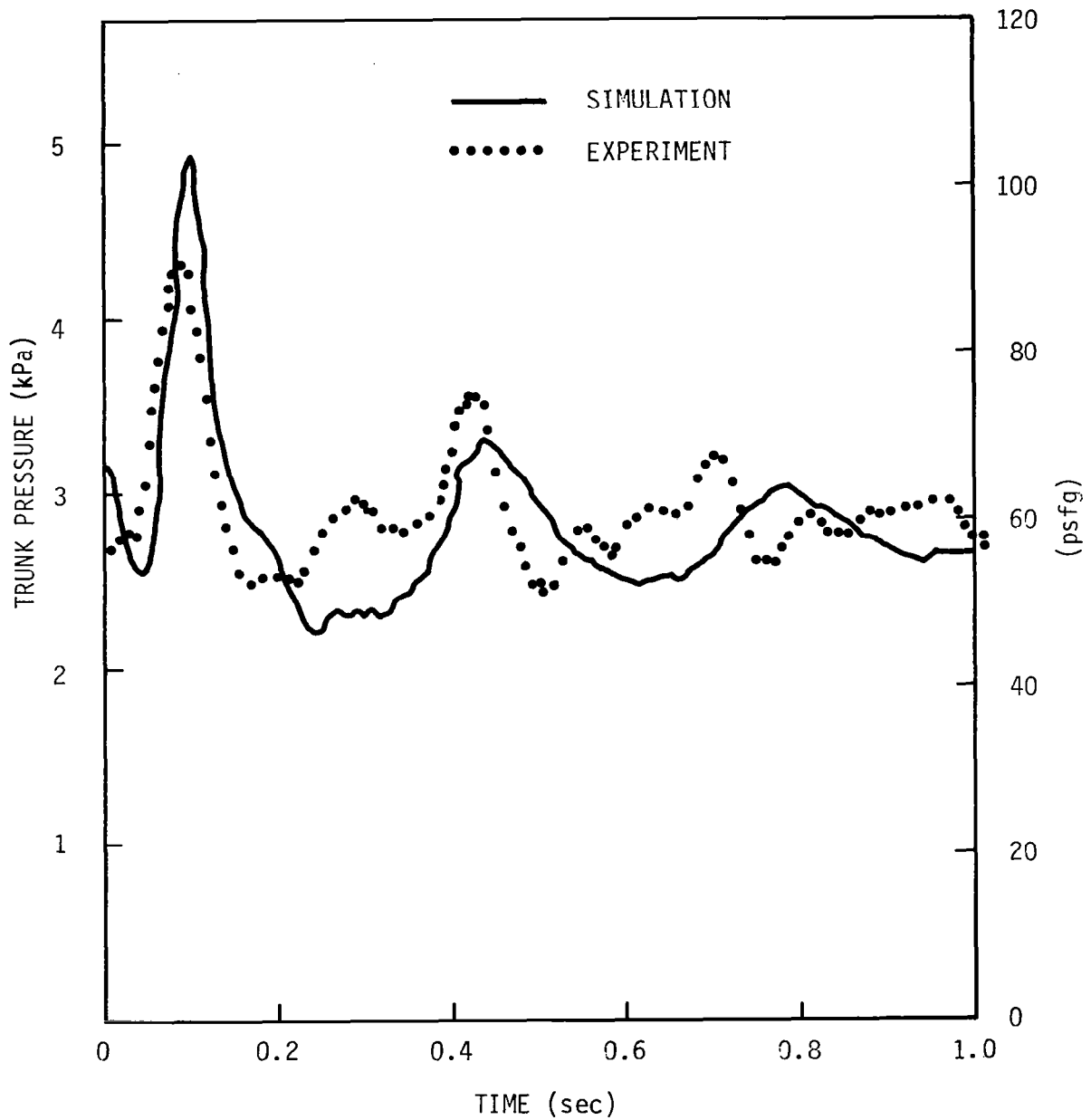


Figure 75. - Comparison between simulation and experiment trunk pressure - baseline system.

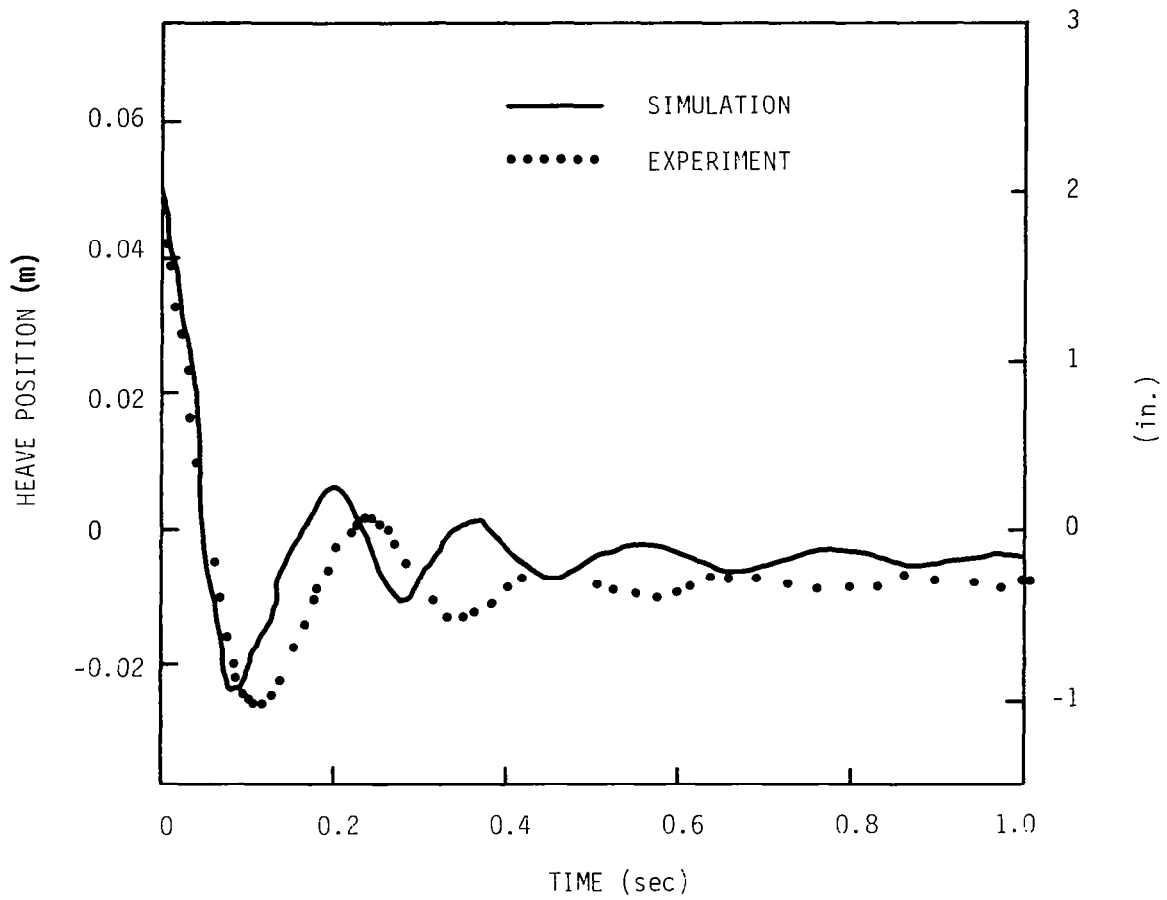


Figure 76. - Comparison between simulation and experiment heave position - damped trunk.

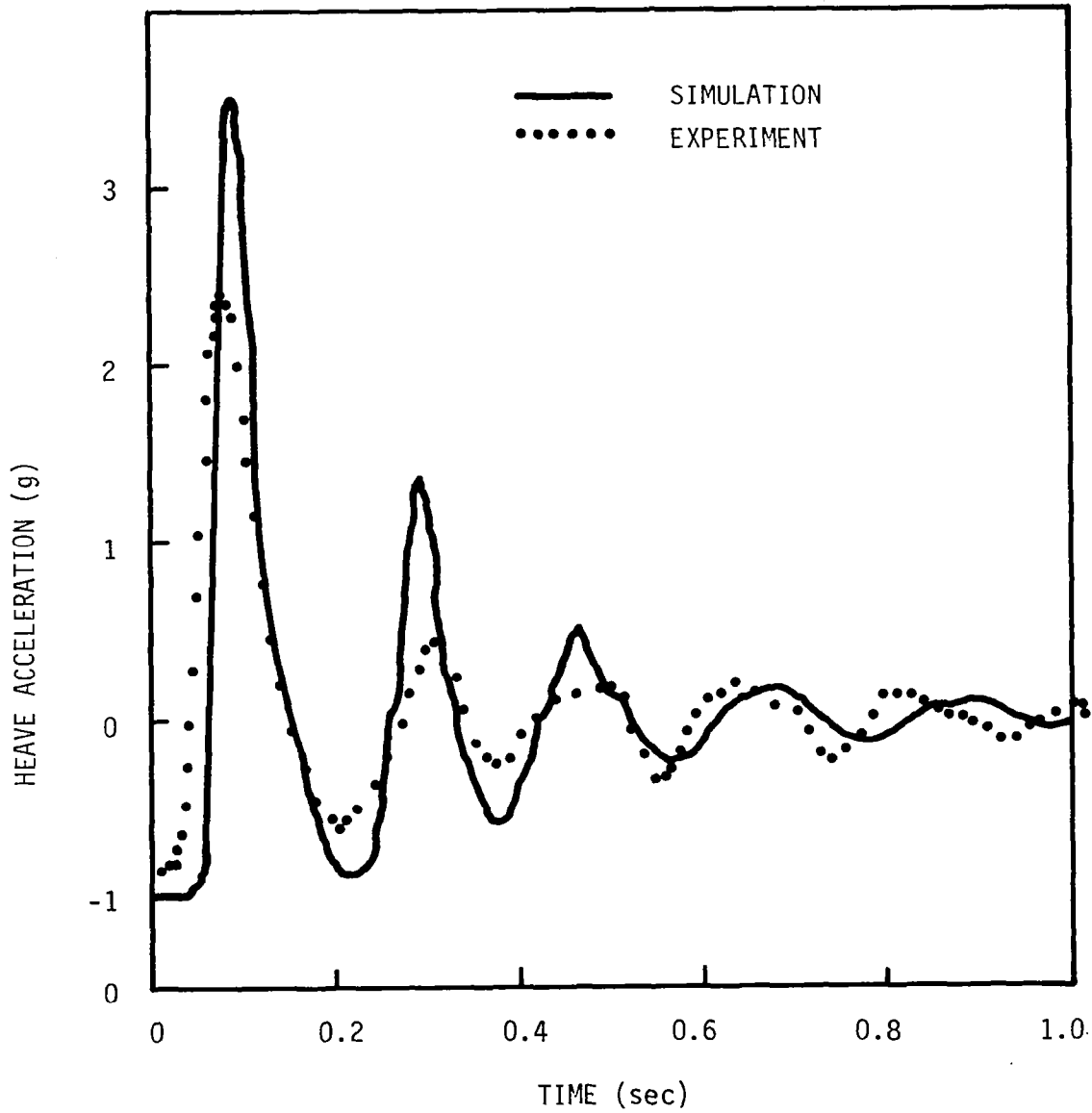


Figure 77. - Comparison between simulation and experiment heave acceleration - damped trunk.

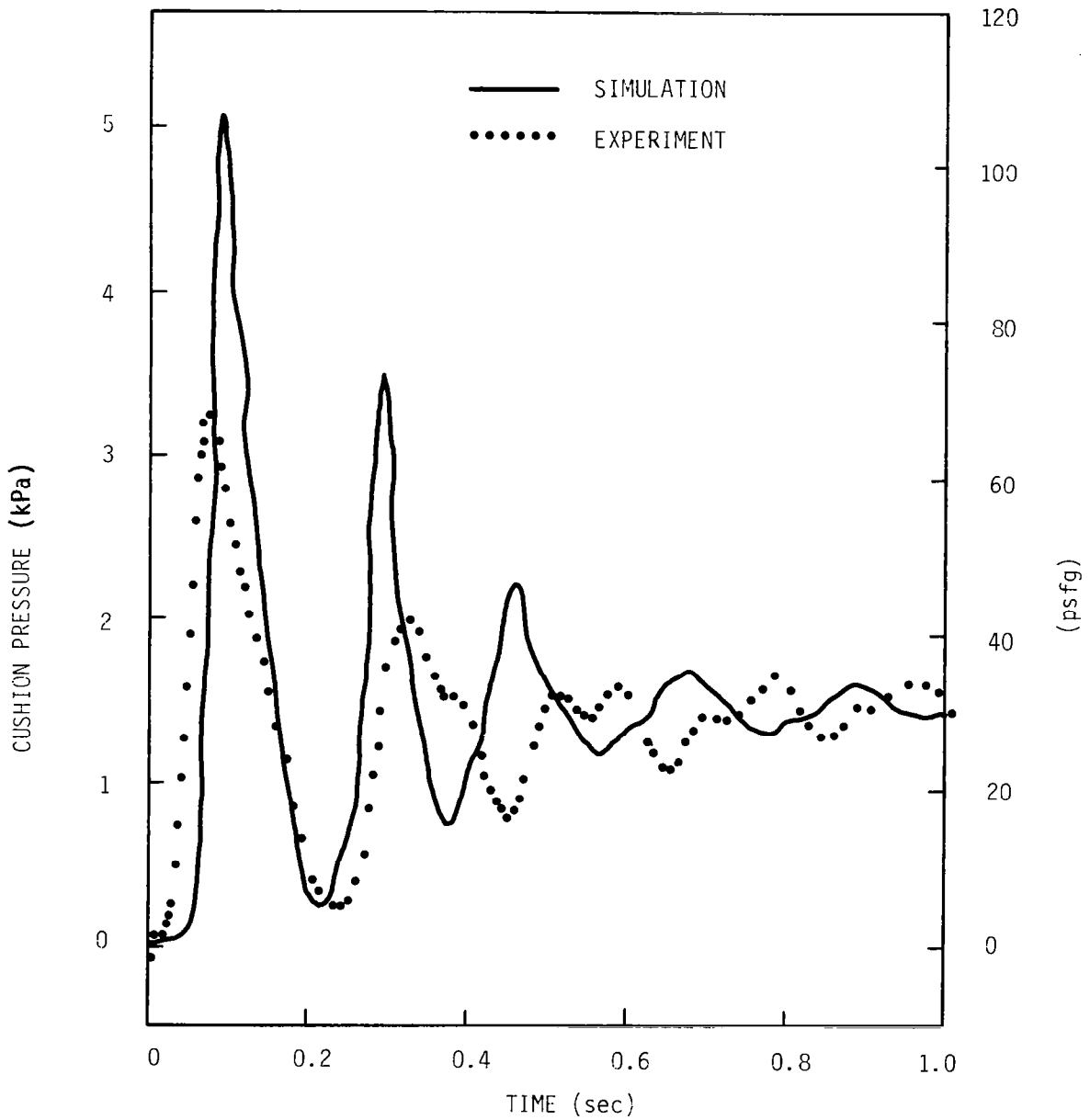


Figure 78. - Comparison between simulation and experiment cushion pressure - damped trunk.

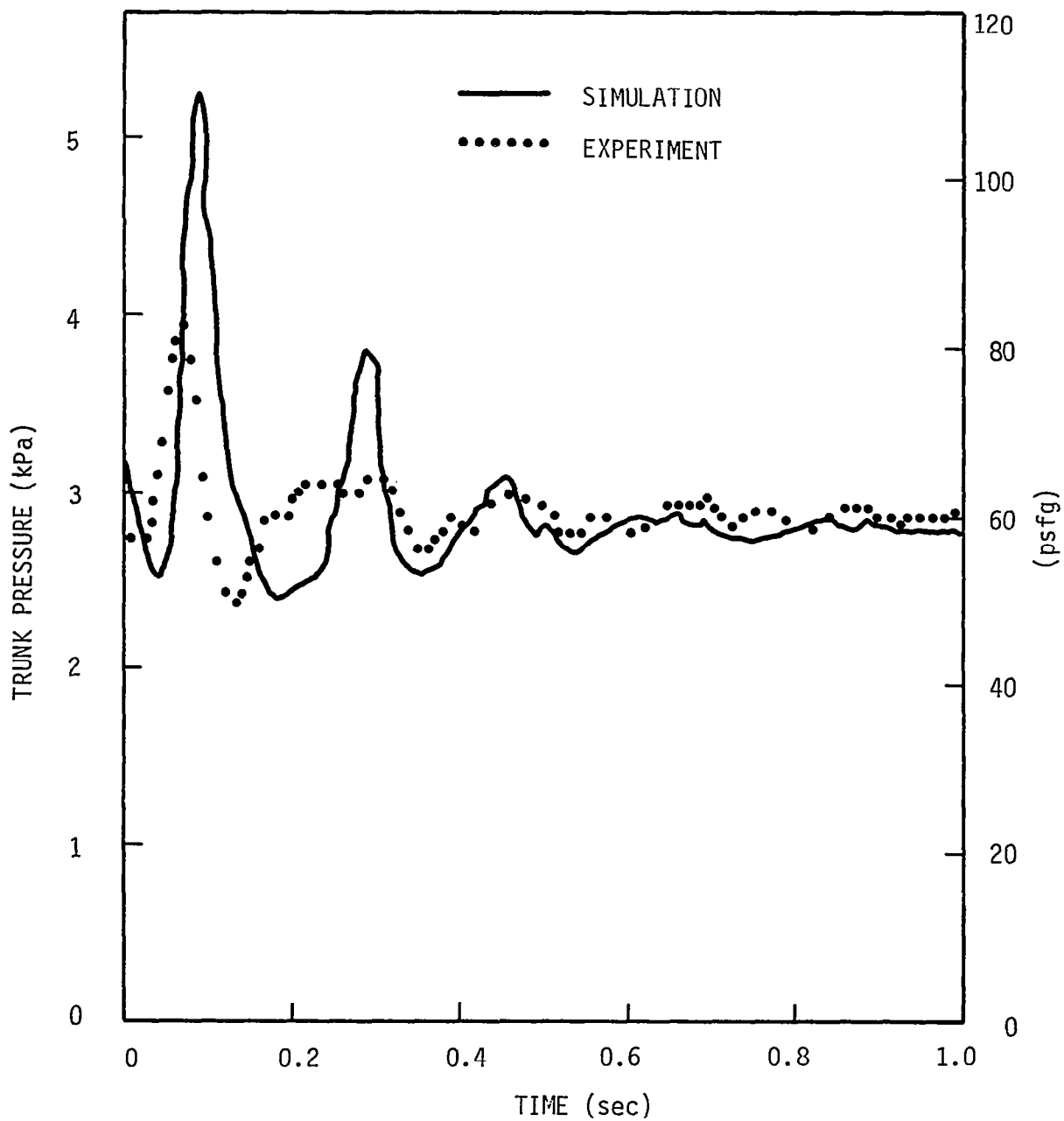


Figure 79. - Comparison between simulation and experiment trunk pressure - damped trunk.

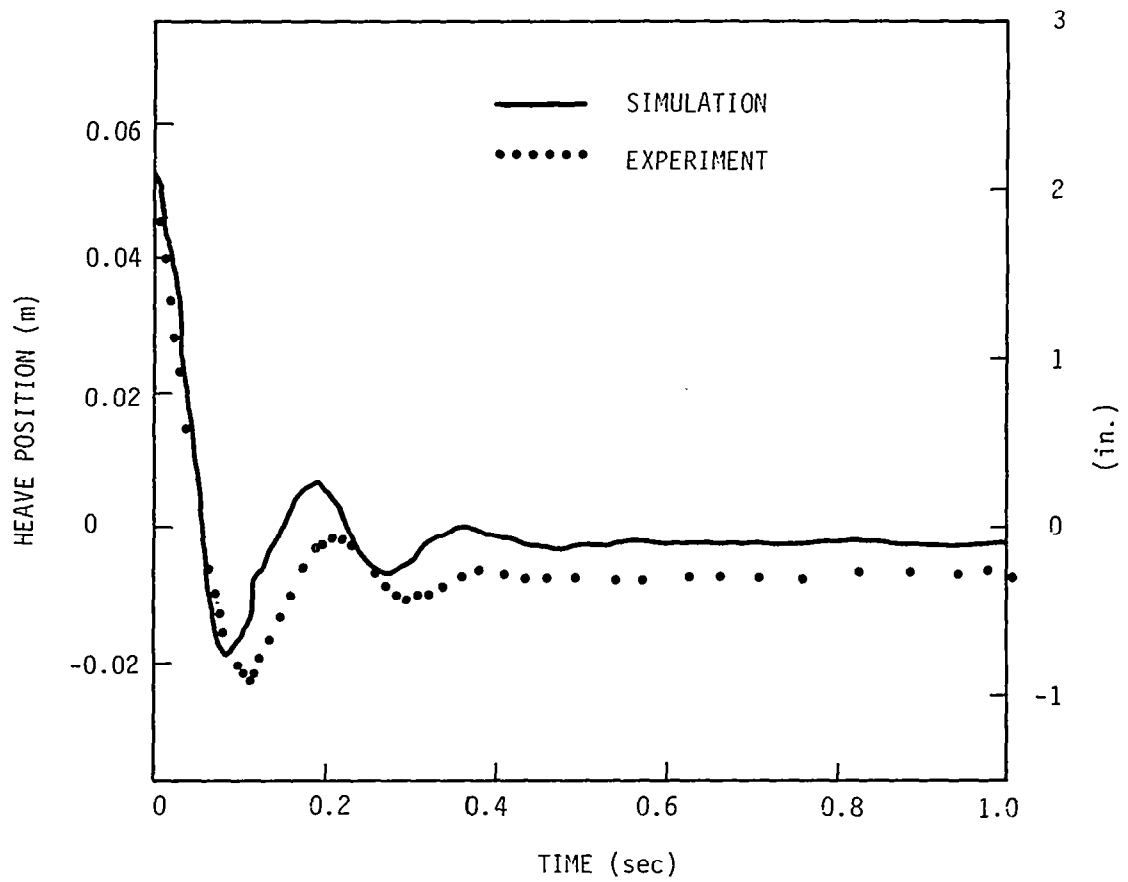


Figure 80. - Comparison between simulation and experiment heave position - filled trunk.

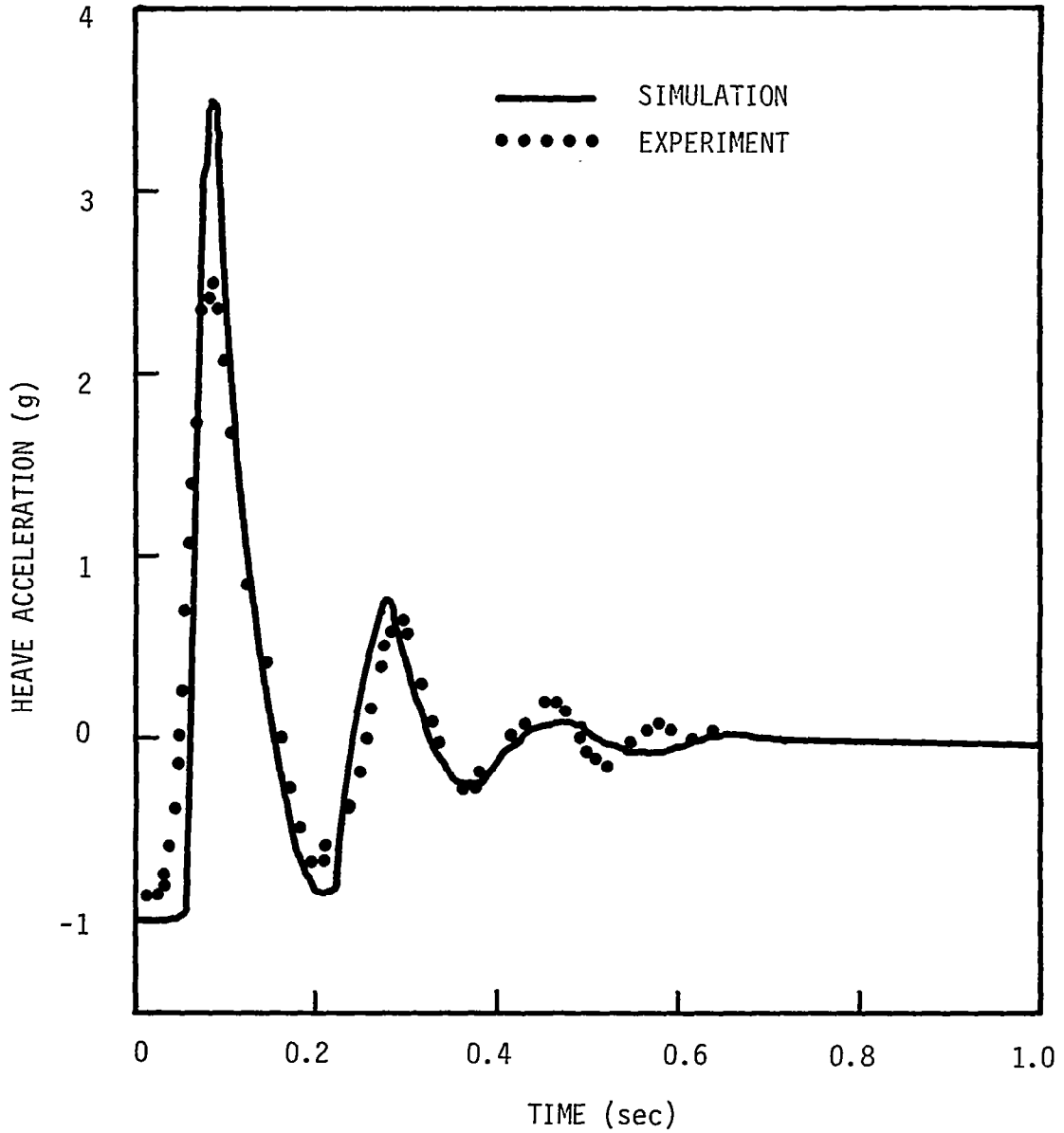


Figure 81. - Comparison between simulation and experiment heave acceleration - filled trunk.

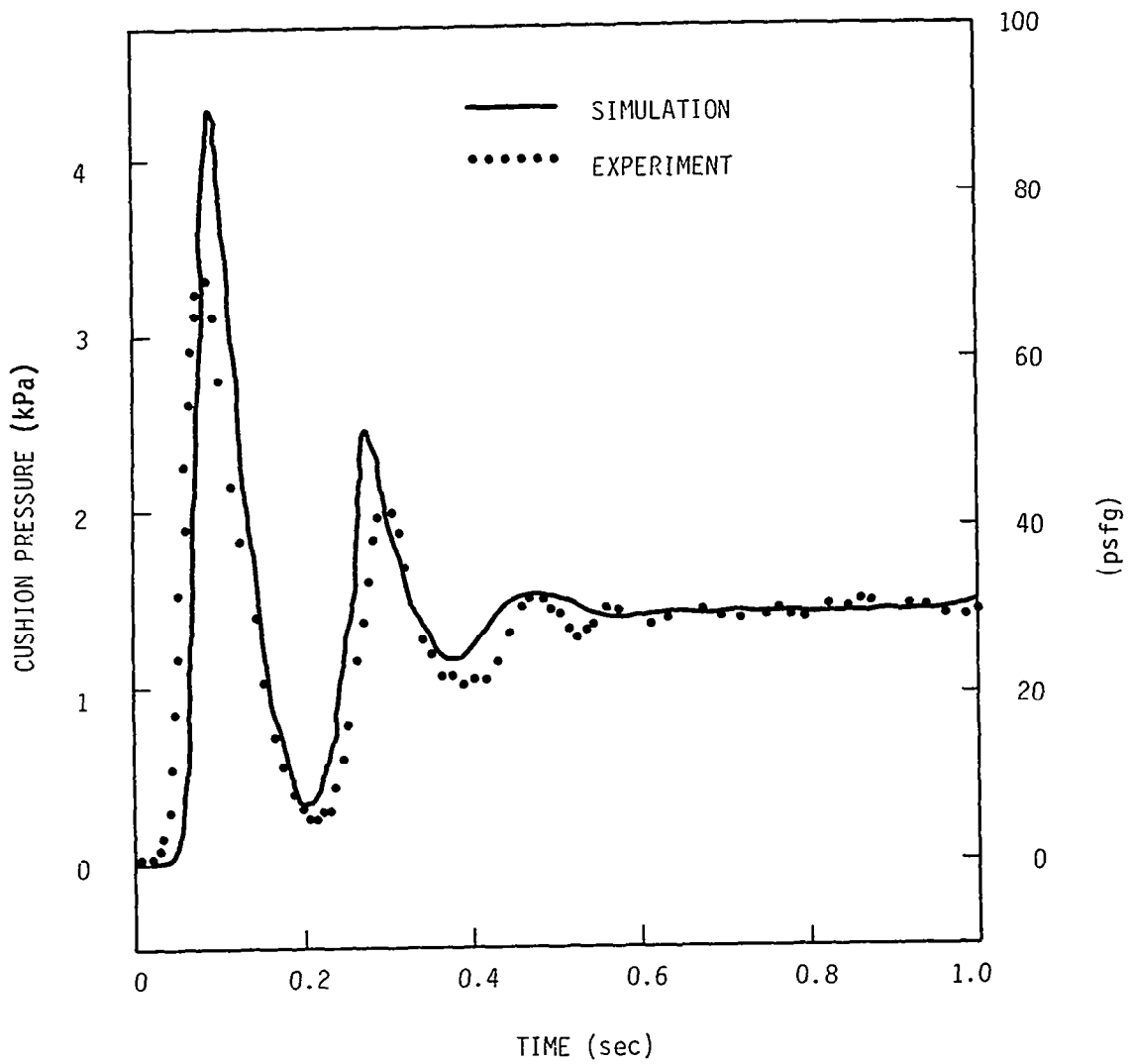


Figure 82. - Comparison between simulation and experiment cushion pressure - filled trunk.

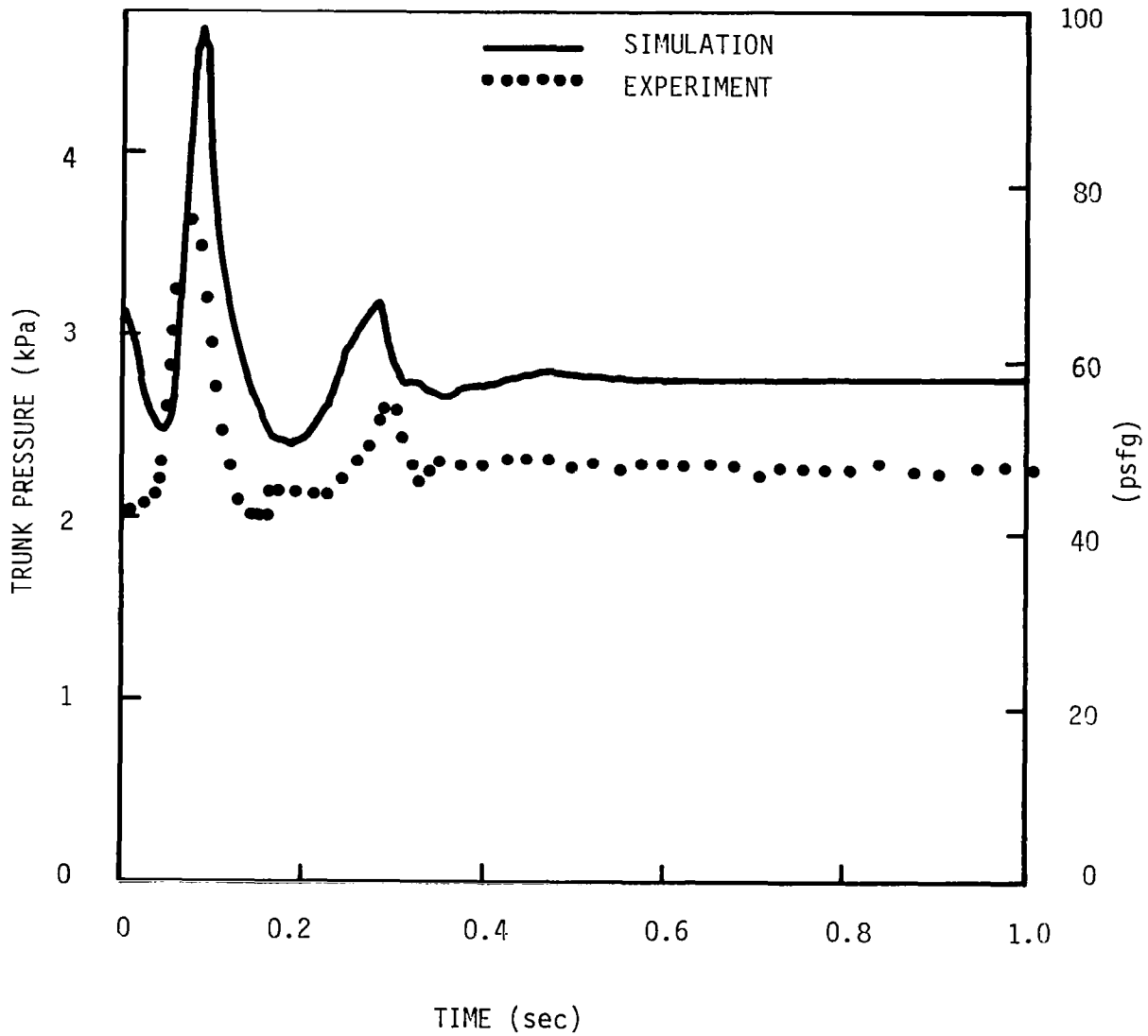


Figure 83. - Comparison between simulation and experiment trunk pressure - filled trunk.

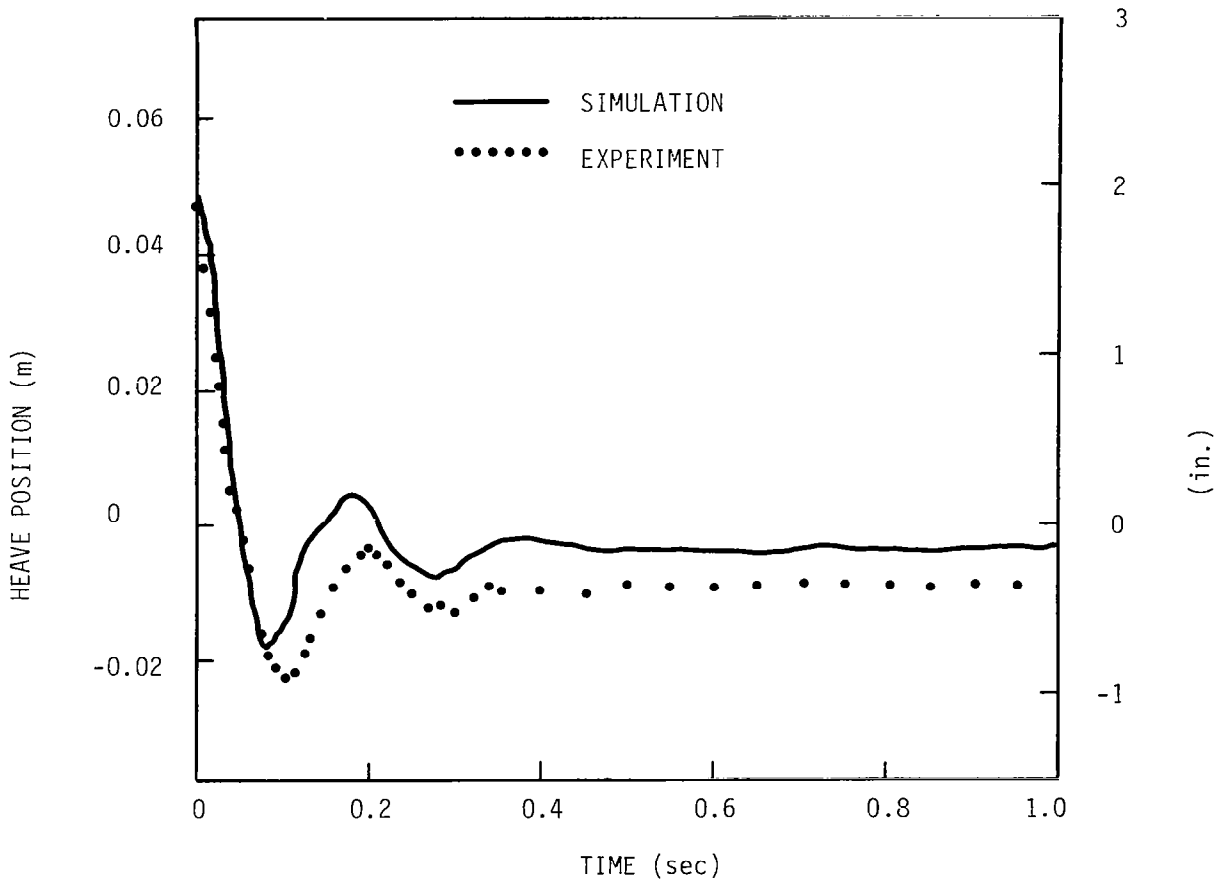


Figure 84. - Comparison between simulation and experiment heave position - compartmented trunk.

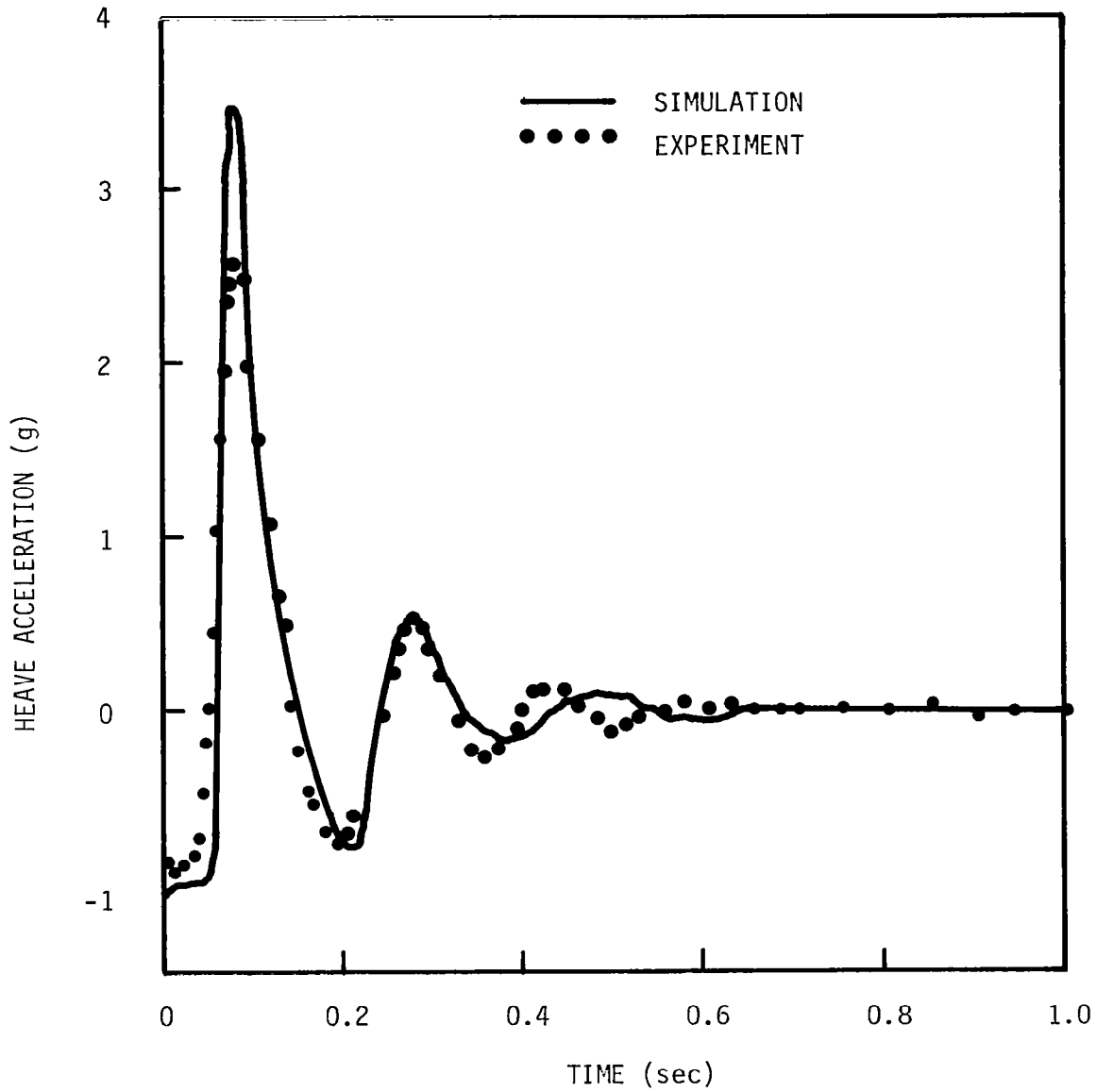


Figure 85. - Comparison between simulation and experiment heave acceleration - compartmented trunk.

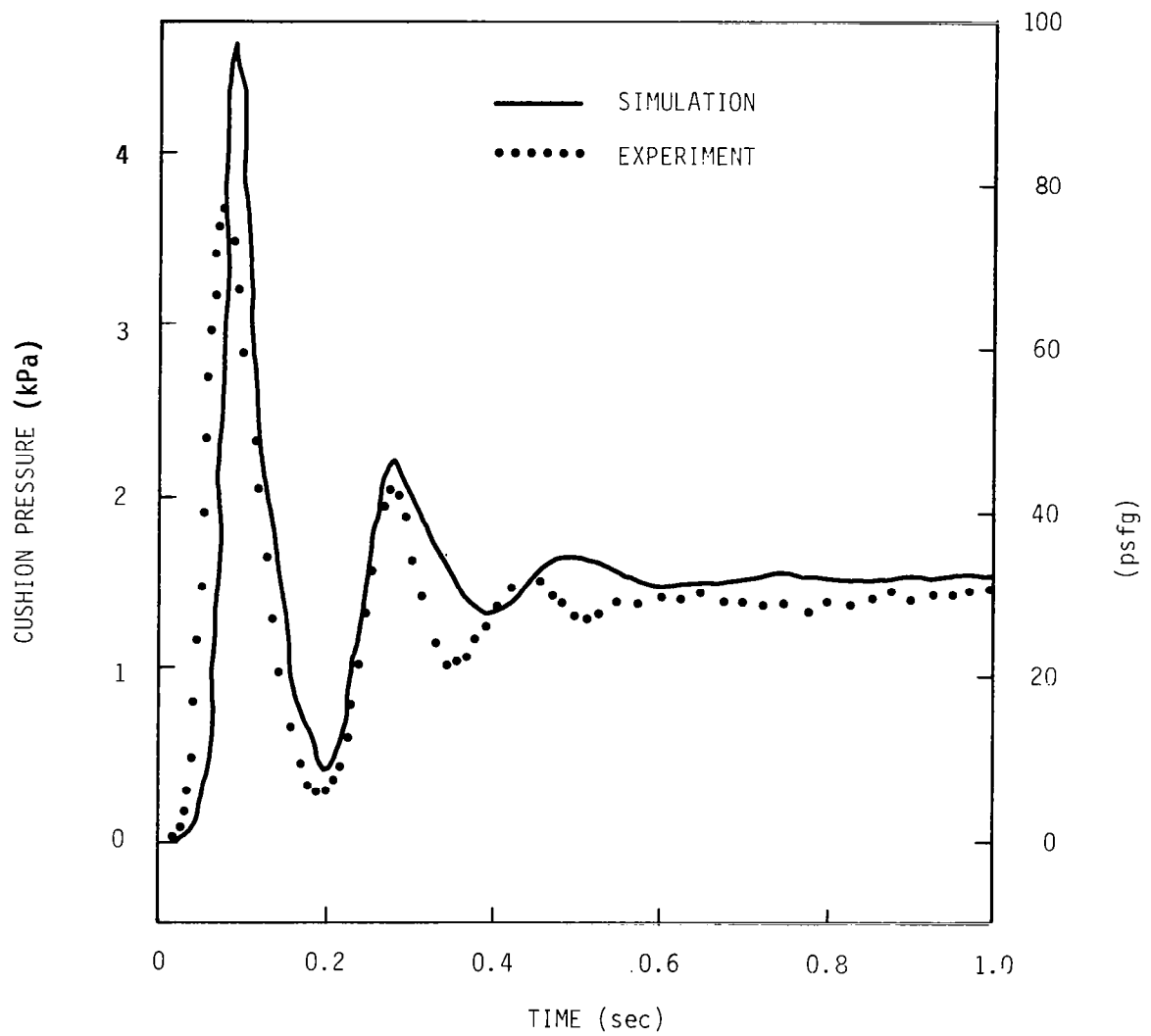


Figure 86. - Comparison between simulation and experiment cushion pressure - compartmented trunk.

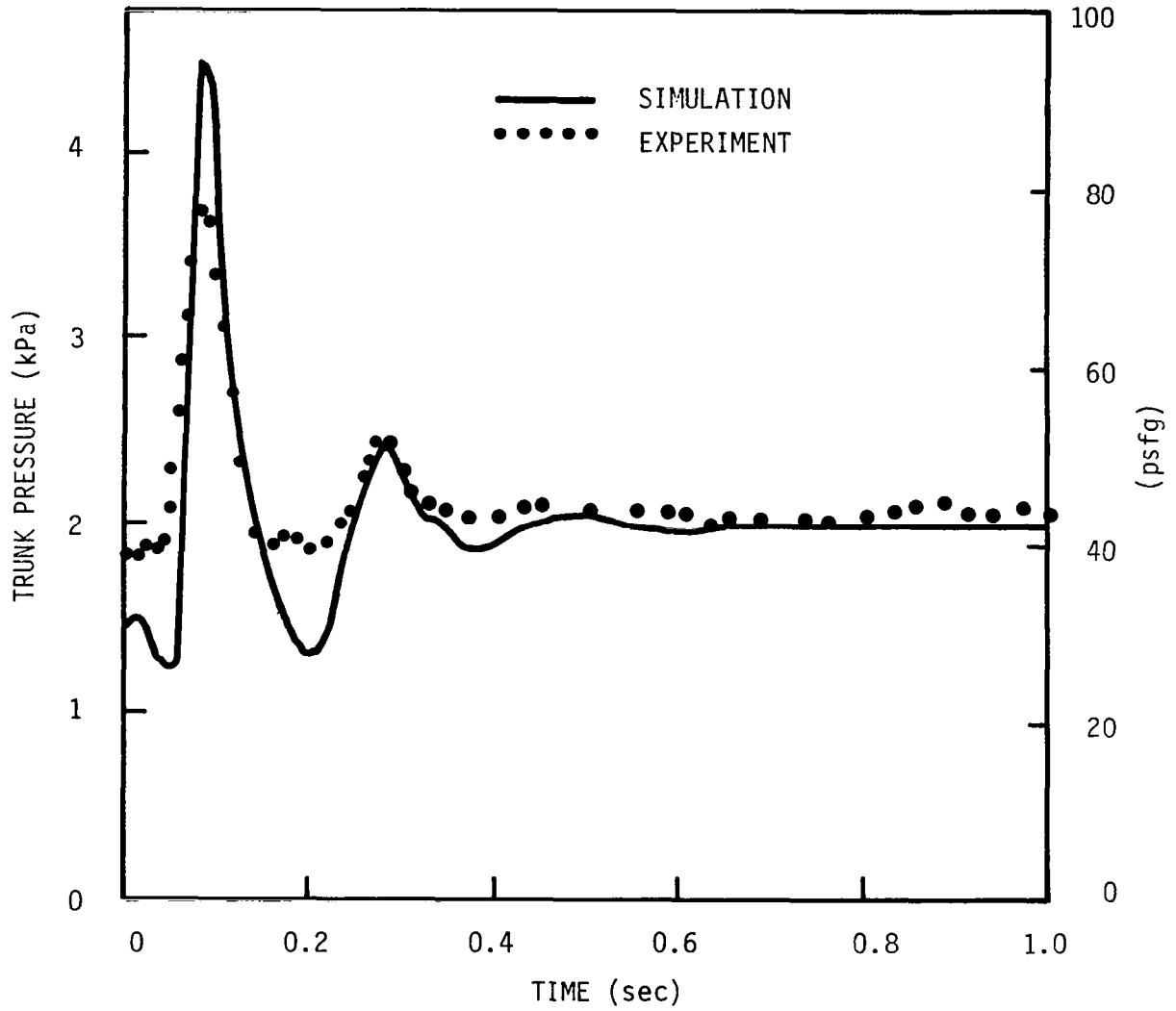


Figure 87. - Comparison between simulation and experiment trunk pressure - compartmented trunk.

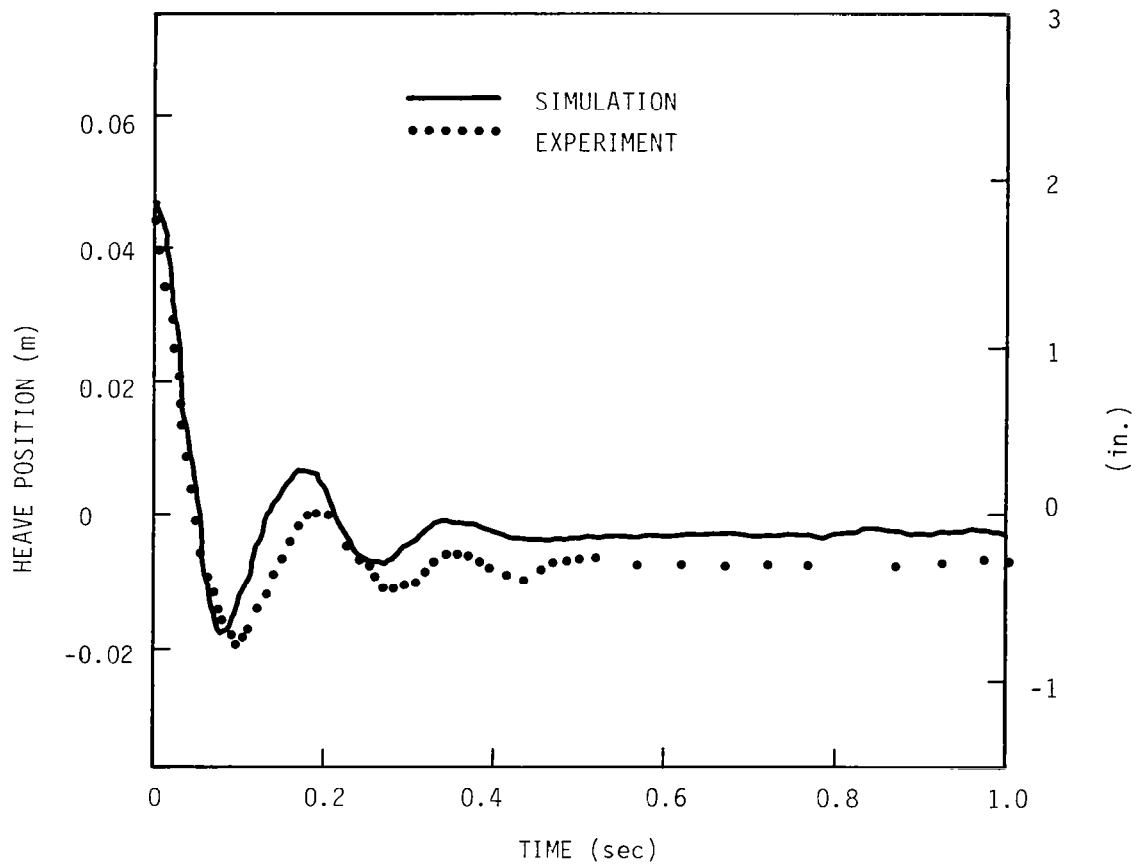


Figure 88. - Comparison between simulation and experiment heave position - segmented trunk.

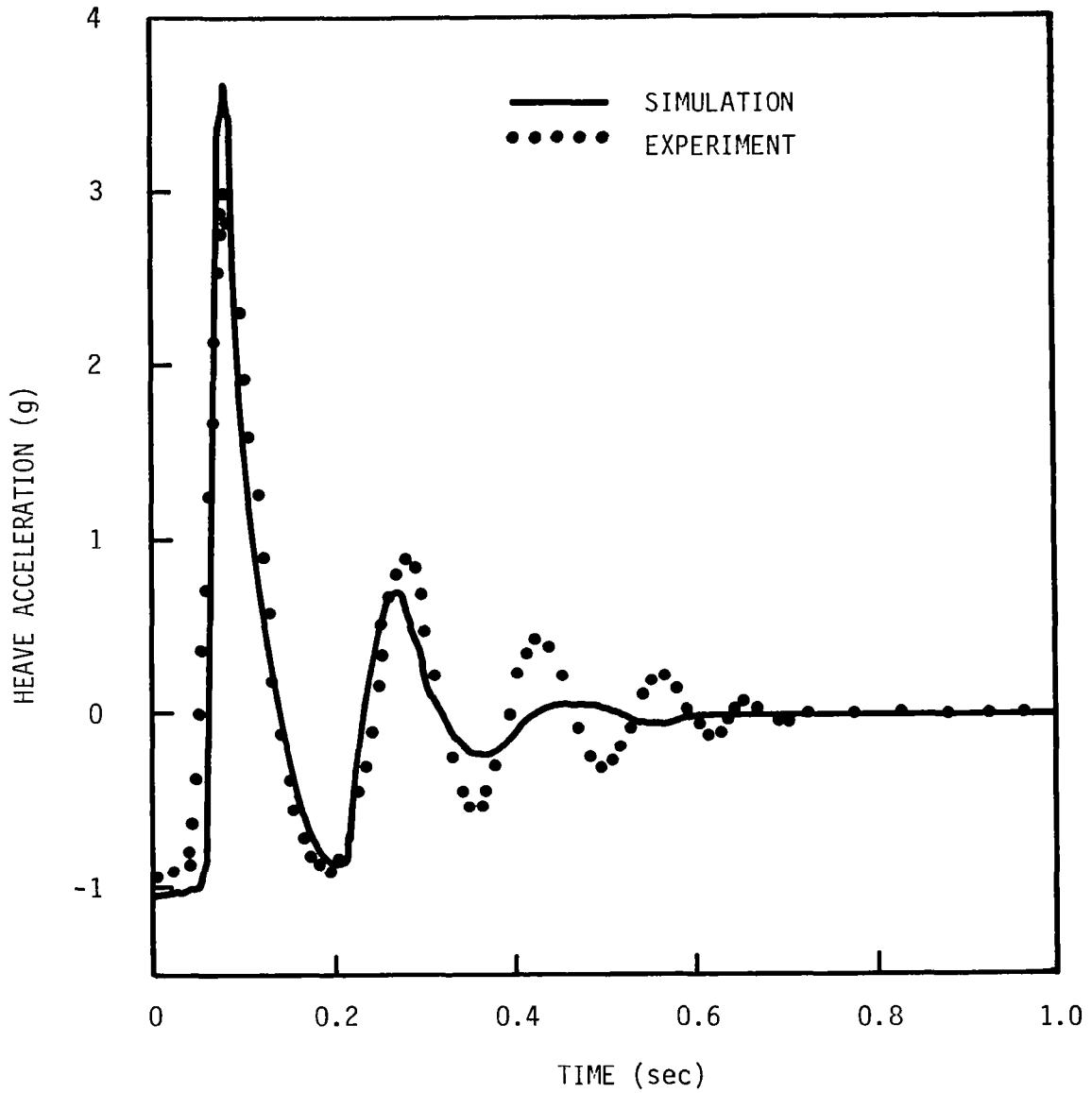


Figure 89. - Comparison between simulation and experiment heave acceleration - segmented trunk.

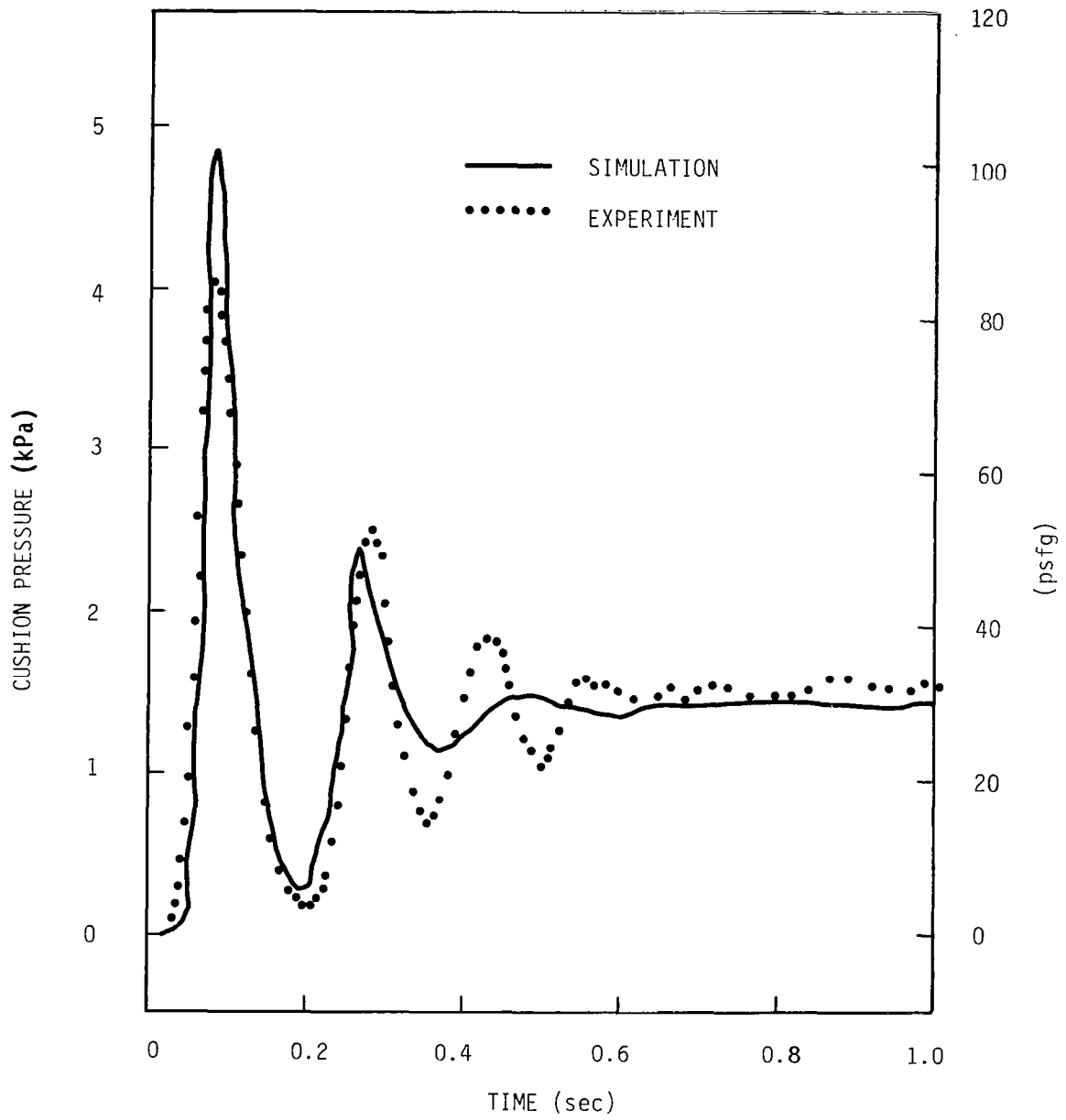


Figure 90. - Comparison between simulation and experiment cushion pressure - segmented trunk.

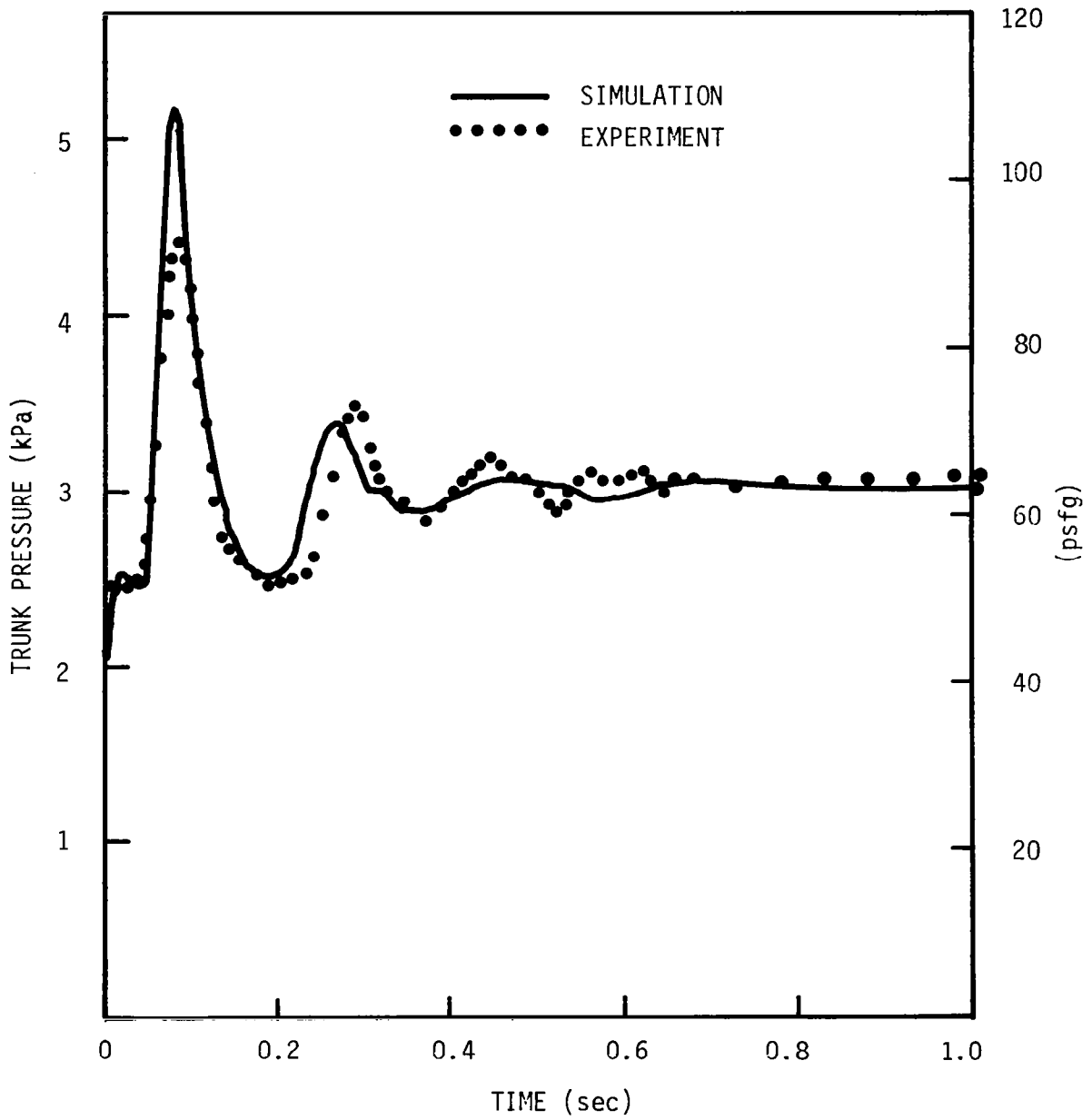


Figure 91. - Comparison between simulation and experiment trunk pressure - segmented trunk.



APPENDIX C

STABILITY ANALYSIS OF NASA TEST VEHICLE

As a first step in a stability analysis of the NASA test vehicle, the stability of a rigid plenum suspension was investigated. This is based on a simple lumped parameter model resulting from a linearized analysis of the fluid suspension in which the sealing region is represented by a quasi-static pressure-displacement-flow relationship and the supply system represented by a pressure source.

The basic result of the rigid plenum analysis is that two time constants, τ_1 and τ_2 , characterize the suspension. The lead time constant τ_1 is essentially the residence time of a fluid particle in the "active" region of fluid suspension. The lag time constant τ_2 is the charging time constant of the cushion volume. These time constants are defined by:

$$\tau_1 = \frac{\rho_{ce} A_e h_e}{W_e b_{c,a}} \quad (C-1)$$

$$\tau_2 = \frac{\rho_{ce} V_{ce}}{W_e \gamma (a_{c,a} - a_{c,s})} \quad (C-2)$$

where:

ρ_{ce} = equilibrium cushion gas density

A_e = area of suspension pad

h_e = equilibrium gap height

$$= \frac{W_e}{Z C_{DC} \{2\rho_{ce} (P_{ce} - P_a)\}^{1/2}}$$

Z = cushion peripheral length

C_{DC} = plenum exit discharge coefficient

W_e = equilibrium supply mass flow rate

$V_{ce} = V_o + A_e h_e$

V_o = volume of cushion ("dead" and "active")

γ = polytropic exponent (=1.4 for air)

$b_{c,a}$ = dimensionless flow - displacement coefficient
(=1 for orifice)

$$a_{c,a} = 1/2 \frac{P_{ce}}{P_{ce} - P_a}$$

$$a_{c,s} = -1/2 \frac{P_{ce}}{P_s - P_{ce}}$$

P_{ca} = equilibrium absolute cushion pressure

P_a = absolute ambient pressure

P_s = absolute supply pressure

When substituting typical values from the one-third scale model static test data for the preceding parameters:

$$A_e = 0.74 \text{ m}^2 \text{ (8 ft}^2\text{)}$$

$$h_e = 0.0305 \text{ m (0.010 ft)}$$

$$W_e = 0.485 \text{ kg/sec (1.07 lb/sec)}$$

$$V_{ce} = 0.084 \text{ m}^3 \text{ (2.96 ft}^3\text{)}$$

$$P_{ce} = 162.11 \text{ kPa (14.81 psia)}$$

$$P_s = 104.05 \text{ kPa (15.09 psia)}$$

$$P_a = 101.36 \text{ kPa (14.7 psia)}$$

and the following equation results:

$$\frac{\tau_1}{\tau_2} = 3.55 \quad \text{(C-3)}$$

which clearly implies stable operation. Using the properly scaled values for trunk and cushion pressures and air flow:

$$W_e = 0.286 \text{ kg/sec (0.63 lbm/sec)}$$

$$P_{ce} = 102.53 \text{ kPa (14.87 psia)}$$

$$P_s = 104.32 \text{ kPa (15.13 psia)}$$

and the result of the stability analysis is:

$$\frac{\tau_1}{\tau_2} = 1.32$$

which still implies a stable system.



APPENDIX D

FLUID SYSTEM ELEMENT REPRESENTATION

The elemental equations for ideal fluid capacitance, C , and inertance, I , are given by ref. 7:

$$Q = C \frac{dP}{dt} \quad (D-1)$$

and

$$P = I \frac{dQ}{dt} \quad (D-2)$$

where

Q = the volume flow through the element

P = the pressure across the element

For incompressible flow, the air volume flow associated with the air inertance, I_a , and air capacitance, C_a , must equal the water volume flow associated with the water inertance, I_w , and water capacitance C_w . By flow conservation the electrical circuit analogous to fluid flow in the test rig is a series connection as shown in Figure 92.

By analogy to the electrical circuit equivalent, the natural frequency is given by:

$$\omega_n = \left(\frac{C_a + C_w}{C_a C_w} \right) \times \left(\frac{1}{I_a + I_w} \right)^{1/2}$$

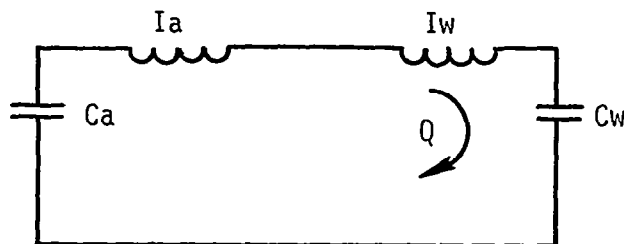


Figure 92. - Test rig fluid element circuit.



APPENDIX E

FLUID MECHANICAL ANALYSIS

The Bernoulli equation for nonsteady, frictionless, incompressible flow in the presence of conservative forces is given by ref. 8:

$$\int_1^2 \frac{\partial V}{\partial t} ds = \frac{V_1^2 - V_2^2}{2} + \frac{P_1 - P_2}{\rho} - (V_1 - V_2) \quad (E-1)$$

where the subscripts 1 and 2 refer to two points on the same streamline.

The main task in applying this equation to the test rig water system is to determine an appropriate streamline along which the integral term can be evaluated. Figure 93 shows a cross-section of the test rig with a streamline constructed in such a manner that the streamline length can be expressed as a function of the water surface levels X_1 and X_2 at points 1 and 2 respectively, relative to a common reference line some distance below the bottom of the trunk.

Consider the flow along the streamline and define V_1 as the fluid velocity along the streamline segment (1, 1'), V_3 along (1', 2') and V_2 along (2', 2). Also define A_1 , A_3 and A_2 as the cross-section areas along the same three streamline segments, respectively. Assuming the velocity is constant over each cross-section area and streamline segment, flow continuity requires that

$$V_1 A_1 = V_2 A_2 = V_3 A_3 \quad (E-2)$$

or

$$V(S) = \begin{cases} V_1; & S \in (1, 1') \\ V_1 (A_1/A_3); & S \in (1', 2') \\ V_1 (A_1/A_2); & S \in (2', 2) \end{cases}$$

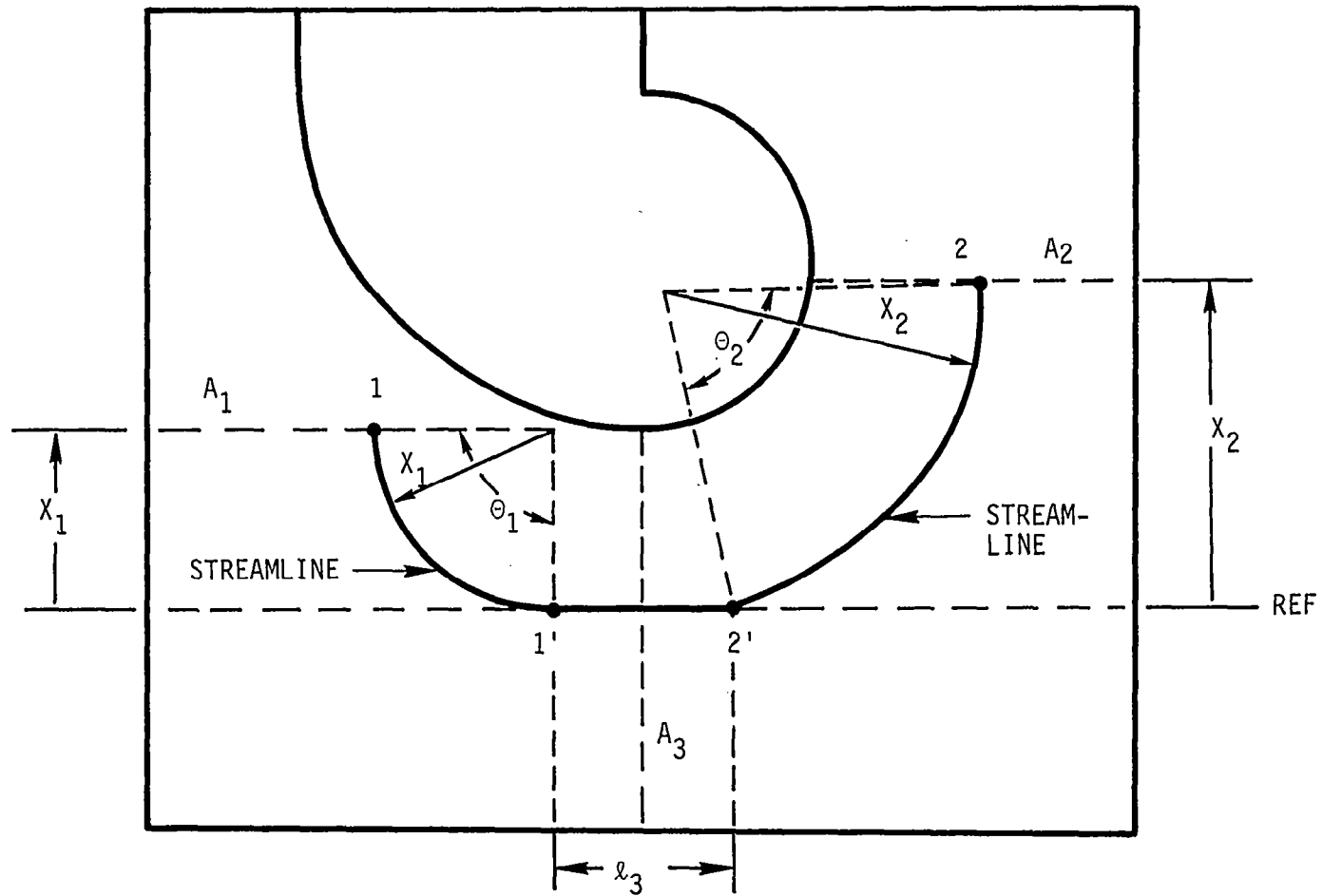


Figure 93. - Streamline construction for evaluating the Bernoulli equation.

The lengths of the streamline segments are $X_1\theta_1$ on $(1, 1')$, ℓ_3 on $(1', 2')$ and $X_2\theta_2$ on $(2', 2)$. Then,

$$\int_1^2 \frac{\partial V}{\partial t} ds = - \frac{dV_1}{dt} \left[X_1\theta_1 + \frac{A_1}{A_3} \ell_3 + \frac{A_1}{A_2} X_2 \right] \quad (E-3)$$

since dV_1/dt is not a function of s on each streamline segment.

The force potential is that due to gravity. Thus,

$$V_i = -gX_i, \quad i = 1, 2 \quad (E-4)$$

The water level, X_2 , at point 2 is not an independent variable. There exists a constant volume, V_{12} such that,

$$V_{12} = A_1X_1 + A_2X_2 \quad (E-5)$$

Noting that V_1 is simply the velocity of the surface at point 1,

$$\frac{dV_1}{dt} = \dot{X}_1 \quad (E-6)$$

Substituting equations (E-2) through (E-6) into (E-1) gives:

$$\begin{aligned} \ddot{X}_1 \left[X_1(\theta_1 - \theta_2 a^2) + \theta_2 a^2 c + b\ell_3 \right] + \dot{X}_1^2 (1 - a^2) \\ + X_1 g(1 + a) = gac - (P_1 - P_2)/\rho \end{aligned} \quad (E-7)$$

where

$$\begin{aligned} a &= A_1/A_2 \\ b &= A_1/A_3 \\ c &= V_{12}/A_2 \end{aligned}$$

Equation (E-7) can be transformed into two first-order differential equations of the form:

$$\dot{y}_1 = f_1(y_1, y_2) \quad (\text{E-8})$$

$$\dot{y}_2 = f_2(y_1, y_2) \quad (\text{E-9})$$

where

$$y_1 = x_1$$

$$y_2 = \dot{x}_1$$

$$f_1(y_1, y_2) = y_2 \quad (\text{E-10})$$

$$f_2(y_1, y_2) = \frac{-y_2^2(1 - a^2) - y_1g(1 - a) + gac - (P_1 - P_2)/\rho}{y_1(\theta_1 - \theta_2 a^2) + \theta_2 a^2 c + b\ell_3} \quad (\text{E-11})$$

Although the differential equations (E-8) and (E-9) are non-linear, they are autonomous and therefore amenable to tractable methods of analysis. By linearizing the differential equations about the singular point (the point for which $f_1 = 0$ and $f_2 = 0$), the behavior of the system about the singular point can be characterized by the normal modes (eigenvalues) of the linearized system.

From equations (E-8) and (E-9), the singular point is found to be:

$$y_1 = \frac{ac - (P_1 - P_2)/(\ell g)}{1 + a}$$

$$y_2 = 0$$

At the singular point the water levels, X_1 and X_2 , are established by the pressure differential $P_1 - P_2$. Define l_1 and l_2 to be the values of X_1 and X_2 , respectively, at the singular point. Furthermore, evaluate the volume term in equation at the singular point. Thus,

$$V_{12} = l_1 A_1 + l_2 A_2$$

$$c = a l_1 + l_2$$

$$l_2 - l_1 = (P_1 - P_2) / (\rho g)$$

and

$$y_1 = l_1$$

at the singular point.

The linear system matrix representation for linearizing the nonlinear differential equations is given by:

$$\underline{A} = \begin{bmatrix} \frac{\partial f_1}{\partial y_1} & \frac{\partial f_2}{\partial y_2} \\ \frac{\partial f_2}{\partial y_1} & \frac{\partial f_2}{\partial y_2} \end{bmatrix}$$

Evaluated at a singular point, the four elements of the matrix \underline{A} are:

$$a_{11} = 0$$

$$a_{22} = 0$$

$$a_{12} = 1$$

$$a_{21} = \frac{-g(1+a)}{\ell_1 \theta_1 + \ell_2 \theta_2 a + \ell_3 b}$$

The eigenvalue equation for the matrix A is:

$$\lambda^2 = a_{21}$$

Since the eigenvalues are purely imaginary, the system is characterized by oscillations about the singular point with a frequency,

$$\omega = \sqrt{|a_{21}|} \quad (\text{E-12})$$

For $A_1 = A_2 = A_3$, equation (E-12) reduces to:

$$\omega = \sqrt{\frac{2g}{\ell}}$$

the oscillation frequency of a fluid on a U-tube of constant cross-sectional area. It happens that the test rig geometry meets this condition approximately. Caution must be used in applying the results of this analysis since the streamline construction shown in Figure 93 is based on the particular geometry of the test rig.

REFERENCES

1. Boghani, A.B., Captain, K.M., and Wormley, D.N., "Heave-Pitch-Roll Analysis and Testing of Air Cushion Landing Systems," NASA Contractor Report No. 2917, February 1978.
2. Saha, Hrishikesh, compiler: "Air Cushion Landing Systems," Univ. of Tennessee Space Inst., c.1973.
3. Ribich, W.A. and Richardson, H.H., "Dynamic Analysis of Heave Motion for Transport Vehicle Suspension," EPL Report No. 76110-3, January 1977 (PB 173 685).
4. Schuring, D.J., "Scale Models in Engineering Fundamentals and Applications," New York: Pergamon Press, 1977.
5. Boghani, A.B., and Fish, R.B., "Analysis of Trunk Flutter in Air Cushion Landing Systems," Technical Report No. AFFDL-TR-79-3102, Wright-Patterson AFB, Ohio, August 1979.
6. Stern, T.E., "Theory of Nonlinear Networks and Systems," Addison-Wesley Publishing Co., Inc., 1965.
7. Shearer, J.L., Murphy, A.T., and Richardson, H.H., "Introduction to System Dynamics," Addison-Wesley Publishing Co., Inc., 1971.
8. Sabersky, R.H., Acosta, A.J., and Hauptman, E.G., "Fluid Flow," Second Ed., The Macmillan Company, 1971.

1. Report No. NASA CR-3476		2.		3. Recipient's Accession No.	
4. Title and Subtitle EXPERIMENTAL AND ANALYTICAL STUDIES OF ADVANCED AIR CUSHION LANDING SYSTEMS				5. Report Date November 1981	
				6.	
7. Author(s) E.G.S. Lee, A.B. Boghani, K.M. Captain, H.J. Rutishauser, H.L. Farley, R.B. Fish, and R.L. Jeffcoat				8. Performing Organization Report No. NAS -7723.5-3	
9. Performing Organization Name and Address Foster-Miller Associates, Inc. 350 Second Avenue Waltham, Massachusetts 02154				10. Project/Task/Work Unit No.	
				11. Contract or Grant No. NAS1-15051	
12. Sponsoring Organization Name and Address National Aeronautics and Space Administration Washington, DC 20546				13. Type of Report Contractor Report	
				14.	
15. Supplementary Notes Langley Technical Monitor: Trafford J.W. Leland Final Report					
16. Abstract Several new concepts were developed for Air Cushion Landing Systems (ACLS) which have the potential for improving performance characteristics (roll stiffness, heave damping, and trunk flutter), and reducing fabrication cost and complexity. After an initial screening, the following five concepts were evaluated in detail: damped trunk, filled trunk, compartmented trunk, segmented trunk, and roll feedback control. The evaluation was based on tests performed on scale models. An ACLS dynamic simulation developed earlier has been updated so that it can be used to predict the performance of full-scale ACLS incorporating these refinements. The simulation was validated through scale-model tests. A full-scale ACLS based on the segmented trunk concept was fabricated and installed on the NASA ACLS test vehicle, where it is currently being used to support advanced system development. A geometrically-scaled model (one-third full scale) of the NASA test vehicle was fabricated and tested. This model, evaluated by means of a series of static and dynamic tests, was used to investigate scaling relationships between reduced and full-scale models. The analytical model developed earlier was applied to simulate both the one-third scale and the full-scale response. A preliminary investigation into the behavior of waterborne ACLS was conducted through experiments, analysis, and computer simulations. The work described consisted of the following three tasks: 1) construction of a two-dimensional, reduced-scale, rigid-impermeable-trunk test rig, 2) formulation of analytical models for the test rig and the trunk discharge process, and 3) computer simulation and model verification against test data.					
17. Originator's Key Words Aircraft landing systems Air cushion landing systems Air cushion technology				18. Availability Statement Unclassified - Unlimited Subject Category 05	
19. U. S. Security Classif. of the Report Unclassified		20. U. S. Security Classif. of This Page Unclassified		21. No. of Pages 186	22. Price A09